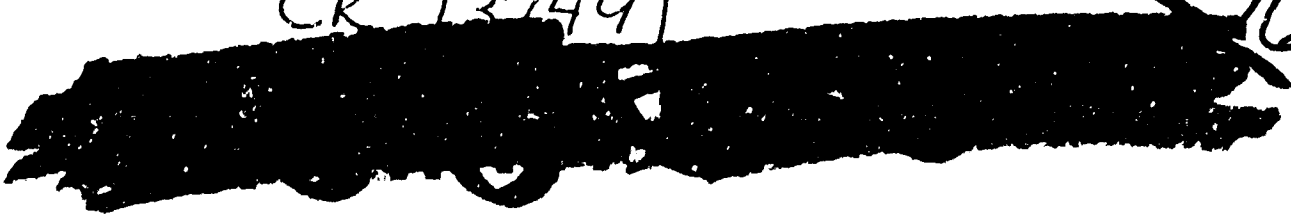


CR 137491

16



# FINAL REPORT SYSTEM DESIGN OF THE PIONEER VENUS SPACECRAFT

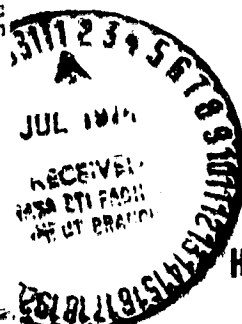
## VOLUME 4 PROBE BUS AND ORBITER SPACECRAFT VEHICLE STUDIES

By  
J. M. BOZAJIAN  
ET AL.

July 1973

Prepared Under  
Contract No. ██████████ NAS 2-7250

By  
HUGHES AIRCRAFT COMPANY  
EL SEGUNDO, CALIFORNIA  
For  
AMES RESEARCH CENTER  
NATIONAL AERONAUTICS AND  
SPACE ADMINISTRATION



(NASA-CF-137491) SYSTEM DESIGN OF THE  
PIONEER VENUS SPACECRAFT. VOLUME 4:  
PROBE BUS AND ORBITER SPACECRAFT VEHICLE  
STUDIES. Final report (Hughes Aircraft  
Co.) 255 P HC \$15.75  
CSCI 228

63/31  
DCLAS  
41559

74-27374



CR 137491

**FINAL REPORT**  
**SYSTEM DESIGN OF THE**  
**PIONEER VENUS SPACECRAFT**

**VOLUME 4**  
**PROBE BUS AND ORBITER**  
**SPACECRAFT VEHICLE STUDIES**

■  
By  
J. M. BOZAJIAN  
ET AL.

■  
July 1973

Prepared Under  
Contract No. ~~XXXXXXXXXX~~ - NAS 2-7250

By  
HUGHES AIRCRAFT COMPANY  
EL SEGUNDO, CALIFORNIA

For  
AMES RESEARCH CENTER  
NATIONAL AERONAUTICS AND  
SPACE ADMINISTRATION

## PREFACE

The Hughes Aircraft Company Pioneer Venus final report is based on study task reports prepared during performance of the "System Design Study of the Pioneer Spacecraft." These task reports were forwarded to Ames Research Center as they were completed during the nine months study phase. The significant results from these task reports, along with study results developed after task report publication dates, are reviewed in this final report to provide complete study documentation. Wherever appropriate, the task reports are cited by referencing a task number and Hughes report reference number. The task reports can be made available to the reader specifically interested in the details omitted in the final report for the sake of brevity.

This Pioneer Venus Study final report describes the following baseline configurations:

- "Thor/Delta Spacecraft Baseline" is the baseline presented at the midterm review on 26 February 1973.
- "Atlas/Centaur Spacecraft Baseline" is the baseline resulting from studies conducted since the midterm, but prior to receipt of the NASA execution phase RFP, and subsequent to decisions to launch both the multiprobe and orbiter missions in 1978 and use the Atlas/Centaur launch vehicle.
- "Atlas/Centaur Spacecraft Midterm Baseline" is the baseline presented at the 26 February 1973 review and is only used in the launch vehicle utilization trade study.

The use of the International System of Units (SI) followed by other units in parentheses implies that the principal measurements or calculations were made in units other than SI. The use of SI units alone implies that the principal measurements or calculations were made in SI units. All conversion factors were obtained or derived from NASA SP-7012 (1969).

The Hughes Aircraft Company final report consists of the following documents:

Volume 1 - Executive Summary - provides a summary of the major issues and decisions reached during the course of the study. A brief description of the Pioneer Venus Atlas/Centaur baseline spacecraft and probes is also presented.

Volume 2 - Science - reviews science requirements, documents the science-peculiar trade studies and describes the Hughes approach for science implementation.

Volume 3 - Systems Analysis - documents the mission, systems, operations, ground systems, and reliability analysis conducted on the Thor/Delta baseline design.

Volume 4 - Probe Bus and Orbiter Spacecraft Vehicle Studies - presents the configuration, structure, thermal control and cabling studies for the probe bus and orbiter. Thor/Delta and Atlas/Centaur baseline descriptions are also presented.

Volume 5 - Probe Vehicle Studies - presents configuration, aerodynamic and structure studies for the large and small probes pressure vessel modules and deceleration modules. Pressure vessel module thermal control and science integration are discussed. Deceleration module heat shield, parachute and separation/despin are presented. Thor/Delta and Atlas/Centaur baseline descriptions are provided.

Volume 6 - Power Subsystem Studies

Volume 7 - Communication Subsystem Studies

Volume 8 - Command/Data Handling Subsystems Studies

Volume 9 - Altitude Control/Mechanisms Subsystem Studies

Volume 10 - Propulsion/Orbit Insertion Subsystem Studies

Volumes 6 through 10 - discuss the respective subsystems for the probe bus, probes, and orbiter. Each volume presents the subsystem requirements, trade and design studies, Thor/Delta baseline descriptions, and Atlas/Centaur baseline descriptions.

Volume 11 - Launch Vehicle Utilization - provides the comparison between the Pioneer Venus spacecraft system for the two launch vehicles, Thor/Delta and Atlas/Centaur. Cost analysis data is presented also.

Volume 12 - International Cooperation - documents Hughes suggested alternatives to implement a cooperative effort with ESRO for the orbiter mission. Recommendations were formulated prior to the deletion of international cooperation.

Volume 13 - Preliminary Development Plans - provides the development and program management plans.



Volume 14 - Test Planning Trades - documents studies conducted to determine the desirable testing approach for the Thor/Delta spacecraft system. Final Atlas/Centaur test plans are presented in Volume 13.

Volume 15 - Hughes IR&D Documentation - provides Hughes internal documents generated on independent research and development money which relates to some aspects of the Pioneer Venus program. These documents are referenced within the final report and are provided for ready access by the reader.

Data Book - presents the latest Atlas/Centaur Baseline design in an informal tabular and sketch format. The informal approach is used to provide the customer with the most current design with the final report.

## CONTENTS

	Page
1. SUMMARY	1-1
1.1 Major Issues	1-1
1.2 Baseline Description	1-4
2. INTRODUCTION	2-1
3. CONFIGURATION	3-1
3.1 Requirements	3-3
3.2 Trades	3-4
Spin Axis Orientation	3-4
Radar Altimeter Integration and Orbiter Periapsis Latitude	3-13
Liquid Versus Solid Propellant for Orbit Insertion	3-17
Magnetometer Integration	3-17
Equipment Shelf Configuration Trade	3-21
Spacecraft Launch Mass and Contingency	3-21
3.3 Thor/Delta Baseline Description	3-27
Probe Bus	3-27
Orbiter Spacecraft	3-49
3.4 Atlas/Centaur Baseline Description	3-51
Mission Configuration and Launch Mass Contingency Trades	3-51
Radio Occultation Experiment Trades	3-53
Magnetometer Boom Installation	3-57
Configuration Descriptions	3-61
4. STRUCTURE SUBSYSTEM	4-1
4.1 Structural Subsystem Requirements	4-2
Structural Design Requirements	4-2
Design Criteria	4-9
Dynamic Loads Analysis	4-10
Mathematic Models	4-11
4.2 Trades	4-15
Beryllium Weight/Cost Considerations	4-15
Stress Analysis	4-19
4.3 Thor/Delta Baseline Description	4-19
4.4 Atlas/Centaur Baseline Description	4-23

PRECEDING PAGE BLANK NOT FILMED

5.	THERMAL CONTROL	5-1
5.1	Requirements	5-3
5.2	Trades	5-13
	Spin Axis Orientation	5-13
	Candidate Thermal Designs	5-15
	Probe Preentry Design Trades	5-17
	Aft Cavity Solar Interreflection Test Evaluation	5-27
	Rocket Exhaust Plume Impingement Study	5-35
5.3	Thor/Delta Baseline Description	5-49
	Spacecraft Design	5-49
	Probe Preentry Design	5-59
	Mass and Power Summary and Hardware Derivation	5-61
	Spacecraft Design Performance	5-61
5.4	Atlas/Centaur Baseline Description	5-80
	Spacecraft Design	5-80
	Probe Preentry Design	5-87
	Mass and Power Summary and Hardware Derivation	5-87
	Spacecraft Design Performance	5-87
	Spacecraft Design Tradeoffs	5-96
	Probe Design Performance	5-99
6.	HARNES SUBSYSTEM	6-1
6.1	Requirements	6-1
6.2	Trades	6-3
6.3	Thor/Delta Baseline Description	6-5
6.4	Atlas/Centaur Baseline Description	6-6
APPENDICES		
A.	Thor/Delta Spacecraft Stress Analysis	A-1
B.	Atlas/Centaur Spacecraft Stress Analysis	B-1

## 1. SUMMARY

This volume discusses the requirements, trades, and design descriptions for the probe bus and orbiter spacecraft configuration, structure, thermal control, and harness. Designs are developed for Thor/Delta and Atlas/Centaur launch vehicles with the latter selected as the final baseline.

### 1.1 MAJOR ISSUES

The principal NASA requirements for spacecraft design are spin stabilization, low cost, maximum commonality of probe bus and orbiter configurations and hardware. The nominal science payload is specified by NASA for the probe bus, a large probe and three identical small probes, and for the orbiter spacecraft.

The major issues examined in achieving the baseline design are shown in Table 1-1. Most of the significant configuration trades center around the orbiter, and in particular, the constraints and performance in Venus orbit. The probe bus design is influenced first by its primary function to transport and separate the probes and the subsequent bus entry mission and, secondly, by the goals of commonality with the orbiter in order to reduce development cost. The specification of one large probe and the use of tangential velocity from the bus spin rate to target three, identical small probes has essentially eliminated any major configuration trade issues in this area.

Spin axis orientation is very important in Venus orbit because of pointing requirements for science experiments and earth communications. The earth pointing spin axis constrains science coverage throughout the mission unless propellant consuming attitude maneuvers are employed periodically. The associated solar angle variation greatly complicates solar power and thermal design. Spin axis perpendicular to ecliptic provides good science coverage with simpler power/thermal configuration. The probe bus retains spin axis orientation perpendicular to the ecliptic during cruise to preserve commonality with the orbiter.

With the spin axis perpendicular to ecliptic, the orbiter high gain antenna (HGA) selection narrows down to use of a mechanically or electrically despun antenna (MDA or EDA). (A stack of three bicone antennas was considered but requires excessive transmitter power to meet the necessary ERP). The configuration can accommodate either an MDA or EDA, but the MDA is selected based on flight experience on many spacecraft (recently, Intelsat IV, Telesat) and lower development cost.

TABLE 1-1. SPACECRAFT CONFIGURATION/STRUCTURE/THERMAL DESIGN ISSUES

Issue	Baseline	Alternatives	Rationale for Selection
Spin axis orientation	Perpendicular to ecliptic	Parallel to earthline or perpendicular to Venus orbit plane	Best science coverage; simpler power and thermal design; low weight
Orbiter HGA	Mechanically despun parabolic reflector	Electronically despun antenna or stacked bicones	Flight proven technology, simpler radio science accommodation; lower cost
Orbiter dual frequency occultation experiment	Separate, 20 deg, X band horn with S band HGA	Dual S/X feed HGA with moving reflector or precessing spacecraft	Lowest cost/weight, high reliability; simple interfaces and mission operations
Orbiter radar altimeter antenna selection and integration	Electronically steered; mounted on forward (HGA) end of spacecraft	Mechanically steered; mount orbit motor end	Simpler installation, deployment not required; no interaction with spacecraft dynamics; all periaapsis latitudes accommodated
Orbiter magnetometer integration	4.4 m, three link boom, deployed in plane perpendicular to spin axis	Shorter booms or five link booms; boom deployed in plane through spin axis	Lower cost of magnetic controls; best science; better stowed failure mode
Orbit insertion motor selection and integration	Solid motor	Biliquid or monoliquid	Simple modification of existing design, lower cost; spacecraft sized for alternate solid motors
Equipment shelf arrangement and thermal approach	Open shelf; instruments and subsystems forward, thermal louvers aft	Compartmented shelf; equipment/louvers on both sides	Lower weight, cost; better access; common installations and thermal approach in probe and orbiter
Probe pre-entry thermal control	Passive finishes; heater power from bus; $\pm 5^{\circ}\text{C}$ uncertainty on entry temperature	Passive design with thermally controlled probe heater for post-separation control	Lower cost, weight, volume; simpler and more reliable
Structural material and weight	Aluminum structure	Selective use of beryllium	Lower cost and development risk; weight acceptable for baseline
Harness wire and connectors	24 AWG wire and crimped contacts, double-density connector	28 AWG wire; soldered contacts, micro miniature connectors	Lower cost; high reliability
Mission opportunities and launch mass contingency	Type I, 1978, multiprobe Type II, 1978, 56°S, orbiter	Type I, 13°N for orbiter	Better science coverage at middle latitudes; mass contingency adequate; simple accommodation of alternate 1978 or 1980 missions

The mechanical despin approach also offers more options in implementation of the dual frequency (S/X band) radio occultation experiment. Approaches involve mounting a separate fixed X band horn with the S band HGA or using a dual feed S/X HGA and using it either with an elevation drive (azimuth is by the despin system) or by precessing the spacecraft. The separate X band horn approach is selected on the basis of lowest cost/weight, high reliability, and simple experiment/bus interfaces.

The radar altimeter antenna selection - mechanically or electronically steered - is influenced by the range or orbit periapsis latitudes required and possible associated requirements to deploy the altimeter to provide adequate viewing. The electronically-steered version is easier to integrate in this regard, and does not couple to the spinning spacecraft dynamics. The requirements of velocity pointed experiments and radar altimeter antenna viewing near periapsis are both satisfied over range of interest (0 to 60° N and S) in periapsis latitudes by mounting the radar antenna on the forward (HGA) end of the spacecraft along with the other experiments on the equipment shelf. The accommodation of a selected periapsis latitude requires only the positioning of the antenna at the appropriate fixed angle to the spin axis by design of the support structure.

The magnetometer boom integration trade begins with the reduction of spacecraft induced magnetic field at the sensor with increased boom length. The cost of spacecraft magnetic cleanliness and controls over the boom length of interest is traded against cost of boom development and issues of "long" boom design and integration, such as methods of articulation, deployment, stowage, mounting locations, spacecraft dynamics, failure modes and effect of spin rate, and orbit insertion acceleration. A long (4.4 m), three link boom is selected for lowest program cost, best science performance, and more favorable failure mode.

The selection of an orbit insertion motor impacts the configuration, since it can be either liquid or solid, and its size is influenced by the desired mission flexibility. Mono-liquid approaches are too heavy because of their low specific impulse. Biliquid systems are competitive with solids in system weight, but are somewhat more difficult to integrate and relatively costly. Existing solid motors are available, with some modifications, for all orbiter mission opportunities in 1978 and 1980 and are selected as the lowest cost approach. The central thrust tube of the spacecraft is sized to accommodate all candidate motors with modification only of the motor attach ring structure.

The equipment shelf arrangement has been selected as an open shelf rather than a compartmentized approach. The open shelf is structurally lighter, more accessible, and is less constraining in achievement of mass balance, lower harness weight, and desired power dissipation distribution for thermal control. The aft (thrust tube) end of the spacecraft is selected for thermal louver radiation as the four probes limit use of the forward side. The louvers are mounted on the aft side of the shelf on the orbiter to maintain commonality with the probe bus. Use of louvers on the aft side and equipment on the forward side also facilitates access, experiment integration

and thermal blanket design and placement. The shelf commonality is further increased by maintaining identical installations of those subsystems and/or experiments that are common to both spacecraft.

The thermal control of probes while on the spacecraft has been evaluated with the condition that passive thermal surface techniques be used to provide a minimum pressure vessel temperature prior to Venus entry. Meeting this condition produces low probe temperatures early in cruise, requiring spacecraft power to probe heaters to maintain acceptable non-operating temperature levels. An alternate design requires probe heater used after separation leading to higher weight and volume in the probes.

Beryllium had been utilized selectively for required weight reduction of spacecraft structure in the Thor/Delta design. Aluminum is selected for the Atlas/Centaur baseline for lower cost and risk.

Matrix-double density subminiature connectors (used on OSO-I) using crimped contacts and 24 AWG wire are selected in the wire harness for lower cost. The alternates include microminiature connectors with soldered contacts and 28 AWG wire.

The final major issue is the selection of the baseline mission set of launch opportunities for multiprobe and orbiter missions. NASA-ARC has directed that both missions be planned for Atlas/Centaur launch vehicles in 1978. A type I probe launch is planned for August 1978 with separated spacecraft mass of 813 kg (1793 lbs) and a mass contingency of 150 kg (330 lbs), which is 19 percent of the dry spacecraft mass less bus science of 13.7 kg (30 lbs). The trade issue involves the trajectory and Venus orbit selection for the orbiter. One possibility is an August 1978 launch (type I, 13° N periapsis in Venus orbit), which has a dry mass in orbit of 405 kg (892 lbs) and contingency of 35 percent of the dry mass in orbit less science of 47.5 kg (105 lbs). The orbiter type I case requires a launch within several weeks of the multiprobe mission launch. The other opportunity is a type II (56° S) launch in May 1978 which has dry mass in orbit of 290 kg (640 lbs) and contingency of 10 percent. This mission has been selected as the orbiter baseline because of better mid-latitude science coverage near periapsis and elimination of closely separated launches. The HGA mast length has been selected to allow radar altimeter antenna positions for all latitudes between 13° and 56° (or higher). For example, a 1980 orbiter type II (26° N) launch has a contingency of 17 percent and can be accommodated, by use of the TEM 616 orbit insertion motor (attach ring modification) and modification to radar antenna support structure.

## 1.2 BASELINE DESCRIPTION

The spin stabilized probe and orbiter spacecraft configurations developed for launch on the Atlas/Centaur are shown in exploded views in Figure 1-1. The configurations are derived from flight-proven communications satellites, particularly the Telesat-Anik and feature a high degree of subsystem hardware commonality.

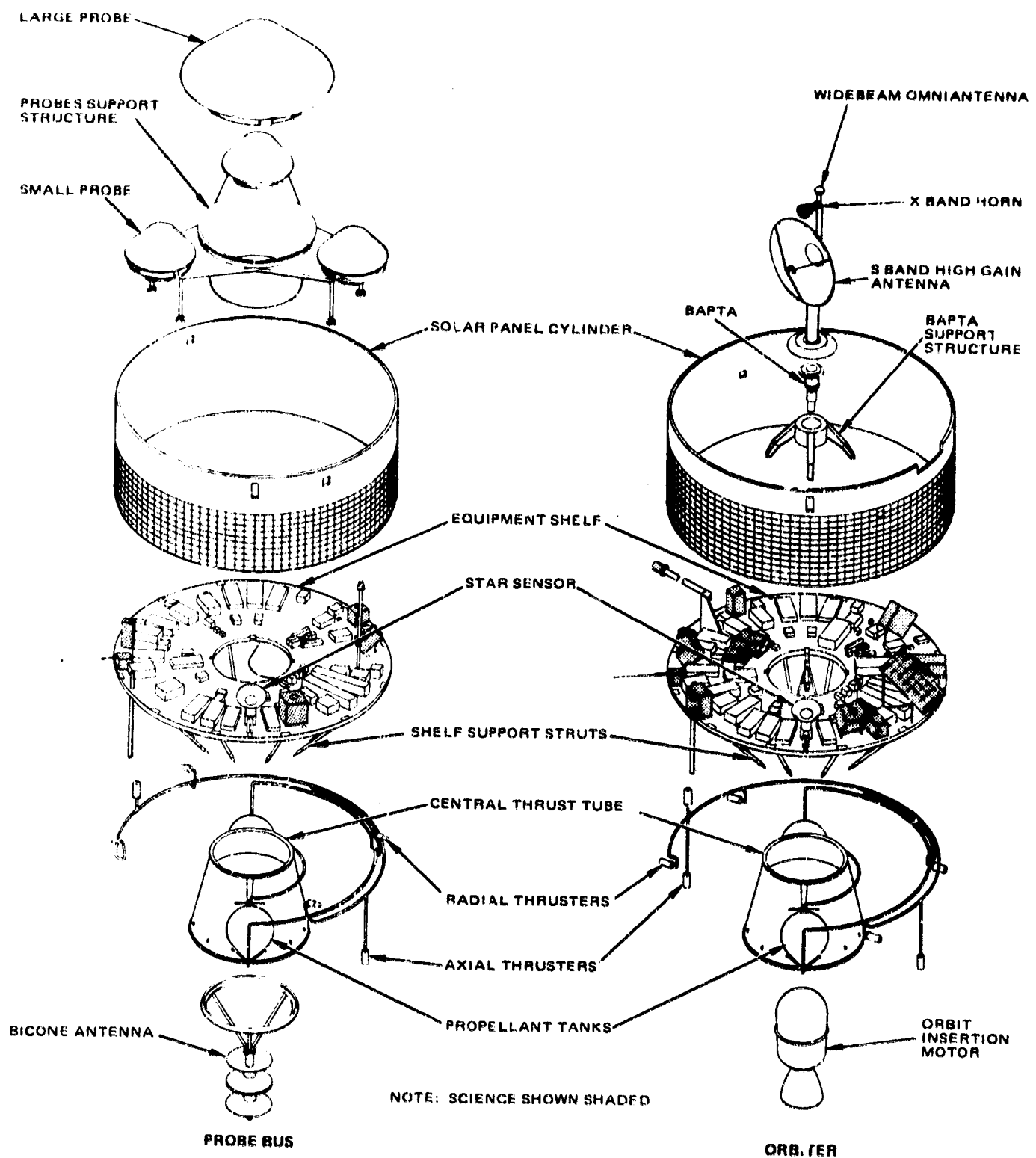


FIGURE 1.1. SPACECRAFT CONFIGURATIONS

REPRODUCIBILITY OF THE ORIGINAL PAGE IS POOR.



Both spacecraft are designed for operation with spin axis perpendicular to the ecliptic except for maneuvers and periods such as trajectory correction, probe release, bus entry, and orbit insertion.

The primary structural elements common to the probe bus and orbiter are the central conical aluminum thrust tube, aluminum honeycomb sandwich equipment shelf, 12 shelf support struts, and the 254 cm (100 in.) diameter solar panel cylinder made of fiberglass face sheets and aluminum honeycomb core. On the probe bus, a central conical support structure with associated secondary structure attaches to the upper end of the thrust tube to support the large probe and three small probes. The large probe is separated axially using springs; the small probes are spin-separated, simultaneously, to minimize targeting errors due to induced nutation. On the orbiter, an existing quadrupod structure (from Telesat) attaches to the forward end of the thrust tube and supports the bearing and power transfer assembly (BAPTA) used to mechanically despun the mast mounted, 82.5 cm (32.5 in.) diameter S band high gain antenna, and X band horn (for the occultation experiment) and the forward omni antenna. The Intelsat IV launch vehicle/spacecraft attach fitting is used with both spacecraft.

The hydrazine propulsion tanks and feed are supported on the thrust tube. Four radial and two axial thrusters on the probe bus and four radial and three axial thrusters on the orbiter are attached through support structures to the equipment shelf. The thrusters provide redundancy in trajectory correction, spin and attitude control. A solid-state star sensor, mounted on the shelf at an angle of  $58^\circ$  with the spin axis, and sun sensors provide the required attitude references.

On the orbiter, the case-stretched TEM-521 solid propellant orbit insertion motor is mounted on the motor attach ring internal to the thrust tube. The bicone antenna is mounted inside the thrust tube on the probe bus.

Five probe bus and nine orbiter experiments are installed, principally, on the equipment shelf. Velocity pointed experiments are positioned for bus entry conditions and Venus orbit periapsis latitude. The three-link, 4.4 m (14.5 ft) magnetometer boom is stowed just above solar cylinder on the orbiter and is deployed, centrifugally, after initial spacecraft spinup, in a plane perpendicular to the spin axis. The electronically steered radar altimeter antenna is positioned with its pointing angle at  $34^\circ$  with the spin axis to provide required radar beam pointing near the baseline orbit periapsis latitude of  $56^\circ$ . Other latitudes are accommodated by varying the fixed angle of the radar antenna installation. The high gain antenna mast length is sufficient to allow repositioning for a periapsis latitude of  $13^\circ$  without RFI.

Spacecraft subsystem components are also mounted on the forward side of the shelf. Identical shelf installations are planned for equipment common to probe bus and orbiter. Ten (12) louver modules are mounted on the aft side of the probe bus (orbiter) shelf for primary thermal control

by radiation out of the aft spacecraft cavity. The body of the spacecraft is enclosed on all external surfaces (except the outer solar panel cylinder) with multilayer aluminized Kapton blankets. In the aft cavity, the blanket is placed over the solar panel cylinder, the outer thrust tube and tanks and the aft shelf with cutouts at each louver module.

The spacecraft mass summary is shown in Table 1-2 for the baseline missions, type I, 1978 for multiprobe and type II, 56° S, 1978 for orbiter. The experiment payloads used are those specified by NASA-ARC in April 1973 and include the recommended 15 percent experiment contingency. The orbiter experiment payload has been increased by 2.13 kg (4.7 lbs) to account for the current Hughes estimate of the additional mass (over the NASA-ARC allowance) required to implement the dual frequency occultation experiment.

TABLE 1-2. SPACECRAFT MASS SUMMARY

Item	Multiprobe Kg (Lb)	Orbiter Kg (Lb)
Bus (dry)	191.5 ( 422.1)	217.6 ( 479.7)
Large probe*	245.1 ( 540.4)	-----
Small probe (3)**	190.8 ( 420.6)	-----
Spacecraft subtotal	627.4 (1383.1)	217.6 ( 479.7)
Contingency	149.6 ( 329.8)	25.3 ( 55.8)
Experiments (bus or spacecraft)	13.7 ( 30.3)	47.5 ( 104.3)
Spacecraft total (dry)	790.7 (1743.2)	290.4 ( 640.3)
Propellant and pressurant	22.4 ( 49.4)	27.0 ( 59.4)
Orbit insertion motor expendables	-----	143.3 ( 316.0)
Spacecraft total (wet)	813.1 (1792.6)	460.7 (1015.7)
Spacecraft attach fitting	31.3 ( 69.0)	31.3 ( 69.0)
Launch Vehicle Payload	844.4 (1861.6)	492.0 (1084.7)

\* Includes 31.6 kg (69.7 lbs) for experiments

\*\* Includes 2.6 kg (5.8 lbs) for experiments (for one probe)

## 2. INTRODUCTION

This volume discusses the probe bus and orbiter spacecraft studies performed during the Pioneer Venus Systems Design Study initiated 2 October 1972. The volume content is limited to vehicular aspects, such as spacecraft configuration, structure, thermal control, and harness. Other spacecraft and probe subsystems are discussed in subsequent volumes. Each section on these vehicular subjects includes a discussion of requirements, trades studies, a description of the baseline design for the Thor/Delta launch vehicle and a description of the final Atlas/Centaur baseline design. These discussions constitute the final report material in satisfaction of selected tasks in subsections 2.1, General Tasks, and 2.2, Design, in the Statement of Work of the Pioneer Venus Mission Systems Design Study, 2-17502, Revision 2, 7 November 1972 and the accompanying requirements specification.

The Study was initiated using the Thor/Delta launch vehicle. Revision 2 of the Statement of Work included an additional parallel study of a design for the Atlas/Centaur launch vehicle. Use of the Atlas/Centaur was predicated on using the greater launch vehicle payload weight and volume for the purpose of achieving low cost objectives. The two baseline designs were developed and evaluated, including cost and weight trades, and presented at the midterm review of the Systems Design Study on February 26 and 27, 1973. Due to phasing of the study, the major trades and issues at midterm were based to greater extent on the Thor/Delta baseline and this is reflected in the final report content. Most of the trades, however, apply in their principal conclusions to the Atlas/Centaur design.

Subsequent to the midterm review, NASA-ARC on 13 April 1973 redirected the balance of the study effort exclusively to the Atlas/Centaur baseline with both multiprobe and orbiter missions to be launched in the 1978 opportunities. A modified science experiment payload was also included in this redirection. The subsections on Atlas/Centaur baseline in this volume are, therefore, responsive to the April redirection. The subsections also include, as required, some additional trade studies pertinent to the Atlas/Centaur design. The Thor/Delta baseline description subsections refer to that design presented at the midterm review.

### 3. CONFIGURATION

Probe bus and orbiter spacecraft configurations have been designed in accordance with basic requirements for spin stabilization, maximum commonality and low cost spacecraft subsystems. Major configuration/structure elements such as equipment shelves, struts, thrust tube propulsion tank installations, solar panel cylindrical substrates are designs common to the probe bus and orbiter. The configuration approach includes use of a mechanically despun antenna (MDA) on the orbiter and is derived from flight-proven Hughes commercial and military satellites, particularly the ANIK-Telesat. The study includes designs for both Thor/Delta and Atlas/Centaur launch vehicles.

The principal configuration trade issues and approaches are summarized in Table 3-1. The selections resulting from these trade studies have resulted in configurations with spin axis orientation perpendicular to the ecliptic except for transient periods of trajectory correction, probe release, probe bus entry, and orbit insertion. Attitude references are provided by sun and star sensors. Attitude/spin control and trajectory corrections are provided by axial and radial hydrazine thrusters.

The probe bus targets the large probe by separating the probe along the spacecraft spin axis. Later, three small probes are released simultaneously and acquire lateral velocity for target separation from the probe bus spin rate.

The orbiter uses flight-proven, mechanical despun technology to point the parabolic high gain antenna toward earth. A separate X-band antenna is mounted with the HGA Atlas/Centaur baseline for the occultation experiment. An electronically steered radar altimeter antenna is positioned at various orbit periapsis latitudes. Existing solid propellant rocket motors are available to accommodate the range of orbit insertion impulse required for the launch vehicles and mission opportunities studied. The magnetometer boom integration is more difficult on Thor/Delta because of weight limitations and specifications limiting spacecraft unbalance during boost. A longer boom is used on the Atlas/Centaur design to reduce the cost of magnetic cleanliness for the spacecraft.

An open equipment shelf design allows maximum flexibility for installing common hardware in probe bus and orbiter without compromising spacecraft balance and thermal design.

TABLE 3-1. SPACECRAFT CONFIGURATION ISSUES AND TRADES

Issue/Approaches	Selection/Status
Spin axis orientation - perpendicular versus parallel to ecliptic	Perpendicular to ecliptic - improved orbiter science coverage and simpler spacecraft power/thermal design
MDA versus EDA for orbiter	MDA - proven technology; facilitates radio science accommodation
Radio occultation by fixed or moving antenna or by precessing spacecraft	Fixed despun antennas (S-band HGA and separate X-band horn) - lowest cost, weight and complexity; simple interfaces
Electronically versus mechanically steered radar altimeter	Electronically steered - simpler integration for various orbit periapsis latitudes
Liquid versus solid propellant for orbit insertion	Solid propellant motor - existing design, lower cost
Magnetometer integration	Short boom and magnetic controls on Thor/Delta due to weight/unbalance constraints; longer boom on Atlas/Centaur
Open equipment shelf versus compartments for experiments and subsystems	Open shelf - lighter, better access, retain common installations in probe spacecraft and orbiter for experiments and subsystems
Launch mass contingency	Marginal/costly for Thor/Delta; liberal (adequate) for Atlas/Centaur multiprobe (orbiter, type II) mission

Spacecraft weight was a substantial problem with the Thor/Delta launch vehicles. Relatively expensive weight reductions were implemented in the midterm design to attain even marginal weight contingency of 6 to 7 percent for either mission. The reductions involved use of beryllium in spacecraft and probe aeroshell structures and large scale integrated (LSI) circuits in spacecraft and probe command and data handling subsystems. In contrast, the Atlas/Centaur contingency was over 20 percent for the allowable launch mass and mission sets applicable at midterm (probe, type I, 1977; orbiter, type I, 1978).

In April, experiment payloads were revised, probe and orbiter launches were both planned for 1978, and allowable Atlas/Centaur payload was increased by 75 kg (165 lb). The trade of type I vs. type II trajectories and associated periapsis latitudes was reviewed for Atlas/Centaur and resulted in selection of type I for the probe mission and type II, 56° S periapsis for the orbiter. The launch weight contingency for the current baseline mission/spacecraft design is 19.3 percent for the probe mission and 10.4 percent for the orbiter mission.

### 3.1 REQUIREMENTS

The spacecraft designs for the two proposed Pioneer Venus missions, probe and orbiter, are influenced by a combination of requirements imposed by several areas. While some of these are common for both missions and can be accommodated in similar fashion, others are unique to each spacecraft.

The initial requirements on the designs are delineated in the Systems Design Study Specification and Statement of Work. These documents direct that for both missions the spacecraft shall be spin stabilized, and provide maximum commonality between probe bus and orbiter spacecraft systems and subsystems consistent with mission objectives and performance requirements.

On the multiprobe mission, the large and small probes and the probe bus are targeted to the desired impact sites by orienting the probe bus to the desired direction. The large probe is separated in an axial direction relative to the spacecraft, the small probes are separated in the same direction but are given a lateral component of velocity from the spacecraft spin rate ( $\approx 70$  rpm at separation). Therefore, the configuration must provide for interference-free axial and lateral separation paths for the four probes and the ability to change spin rate. Also, the small probes must be arranged symmetrically about the spin axis for static and dynamic balance which results in a symmetrical targeting since, for effective separation, the small probes must be separated simultaneously. A final reorientation is made for targeting the probe bus for entry with spin axis orientated along the earth line and close to the velocity vector.

For the orbiter mission the selection of a type I or type II transit trajectory determines the size of the orbit insertion motor that must be

accommodated by the configuration. It also establishes the range of periapsis latitudes that are available. The selection of a latitude establishes pointing angle requirements for those experiments that desire orientation in the direction of velocity at periapsis or for the radar altimeter which points along the planet radius vector.

A nominal payload of science experiments was established for each mission and these are discussed in Volume 2. Most of the experiments have desired line of sight angles relative to the spacecraft and need unobstructed fields of view to permit their proper operation. Also, the neutral mass spectrometer, assumed to be of the magnetically focused type, must be located remotely from those instruments affected by a magnetic field such as a magnetometer, retarding potential analyzer, electronic temperature probe and ion mass spectrometer. These requirements thus impose limitations to the locations of the experiments on the spacecraft. Velocity oriented experiments must be installed on the probe bus for proper attitude during bus entry and on the orbiter for near-periapsis operations.

The final spacecraft configuration is the end result of integrating the subsystems necessary for accomplishment of the mission. The individual subsystem requirements, mass, volume, and form factor and their interaction with each are all factors to be dealt with in establishing the best arrangement. For subsystem units that are to be shelf mounted, consideration must be given to their locations for reasons of mass balance, thermal distributions, interconnect harness lengths to minimize line losses, in addition to functional arrangement. The need for maintaining unobstructed fields for attitude control sensors and rf antenna beams, prevention of solar array shadowing, clearance from motor exhaust plumes, are some of the requirements affecting the external arrangement.

Two different launch vehicles are considered, Thor/Delta and the Atlas/Centaur. The major areas of constraint to the spacecraft for each launch vehicle as shown in the Design Study Specification Appendices C and D, are noted in Table 3-2.

### 3.2 TRADES

The principal trade considerations in development of the probe bus and orbiter spacecraft configurations are presented in this subsection. Most of these trades were conducted for Thor/Delta design conditions, however, most of the results apply to Atlas/Centaur versions. Additional trades performed specifically for the final Atlas/Centaur baseline design are discussed in subsection 3.4.

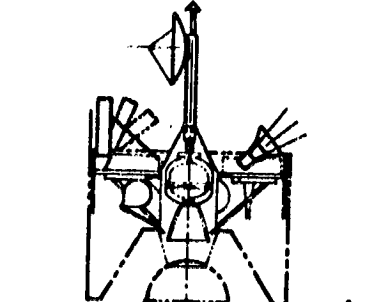
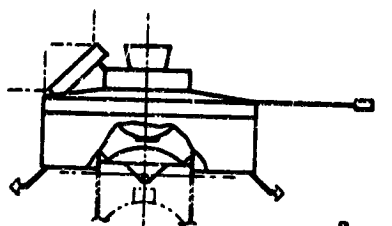
#### Spin Axis Orientation

Spacecraft spin axis orientation is a driving factor in configuration and subsystem design. On the orbiter, orientation is critical to the viewing direction of the science experiments over the Venusian year. The science coverage and mission trades of this selection are discussed in Volumes 2 and 3. The spacecraft design trades are summarized in this volume.

TABLE 3-2. CONFIGURATION CONSTRAINTS IMPOSED BY THE LAUNCH VEHICLES

Configuration Constraints	Thor/Delta	Atlas/Centaur
Maximum probe bus payload mass (includes spacecraft adapter)	405.65 kg (894.3 lb) (includes telemetry unit)	844.4 kg (1861.6 lb)
Maximum orbiter payload mass (includes spacecraft adapter)	314.38 kg (693.1 lb) (includes telemetry unit)	492 kg (1084.7 lb)
Maximum payload diameter (launch configuration)	218.4 cm (86.0 in.)	266.7 cm (105 in.)
Spacecraft c.m. alignment (launch configuration)	c.m. offset to spacecraft centerline no greater than 0.38 mm (0.015 in.)	Not specified
Spacecraft inertial axis alignment (launch configuration)	Principal axis of inertia tilt not greater than 0.002 rad (0.1 deg)	Not specified
Launch vehicle spin rates	Spin rates up to 100 rpm	Spin rates up to 12 rpm-optional (if Delta spin table and adapter used, spin rates up to 120 rpm-optional)
Maximum center of mass height above separation plane	107 cm (42 in.) for 408 kg (900 lb) payload on 63.5 cm (25 in.) adapter	Not specified
Adapter or attach fitting interface diameter options	45.7 cm (18.0 in.) 63.5 cm (25.0 in.) 94 cm (37.0 in.)	94 cm (37.0 in.) 113 cm (44.5 in.) 140 cm (55.0 in.)



SPIN AXIS ORIENTATION	FEATURE	CONFIGURATION
1. PERPENDICULAR TO ECLIPTIC	SIMPLEST THERMAL CONTROL & POWER SUBSYSTEM DESIGNS	 <p style="text-align: right;">A</p>
2. DIRECTED TO EARTH  3. PERPENDICULAR TO ORBIT PLANE (AROUND VENUS)	FIXED HIGH GAIN ANTENNA  BEST FOR PLANET AND VELOCITY POINTED EXPERIMENTS	 <p style="text-align: right;">B</p>

30163-333(U)

FIGURE 3-1. ORBITER SPIN AXIS ORIENTATION OPTIONS

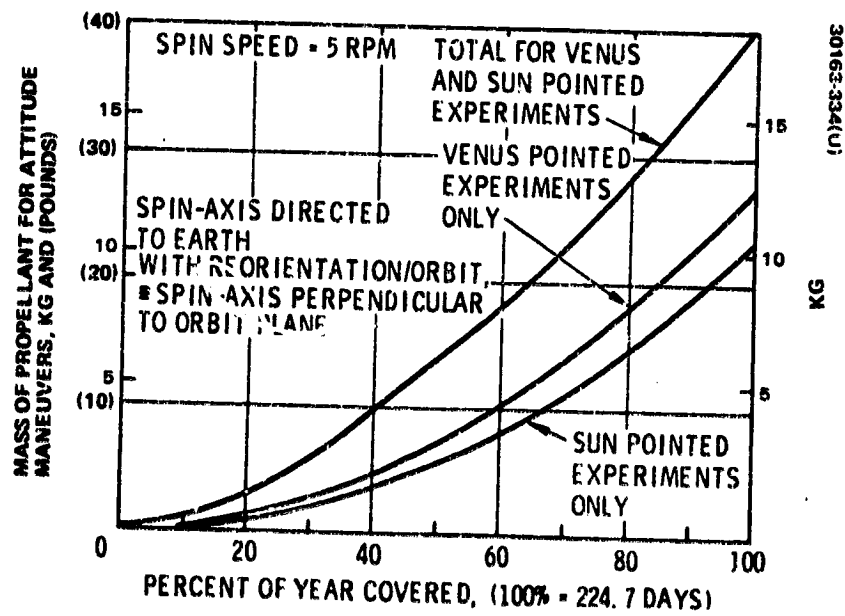


FIGURE 3-2. PROPELLANT REQUIRED FOR EXPERIMENT ORIENTED ATTITUDE MANEUVERS

Figure 3-1 illustrates the options on spin axis orientation for the orbiter: 1) perpendicular to the ecliptic, 2) directed to the earth, and 3) perpendicular to the orbit plane around Venus. Also shown are configuration approaches compatible with the particular spin axis orientation. Configuration A requires use of a despun antenna system (MDA is shown) for the data rates in the orbital phase of the mission and uses a cylindrical solar panel with thermal louvers on bottom surface of the equipment shelf. Large solar angle variations occur for configuration B (Figure 3-1) requiring use of solar panels on fore and aft surfaces of the spacecraft in addition to that on the cylindrical surface. The solar angle variation also complicates the thermal design (see subsection 5.2) and requires a capability of radiating from both ends of the spacecraft with the associated need for additional louvers and shelf area. Configuration B uses an earth pointing high gain antenna (HGA) and spacecraft spin for use in a conical scan as an attitude reference. Attitude reference studies (Volume 9) have shown, however, that configuration B also requires a star sensor for spin sector reference.

The science coverage studies (Volume 2) indicate the spin axis perpendicular to the ecliptic is preferred (case 1, Figure 3-1) to the earth pointing mode (case 2). Case 3, perpendicular to Venus orbit plane is well-suited for planet and velocity pointed experiments but requires a reorientation on every orbit for downlink data dump near apoapsis. This maneuver is costly in propellant (see Figure 3-2) and is restrictive operationally.

Table 3-3 summarizes the major issues in the Thor/Delta orbiter spacecraft mechanization trades as a function of spin axis orientation. The structure and adapter mass increase for configuration B as a result of thermal/power complexity and the method of integrating the 81 cm (32 in) HGA. The weight is crucial for a Thor/Delta mission and, combined with the science and operations factors, results in one more factor to favor the spin axis perpendicular to ecliptic for the baseline. The weight trade is also significant for the Atlas/Centaur mission particularly for the 1978 type II orbiter mission. Note that accommodation of an occultation experiment, with an elevation excursion of  $\pm 20$  deg would probably require reorientation of the spacecraft for configuration B. The antenna positioning aspects are major complications to configuration B but only minor extensions of configuration A (when using an MDA).

The largest cost element in the trade is the despun system consisting of the bearing and transfer assembly (BAPTA) and the associated despun electronics which is estimated at \$1.5 M in configuration A. The cost of added solar panel, structure and thermal design complexity of configuration B is estimated to be within \$300 to 400 K of the above cost of the despun system.

Spin axis perpendicular to the ecliptic is selected for the orbiter baseline because of:

- 1) Improved science instrument pointing and coverage over mission life

TABLE 3-3. ORBITER SPACECRAFT MECHANIZATION/SYSTEM  
DESIGN COMPARISONS

Affected Area	Change From Spin Axis Perpendicular to Elliptic to Spin Axis Directed to Earth	
	Pro	Con
Power subsystem		<ul style="list-style-type: none"> <li>• Add solar cells front and back</li> </ul>
Thermal control subsystem		<ul style="list-style-type: none"> <li>• Increased louver areas; possible need for heat pipes</li> </ul>
Attitude control subsystem	<ul style="list-style-type: none"> <li>• Conscan earth reference (additional attitude reference)</li> </ul>	<ul style="list-style-type: none"> <li>• Greater propellant requirement +2.7 kg (+6 lb) for transit +11 to 18 kg (+25 to 40 lb) if reorient for science in orbit</li> </ul>
Spacecraft structure subsystem		<ul style="list-style-type: none"> <li>• 16 kg (+35 lb)</li> </ul>
Adapter		<ul style="list-style-type: none"> <li>• 13 kg (+26 lb)</li> </ul>
Communication subsystem	<ul style="list-style-type: none"> <li>• Delete bearing and power transfer assembly and despin electronics</li> </ul>	
Science		<ul style="list-style-type: none"> <li>• Reduced coverage if not allowed to reorient</li> </ul>
Mission operations		<ul style="list-style-type: none"> <li>• Break rf downlink if reorient for science every orbit</li> </ul>
Overall mass change		<ul style="list-style-type: none"> <li>• 43 kg (+95 lb) (not including fuel for reorientation)</li> </ul>

- 2) Simpler power and thermal design
- 3) Lower weight

Spin axis perpendicular to ecliptic is used on the probe bus spacecraft in cruise phase for commonality with the orbiter spacecraft. Off-normal angles occur only transiently for trajectory correction, probe release maneuvers, and during bus entry.

#### High Gain Antenna Approaches for the Orbiter

The orbiter spacecraft requires a high gain antenna for data transmission in Venus orbit. The trade consideration between mechanically despun antenna (MDA) or electrically despun antenna (EDA) approaches has been evaluated in Volumes 3 and 7. The impact on spacecraft configuration and weight will be reviewed herein. The principal trades were made for the midterm Thor/Delta design, but the conclusions apply generally to the Atlas/Centaur version.

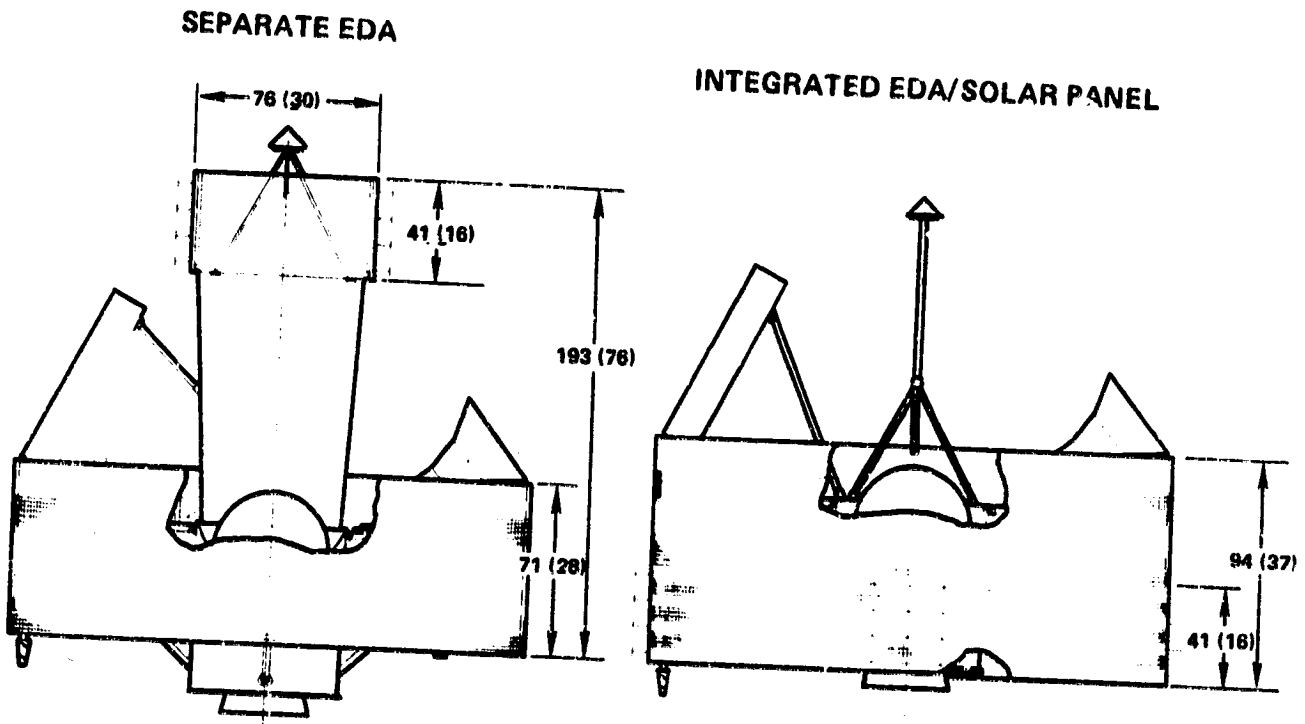
A comparison for the various antenna approaches, based on significant performance parameters and relative weights, is shown in Table 3-4 for the Thor/Delta design. The common performance parameter used was to design each system to essentially the same ERP.

The MDA candidate configuration designed for spin axis perpendicular to the ecliptic is described in subsection 3.4. The MDA is a focal point fed, 82.5 cm (32.5 in) diameter, 23.5 dBi gain, parabolic reflector antenna. Two configurations using alternate EDA approaches are shown in Figure 3-3. The EDA preliminary designs are taken from a Texas Instrument Study. The separate EDA design is similar to the TI nominal. The integrated EDA is built into an extension of the solar panel.

Also shown in Table 3-4 is a summary of parameters obtained from ARC for a Philco-Ford SMS antenna adapted for Pioneer Venus. The weight trade shows the MDA baseline and separable EDA design as comparable. The integrated EDA solar panel design appears to offer no real advantages and complicates somewhat the commonality of the solar cell array cylinder with the probe bus. The weight penalty of the SMS design is prohibitive for the Thor/Delta mission and is significant for the Atlas/Centaur type II 1978 orbiter mission.

A summary of other selection factors is listed in Table 3-5. The despin system consisting of the bearing and power transfer assembly (BAPTA) and the despin control electronics (DCE) has been used on many Hughes flight spacecraft with a mission lifetime up to 7 years. The MDA approach, therefore, represents flight-proven technology. It is estimated that the cost of development of an EDA would equal or exceed cost of providing the MDA system. The MDA also will accommodate, relatively easily, radio science capability such as two dimensional steering or dual-frequency occultation. Based on the factors presented, the MDA has been selected in the orbiter configuration baseline.

30163-335(U)



DIMENSIONS IN CENTIMETERS AND (INCHES)

FIGURE 3-3. EDA CONFIGURATIONS

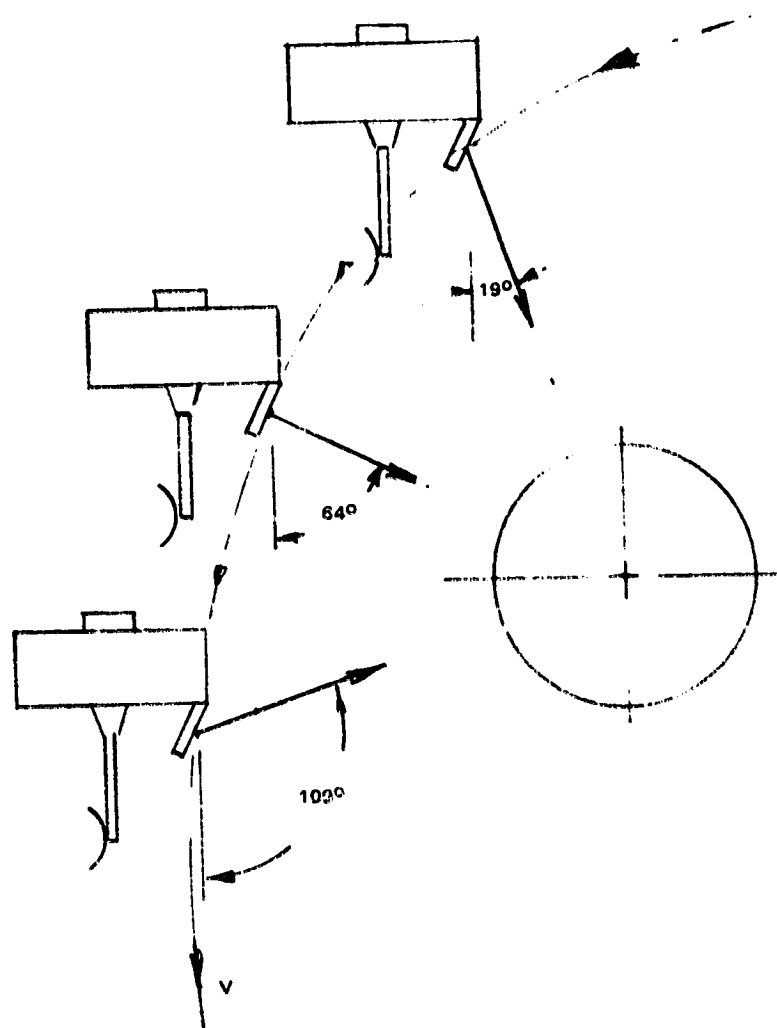
REPRODUCIBILITY OF THE ORIGINAL PAGE IS POOR.

TABLE 3-4. MDA/EDA COMPARISONS AND MASS TRADE

	MDA	EDA (II)		EDA (SMS)
		Separate	Integrated	
<b>Antenna Parameters</b>				
Size, cm (in.)	82.6 (32.5) dia.	76.2 (30) dia. x 40.6 (16) high	213.4 (84) dia. x 40.6 (16) high	76.2 (30) dia. x 48.1 (19) high
Bear-width - 3 dB, deg	11.0	13 x 16	6 x 16	
Gain, dBi	23.5	21.0 <sup>1</sup>	24.5	16.15
<b>Transmitter Parameters</b>				
RF power, W	5.0	10.0 <sup>1</sup>	5.0	20.0
DC power, W	25.2	31.8	15.9	103.4
Effective Radiated Power, dBm	60.5	61.0	61.5	59.15
<b>Mass Summary, kg (lb)</b>				
Antenna	0.8 ( 1.7)	4.0 ( 8.9)	3.6 ( 8.0) <sup>5</sup>	4.6 (10.1)
Coax	0.3 ( 0.6)	0.7 ( 1.6)	1.9 ( 4.2)	1.6 ( 3.5)
Support	1.0 ( 2.2)	2.5 ( 5.5)	2.8 ( 6.1) <sup>9</sup>	2.5 ( 5.5)
Feed	0.2 ( 0.4)	-	-	-
Feed support	0.2 ( 0.4)	-	-	-
Circulator, switch, filter	0.7 ( 1.5)	-	-	-
DCE <sup>2</sup>	3.4 ( 7.4)	0.9 ( 2.0)	0.9 ( 2.0)	3.0 ( 6.6) <sup>3</sup>
Logic cabling	-	0.8 ( 1.7)	1.5 ( 3.4)	0.7 ( 1.5)
Power amplifier, HGA	0.5 ( 1.0)	1.8 ( 4.0) (32 x 2 oz)	2.7 ( 6.0) (48 x 2 oz)	2.9 ( 4.3)
Power amplifier, omni <sup>4</sup>	0.5 ( 1.1)	1.0 ( 2.1)	1.0 ( 2.1)	-
BAPTA <sup>5</sup>	5.1 (11.2)	-	-	-
BAPTA support	0.8 ( 1.8)	-	-	-
Omni antennas <sup>6</sup>	0.6 ( 1.3)	1.3 ( 2.8)	0.7 ( 1.5)	0.7 ( 1.6)
Solar panel (relative) <sup>7</sup>	-	0.4 ( 0.9)	-0.7 (-1.5)	5.4 (11.9)
Total Relative Mass, kg (lb)	13.9 (30.6)	13.4 (29.5)	14.4 (31.8)	20.4 (45.0)

- NOTES: 1. Eight modules active, change from II baseline  
 2. DCE - despun control electronics. All cases use redundant DCE, change from II baseline  
 3. 0.9 kg (2.0 lb) DCE (optimistic estimate), 2.1 kg (4.6 lb) switches  
 4. Additional power amplifier to provide a total of 10 rf W to omnis for nonstandard attitudes  
 5. BAPTA - bearing and power transfer assembly. Includes rotary joint.  
 6. Omni weights include masts.  
 7. 0.068 kg (0.15 lb)/de W including substrate  
 8. Structure included in support. Includes dipoles and manifolds  
 9. Additional substrate and axial jet support

REPRODUCIBILITY OF THE ORIGINAL PAGE IS POOR



30:43-336(U)

FIGURE 3-4. RADAR ALTIMETER 1000 KM AND LOWER ORBIT ALTITUDE LINE OF SIGHT

TABLE 3-5. SUMMARY OF OTHER MDA/EDA SELECTION FACTORS

Consideration	Hughes Baseline MDA	TI EDA
Technological maturity	Flight proven Hughes technology	Predevelopment status
Reliability	Good. Possible single point failure with BAPTA	Good. Graceful degradation with distributed amplifier module failures
Magnetic cleanliness	Motor requires compensation	Good
Radio science accommodation	Easy dual-frequency and two dimensional steering modifications	Difficult. Beamforming phasing must be compensated
Growth capability	Good. Lumped amplifier design allows easy growth	Limited without complete system redesign

Radar Altimeter Integration and Orbiter Periapsis Latitude

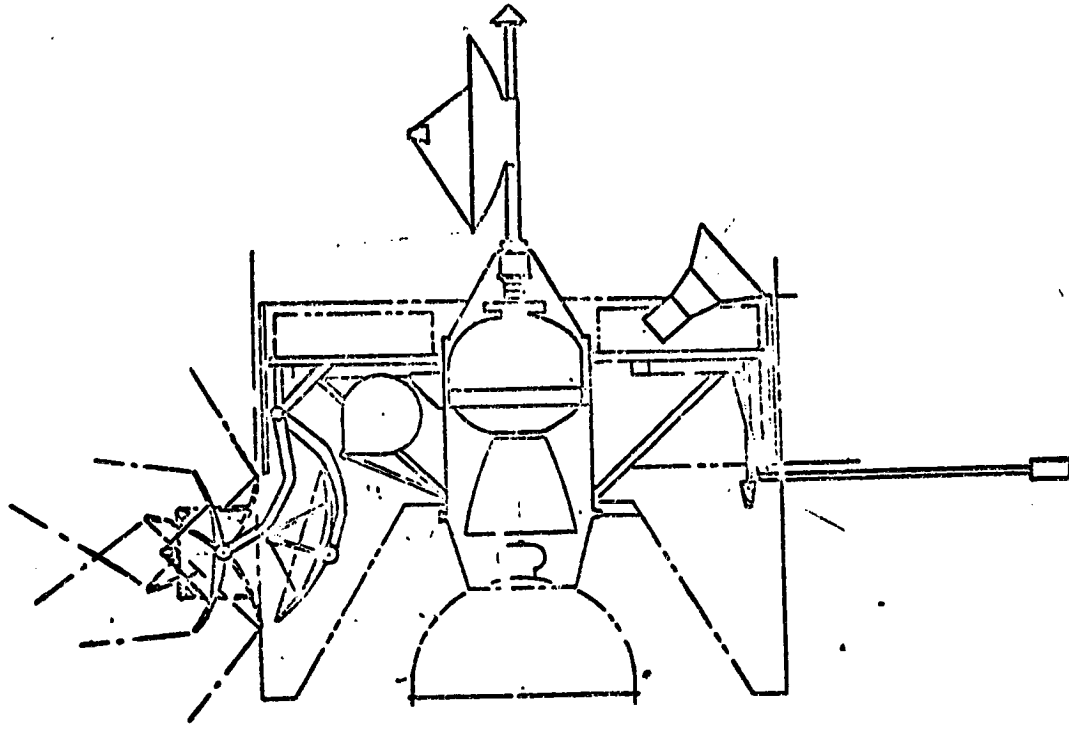
The possible periapsis latitudes for the Thor/Delta mission are:

- Type I transit trajectory: 4° to 13° N latitude; 81° to 90° S latitude
- Type II transit trajectory: 21° to 31° N latitude; 45° to 55° S latitude

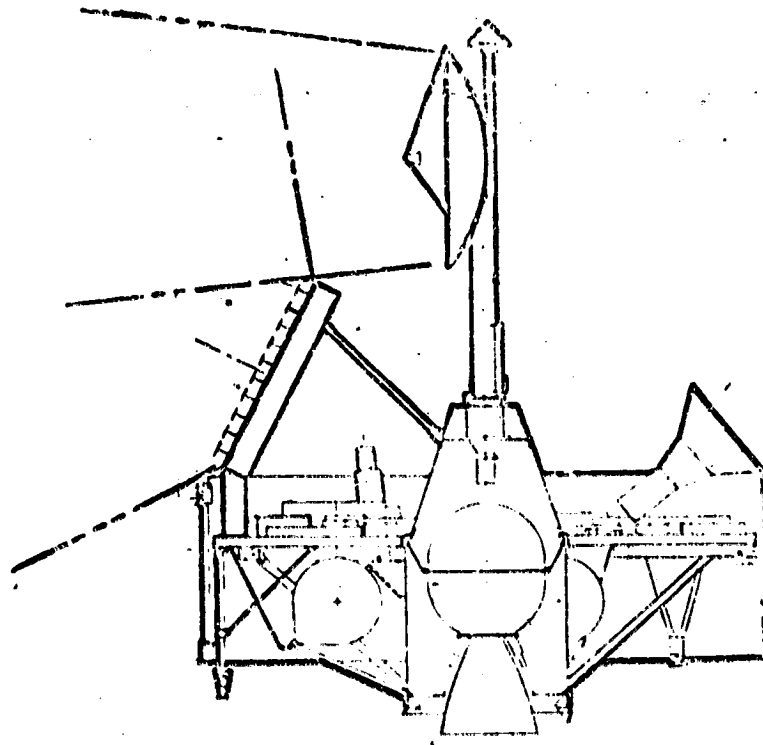
The selection of the periapsis latitude and the spacecraft spin axis orientation defines required pointing angles for the radar antenna relative to the spacecraft. These angles along with the antenna beam field of view combine to place restrictions on the science instrument location on the spacecraft.

The altimeter experiment objective is to measure surface height variation, reflectivity and roughness at an orbit altitude range of 1000 km and lower. For a 26° N latitude periapsis this corresponds approximately to a line of sight from the spacecraft spin axis from 19 to 109 deg as periapsis is approached and then passed (see Figure 3-4). The altimeter rf beam must be steered in elevation + 45 deg from the nominal pointing angle in order to maintain a line of sight in the orbit plane, normal to the planet surface. By mounting the antenna on the spinning section of the spacecraft,





a) MECHANICALLY STEERED



b) ELECTRONICALLY STEERED

FIGURE 3-5. RADAR ANTENNA

the planet will be scanned in azimuth once per spacecraft revolution, permitting the planet subspacecraft surface to be mapped.

Two methods of implementing the elevation scan were given by NASA/ARC. One uses a focal point fed elliptical paraboloid for the antenna and elevation steering is provided by a mechanically driven single axis gimbal. The other option is a planar array with electronic beam steering in the elevation plane.

The mechanically steered antenna must be positioned on the spacecraft to not only provide for an unobstructed rf beam but also assure the volume swept by the reflector during scan is clear. In addition, the mass movement of the antenna during scanning must be considered in the spacecraft dynamics. However, the electronically-steered radar antenna only requires the rf beam field to be kept clear, and since no mass is moved during the operation, it has no affect on spacecraft dynamics. The electronic scan planar array was assumed for baseline on the basis of least complexity of integration and dynamic affects to the spacecraft.

Figure 3-5 depicts an aft installation for a mechanically steered version of the radar antenna, with pointing angles for a near equatorial periapsis orbit. Also shown in Figure 3-5 is the forward installation of an electronically steered planar array type with pointing angles for higher latitude periapsis.

The spacecraft orientation in orbit is such that the forward end is in the direction of velocity at periapsis to accommodate other science experiment pointing requirements. Hence, the radar antenna line of sight initially desires to be offset from the spin axis in a forward direction. The planar array can be located on either the aft or forward end of the spacecraft. Antenna installation on the aft end of the spacecraft would need a deployment scheme to place the antenna outside the solar panel periphery to maintain an interference free field of view in the elevation plane for all but near equatorial latitudes. The required extension gets greater with increase of latitude increasing dynamic balance problems. Another area of concern for aft installation is insertion motor plume heating, necessitating thermal protection.

Installing the antenna at the forward end of the spacecraft will permit latitudes above 4 deg to be accommodated without requiring deployable schemes and eliminates potential plume impingement problems. In addition, the dynamic balance problem is minimized because the antenna is nearer the spacecraft center of gravity. However, this location does require a higher mast for the S-band HGA (see Figure 3-5b). The maximum mast length increase is associated with type I near equatorial latitudes and is estimated to be approximately 45.7 cm (18 in). The higher latitudes require less mast height.

On the Thor/Delta baseline, the radar antenna is installed on the forward end of the spacecraft, eliminating deployment mechanisms, plume heating protection, and reducing counterbalancing which minimize weight and complexity. An additional benefit from the forward installation is realized if

REPRODUCIBILITY OF THE ORIGINAL PAGE IS POOR.

30163-338(U)

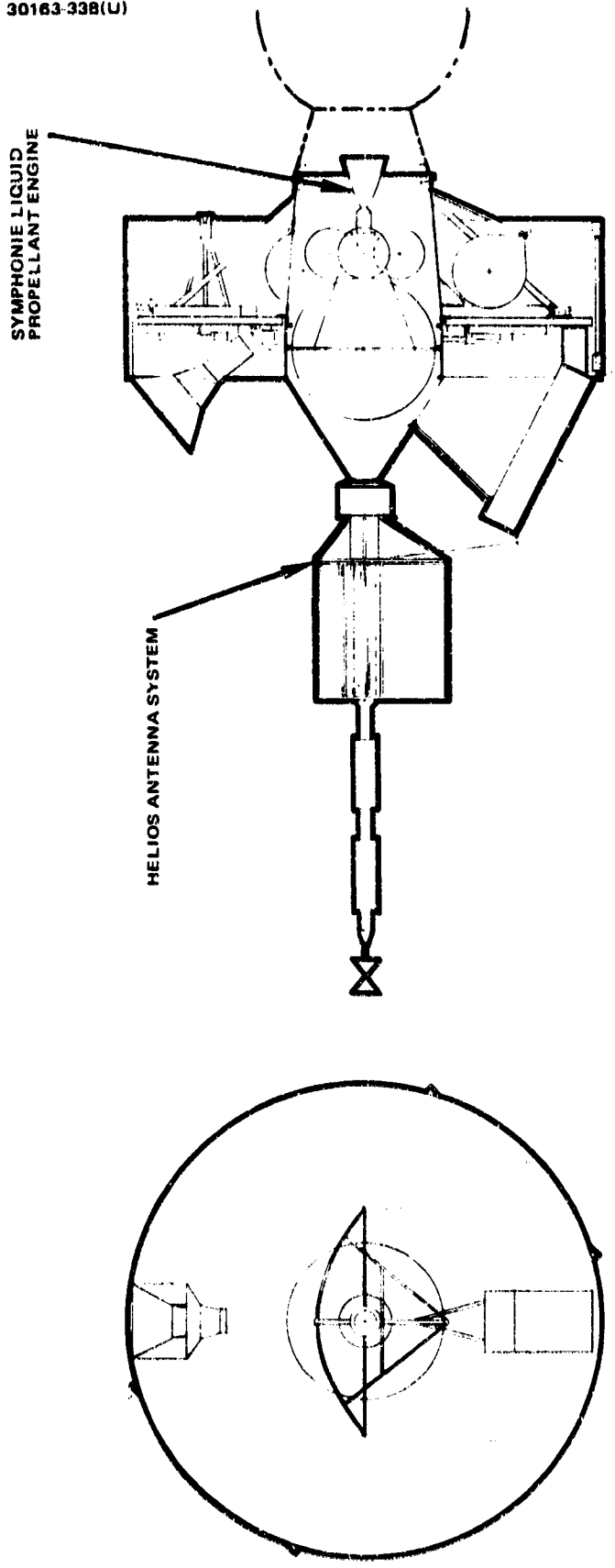


FIGURE 3-6. ORBITER WITH LIQUID ORBIT INSERTION

it becomes desirable to change the transit trajectory from type II - 26° N periapsis latitude to the southern range of latitudes or to type I near equatorial latitudes since this change in latitude can be accommodated by the antenna with no difficulty. For southern periapsis latitude, the spacecraft orientation is inverted and, in orbit, the HGA, radar altimeter and star sensor would be toward the northern hemisphere. For latitudes higher than the baseline selection, the HGA mast can either be reduced in overall height or left unchanged, and for latitudes below 26 deg, a slight increase in mast height and weight is necessary to maintain an unobstructed field of view between the HGA and the radar altimeter.

### Liquid Versus Solid Propellant for Orbit Insertion

A major subsystem selection influencing orbiter configuration is the type of orbit insertion motor - solid or liquid. Monopropellant systems have too low a specific impulse for this application (see Volume 10). An existing bipropellant system was reviewed (also with regard to International Cooperation approaches, Volume 13) for application to the Thor/Delta baseline. Figure 3-6 shows a slightly modified, 400 N (90 lbf) thrust, biliquid system developed by Messerschmitt-Boelco-Blohm (MBB) for the Symphonic satellite.

The existing propellant tank has a usable capacity of 148 kg (326 lb), more than adequate for type I and II Thor/Delta missions and for some Atlas/Centaur missions. The principal modification is relocation of the helium tanks to fit within the orbiter thrust tube which has been tapered slightly to accept main tank.

The dry mass of the biliquid system was estimated at about 19 kg (42 lb) versus about 10 kg (22 lb) for the modified (shortened) TEM-521 solid motor (Thor/Delta baseline). The higher specific impulse of the biliquid (300 to 305 sec versus 286 sec for the solid) would allow about 3.6 kg (8 lb) increase in dry mass in orbit which combined with the difference in inert motor mass still produces an in-orbit penalty of about 5 to 6 kg (11 to 13 lb) for the liquid design. The liquid system offers some potential possible advantages in mission flexibility. However, with adequate lead time provisions, the solid motors can be modified/sized to accommodate a range of acceptable mission opportunities (see Volume 10). The program cost increase in using the biliquid system is estimated to be in excess of \$1.0M.

In view of the cost and weight factors, the solid motor has been selected for the orbiter baseline. The thrust tube has been sized to accommodate the solid motors applicable to type I or type II missions for Thor/Delta or Atlas/Centaur.

### Magnetometer Integration

The midterm baseline instrument payloads for both probe bus and orbiter spacecraft included a magnetometer experiment. The instrument

TABLE 3-6. MAGNETOMETER INTEGRATION CONSIDERATIONS

Spacecraft Location	Pro		Con	
	Probe Bus	Orbiter	Probe Bus	Orbiter
(A) Forward Plane	<ul style="list-style-type: none"> <li>• Easiest to dynamic balance spacecraft</li> <li>• Larger off normal sun line angle before shadowing solar panel</li> <li>• Simple stowage and deployment mechanization</li> <li>• Minimal structural support mass</li> <li>• RF beam clearance</li> <li>• Minimal structural support mass</li> <li>• Good rf beam clearance</li> <li>• Less restriction on experiment and sensors with radial line of sight</li> <li>• Good clearance for small probe separation</li> <li>• Least restriction on experiment locations for unobstructed field of view</li> <li>• Best clearance for small probe separation</li> </ul>	<ul style="list-style-type: none"> <li>• Same</li> <li>• Same</li> <li>• Same</li> <li>• Same</li> <li>• Same</li> <li>• Same</li> <li>• Same</li> <li>• Same</li> <li>• Same</li> </ul>	<ul style="list-style-type: none"> <li>• Experiments and sensors with radial line of sight must be positioned away from boom</li> <li>• Must be positioned near small probe to insure maximum separation clearance</li> </ul>	<ul style="list-style-type: none"> <li>• Same</li> </ul>
(B) Mid Plane	<ul style="list-style-type: none"> <li>• Good clearance for small probe separation</li> </ul>	<ul style="list-style-type: none"> <li>• Same</li> </ul>	<ul style="list-style-type: none"> <li>• Unacceptable solar panel shadowing</li> <li>• Stowage difficult</li> </ul>	<ul style="list-style-type: none"> <li>• Same</li> <li>• Same</li> </ul>
(C) Aft Plane	<ul style="list-style-type: none"> <li>• Best clearance for small probe separation</li> </ul>	<ul style="list-style-type: none"> <li>• Same</li> </ul>	<ul style="list-style-type: none"> <li>• Most difficult to dynamic balance spacecraft</li> <li>• Extensive support structure</li> <li>• Small off normal sun angle shadows solar panel</li> <li>• Bicone antenna beam interference</li> </ul>	<ul style="list-style-type: none"> <li>• Same</li> <li>• Same</li> <li>• Possible plume impingement problem</li> </ul>

will be used to measure interplanetary magnetic fields in addition to those fields at Venus. Therefore, it will be operative throughout the mission starting with separation of the spacecraft from the launch vehicle.

The sensitivity of the sensor dictates that it be remotely located from the spacecraft to minimize the magnetic influences of the spacecraft. The Thor/Delta magnetometer is deployed 107 cm (42 in) from any surface, in a plane perpendicular to the spacecraft spin axis (Volume 2, Task No. EX-15). The spacecraft induced magnetic field with the magnetometer on the 107 cm boom is 17  $\gamma$  (magnetized) and 2.5  $\gamma$  (demagnetized). These levels of magnetic field require magnetic cleanliness controls on design, parts and materials with an estimated total program cost of about \$1.4 M.

The launch vehicle payload envelope precludes a magnetometer fixed radial placement of 107 cm; therefore, it is necessary to consider the use of a boom installation. The boom will be stowed during the launch sequence and deployed to the desired position after separation from the launch vehicle. The boom design must have minimum impact on spacecraft balance and the location must not compromise other subsystems.

The 107 cm (42 in) clearance from spacecraft structure is achievable by placement of the magnetometer on a boom extended radially from the spacecraft and in a plane located generally aft, at midpoint, or forward of the solar array structural cylinder. The major considerations for probe bus and orbiter in each of these areas are summarized in Table 3-6. Probe bus magnetometer placement in the plane forward of the structural cylinder must not interfere with small probe release. A small probe separation study indicated a radial boom position adjacent to a probe, on the leading spin side, provides maximum in plane clearance with the probe separation path. For the boom length being considered an adequate clearance will exist.

A boom located in the aft plane presents a more difficult spacecraft dynamic balance problem, as well as structural support weight penalties and solar panel shadowing (sun angles  $> 2$  deg) for both the orbiter and bus spacecraft. The orbiter insertion motor plume heating and impingement effects on the magnetometer may require additional thermal protection aggravating the dynamic balance and increasing the weight penalty for the orbiter.

As noted in Table 3-6, the midplane is approximately equal to the forward plane location except for solar panel shadowing by the boom and magnetometer, at all sun angles, which makes this an unacceptable approach.

The forward plane installation design (see Volume 9) weighs 1.36 kg (3.0 lb) including deployment mechanism and boom, plus 0.54 kg (1.2 lb) for the magnetometer sensor.

The spacecraft must be balanced in the mission operational configuration so that the spin axis and the spacecraft centerline are coincident. This is to ensure proper separation of the four probes from the probe bus and prevent misalignment of experiment pointing angles due to spacecraft wobble.

When the boom is in the stowed position the orbiter spacecraft center of mass (c. m. ) shifts laterally  $\approx 5.3$  mm (0.21 in. ) and the principal axis tilt of  $\approx 0.011$  rad (0.62 deg) occurs. These values are in excess of the Thor/Delta launch vehicle requirement noted in System Design Specification No. 2-17502, Appendix C. A Thor/Delta spacecraft launch configuration c. m. offset from its centerline is required to be no greater than 0.38 mm (0.015 in. ) and the principal axis of inertia tilt not greater than 0.002 rad (0.1 deg). It is noted that the August 1972 revision of the Delta Spacecraft Design Restraints Manual DAC-61687 allows c. m. offset of 0.13 cm (0.05 in. ) and spin axis tilt of 0.020 rad (1.4 deg). The Atlas/Centaur launch vehicle does not have requirements of this nature.

The direct approach to solve the axis tilt and c. m. shift problem is to stow and deploy a dummy magnetometer on a boom diametrically opposite of the magnetometer. The weight increase is a severe penalty for the Thor/Delta spacecraft.

Some reduction in the c. m. offset may be realized by selectively locating the 8.4 kg (18.5 lb) telemetry kit that is attached to the spacecraft adapter.

The use of a longer boom was investigated to reduce cost of a magnetic control program. The Thor/Delta spacecraft boom length was increased to 3.05 m (10.0 ft). A counterbalance boom is required to satisfy the balance requirement for the Thor/Delta launch vehicle as demonstrated in Table 3-7. The net total program savings (reduced magnetic cleanliness versus added boom cost) is approximately \$700 K.

The increased mass of  $\approx 5.6$  kg (12.4 lb) necessary for the 3.05 m magnetometer and balance boom system was highly undesirable in view of the small mass contingency. Therefore, the shorter 107 cm, and lighter mass boom was chosen as baseline for the Thor/Delta configurations.

TABLE 3-7. EXTENDED MAGNETOMETER  
BOOM DATA (3.05 m BOOM LENGTH)

Magnetometer, boom, harness, mechanism	= 4.15 kg (9.15 lb)
c. m. offset, stowed	= 9.4 mm (0.37 in. )
c. m. offset, deployed	= 52.32 mm (2.06 in. )
Spin axis tilt, stowed	= 1.05 deg
Spin axis tilt, deployed	= 2.26 deg
Counterbalance boom and balance weight	= 3.37 kg

Note: Offset and tilt are for the addition of the magnetometer boom assembly only, on a spacecraft that was initially dynamically balanced.

The location required in the spacecraft forward plane to provide small probe separation clearance can also be accommodated on the orbiter spacecraft without penalty, hence, commonality of boom location on the two spacecraft is achievable. Therefore, the integration of the magnetometer at the forward end of the probe bus and orbiter spacecraft was selected for the Thor/Delta baseline configuration. A longer boom can be accommodated on the Atlas/Centaur design because the imbalance of the stowed boom can be tolerated on the launch vehicle and also because of higher allowable spacecraft weights.

### Equipment Shelf Configuration Trade

One of the basic NASA requirements of the Pioneer Venus spacecraft is that they are spin stabilized. This demands a spin to transverse mass ratio greater than unity to achieve stability. Such ratios are a natural consequence of disc like physical arrangements with the mass distribution out near the perimeter. For this reason a subsystem single level arrangement (open equipment shelf) facilitates mass distribution toward the perimeter, and as such is a candidate approach to configure the spacecraft equipment.

NASA/Hughes OSO-III scientific spacecraft program uses an arrangement philosophy of dedicated compartments for each instrument providing subsystem isolation. The compartmentalized and open shelf arrangement approaches were evaluated to determine the best for the Pioneer Venus spacecraft. Figure 3-7 schematically depicts an arrangement for both methods and lists some considerations for each.

The study conclusion is that a compartment approach constrains mass and thermal balance by restricting the location of units, requires additional structure to form the compartments, creates a more complex wire harness and restricts accessibility to the subsystem units. All of these considerations are readily met by the open shelf approach. Hence, the baseline is an open shelf maintaining subsystem and payload location commonality between the probe bus and orbiter. Also, the open shelf arrangement allows the underside of the shelf to be used if necessary.

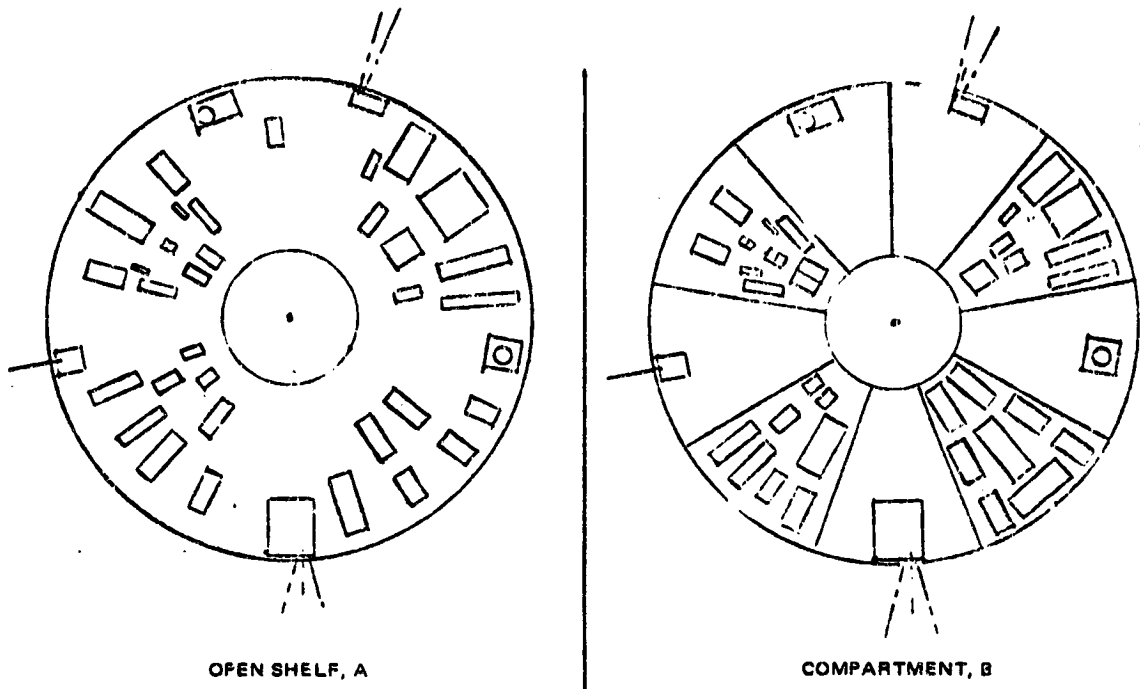
### Spacecraft Launch Mass and Contingency

A very significant trade issue for Pioneer Venus is spacecraft mass and contingency allowance especially for the Thor/Delta. In fact, rather costly weight reductions were required in the midterm design to attain even a marginal contingency.

A weight comparison summary is shown in Table 3-8 for probe and orbiter spacecraft midterm baselines for Thor/Delta and Atlas/Centaur. The liquid propellant and orbit insertion expendables were determined for the full weight of the spacecraft including contingency. The trajectory types and contingencies at the midterm briefing are summarized in Table 3-9. From this summary, it is apparent that approximately 7 percent contingency for Thor/Delta mission is marginal, but the Atlas/Centaur contingency is good.



30163-339(U)



OPEN SHELF, A

COMPARTMENT, B

**ADVANTAGES**

- LESS RESTRICTIVE IN EQUIPMENT ARRANGEMENT
- MASS BALANCE EASIER TO ACHIEVE
- THERMAL DISTRIBUTION EASIER TO ACHIEVE
- LIGHTER WEIGHT STRUCTURE

- DEDICATED AREA FOR SCIENCE
- ISOLATION FROM OTHER SUBSYSTEM EFFECTS EASIER TO ACCOMPLISH

**DISADVANTAGES**

- DIFFICULT TO ISOLATE SCIENCE INSTRUMENTS FROM THERMAL AND MAGNETIC EFFECTS

- LESS EFFICIENT USE OF SPACE
- LESS FREEDOM FOR ADJUSTMENT FOR MASS BALANCE
- LESS FREEDOM FOR ADJUSTMENT FOR THERMAL BALANCE
- HEAVIER STRUCTURE DUE TO VERTICAL WALLS
- FUNCTIONAL ARRANGEMENT OF SUBSYSTEMS MORE RESTRICTED

FIGURE 3-7. OPEN EQUIPMENT SHELF VERSUS COMPARTMENTALIZATION

TABLE 3-8. MASS COMPARISON - THOR/DELTA VERSUS ATLAS/CENTAUR MIDTERM BASELINES

Item/Subsystem	Probe Spacecraft				Orbiter Spacecraft			
	Thor/Delta		Atlas-Centaur		Thor/Delta		Atlas-Centaur	
	kg	lb	kg	lb	kg	lb	kg	lb
RF	8.8	19.5	10.0	22.1	8.5	18.8	9.7	21.4
Antenna	3.1	6.8	3.4	7.4	2.5	5.6	3.5	7.6
Data Handling	5.8	12.8	7.7	17.0	9.9	21.8	13.2	29.0
Command	7.0	15.5	12.3	27.2	6.6	14.5	11.0	24.2
Attitude control, mechanisms	11.2	24.6	14.7	32.3	18.1	40.0	26.6	58.6
Structure	36.5	80.4	96.4	212.5	32.5	71.7	83.3	183.7
Power	16.0	35.3	27.2	60.0	22.4	49.4	29.1	64.1
Harness	4.7	10.3	9.1	20.0	6.8	14.9	13.6	30.0
Thermal control	10.3	22.5	19.0	41.9	11.3	24.9	20.9	46.0
Propulsion (dry)	9.1	20.0	10.4	22.9	9.8	21.7	11.2	24.6
Orbit insertion motor case								
Bus total	112.4	247.8	210.2	463.3	138.6	305.6	248.7	548.3
Large probe	114.6	252.6	198.7	438.0				
Small probe (3)	101.9	224.7	169.1	372.9				
Spacecraft subtotal	328.9	425.1	578.0	1274.2	138.6	305.6	248.7	548.3
Contingency	22.8	50.3	140.0	308.7	10.0	22.1	91.4	201.5
Experiments (bus only)	11.6	25.6	12.6	27.7	31.1	68.6	35.0	77.2
Spacecraft total (dry)	363.3	801.0	730.6	1610.6	179.8	396.3	375.1	827.0
Propellant	20.7	45.7	17.7	39.0	24.3	53.6	29.0	64.0
Pressurant	0.0	0.1	0.2	0.4	0.0	0.1	0.5	1.0
Orbit insertion expendables								
Spacecraft total (wet)	384.1	846.8	748.4	1650.0	292.8	645.6	733.0	1616.0
Spacecraft adapter	13.2	29.0	31.3	69.0	13.2	29.0	31.3	69.0
Telemetry and C band	8.4	18.5			8.4	18.5		
Launch vehicle payload	405.7	894.3	779.7	1719.0	314.4	693.1	764.3	1685.0

To achieve the Thor/Delta launch contingency of Tables 3-8 and 3-9, certain weight reductions were implemented as shown in Table 3-10. These reductions involved the use of beryllium in spacecraft structure (subsection 4.2) in the bearing and power transfer assembly (BAPTA) (Volume 9), and in the deceleration module structure (Volume 5). It also required the use of additional large scale integrated circuits (LSI) in both the spacecraft and probe data handling and command subsystems (Volume 8) and use of light-weight (28 gauge) wire in spacecraft (Section 6) and probe (Volume 5) cabling. The change in parachute and jettison altitude in Table 3-10 results in reduction in battery and insulation weight permitted by a more rapid pressure vessel descent.

The cost impact of the Thor/Delta major weight reduction is estimated at about \$1.5 M for use of beryllium (highest for the aeroshells) and additional \$1.3 M for 14 new LSI development and a risk allowance for potential problems in probe packaging caused by the low contingency. The total cost savings potential afforded by using the Atlas/Centaur allowance and approach is discussed in Volume 11.

Possible weight reductions in redundancy for Thor/Delta are listed in Table 3-11, but were not implemented because spacecraft reliability was excessively reduced. Other weight trades involving reduction of science payload or experiment objectives, particularly for the probe mission, are discussed in Volumes 2, 3 and 5.

A brief summary of the trade study results follows:

- Thor/Delta missions have a marginal weight contingency
- Cost increases have already been imposed on the Thor/Delta mission designs in order to attain an even marginal contingency
- Atlas/Centaur launch contingency is considerably higher than for Thor/Delta and would minimize weight and cost risk and potential compromises in experiment weight and science performance objectives

TABLE 3.9. MISSION SET/MASS CONTINGENCY SUMMARY  
(AT MIDTERM)

Item	Thor/Delta Spacecraft		Atlas/Centaur Spacecraft	
	Probe 1977	Orbiter 1978	Probe 1977	Orbiter 1978
Trajectory type	I	II	I	I
Contingency, kgs (lb)	23 (50)	10 (22)	140 (309)	92 (202)
Percent contingency*	6.5	6.7	20	27

\*Percent of spacecraft dry mass less bus or orbital experiments.

TABLE 3-10. MASS REDUCTIONS IMPLEMENTED (THOR/DELTA)

Item	Mass Reduction, kg (lb)	
	Multiprobe Mission	Orbiter
Use beryllium in spacecraft structure	4.8 ( 10.6)	2.5 ( 5.5)
Use beryllium in spacecraft BAPTA	—	1.1 ( 2.5)
Use beryllium in large probe aeroshell	13.2 ( 29.0)	—
Use beryllium in small probe aeroshells (3)	8.0 ( 17.7)	—
Add LSI to telemetry processor	1.5 ( 3.2)	1.5 ( 3.2)
Add LSI to central decoder	2.3 ( 5.0)	2.3 ( 5.0)
Add LSI to large probe data unit	1.8 ( 3.9)	—
Add LSI to small probe data unit (3)	3.8 ( 8.4)	—
Use 28 gage wire in spacecraft cabling	2.2 ( 4.9)	3.1 ( 6.9)
Use 28 gage wire in probes	0.8 ( 1.7)	—
Delete redundant remote multiplexers	1.4 ( 3.0)	1.4 ( 3.0)
Delete one propulsion tank	1.5 ( 3.4)	1.5 ( 3.4)
Change large probe parachute size and raise jettison altitude from 40 to 55 km	11.7 ( 25.7)	—
	<hr/> 52.8 (116.5)	<hr/> 13.4 (29.5)

TABLE 3-11. ADDITIONAL MASS REDUCTION CANDIDATES

Item	Mass Reduction, kg (lb)		Comment
	Multiprobe Mission	Orbiter	
Delete redundancy in command	2.7 ( 5.9)	2.7 ( 5.9)	Reliability 0.978 → 0.862 probe bus
Delete redundancy in data handling	2.0 ( 4.4)	2.0 ( 4.4)	0.918 → 0.605 orbiter
Delete redundancy in attitude control	1.6 ( 3.6)	3.3 ( 7.3)	
Delete one pair radial thrusters	1.5 ( 3.4)	1.5 ( 3.4)	
Raise periapsis altitude from 150 to 200 km	—	3.2 ( 7.0)	
Use 36 h orbit	—	4.1 ( 9.0)	
	<u>7.9 (17.3)</u>	<u>16.8 (37.0)</u>	

### 3.3 THOR/DELTA BASELINE DESCRIPTION

A major objective to configuring the probe and orbiter spacecraft was maximum commonality to reduce program cost, and the following descriptions of the spacecraft configurations highlight this point.

Inboard profiles, forward and aft end views, of the baseline spacecraft configurations for the multiprobe and orbiter missions are presented in Figures 3-8 and 3-9, respectively. Equipment shelf arrangements for each spacecraft, with subsystem elements and experimental locations noted, are depicted in Figures 3-10 and 3-11. A mass summary for major subsystems is presented in Table 3-12 and detailed mass statements in Tables 3-13 through 3-15.

#### Probe Bus

In the launch configuration, the probe bus has a mass of 384.1 kg (846.8 lb) with the center of mass located 107 cm (42.3 in.) above the launch vehicle separation plane. The roll to transverse inertia ratio varies from a minimum value of 1.20 at launch to a maximum of 1.79 after release of all probes. The inertia ratio range assures adequate spin stability. A maximum diameter of 213 cm (84 in.) and an overall length of 180 cm (71 in.) allows for radial and longitudinal clearances from the allowable payload envelope.

The basic arrangement consists of a central thrust tube with a ring sized to mate with the Thor/Delta 2512 spacecraft to launch vehicle adapter; a circular shelf for mounting subsystem equipment positioned at the upper end of the thrust tube; six equally spaced support struts attached at the shelf perimeter and extending radially to the thrust tube lower end, and a cylindrical substrate surrounding the shelf and positioned so as to provide an enclosed volume above and below the shelf. The solar electric array is mounted on the substrate extension at and below the shelf level. The length of the substrate is sized for the larger array required for the orbiter mission and for commonality kept the same for the probe bus.

The hydrazine propellant tanks are located beneath the shelf opposite each other and supported from the thrust tube. This arrangement allows the shelf to be assembled without disturbing the tank installation and keeps the shelf upper surface and volume entirely available for the mounting and positioning of subsystem units and experiments. The basic arrangement is identical for probe and orbiter spacecraft.

An inverted right conical frustum installed at the upper end of the thrust tube provides for support and installation of the large probe. Three attach fittings 120 deg apart provides for the mechanical interface with the probe. The three small probes are positioned symmetrically around the large probe adapter and are supported by structural elements extending radially from the adapter and vertically to the shelf.

The large probe is separated in an axial direction with a small  $\Delta V$  being applied from prestressed springs located at each attach fitting. After

the large probe separates, the three small probes are released simultaneously and the forces from the probe bus spin provide a lateral separation velocity. Since the small probes leave in a lateral direction, they trace a spiral path in spacecraft coordinates, opposite in direction to the spin, over the upper surface of the spacecraft. Therefore, this region is free of protuberances above the forward plane of the substrate. This path is shown for one of the probes on Figure 3-8.

Two of the bus experiments, the ion and neutral mass spectrometers require unobstructed 60 deg conical fields of view in an axial direction, but only after probe release. Therefore, the instruments were located on the spacecraft to assure the proper FOV. Since the Langmuir probe and UV fluorescence experiments deploy appendages radially, they are positioned near the shelf outer edge. The magnetometer is mounted on a pivoted boom to permit stowage during launch. The extended boom position was selected to obtain maximum clearance from the small probe separation paths.

The units are arranged on the shelf in a manner that provides for functional grouping and mass and thermal distribution. Sufficient space exists on the shelf permitting units to be repositioned if necessary to accommodate changes in thermal or mass distribution. Six thermal control louvers are placed on the lower surface of the shelf and radiate out of the aft cavity. Identical shelf locations are maintained for those units and thermal control louvers that are common to both probe and orbiter spacecraft. These features can be seen by comparison of Figures 3-10 and 3-11.

The bicone antenna has 360 deg beam in a plane normal to the spin axis and 30 deg in elevation. In order to place the antenna on the spin axis, it was necessary to store it inside the thrust tube during launch. Since its deployment is axial along the spacecraft centerline, a dynamic unbalance is not incurred.

A medium gain horn antenna, with a 45.7 cm (18.0 in.) diameter aperture and an rf beam width of 20 deg, is attached to the shelf aft side and is pointed parallel with the spacecraft centerline. By locating it near the shelf outer edge, the beam is unobstructed by the bicone antenna. To prevent blockage of the thermal control louver view by the large diameter aperture of the antenna, it is placed near one of the hydrazine tanks.

A narrowbeam angle (140 deg) omni antenna mounted on the forward end of the spacecraft and a widebeam omni antenna (220 deg) attached to the bicone assembly complete the antenna complement.

The star sensor line of sight required is 55 deg from the spin axis on the forward end and has a 25 deg field of view. It is located near the outer perimeter and midway between two of the probes to minimize possible reflections from the spacecraft entering the sun shield. The three sun sensors have a combined field of view of 150 deg in a plane containing the spin axis and is centered about a normal to the axis. Again, to preclude false readings due to reflections, the sensors are located at the periphery of the substrate and at a location free of extensions.

**WALDOUT FRAME**

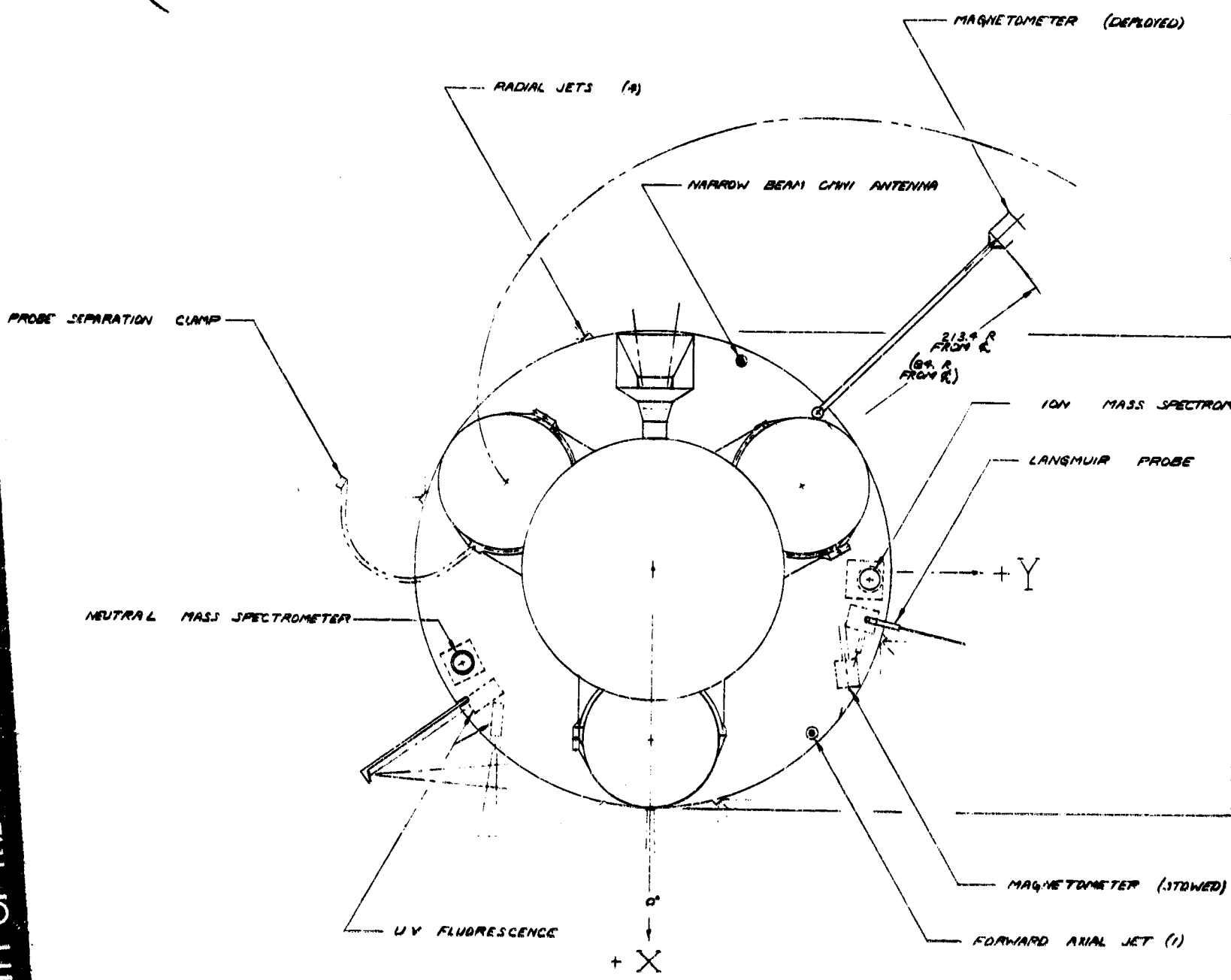


FIGURE 3-8. THOR/DELTA PROBE SPACECRAFT BASELINE DESIGN

REPRODUCIBILITY OF THE ORIGINAL PAGE IS



# FOLDOUT FRAME

2

(DEPLOYED)

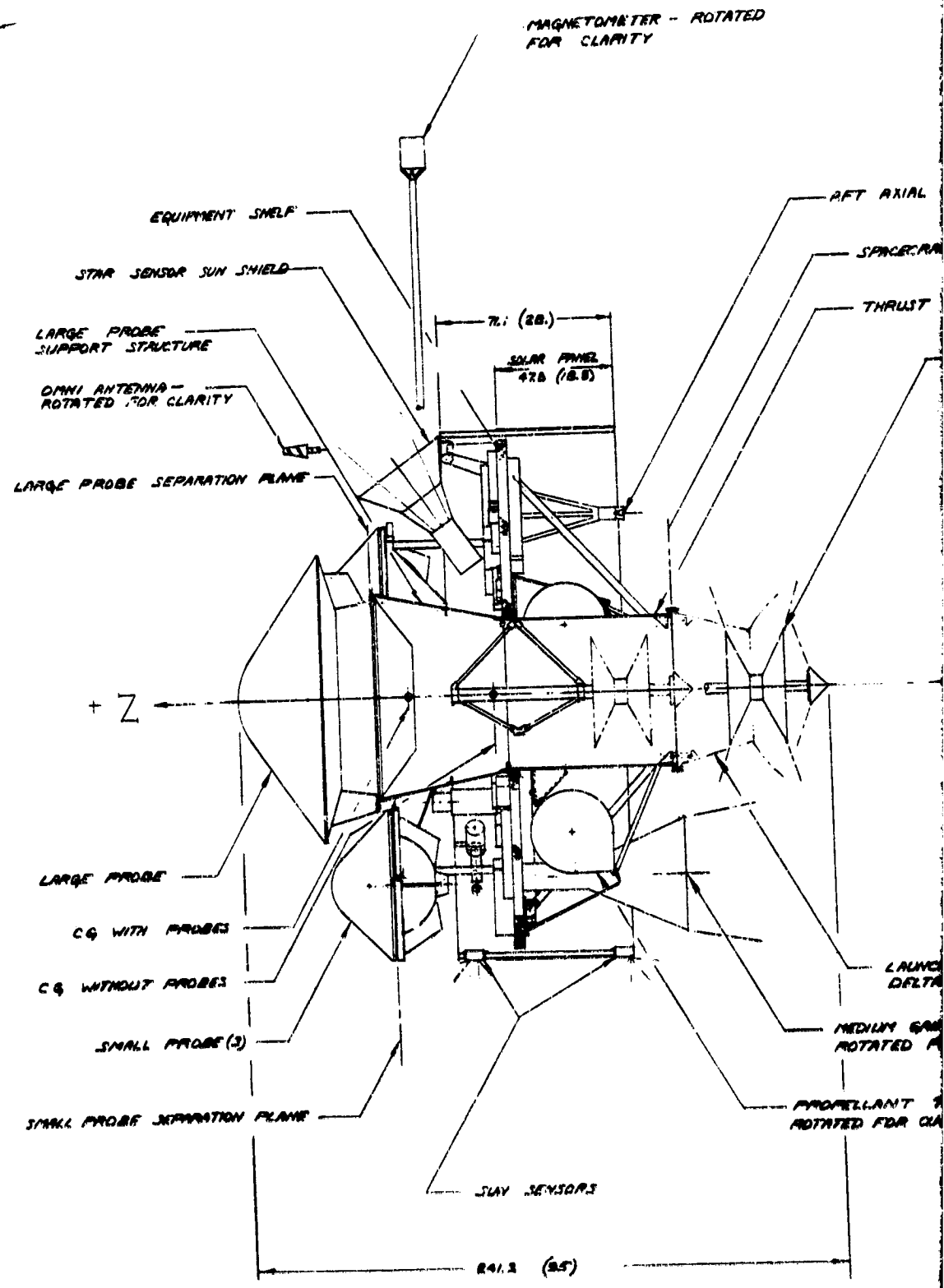
ION MASS SPECTROMETER

LANGMUIR PROBE

213.4 DIA  
(89 DIA)

MAGNETOMETER (STOWED)

AXIAL JET (1)



REPRODUCTION OF THE ORIGINAL PAGE IS FOR

5

30163-340(U)

AXIAL JET (1)

SPACECRAFT SEPARATION PLANE

THRUST TUBE

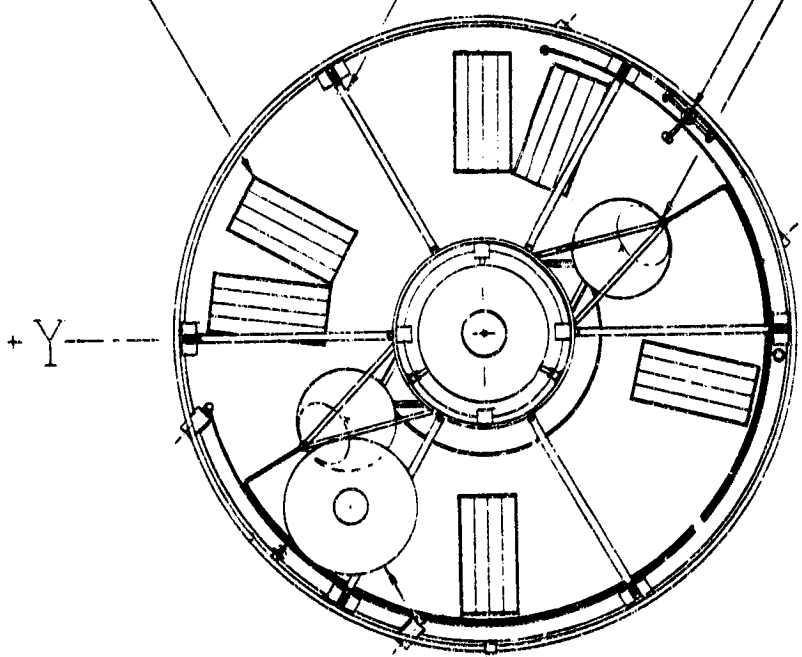
BICOINE WIDE BEAM  
OMNI ANTENNA (DEPLOYED)

LOUVER (6)

SUPPORT STRUT (6)

AFT AXIAL JET (1)

PROPELLANT TANK (2)



REPRODUCTION OF THE ORIGINAL PAGE IS FOR

LAUNCH VEHICLE ADAPTER  
DELTA 2512

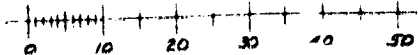
GAIN ANTENNA -  
ED FOR CLARITY

TANK (2) -  
ED FOR CLARITY

MEDIUM GAIN ANTENNA



CENTIMETERS

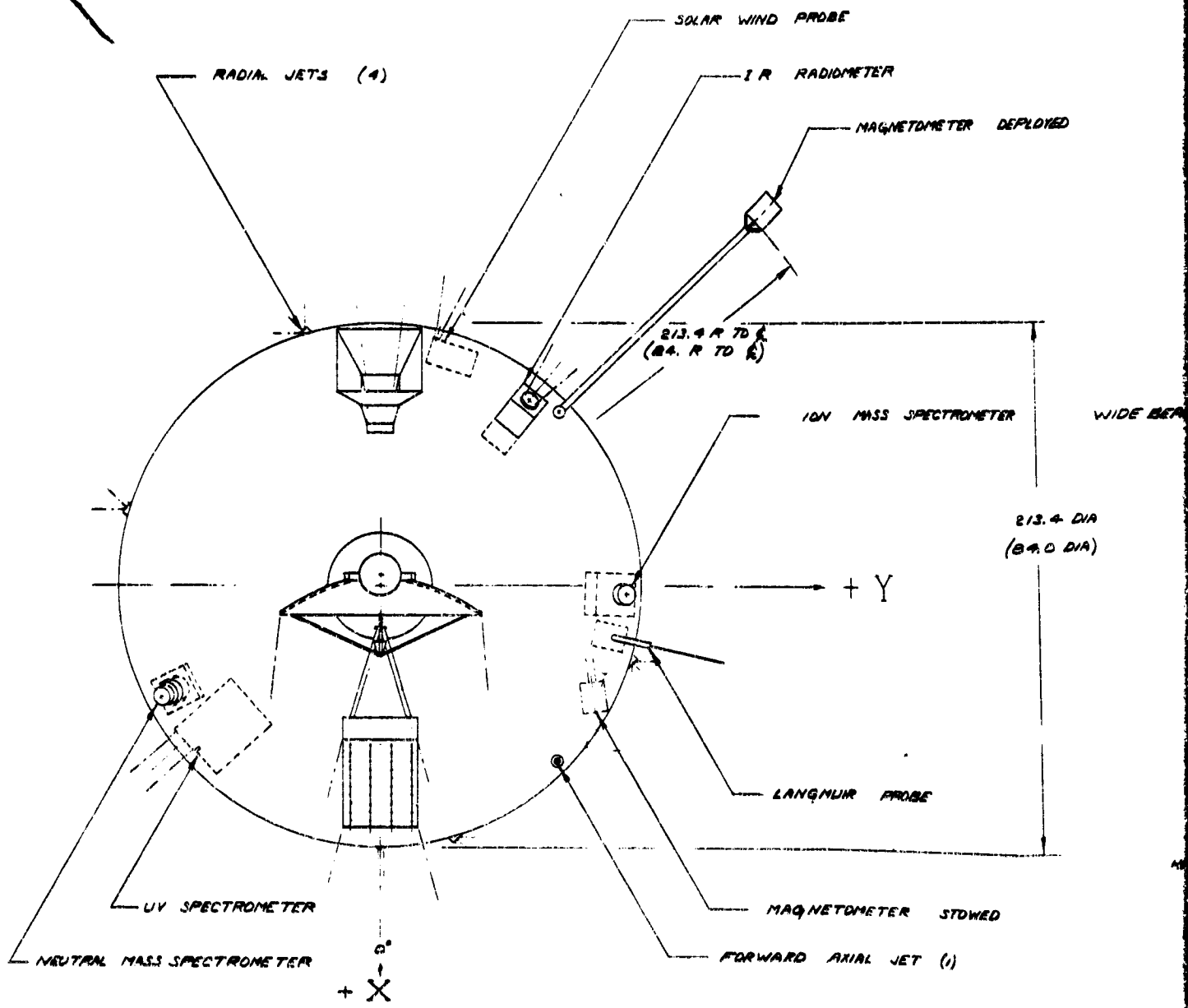


(INCHES)

NOTE: THERMAL INSULATION OMITTED FOR CLARITY

FOLDOUT FRAME

FOLDOUT

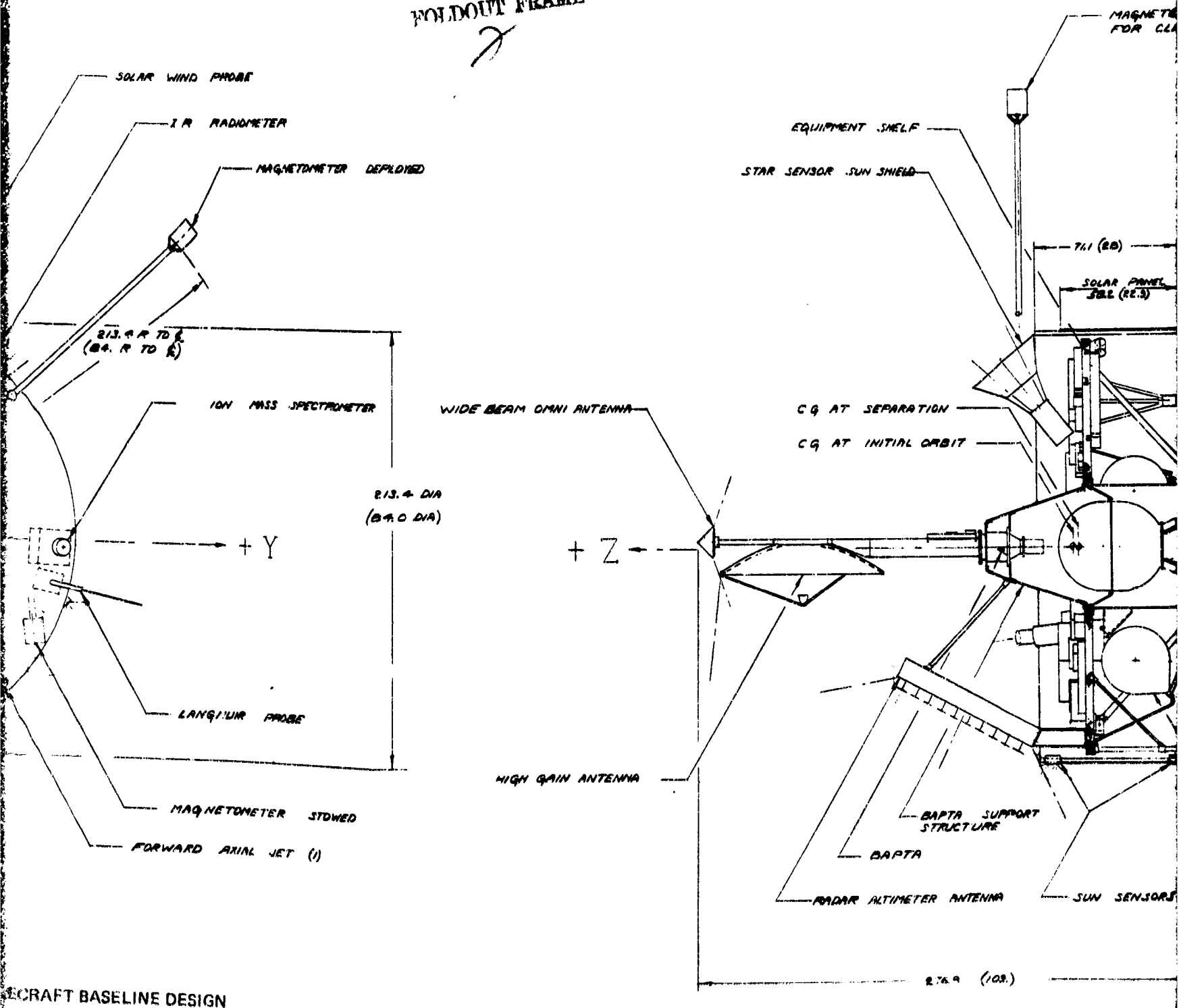


REPRODUCIBILITY OF THE ORIGINAL PAGE IS POOR.

FIGURE 3-9. THOR/DELTA ORBITER SPACECRAFT BASELINE DESIGN

# FOLDOUT FRAME

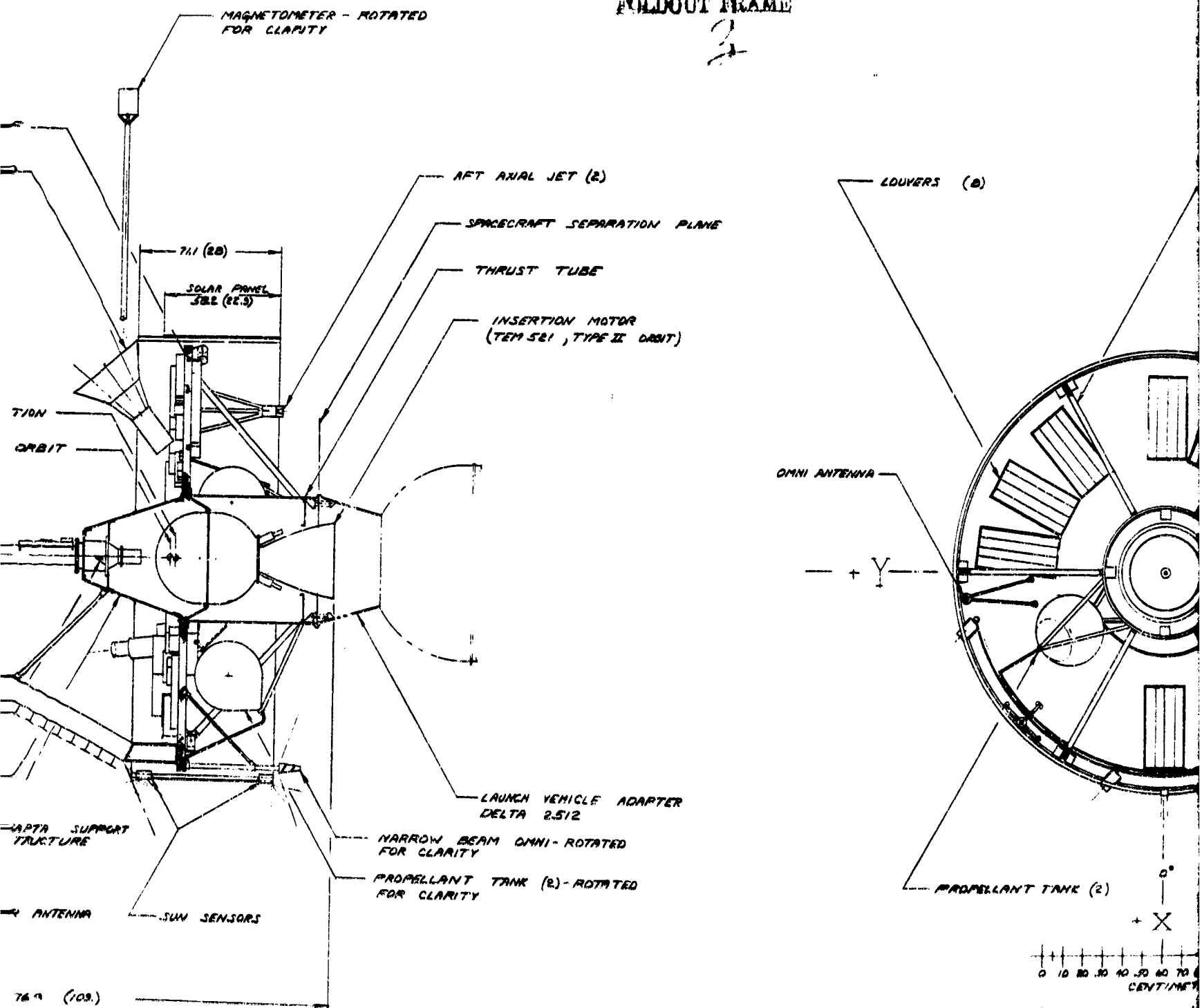
2



REPRODUCIBILITY OF THE ORIGINAL PAGE IS POOR.

# FOLDOUT FRAME

3



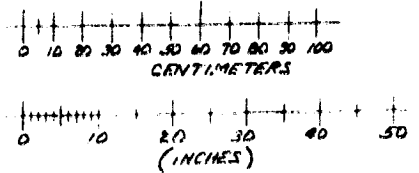
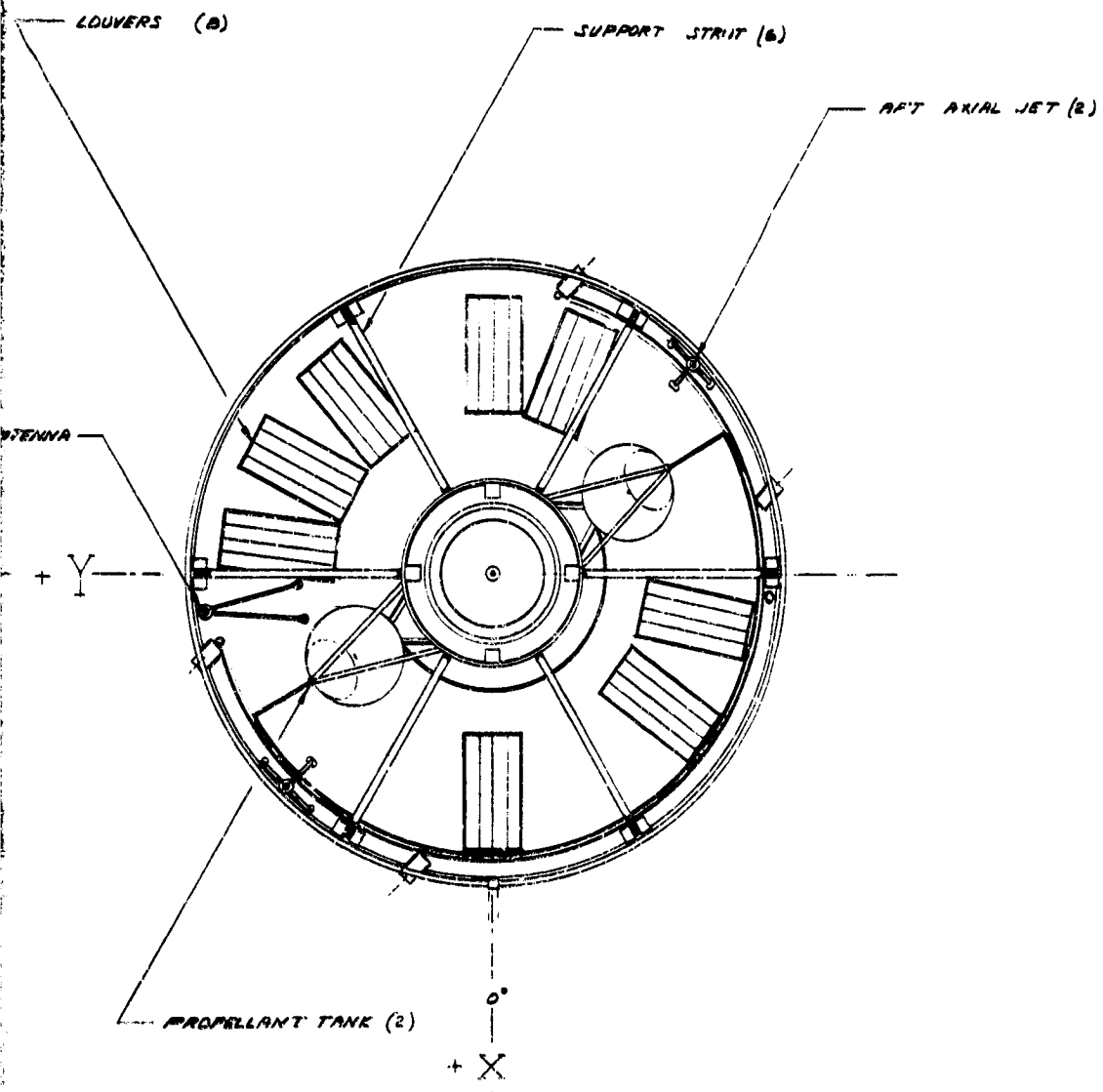
NOTE: INSULATION OMITTED

REPRODUCIBILITY OF THE ORIGINAL PAGE IS POOR.

WHITE FRAME

4

30163-341(U)



NOTE: INSULATION OMITTED FOR CLARITY

REPRODUCIBILITY OF THE ORIGINAL PAGE IS POOR.

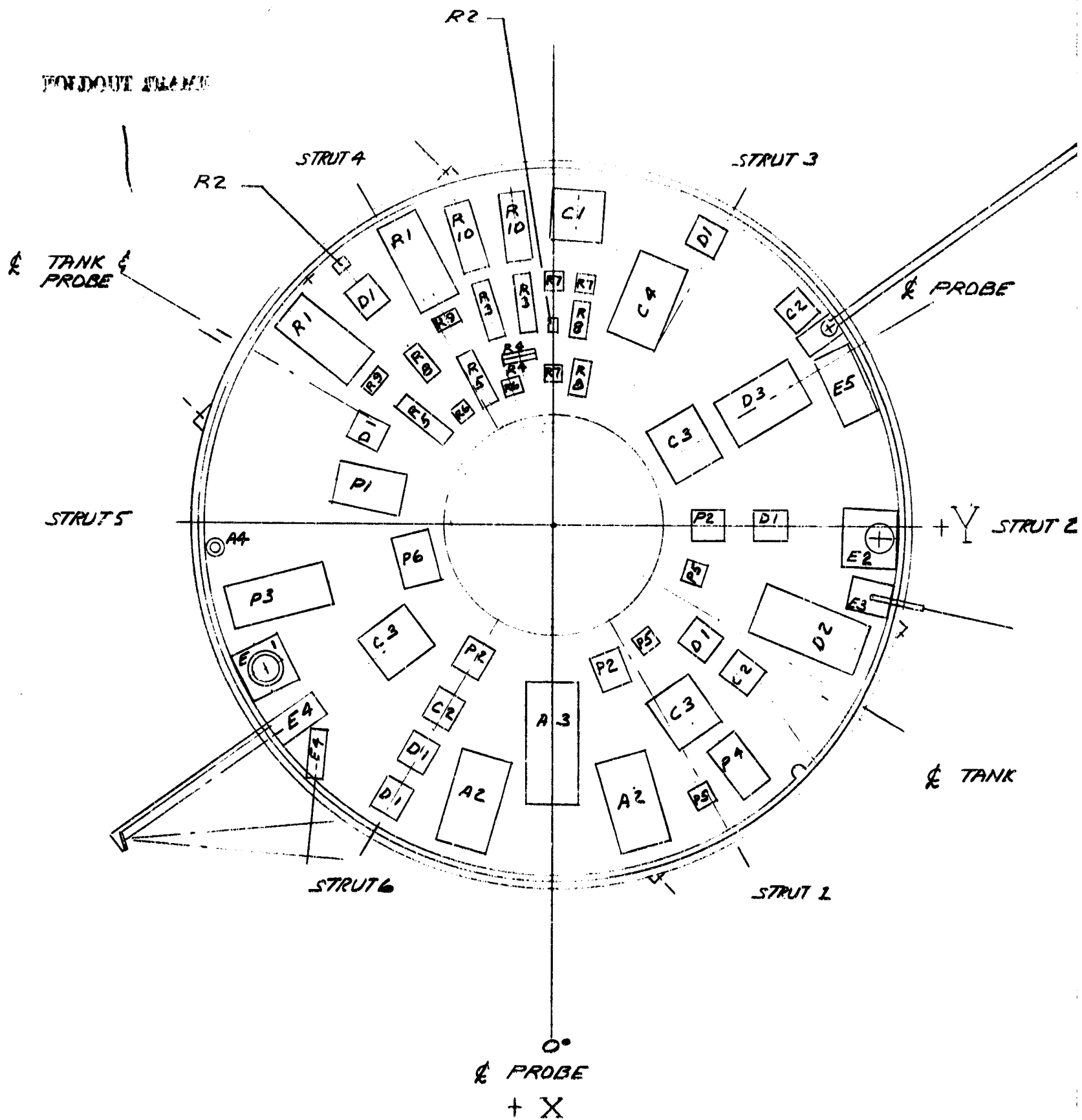
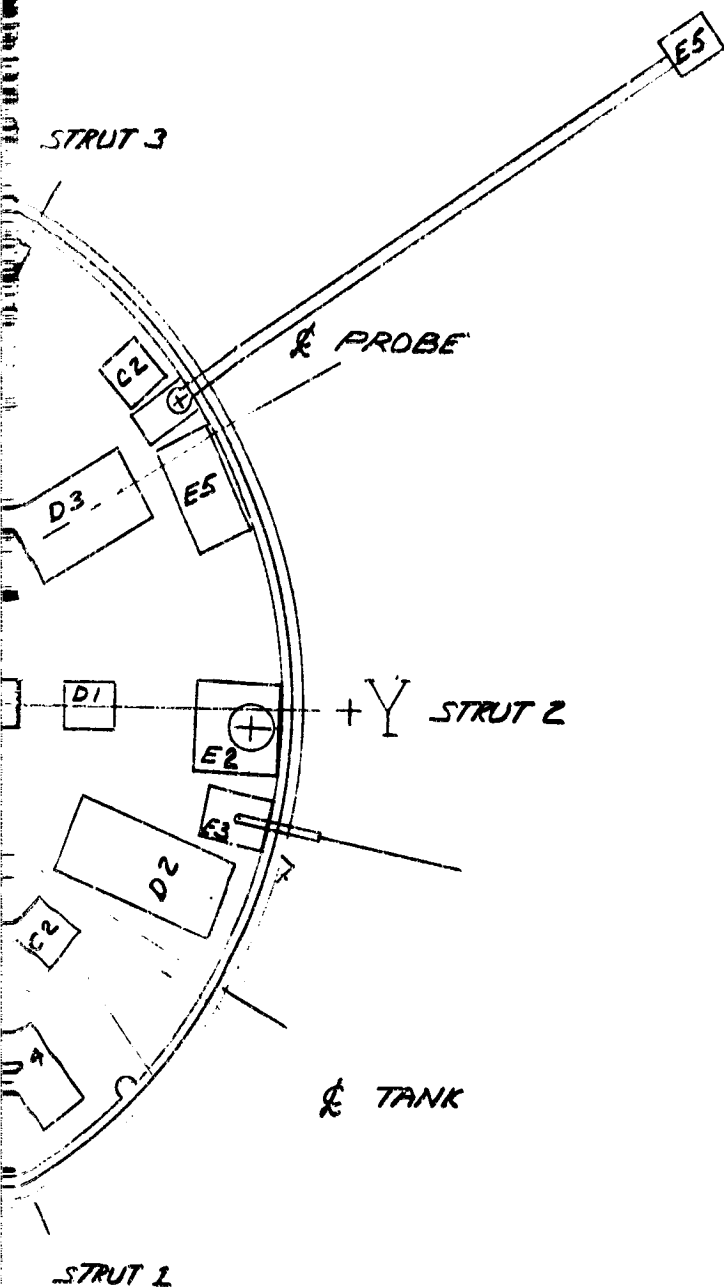


FIGURE 3-10. THOR/DELTA PROBE SPACECRAFT SHELF ARRANGEMENT

REPRODUCIBILITY OF THE ORIGINAL PAGE IS POOR.

2



CODE	UNIT	NO. REQD
E 1	NEUTRAL MASS SPECTROMETER	1
2	ION MASS SPECTROMETER	1
3	LANGMUIR PROBE	1
4	UV FLUORESCENCE	1
5	MAGNETOMETER	1
R 1	EXCITER / RCVR	2 2 2 2 2 2 2 2 2 2
2	HYBRID	
3	FILTER, TXBP	
4	FILTER, HARMONIC	
5	FILTER, RCBP	
6	CIRCULATOR + ISOLATOR	
7	SPDT SWITCH	
8	TRANSFER SWITCH	
9	PREAMPLIFIER	
10	POWER AMPLIFIER	
D 1	REMOTE MULTIPLEXER	7
2	PCM ENCODER, DUAL	1
3	TELEMETRY PROCESSOR, DUAL	1
C 1	DEMODULATOR	1 1 1 1
2	DUAL REMOTE DECODER	
3	FYRD CONTROL UNIT	
4	CENTRAL DECODER / COMMAND MEMORY, DUAL	
A 1	STAR SENSOR	1
2	ATTITUDE DATA PROCESSOR	2
3	SOLENOID DRIVERS	1
4	INUTATION DAMPER	1
P 1	DISCHARGE REGULATOR	1
2	BUS LIMITER	3
3	BATTERY	1
4	OVERLOAD CONTROL UNIT	1
5	CURRENT SENSOR	1
6	BATTERY CHARGER	1

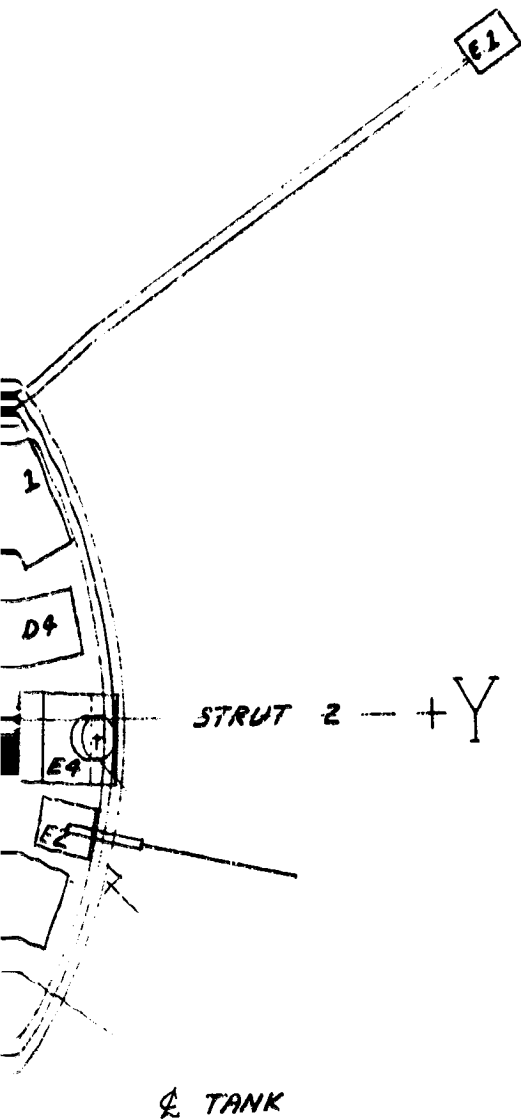
REPRODUCIBILITY OF THE ORIGINAL PAGE IS POOR.





FOLDOUT FRAME

20163-543(1)



CODE	UNIT	NO	RQD
E	1	MAGNETOMETER	1
	2	LANGMUIR PROBE	1
	3	NEUTRAL MASS SPECTROMETER	1
	4	ION MASS SPECTROMETER	1
	5	UV SPECTROMETER	1
	6	IR RADIOMETER	1
	7	S-BAND RADIO OCCULTATION	1
	8	S-BAND RADAR ALTIMETER	1
	9	SOLAR WIND PROBE	1
R	1	EXCITER / RCVR	2
	2	HYBRID	2
	3	FILTER, TXBP	2
	4	FILTER, HARMONIC	2
	5	FILTER, RCBP	2
	6	CIRCULATOR + ISOLATOR	4
	7	SPDT SWITCH	3
	8	TRANSFER SWITCH	2
	9	PRE-AMPLIFIER	2
	10	POWER AMPLIFIER	2
D	1	REMOTE MULTIPLEXER	7
	2	PCM ENCODER, DUAL	1
	3	TELEMETRY PROCESSOR, DUAL	1
	4	DATA STORAGE	1
C	1	DEMODULATOR	1
	2	DUAL REMOTE DECODER	3
	3	PYRO CONTROL UNIT	1
	4	CENTRAL DECODER / COMMAND MEMORY, DUAL	1
A	1	STAR SENSOR	1
	2	ATTITUDE DATA PROCESSOR	2
	3	SOLENOID DRIVERS	1
	4	NUTATION DAMPER	1
	5	DESIGN CONTROL ELECTRONICS	2
P	1	DISCHARGE REGULATOR	1
	2	BUS LIMITER	4
	3	BATTERY	1
	4	OVERLOAD CONTROL UNIT	2
	5	CURRENT SENSOR	3
	6	BATTERY CHARGER	1

REPRODUCIBILITY OF THE ORIGINAL PAGE IS POOR.

TABLE 3-12. PIONEER VENUS MASS SUMMARY BY MAJOR SUBSYSTEM FOR THOR/DELTA BASELINE

Item Subsystem	Spacecraft Mass			
	Probe		Orbiter	
	kg	lb	kg	lb
RF				
Antenna	8.85	19.5	8.53	18.8
Data handling	3.08	6.8	2.54	5.6
Command	5.81	12.8	9.89	21.8
Attitude control, mechanisms	7.03	15.5	6.58	14.5
Structure	11.16	24.6	18.14	40.0
Power	35.97	79.3	32.52	71.7
Cabling	16.01	35.3	22.41	49.4
Thermal control	4.67	10.3	6.76	14.9
Propulsion (dry)	10.25	22.6	11.29	24.9
Orbit insertion motor case	9.07	20.0	9.84	21.7
Bus total (dry)	111.90	246.7	138.62	305.6
Large probe	114.58	252.6		
Small probe (3)	101.91	224.7		
Spacecraft subtotal	328.40	724.0	138.62	305.6
Contingency	23.31	51.4	10.02	22.1
Experiments (bus only)	11.61	25.6	31.12	68.6
Spacecraft total (dry)	363.33	801.0	179.76	396.3
Propellant	20.73	45.7	24.31	53.6
Pressurant	.05	0.1	.05	0.1
Orbit insertion motor expendables			88.72	195.6
Spacecraft total (wet)	384.10	846.8	292.84	645.6
Spacecraft adapter	13.15	29.0	13.15	29.0
Telemetry and C band	8.39	18.5	8.39	18.5
Launch vehicle payload	405.65	894.3	314.38	693.1

TABLE 3-13. MASS PROPERTY SUMMARY DETAIL MASS STATEMENT  
 PROBE SPACECRAFT - THOR/DELTA BASELINE

Description	Mass	
	kg	lb
<u>RF Subsystem</u>	<u>9.85</u>	<u>19.5</u>
Exciter/receiver (2)	3.63	8.0
Hybrid (2)	0.05	0.1
Filter - TxBP (2)	0.73	1.6
Filter - harmonic (2)	0.09	0.2
Filter - RC BP (2)	0.73	1.6
Circulator - isolator (4)	0.45	1.0
SPDT switch (3)	0.36	0.8
Transfer switch (3)	0.95	2.1
Preamplifier (2)	0.23	0.5
Power amplifier	0.91	2.0
Coax cables	0.73	1.6
<u>Antenna Subsystem</u>	<u>3.08</u>	<u>6.8</u>
Bicone antenna	1.72	3.8
Medium gain antenna	0.91	2.0
Omni (wide beam)	0.27	0.6
Omni (narrow beam)	0.18	0.4
<u>Data Handling Subsystem</u>	<u>5.81</u>	<u>12.8</u>
Remote multiplexer (7)	1.36	3.0
Dual telemetry processor	1.59	3.5
Dual PCM encoder	2.86	6.3
<u>Command Subsystem</u>	<u>7.03</u>	<u>15.5</u>
Dual demodulator	2.09	4.6
Dual central decoder	1.77	3.9
Dual remote decoder (3)	1.81	4.0
Pyro control unit	1.36	3.0
<u>Attitude Control, Mechanisms</u>	<u>11.16</u>	<u>24.6</u>
Sun sensor (3)	0.27	0.6
Star sensor (includes sunshade)	2.49	5.5
Attitude data processor (2)	3.27	7.2
Solenoid driver	1.00	2.2
Nutation damper	0.86	1.9
Magnetometer boom and deployment	1.36	3.0
UV fluorescence deployment	0.59	1.3
Bicone deployment	0.86	1.9
Separation arm switch (2)	0.45	1.0

Table 3-13 (continued)

Description	Mass	
	kg	lb
<u>Structure Subsystem</u>	<u>35.97</u>	<u>79.3</u>
Equipment shelf	11.29	24.9
Shelf support struts (Be)	1.04	2.3
Shelf support brackets (Be)	0.23	0.5
Shelf support doublers (Be)	0.14	0.3
Thrust tube (Be)	3.63	8.0
Large probe attach structure (Be)	2.95	6.5
Large probe structure longerons (6) (Be)	0.86	1.9
Omni boom mounting	0.18	0.4
Medium gain antenna bracketry	0.09	0.2
Bicone deployment support	0.36	0.8
Substrate	8.03	17.7
Small probe attach structure (Be)	2.00	4.4
Propellant tank supports	1.04	2.3
Thruster supports	1.41	3.1
Balance weights	1.81	4.0
Miscellaneous hardware	0.91	2.0
<u>Power Subsystem</u>	<u>16.01</u>	<u>35.3</u>
Battery	4.22	9.3
Discharge regulator	2.72	6.0
Battery charger	1.81	4.0
Bus limiter	1.91	4.2
Solar array (excludes substrate)	4.04	8.9
Experiment overload control	0.91	2.0
Current sensors (3)	0.41	0.9
<u>Harness</u>	<u>4.67</u>	<u>10.3</u>
Wire harness	4.67	10.3
<u>Thermal Control</u>	<u>10.25</u>	<u>22.6</u>
Coatings	.45	1.0
Blankets	6.44	14.2
Louvers (6)	1.77	3.9
Shelf doublers	1.50	3.3
Temperature sensors	0.09	0.2
<u>Propulsion Subsystem (dry)</u>	<u>9.07</u>	<u>20.0</u>
Propellant tanks (2)	3.13	6.9
Thrusters (6)	1.63	3.6
Propellant valve (6)	1.36	3.0
Latch valve	0.54	1.2

Table 3-13 (continued)

Description	Mass	
	kg	lb
Fill valve	0.14	0.3
Filter (4)	0.54	1.2
Pressure transducer	0.23	0.5
Tubing	0.32	0.7
Fittings	0.45	1.0
Valve and catalyst bed heaters	0.18	0.4
Thruster insulation	0.45	1.0
Temperature sensors	0.09	0.2
<u>Bus Total (Dry)</u>	<u>111.90</u>	<u>246.7</u>
<u>Large Probe</u>	<u>114.58</u>	<u>252.6</u>
<u>Deceleration Module</u>	( 39.46 )	( 87.0 )
Heat shield	12.02	26.5
Structure - aeroshell	5.13	11.3
Structure - internal	10.34	22.8
Aft cover	3.90	8.6
Parachute	( 3.72 )	( 8.2 )
Main parachute	2.36	5.2
Pilot parachute	0.45	1.0
Mortar	0.41	0.9
Separation nuts	0.50	1.1
Cabling	1.04	2.3
Separation	( 1.27 )	( 2.8 )
Explosive nuts (5)	0.68	1.5
Inflight disconnect	0.59	1.3
Instrumentation	( 0.18 )	( 0.4 )
Sensors	0.18	0.4
Ballast	0.73	1.6
Shock layer radiometer	1.13	2.5
<u>Pressure Vessel Module</u>	( 73.07 )	( 161.1 )
Structure	( 24.99 )	( 55.1 )
Shell	13.20	29.1
Shelves (2)	4.13	9.1
Flanges	3.58	7.9
Penetrations	1.27	2.8
Adapter	1.36	3.0
Insulation retainer	1.32	2.9
Strain gauges	0.14	0.3
Thermal control	( 7.48 )	( 16.5 )
Insulation	7.26	16.0
Temperature sensors	0.23	0.5

Table 3-13 (continued)

Description	Mass	
	kg	lb
RF subsystem	( 3.63)	( 8.0 )
Receiver/exciter	1.81	4.0
Hybrid	0.05	0.1
Filter - Tx BP	0.36	0.8
Filter - harmonic	0.05	0.1
Filter - Rc BP	0.36	0.8
Circulator	0.11	0.25
Preamplifier	0.11	0.25
Power amplifier	0.45	1.0
Coax cables	0.32	0.7
Digital	2.13	4.7
Command/data unit	1.13	2.5
Pyro control unit	1.00	2.2
Power	( 11.20)	( 24.7 )
Battery	6.67	14.7
Discharge regulator/ current sensor	2.72	6.0
Experiment interface (3)	1.13	2.5
Pyro switch	0.68	1.5
Antenna	0.68	1.5
Harness	( 0.86)	( 1.9 )
Internal	0.73	1.6
External	0.14	0.3
Equipment	( 0.73)	( 1.6 )
G switch	0.45	1.0
Pressure gauge	0.09	0.2
Pressure switch	0.18	0.4
Experiments	( 21.36)	( 47.1 )
Temperature sensors (2)	0.59	1.3
Pressure sensors (2)	0.82	1.8
Nephelometer	1.13	2.5
Planetary flux detector	2.27	5.0
Accelerometer	1.13	2.5
Solar flux detector	1.81	4.0
Mass spectrometer	7.71	17.0
Aureole extinction detector	1.81	4.0
Cloud particle size analyzer	3.63	8.0
Hygrometer	0.45	1.0
<u>Bus Separation Module</u>	( 2.04)	( 4.5 )
Explosive nut (3)	0.68	1.5
Separation spring (3)	0.68	1.5
Inflight disconnect	0.68	1.5

Table 3-13 (continued)

Description	Mass	
	kg	lb
<u>Small Probe</u>		
<u>Deceleration Module</u>	<u>33.97</u>	<u>74.9</u>
Heat shield	( 9.12 )	( 20.1 )
Structure	4.63	10.2
Aeroshell	( 3.86 )	( 8.5 )
Internal structure	1.50	3.3
Harness	2.36	5.2
Experiment (temperature probe)	0.14	0.3
	0.50	1.1
<u>Pressure Vessel Module</u>		
Structure	( 23.59 )	( 52.0 )
Shell	( 6.76 )	( 14.9 )
Shelf	2.77	6.1
Flanges	1.18	2.6
Penetrations	1.22	2.7
Electrical feedthrough	( 0.23 )	( 0.5 )
Ports	0.05	0.1
Windows	0.05	0.1
Adapter	0.14	0.3
Insulation retainer	0.77	1.7
Antenna cover	0.54	1.2
Harness	0.05	0.1
Thermal control	0.27	0.6
Insulation	( 4.90 )	( 10.8 )
Temperature sensors	4.76	10.5
RF	0.14	0.3
Exciter	( 1.13 )	( 2.5 )
Stable oscillator	0.45	1.0
Power amplifier	0.36	0.8
Coax cable	0.23	0.5
Digital	0.09	0.2
Command/data	( 1.22 )	( 2.7 )
Pyro control	1.00	2.2
Power	0.23	0.5
Battery	( 7.08 )	( 15.6 )
Discharge regulator/current sensor	4.13	9.1
Experiment interface	1.59	3.5
Pyro switch	0.68	1.5
Antenna	0.68	1.5
Equipment - G switches	0.23	0.5
Science	0.23	0.5
Pressure gauge	( 1.77 )	( 3.9 )
Nephelometer	0.41	0.9
	0.45	1.0



Table 3-13 (continued)

Description	Mass	
	kg	lb
Accelerometer	0.18	0.4
Magnetometer	0.50	1.1
Temperature probe electronics	0.23	0.5
<u>Separation - Despin Module</u>	<u>( 1.27 )</u>	<u>( 2.8 )</u>
Spin rocket (3)	0.32	0.7
Bolt thruster	0.14	0.3
Hinge-arm and open hatch	0.41	0.9
Inflight disconnect	0.41	0.9
<u>Spacecraft Subtotal</u>	<u>328.40</u>	<u>724.0</u>
<u>Contingency</u>	<u>23.31</u>	<u>51.4</u>
<u>Experiments</u>	<u>11.61</u>	<u>25.6</u>
Neutral mass spectrometer	4.99	11.0
Ion mass spectrometer	1.36	3.0
Electron temperature probe	1.59	3.5
UV fluorescence	1.36	3.0
Magnetometer	2.31	5.1
<u>Spacecraft Total (Dry)</u>	<u>363.33</u>	<u>801.0</u>
<u>Propellant</u>	<u>20.73</u>	<u>45.7</u>
<u>Pressurant</u>	<u>0.05</u>	<u>0.1</u>
<u>Spacecraft Total (Wet)</u>	<u>384.10</u>	<u>846.8</u>
<u>Spacecraft Adapter</u>	<u>13.15</u>	<u>29.0</u>
<u>Telemetry and C band</u>	<u>8.39</u>	<u>18.5</u>
<u>Launch Vehicle Payload</u>	<u>405.65</u>	<u>894.3</u>

TABLE 3-14. MASS PROPERTY SUMMARY DETAIL MASS STATEMENT  
ORBITER SPACECRAFT - THOR/DELTA BASELINE

Description	Mass	
	kg	lb
<u>RF Subsystem</u>	<u>8.53</u>	<u>18.8</u>
Exciter/receiver (2)	3.63	8.0
Hybrid (2)	0.05	0.1
Filter - TxBP (2)	0.73	1.6
Filter - harmonic (2)	0.09	0.2
Filter - RcBP (2)	0.73	1.6
Circulator - isolator (4)	0.45	1.0
SPDT Switch (3)	0.36	0.8
Transfer switch (3)	0.64	1.4
Preamp (2)	0.23	0.5
Power amplifier (2)	0.91	2.0
Coax cables	0.73	1.6
<u>Antenna Subsystem</u>	<u>2.54</u>	<u>5.6</u>
High gain antenna	1.41	3.1
Omni (widebeam)	0.27	0.6
Omni (narrow beam)	0.18	0.4
Circulator	0.14	0.3
SPDT switch	0.09	0.2
Notch filter	0.45	1.0
<u>Data Handling Subsystem</u>	<u>9.89</u>	<u>21.8</u>
Remote multiplexer	1.36	3.0
Dual telemetry processor	1.59	3.5
Data storage unit	4.08	9.0
Dual PCM encoder	2.86	6.3
<u>Command Subsystem</u>	<u>6.58</u>	<u>14.5</u>
Dual demodulator	2.09	4.6
Dual central decoder	1.77	3.9
Dual remote decoder (3)	1.81	4.0
Pyro control unit	0.91	2.0
<u>Attitude Control, Mechanisms</u>	<u>18.14</u>	<u>40.0</u>
Sun sensor (3)	0.27	0.6
Star sensor (includes sun shade)	2.49	5.5
Attitude data processor (2)	3.27	7.2
Despin control electronics (2)	3.36	7.4
Solenoid driver	1.00	2.2
Nutation damper	0.86	1.9

Table 3-14 (continued)

Description	Mass	
	kg	lb
BAPTA	5.08	11.2
Magnetometer boom and deployment	1.36	3.0
Separation and arm switch (2)	0.45	1.0
	<u>32.52</u>	<u>71.7</u>
<u>Structure Subsystem</u>		
Equipment shelf	11.29	24.9
Shelf support struts (Be)	1.04	2.3
Shelf support brackets (Be)	0.23	0.5
Shelf support doublers (Be)	0.14	0.3
Thrust tube (Be)	3.63	8.0
BAPTA support (Be)	0.82	1.8
HGA boom	1.00	2.2
Omni booms (2)	0.18	0.4
Substrate	8.03	17.7
Propellant tank supports (2)	1.04	2.3
Thruster supports (8)	1.50	3.3
Motor attach ring	0.54	1.2
Balance weights	1.81	4.0
RF altimeter support	0.36	0.8
Miscellaneous hardware	0.91	2.0
	<u>22.41</u>	<u>49.4</u>
<u>Power Subsystem</u>		
Battery	7.85	17.3
Discharge regulator	2.72	6.0
Solar array (excludes substrate)	4.99	11.0
Bus limiter (4)	2.49	5.5
Battery charger	1.22	2.7
Overload control unit	2.72	6.0
Current sensors	0.41	0.9
	<u>6.76</u>	<u>14.9</u>
<u>Harness</u>		
Wire harness	6.76	14.9
	<u>11.29</u>	<u>24.9</u>
<u>Thermal Control</u>		
Thermal coatings	0.15	1.0
Insulation blankets	6.44	14.2
Thermal louvers (8)	2.36	5.2
Shelf doublers	1.91	4.2
Temperature sensors (17)	0.14	0.3

Table 3-14 (continued)

Description	Mass	
	kg	lb
<u>Propulsion Subsystem (dry)</u>	<u>9.84</u>	<u>21.7</u>
Propellant tanks (2)	3.13	6.9
Thrusters (7)	1.91	4.2
Propellant valve (7)	1.59	3.5
Latching valve (2)	0.54	1.2
Fill valve	0.14	0.3
Filter (4)	0.54	1.2
Pressure transducer	0.23	0.5
Tubing	0.45	1.0
Fittings	0.45	1.0
Valve and catalyst bed heaters	0.23	0.5
Thruster insulation	0.54	1.2
Temperature sensors	0.09	0.2
<u>Orbit Insertion Motor Case</u>	<u>10.12</u>	<u>22.3</u>
Motor case (burned out)	9.93	21.9
Heater	0.18	0.4
<u>Bus Total (dry)</u>	<u>138.62</u>	<u>305.6</u>
<u>Spacecraft Subtotal</u>	<u>138.62</u>	<u>305.6</u>
<u>Contingency</u>	<u>10.02</u>	<u>22.1</u>
<u>Experiments (Bus Only)</u>	<u>31.12</u>	<u>68.6</u>
RF altimeter	9.07	20.0
IR radiometer	4.08	9.0
UV spectrometer	5.44	12.0
Neutral mass spectrometer	4.54	10.0
Ion mass spectrometer	1.36	3.0
Electron temperature probe	1.59	3.5
Magnetometer	2.31	5.1
Solar wind probe	2.72	6.0
<u>Spacecraft Total (dry)</u>	<u>179.76</u>	<u>396.3</u>
<u>Propellant</u>	<u>24.31</u>	<u>53.6</u>
<u>Pressurant</u>	<u>0.05</u>	<u>0.1</u>
<u>Orbit Insertion Motor Expendables</u>	<u>88.72</u>	<u>195.6</u>

Table 3-14 (continued)

Description	Mass	
	kg	lb
<u>Spacecraft Total (wet)</u>	<u>292.84</u>	<u>645.6</u>
Spacecraft adapter	13.15	29.0
Telemetry and C band	8.39	18.5
<u>Launch Vehicle Payload</u>	<u>314.38</u>	<u>693.1</u>

TABLE 3-15. PIONEER VENUS SPACECRAFT MASS PROPERTIES ANALYSIS  
 THOR/DELTA BASELINE - MISSION PROFILE

Condition	Mass		Center of Gravity		Moment of Inertia						$I_R / I_T$	
	kg	lb	M	In	$I_x$		$I_y$		$I_z$			
					kg-M <sup>2</sup>	Slug-ft <sup>2</sup>	kg-M <sup>2</sup>	Slug-ft <sup>2</sup>	kg-M <sup>2</sup>	Slug-ft <sup>2</sup>		
<u>Probe Spacecraft</u>												
At launch, boom retracted	384.10	(846.8)	1.07	(42.3)	139.8	(103.1)	132.5	(97.7)	163.8	(120.8)		1.20
At launch, boom extended	384.10	(846.8)	1.07	(42.3)	141.0	(104.0)	134.6	(99.3)	167.2	(123.3)		1.21
After large probe separation	248.75	(548.4)	0.94	(37.1)	94.8	(69.9)	96.1	(70.9)	147.6	(108.9)		1.55
After small probe separation	146.83	(323.7)	0.73	(28.8)	48.8	(36.0)	50.3	(37.1)	38.4	(65.2)		1.79
<u>Orbiter Spacecraft</u>												
At launch, boom retracted	292.84	(645.6)	0.71	(28.0)	72.1	(53.2)	64.8	(47.8)	111.0	(81.9)		1.62
At launch, boom extended	292.84	(645.6)	0.71	(28.0)	73.5	(54.2)	67.0	(49.4)	114.4	(84.4)		1.63
Before Venus orbit insertion	279.83	(616.9)	0.72	(28.4)	68.3	(50.4)	65.9	(48.6)	110.1	(81.2)		1.64
In Venus orbit	191.10	(421.3)	0.74	(29.1)	66.3	(48.9)	63.9	(47.1)	108.2	(79.8)		1.66
Spent spacecraft	179.75	(396.3)	0.75	(29.7)	61.0	(45.0)	62.5	(46.1)	103.9	(76.6)		1.68

## Orbiter Spacecraft

The orbiter spacecraft in launch configuration has a total mass of 292.84 kg (645.6 lb) with the center of mass located 71 cm (28.0 in.) above the separation plane from the launch vehicle. The roll to transverse inertia ratio varies from a minimum value of 1.62 to a maximum of 1.68 at end of life. This ratio provides good spin stability throughout the mission. A maximum diameter of 213.4 cm (84.0 in.) and an overall length of 276.9 cm (109.0 in.) allows for radial and longitudinal clearances from the allowable payload envelope.

The basic arrangement primary elements, i. e., thrust tube, equipment shelf, substrate, struts, and hydrazine tanks, as previously noted, are identical to the probe bus.

A right conical frustum installed at the upper end of the thrust tube provides for support and installation of the bearing and power transfer assembly (BAPTA). The high gain antenna (HGA) mast is attached to the despun flange of the BAPTA and positions the center line of the HGA 121.9 cm (48 in.) above the forward plane of the substrate. At this position, the 11 deg beamwidth of the HGA maintains clearance with the radar altimeter mounted above the substrate and the radially deployed magnetometer. The wide beam (220 deg) omni antenna is located 45.7 cm (18 in.) above the HGA center line to maintain beam clearance with the reflector.

Of nine specified payload experiments, all but one require physical accommodation on the spacecraft. The exception, radio occultation, will use the existing spacecraft RF subsystem.

The magnetometer, langmuir probe, ion and neutral particle mass spectrometers are similar to those specified for the probe spacecraft. Therefore, their locations on the equipment shelf remain the same. For the ion and neutral particle mass spectrometers, a nominal pointing angle of 15 deg from the spin axis was established for the orbiter mission. This orientation allows the HGA and widebeam omni antenna to remain well outside of the experiments 30 deg field of view. The UV spectrometer, with line of sight pointed radially, is located at the shelf position used by the UV fluorescence experiment on the probe bus. The subsystem unit shelf arrangement developed for the probe bus will accommodate the solar wind probe and IR radiometer experiments and several additional subsystem units with no rearrangement required. The additional experiments and subsystem units increased the thermal load on the shelf from that of the probe bus. Therefore, two thermal control louver modules are added to the bottom of the shelf, making a total of eight.

The pointing angle for the radar altimeter is determined by the periapsis latitude. For the Thor/Delta baseline (26°N nominal periapsis), the angle is 64 deg from the spin axis. A reduction in latitude requires a corresponding increase in the pointing angle. If it should become desirable to lower the periapsis latitude, only a slight change to the spacecraft

configuration is needed, i. e., a minor increase in the HGA mast height to maintain clearance between the HGA beam and the radar altimeter. For increases in latitude, the mast may remain as is or be shortened.

For the baseline Type II transit trajectory, a Thiokol TE-M-521 solid propellant motor was selected to provide orbit insertion. The 44.5 cm (17.5 in.) diameter motor is easily accommodated in the thrust tube and is supported by a motor attach ring located near the upper end.

For the other option, Type I transit trajectory, the candidate motor for insertion was an Aerojet SVM-2. This motor is larger in diameter, 56.6 cm (22.3 in.), but can also be readily installed in the thrust tube, requiring only a change in motor attach rings.



### 3.4 ATLAS/CENTAUR BASELINE DESCRIPTION

This subsection includes additional trade studies conducted for the Atlas/Centaur design and the final study baseline configuration achieved after redirection of the study effort in April 1973 to use the Atlas/Centaur launch vehicle.

#### Mission Configuration and Launch Mass Contingency Trades

The baseline mission plan was redirected after midterm to one probe and one orbiter Atlas/Centaur launch in 1978. The probe launch is essentially the same as for 1977. However, a new issue is the tradeoff of mission set case A, using type I opportunity for the multiprobe mission and the earlier (May 1978) type II opportunity for the orbiter or case B, with both probe and orbiter launches in the type I (August 1978) opportunity separated by several weeks.

The mission sets, launch mass, and contingencies are summarized in Table 3-16. The experiment payload update received in April 1973 is used in these comparisons. Including the 15 percent experiment weight contingency specified by NASA-ARC results in payloads of 13.74 kg (30.3 lb) for the probe bus (not including probes) and 45.41 kg (100.1 lb) for the orbiter spacecraft. The Hughes baseline approach for the dual-frequency occultation is estimated to be 2.13 kg (4.7 lb) greater (with contingency) than that specified by NASA-ARC. Therefore, an orbiter experiment payload of 47.54 kg (104.8 lb) is used in the baseline design. Accordingly since experiment contingency has already been allowed in the experiment payload mass, the contingency levels shown in Table 3-16 are included in and apply to the dry spacecraft less the bus or orbiter science. The propellant loading assumed is for the spacecraft mass including all contingency. The spacecraft mass includes the additional 75 kg (165 lb) specified in April by ARC for Atlas/Centaur payload, but does not include the mass of the Intelsat IV attach fitting selected for the baseline design.

Case A results in Table 3-16 show that the launch mass contingency is liberal for the probe mission and adequate for the orbiter. Case B differs in that, the contingency is greatly increased for a type I orbiter launch. The type I orbiter periapsis of 130N is inferior in science coverage, however, to the 560S given by type II in Case A.

To achieve adequate ( $\approx 10$  percent) orbiter launch mass contingency for Case A, several changes were made relative to the midterm Atlas/Centaur design. The thrust tube was revised to a shorter, single conical frustrum rather than the earlier cylinder-cone design saving about 10.5 kg (23 lb). All possible structural commonality between probe bus and orbiter has been preserved. Revised requirements permitted use of a 5 A-h, cell battery (common to probe bus and orbiter) rather than the 7 A-h cell battery with a reduction of 2.91 kg (6.4 lb). The magnetometer boom was redesigned using boom segments of beryllium tubing saving 1.45 kg (3.2 lb). Beryllium is also used in the bearing and power transfer assembly (BAPTA) saving 1.45 kg (3.2 lb). The total cost increase for these changes should not exceed \$150K.

TABLE 3-16. MISSION SET/WEIGHT CONTINGENCY SUMMARY

Case	Probe Spacecraft				Orbiter Spacecraft				Comments	
	Launch Date	Type	Spacecraft Mass, kg (lb)	Contingency, kg (lb) %	Launch Date	Type	Spacecraft Mass, kg (lb)	Dry Mass in Orbit, kg (lb)		Contingency, kg (lb) %
A	Aug 1978	I	813.1 (1793 )	149.6 (327.8) 19.3	May 1978	II, 56°S	460.7 (1015.7)	290.4 (640.3)	25.3 ( 55.8) 10.4	Baseline Orbiter arrives first Best orbit science
B	Aug 1978	I	813.1 (1793 )	149.6 (329.8) 19.3	Aug 1978	I, 13°N	760 (1673 )	405 (892 )	124 (274 ) 34.8	Two launches in same opportunity Uses TEM 616 orbit motor
C	Mar 1980	I	692 (1525 )	31.7 ( 70 ) 4.7	Apr 1980	II, 26°N	682 (1515 )	327 (720 )	46.3 (102 ) 16.6	Orbiter cont. assumes TEM 616 not stretched
	Apr 1980	II	805 (1775 )	142 (313 ) 18.5						

\*Percent of spacecraft dry weight without bus 13.74 kg (30.3 lb) or orbiter: 47.53 kg (104.8 lb) science

The type II (case A) orbiter will use a stretched TEM 521 motor as discussed in Volume 10 while the type I (case B) uses the heavier TEM 616. The stretched-case modification of the TEM 521 traded against the heavier 616 makes this cost trade almost even. The thrust tube has been sized to accept either motor with modification of the motor attach ring.

Also shown in Table 3-16 is case C, describing possible launch opportunities for 1980. The payload for the orbiter type II opportunity has been limited to that corresponding to the maximum propellant load of 333 kg (734 lb) for an unmodified TEM 616 motor. It is estimated that the motor procurement need not be placed until the tenth month of the execution phase. This allows maximum flexibility in selecting orbiter missions. The weight estimates include structural changes for the motor attach ring and the repositioning of the radar altimeter antenna for other periapsis latitudes ( $13^{\circ}\text{N}$  or  $26^{\circ}\text{N}$ ). The high gain antenna mast length is adequate to accommodate all missions considered.

Based on the above considerations, the baseline mission design has been selected as case A, type I probe and type II, 56 $^{\circ}\text{S}$  for the orbiter for the following reasons:

- The probe mission has liberal launch mass contingency and the orbiter contingency is adequate for a design using all applicable common hardware from the probe spacecraft
- Type II orbiter mission provides superior science coverage
- The type II orbiter mission avoids any potential problem associated with achieving two launches during the same 1978 type I opportunity
- The orbiter design can accommodate changes required (e. g., orbit motor, radar altimeter antenna installation) for type I, 1978 or type II, 1980 mission

#### Radio Occultation Experiment Trades

A significant trade for the Atlas/Centaur orbiter is the approach to be used for the dual frequency radio occultation experiment. RF beam refractive angles in the ranges of  $\pm 10$  to  $\pm 20$  deg have been considered in this trade.

The mechanically despun high gain antenna (HGA) reflector selected for the spacecraft communications subsystem facilitates the options available for S/X band occultation. This results from use of the despun system for azimuth pointing, as required, combined with adequate ERP at S-band for refractions to  $\pm 10$  deg. The trade involves approaches to the required ERF at S and X band by use of a fixed antenna/higher power (for X band), by pointing dual feed antenna using an elevation positioner or by moving (precessing) the spacecraft.

TABLE 3-17. DUAL FREQUENCY OCCULTATION TRADES

Configuration (All Antenna Assemblies are Despun in Azimuth)		A		B		C	
Design approach		Fixed S band HGA, Separate X band horn 3 W X band transmitter	Moving HGA reflector Fixed S/X feed 0.2 W X band transmitter	Moving spacecraft Fixed antenna with S/X feed 3 W X band transmitter			
	Increases to add occultation experiment	Cost K\$	750	1020	770		
Reliability		Best	Must accommodate ele- vation drive failure	Additional thruster pulses required			
	Science	Adequate (to $\pm 10$ deg), pointing accuracy $< 1$ deg. Best interface (separate X band)	Best boresight to earth, $\pm 20$ deg; pointing accuracy $< 1$ deg	Worst attitude uncertainty, pointing accuracy $< 2.5$ deg. Impacts radar altimeter usage			
Mission operations		Best	Some additional operations				
							Worst - requires daily attitude control. Uses 1.9 kg (4.2 lb) propellant in 40 days at $\pm 10$ deg

The communications requirements and implementation for radio occultation have been discussed in Volume 7. The influence of this trade on spacecraft configuration is reviewed here. Three approaches are shown and described in Table 3-17.

- 1) Adding a fixed, separate 20 deg beamwidth X band horn antenna and a 3 W, TWTA transmitter for  $\pm 10$  deg capability
- 2) Adding a  $\pm 10$  deg elevation positioner for the HGA reflector, which provides  $\pm 20$  deg beam steering capability with a fixed dual S/X feed, and an 0.2 W X band solid state transmitter
- 3) Adding a defocused X band feed to the fixed HGA and a 3 W TWTA transmitter and using precession of the spacecraft to achieve pointing to  $\pm 10$  deg

Table 3-17 summarizes the major issues of the trade selection. The mass and cost increments are those required to implement the S/X dual frequency occultation capability relative to a baseline spacecraft S band communications subsystem using a mechanically despun HGA. The detailed mass and cost increment data for the three approaches are shown in Table 3-18 for the required additions or modifications.

Approach A, using the separate X band horn requires careful calibration of the antenna pattern since the refractive effects will be established by gain variations away from boresight. Approaches A and C require higher transmitter power which is provided by use of an existing 3 W TWT amplifier. The difference in total dc power requirements for the three approaches is small and has been neglected in the trade. Approach A is the simplest to implement in design and operations, in lowest in cost and weight and has simplest experiment/spacecraft interfaces. Because of its shorter length, a common HGA mast length can be used for all radar altimeter angle positions associated with other candidate missions.

The moving reflector approach (B) provides the best science performance; refractive angles of  $\pm 20$  deg can be accommodated relatively easily with some penalty in HGA antenna mast length. The effective boresight angle to earth is measured directly using elevation positioner angle data. The technique of fixed feed and moving reflector require use of an elevation positioner mechanism (with  $\pm 10$  deg capability) with associated cost/weight increases. A squib activated, "return to zero" elevation angle provision has been provided to eliminate a critical failure mode in case of failure of the nonredundant elevation drive and electronics.

Approach C requires moving (precessing) the spacecraft through a total angle range of 40 deg at rates up to 7 deg/min for every performance of 10 deg. This periodic maneuver uses propellant, as shown in Table 3-17, produces nutation leading to increased attitude uncertainty, and may impact the near-periapsis operations of other science instruments, particularly the radar altimeter. The attitude uncertainty of 2.5 deg is caused, in part, by nutation accompanying the precessing maneuver and requires defocusing the X-band beamwidth from 3 to 6 deg.

TABLE 3-18. MASS AND COST INCREASES FOR A DUAL FREQUENCY OCCULTATION EXPERIMENT

Item Required	Design Approach						
	A		B		C		
	Mass, kg (lb)	Cost, \$K	Mass, kg (lb)	Cost, \$K	Mass, kg (lb)	Cost, \$K	
Add X-band horn	0.23 ( 0.5)	160	-	-	-	-	
Add X-band coax	0.27 ( 0.6)	130	0.27 ( 0.6)	85	0.27 ( 0.6)	130	
Modify HGA for dual feed	-		0.54 ( 1.2)		-		0.32 ( 0.7)
Add S band coax	-		0.14 ( 0.3)		-		-
Add rotary joint	0.41 ( 0.9)	85	0.41 ( 0.9)	85	0.41 ( 0.9)	85	
Modify HGA mast and support	-	-	1.23 ( 2.7)	30	-	-	
Add elevation positioner for HGA reflector (mechanism and electronics)	-	-	3.22 ( 7.1)	400	-	-	
Add X band solid state driver or transmitter	1.40 ( 3.1)	375	1.50 ( 3.3)	375	1.40 ( 3.1)	375	
Add X band TWA(3 W)	2.27 ( 5.0)	130	-	-	2.27 ( 5.0)	130	
Process spacecraft (propellant for 40 days) (electronics)	-	-	-	-	2.00 ( 4.4)	50	
Experiment contingency (15 percent)	0.68 ( 1.5)	-	1.09 ( 2.4)	-	(-1.90)( 4.2)		
Totals	5.26 (11.6)	750	8.40 (18.5)	1020	7.67 (16.9)	770	

Approach A has been selected as baseline for following reasons:

- Lowest cost, weight, and complexity
- Adequate science performance, best experiment/spacecraft interface
- High reliability
- Simple mission operations

The selected approach requires an increase in spacecraft (experiment) mass 2.14 (1.7 lb) greater (including contingency) than allocated by NASA-ARC for this experiment.

#### Magnetometer Boom Installation

At midterm the nominal science payload used for the study included a magnetometer for both the probe and orbiter mission. Since then a modified payload has been established and retains the magnetometer only for the orbiter mission.

A previous study (see Volume 2) established that a minimum distance of 4.4 m (14.5 ft) would permit a relatively low magnetic control on the spacecraft to meet background requirements. A boom of this length necessitated a folding scheme to permit stowage during launch. On the probe bus the three small probes presented restrictions on the placement of the stowed boom in a plane at the forward end of the spacecraft and therefore, at midterm it was positioned parallel to the substrate for launch for both spacecraft and deployed radially in a plane near the forward end. This installation can be seen in Volume 11.

Since only the orbiter spacecraft now carries a magnetometer a new study for boom installation was made. In addition to rigid articulated booms an extendable/retractable boom (ASTROMAST) was also investigated. The rigid booms are designed to accept orbit insertion loads, but the Astromast does not have that capability and must be retracted prior to motor firing. Details of the two types of boom may be found in Volume 9.

The spacecraft is designed to be statically and dynamically balanced with the boom deployed for rigid type designs, and dynamically balanced when deployed and statically balanced when retracted for the Astromast type. The center of mass (c. m.) offset incurred when the booms are stored present no problems to the launch vehicle but the Astromast must be retracted for orbit motor firing and at that time; the c. m. must be near the center line of thrust to minimize injection errors.

Installations in a plane forward of the substrate for articulated type booms, each approximately 4.42 m (14.5 ft) in deployed length, are depicted in Figures 3-12 and 3-13.

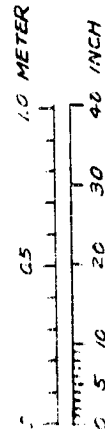
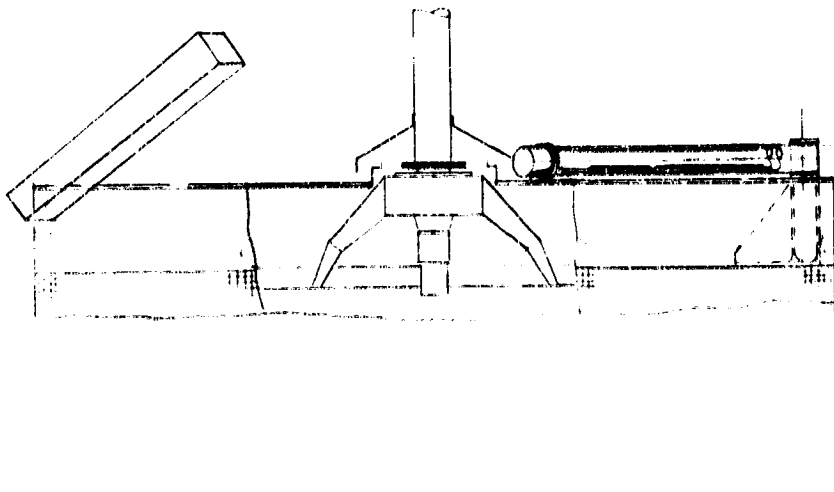
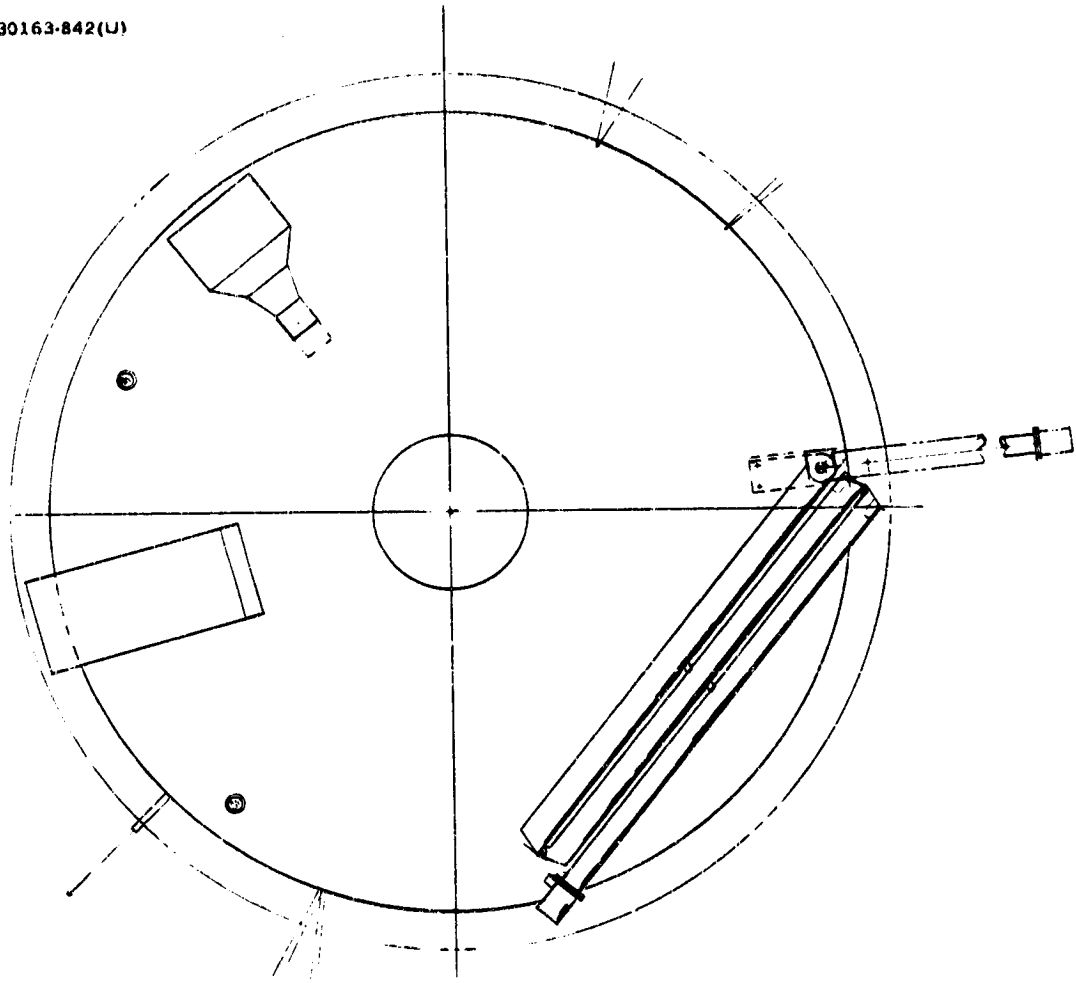


FIGURE 3-12. THREE LINK MAGNETOMETER BOOM

REPRODUCIBILITY OF THE ORIGINAL PAGE IS POOR



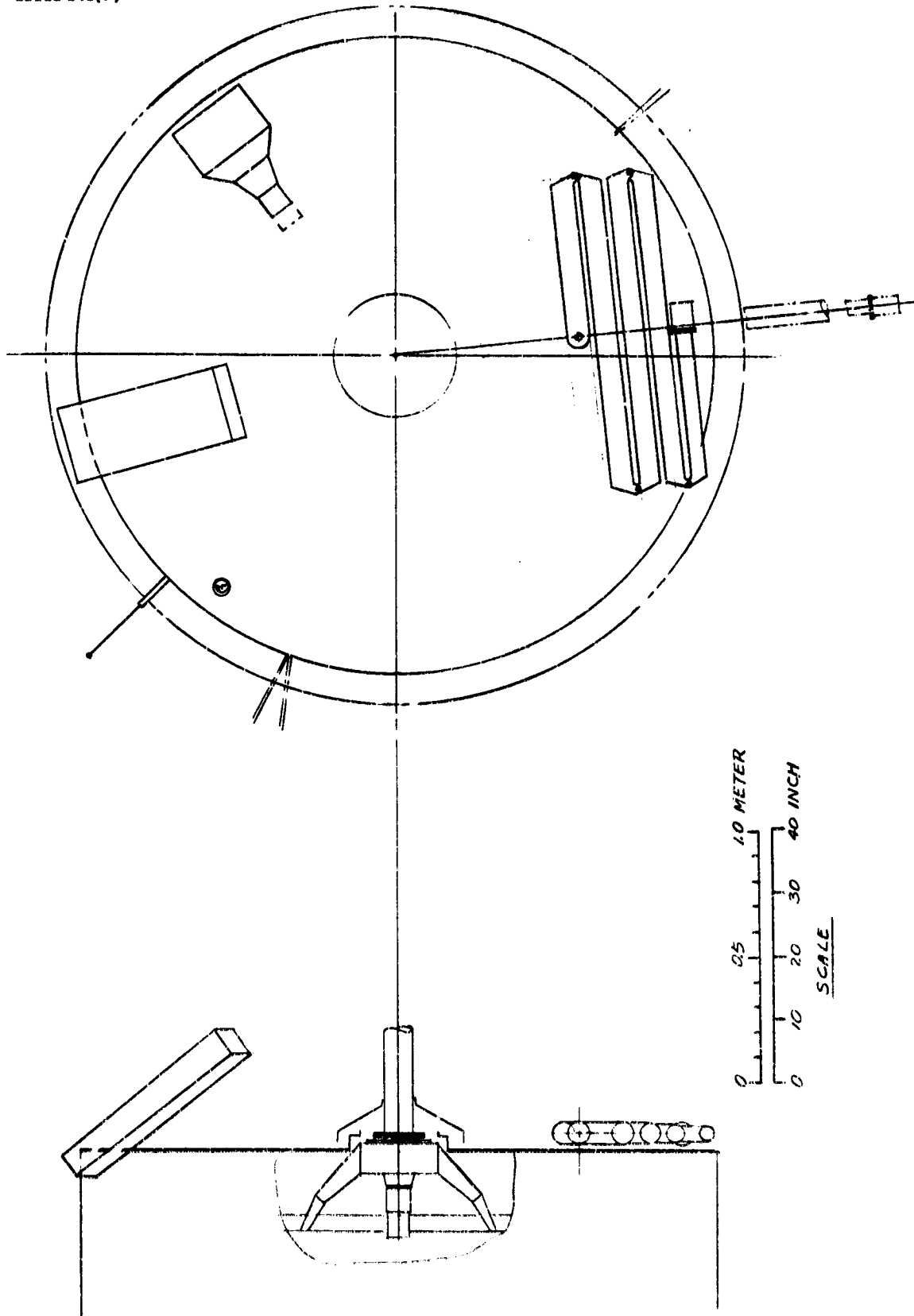


FIGURE 3-13. FIVE LINK MAGNETOMETER BOOM

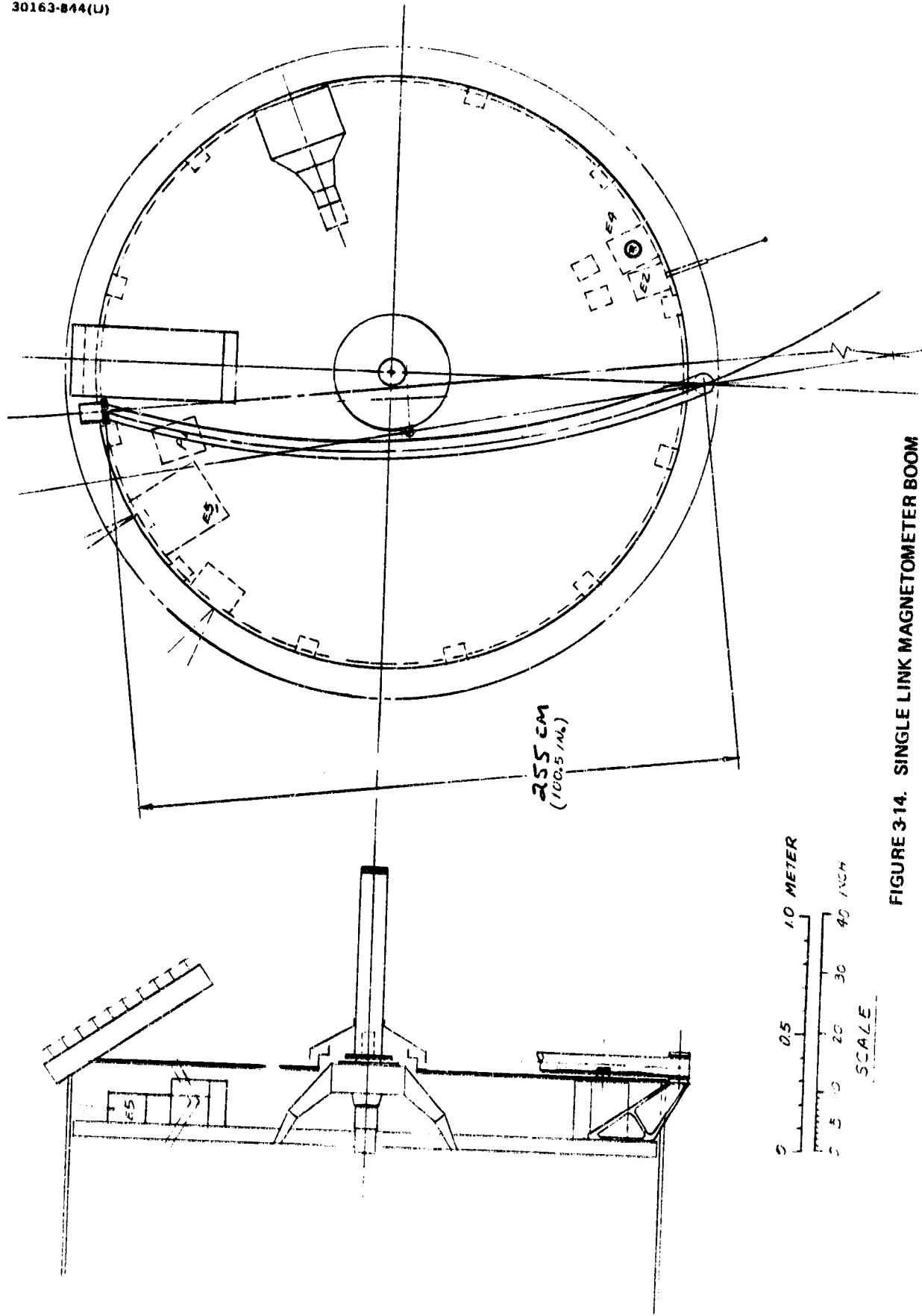


FIGURE 3-14. SINGLE LINK MAGNETOMETER BOOM

In Figure 3-12 the three links are of equal length, has two hinged joints and is pivoted near the perimeter of the spacecraft. The arrangement shown in Figure 3-13 uses three long links and two shorter links of equal lengths, four hinged joints and is pivoted near the shelf mid radius. Each of these arrangements can be accommodated within one quadrant of the upper surface leaving three quadrants unobstructed for science instrument viewing and other protuberances.

In the interest of simplicity a one piece boom was considered. By making the boom curved a maximum separation distance of 2.55 m (8.38 ft) was obtainable. This would require more magnetic control than the longer booms and also sweeps over two of the upper surface quadrants when deploying. Figure 3-14 shows this type of installation.

The integration of the astromast presents the least restriction to placement of other equipment, such as star sensors, axial jets, etc., in the upper plane. The mast is housed in a cylindrical container ~17.78 cm (7.0 in.) in diameter by 25.4 cm (10.0 in.) long. The mast deploys radially and, therefore, is positioned near the shelf outer edge as shown in Figure 3-15.

For all installations depicted, the science instruments and spacecraft equipment were arranged such that nondeployment of the boom would not obscure their field of view. The failure mode of boom nondeployment introduces a pointing error for orbit injection. By increasing the spacecraft spin rate for motor burn from the planned rate of 25 rpm to 60 to 70 rpm the error will be reduced to approximately 2 deg. The effect on c.m. displacement and spin axis tilt for nondeployment is noted in Table 3-19 for the design used at midterm (for reference) for one, three, and five links (see Figures 3-12 through 3-14) and for the Astromast installation (see Figure 3-15).

The approach shown in Figure 3-12 was selected for baseline. It offers minimal magnetic control requirement, lightest mass and fewer hinges (other than the curved one piece boom).

### Configuration Descriptions

The probe and orbiter spacecraft baseline configuration are designed to accommodate the science payload as defined in Volume 2. Another major consideration in the approach to configuring the spacecraft was the objective for maximum commonality between them in the interest of reducing program cost. This was achieved for many aspects and will be noted in the following descriptions of the spacecraft configuration.

Inboard profiles, forward and aft end views, of the baseline spacecraft configurations for the multiprobe and orbiter missions are presented in Figures 3-16 and 3-17, respectively. Equipment shelf arrangements for each spacecraft, with subsystem elements and science instrument locations noted, are depicted in Figures 3-18 and 3-19. A mass summary for major subsystem is presented in Table 3-20 and detailed mass statements in Tables 3-21, 3-22 and 3-23.

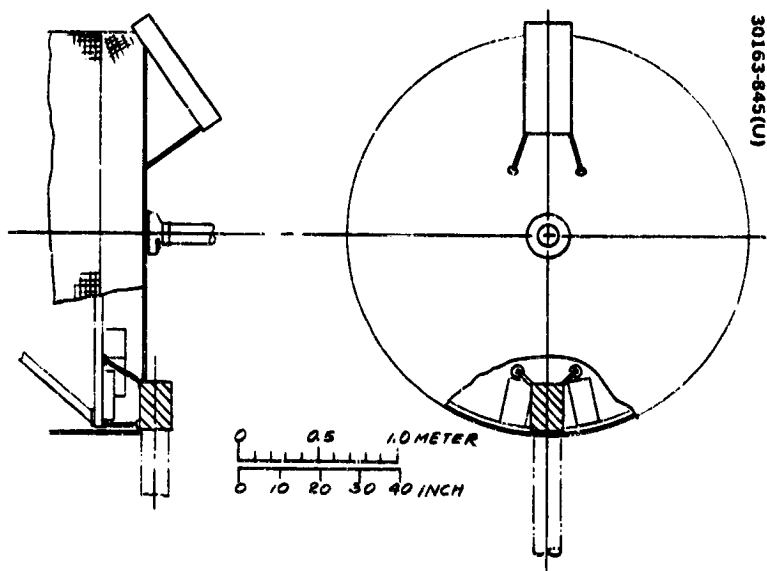


FIGURE 3-15. ASTROMAST MAGNETOMETER BOOM

TABLE 3-19. MAGNETOMETER BOOM CHARACTERISTICS

Condition	Midterm Configuration	Three Equal Links (Figure 3-12)	Five Links (Figure 3-13)	Single Link (Figure 3-14)	Astromast (Figure 3-15)
<b>Stowed, transit</b>					
Spin axis tilt, deg	8.5	5.1	5.2	3.5	3.8
C.M. offset, cm (in.)	2.29 ( 0.90 )	1.52 ( 0.60 )	1.85 ( 0.73 )	0.84 ( 0.33 )	0.84 ( 0.33 )
<b>Stowed, post-orbit injection</b>					
Spin axis tilt, deg	3.9	1.9	1.9	1.3	1.4
C.M. offset, cm (in.)	3.45 ( 1.36 )	2.36 ( 0.93 )	2.84 ( 1.12 )	1.30 ( 0.51 )	1.30 ( 0.51 )
Boom system mass, kg (lb)	3.49 ( 7.7 )	3.27 ( 7.2 )	3.81 ( 8.4 )	2.27 ( 5.0 )	4.13 ( 9.1 )
Boom length*, m (ft)	4.4 ( 14.5 )	4.4 ( 14.5 )	4.4 ( 14.5 )	2.5 ( 8.3 )	4.4 ( 14.5 )

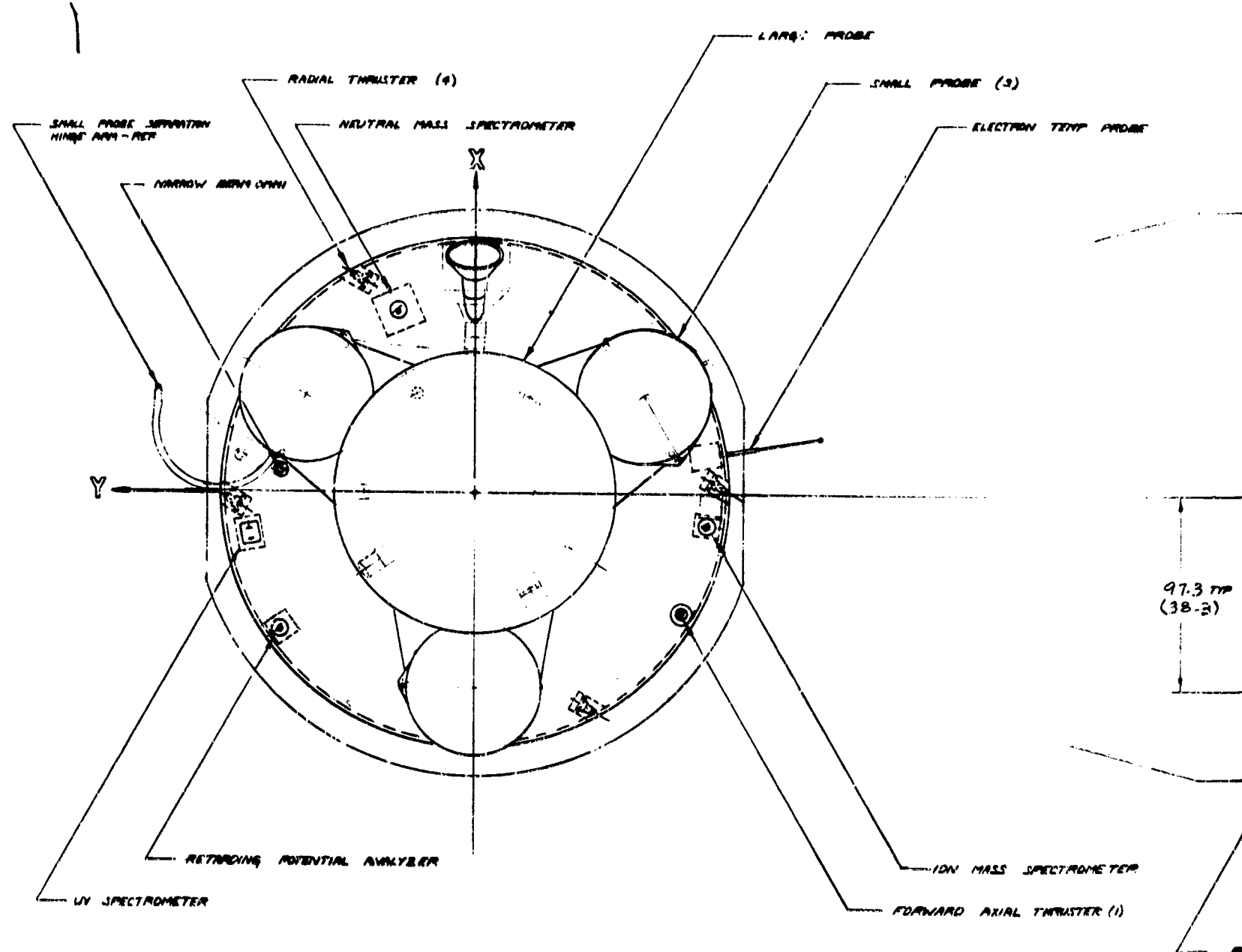
\*Measured from solar panel cylinder

TABLE 3-20. MASS SUMMARY BY MAJOR SUBSYSTEM  
 - ATLAS/CENTAUR BASELINE

Item/Subsystem	Multiprobe Spacecraft Mass		Orbiter Spacecraft Mass	
	kg	lb	kg	lb
Communications subsystem	14.24	31.4	12.84	28.3
Data handling subsystem	7.80	17.2	16.87	37.2
Command subsystem	9.84	21.7	9.84	21.7
Controls subsystem	11.89	26.2	26.26	57.9
Structure and harness subsystem	100.68	235.2	96.03	211.7
Power subsystem	29.44	64.9	30.89	68.1
Propulsion subsystem (dry)	11.57	25.5	12.29	27.1
Orbit insertion motor case	-	-	12.58	27.7
Bus total (dry)	191.46	422.1	217.59	479.7
Large probe	245.12	540.4	-	-
Small probe (3)	190.78	420.6	-	-
Spacecraft subtotal	627.36	1383.1	217.59	479.7
Contingency	149.59	329.8	25.31	55.8
Experiments (bus only)	13.74	30.3	47.54	104.8
Spacecraft total (dry)	790.70	1743.2	290.44	640.3
Propellant	22.23	49.0	26.76	59.0
Pressurant	0.18	0.4	0.20	0.4
Orbit insertion motor expendables	-	-	143.33	316.0
Spacecraft total (wet)	813.11	1792.6	460.70	1015.7
Spacecraft attach fitting	31.30	69.0	31.30	69.0
Launch vehicle payload	844.41	1861.6	492.00	1084.7

FOLDOUT

# FOLDOUT FRAME



REPRODUCIBILITY OF THE ORIGINAL PAGE IS POOR

FIGURE 3-18. ATLAS/CENTAUR PROBE SPACECRAFT BASELINE  
3-65

FOLDOUT FRAME

2

(3)

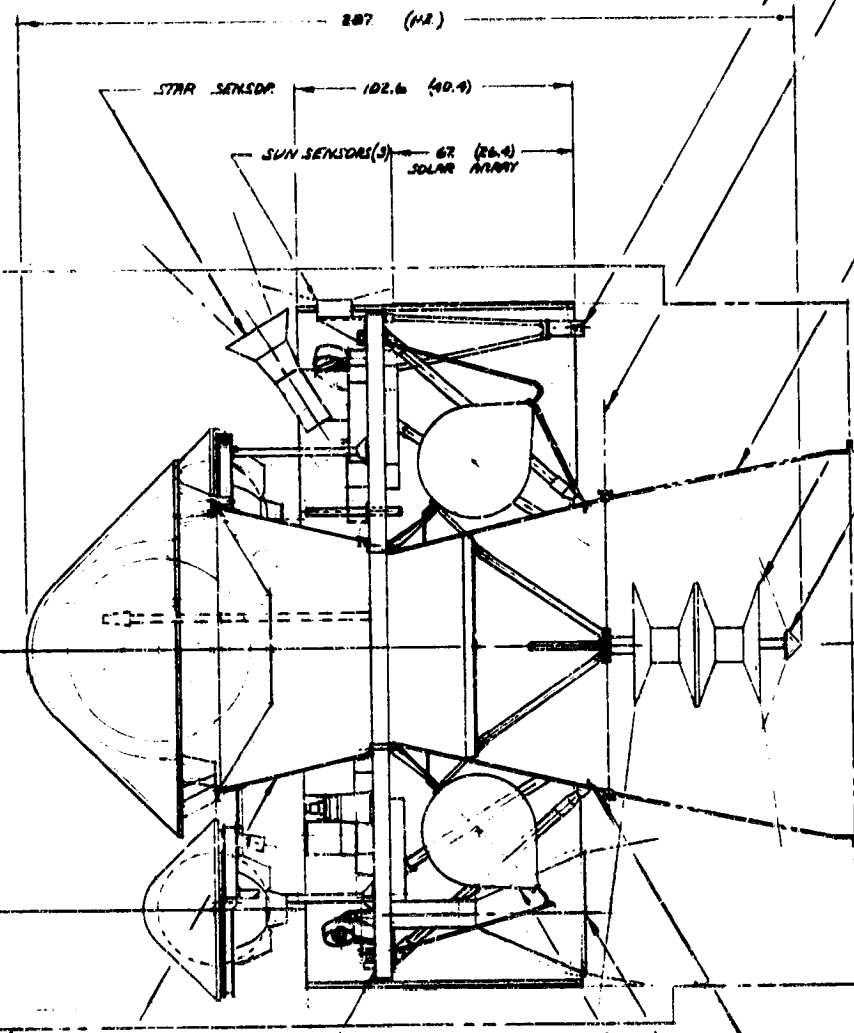
ELECTRON TEMP PROBE

AFT AXIAL THRUSTER - NOT  
ROTATED FOR CLARITY  
SPACECRAFT SEPARATION PLANE

INTELSAT DE ATTACH FITTING

BICOINE ANTENNA

WIDE BEAM GAIN



207 (82)

STAR SENSOR 102.6 (40.4)

SUN SENSOR(S) 62 (26.4)  
SOLAR ARRAY

97.3 mm  
(38.3)

8.5" DIA  
(100)

MASS SPECTROMETER

AXIAL THRUSTER (1)

PAYLOAD DYNAMIC ENVIRONMENT

EQUIPMENT SHELF

LARGE PROBE ATTACH STRUCTURE

THRUST TUBE

MEDIUM GAIN ANTENNA - 17dB

PROPELLANT TANK (8)

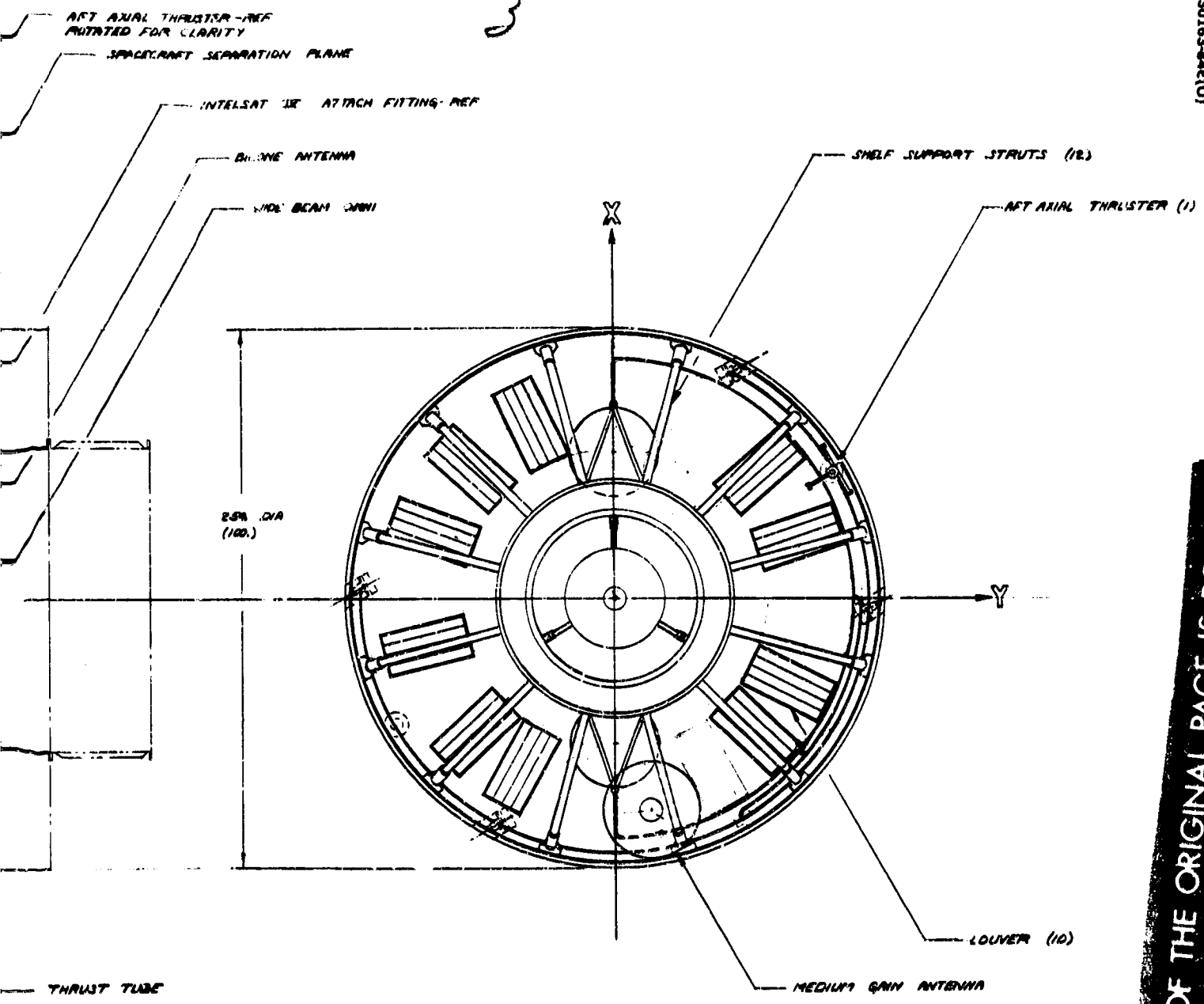
REPRODUCIBILITY OF THE ORIGINAL PAGE IS POOR.



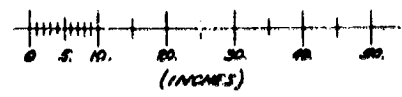
# FOLDOUT FRAME

3

30163-846(U)

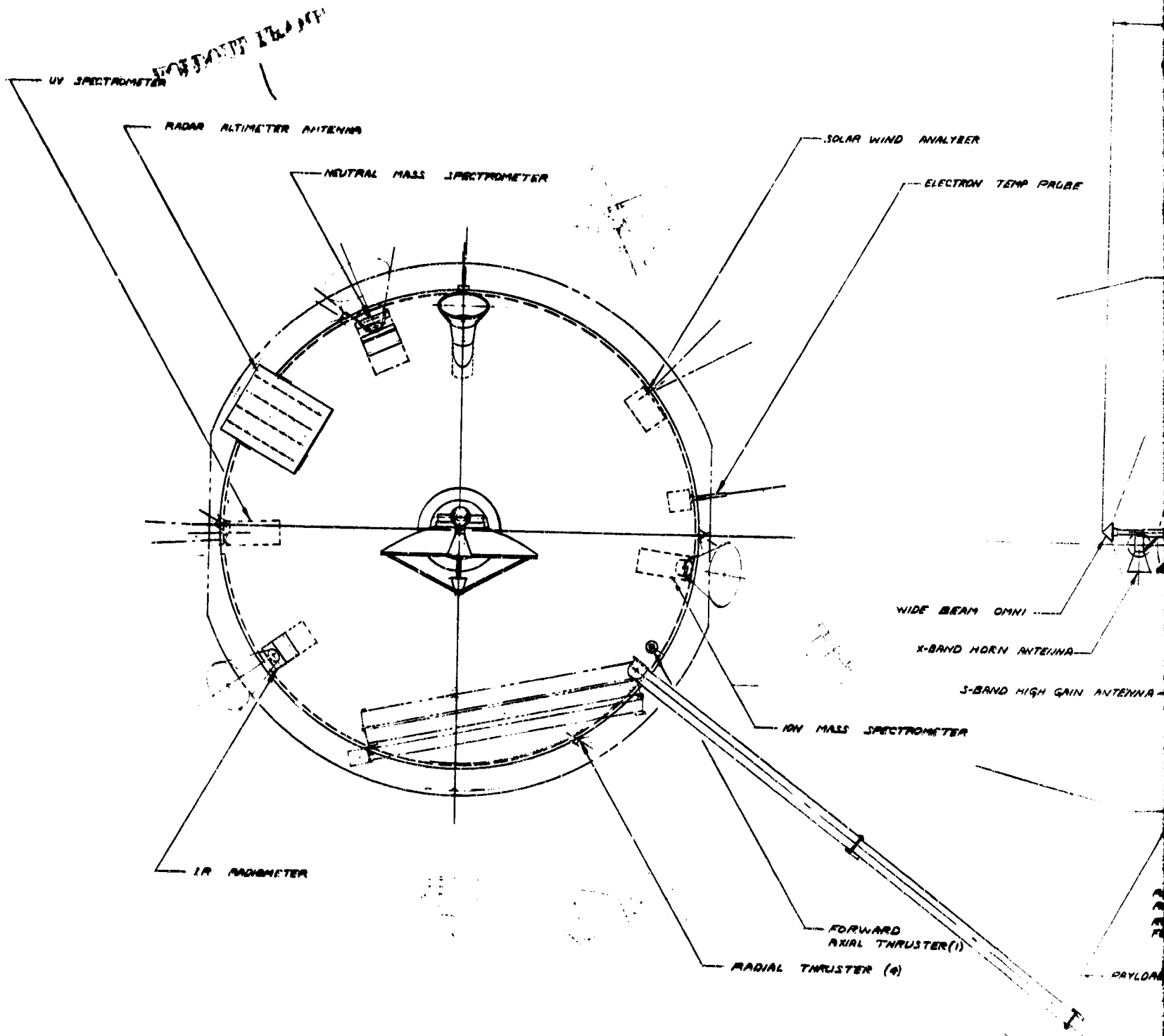


NOTE: INSULATION OMITTED FOR CLARITY



SCALE 1/10

REPRODUCIBILITY OF THE ORIGINAL PAGE IS POOR.

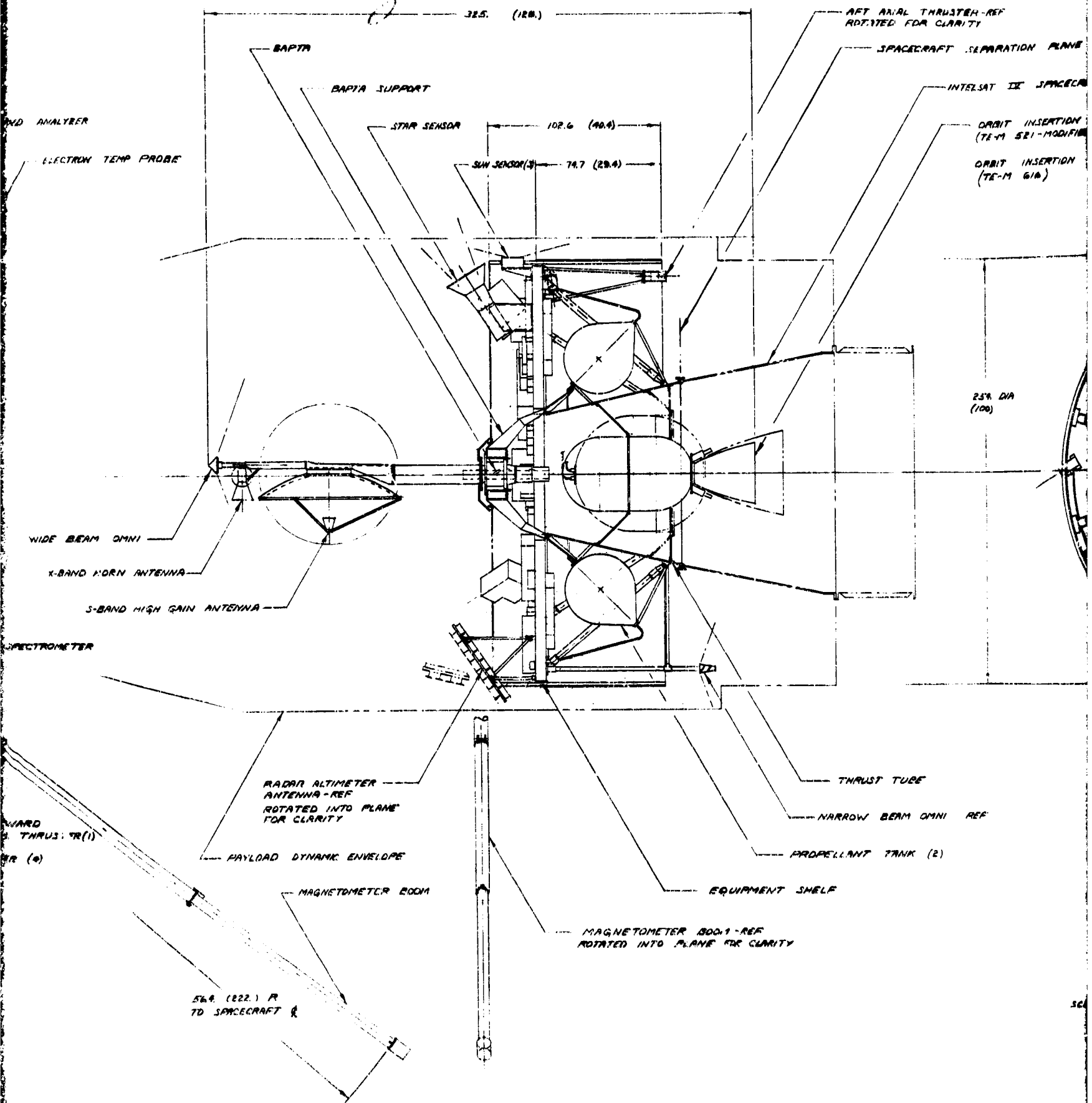


REPRODUCIBILITY OF THE ORIGINAL PAGE IS POOR.

564 (222) M  
TD SPACECRAFT

FIGURE 3-17. ATLAS/CENTAUR ORBITER SPACECRAFT BASELINE  
3-67

HYDRAULIC ALARM

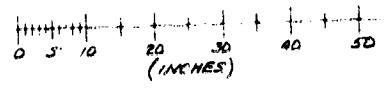
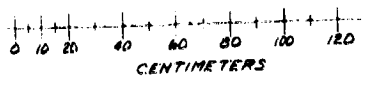
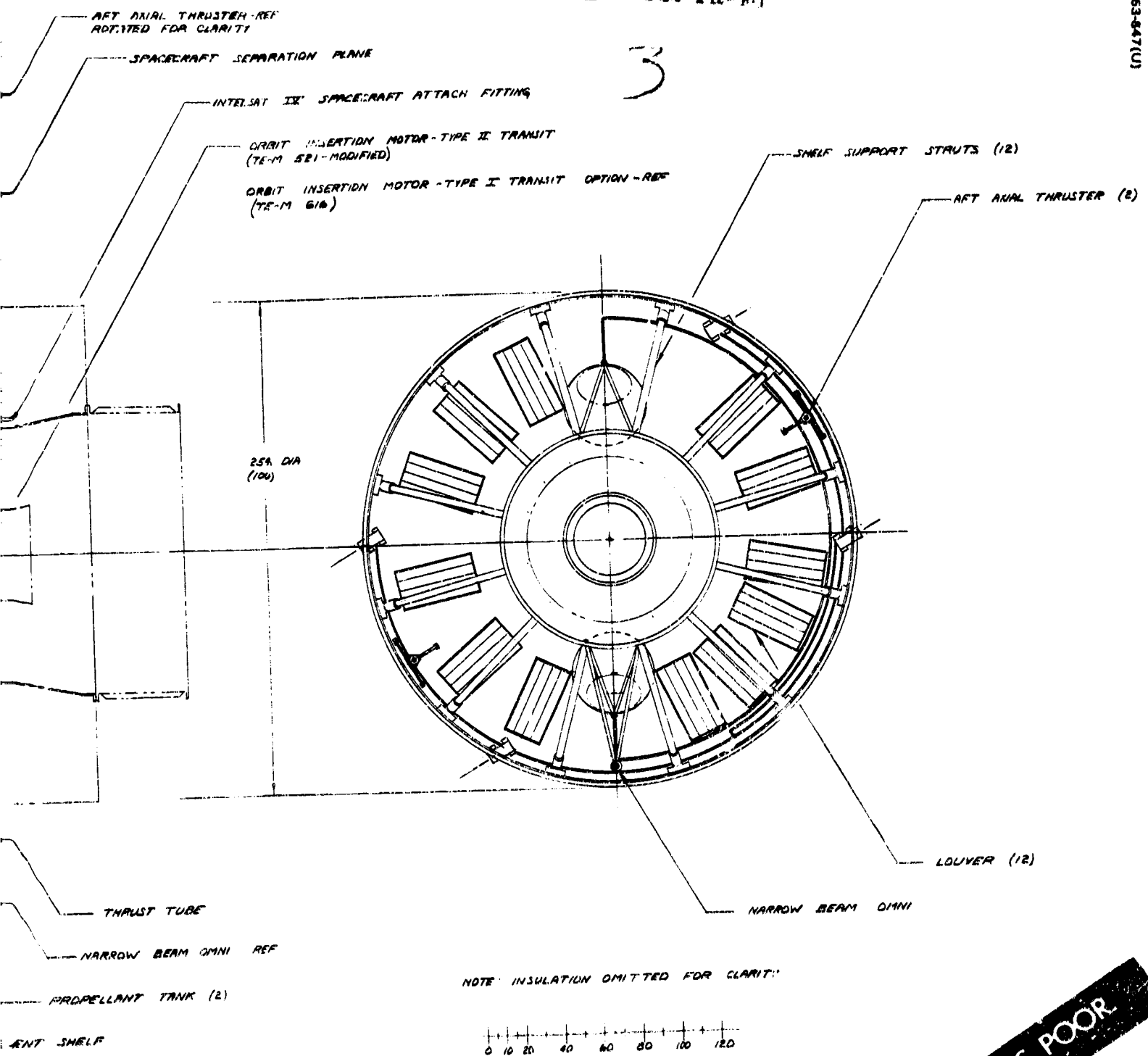


REPRODUCIBILITY OF THE ORIGINAL PAGE IS POOR.

# LOADOUT PLAN

30163-847(U)

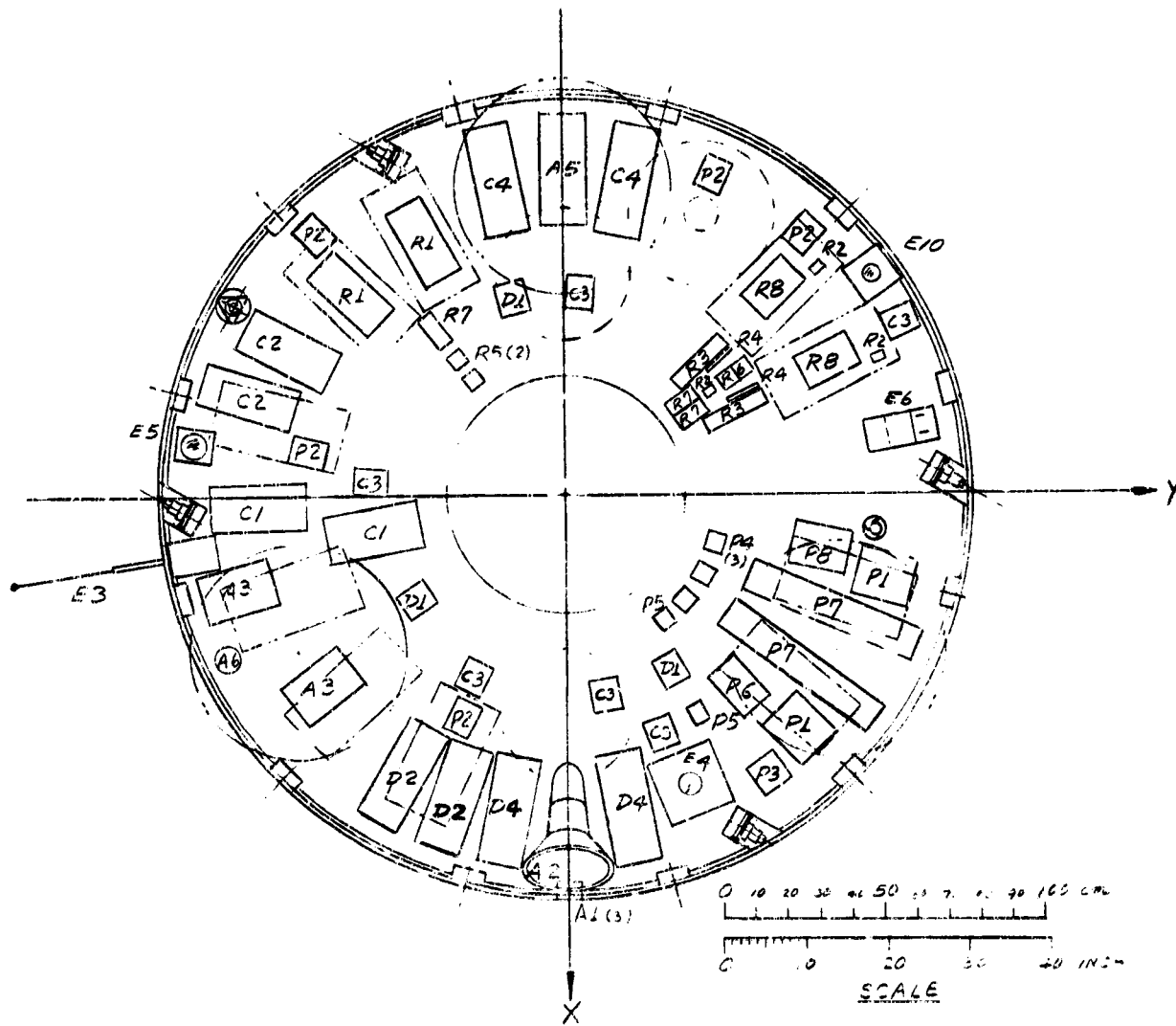
3



SCALE 1/10

**REPRODUCIBILITY OF THE ORIGINAL PAGE IS POOR**

FOLDOUT FRAME



CODE	NOMENCLA
E 1	MAGNETOMETER
2	SOLAR WIND ANALY
3	ELECTPON TEMPERA
4	NEUTRAL MASS SPEC
5	ION MASS SPECTROM
6	UV SPECTROMETER
7	IR RADIOMETER
8	X-BAND OCCULTATIO
9	HADAR ALTIMETER
E 10	RETARDING POTENT
R 1	TRANSPONDER
2	HYBRID
3	FILTER, Tx BP
4	FILTER, HARMONIC
5	CIRCULATOR
6	SPDT SWITCH
7	TRANSFER SWITCH
R 8	POWER AMPLIFIER
U 1	DUAL REMOTE MUL
2	TM PROCESSOR
3	DATA STORAGE
D 4	PCM ENCODER
C 1	COMMAND DEMODU
2	CENTRAL DECODER
3	REMOTE DECODER
C 4	PYRO CONTROL UN
A 1	SUN SENSOR ASSEM
2	STAR SENSOR
3	ATTITUDE DATA PR
4	DESPIN CONTROL E
5	SOLENOID DRIVER
6	NUTATION DAMPER
7	BAPTA
A 8	MAGNETOMETER D
P 1	CHARGE DISCHARG
2	BUS LIMITER
3	UNDERVOLTAGE S
4	CURRENT SENSOR
5	HEATER SWITCH
6	POWER INTERFAC
7	BATTERY
P 8	PROBE BATTERY C

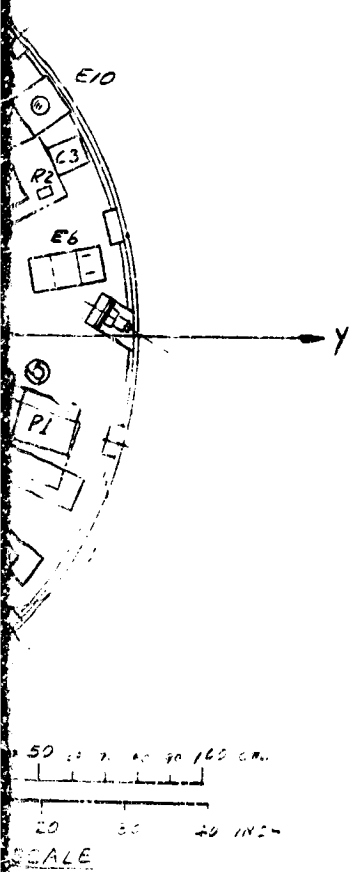
FIGURE 3-18. PROBE BUS SHELF ARRANGEMENT

REPRODUCIBILITY OF THE ORIGINAL PAGE IS POOR.

# BOLDOUT FRAME

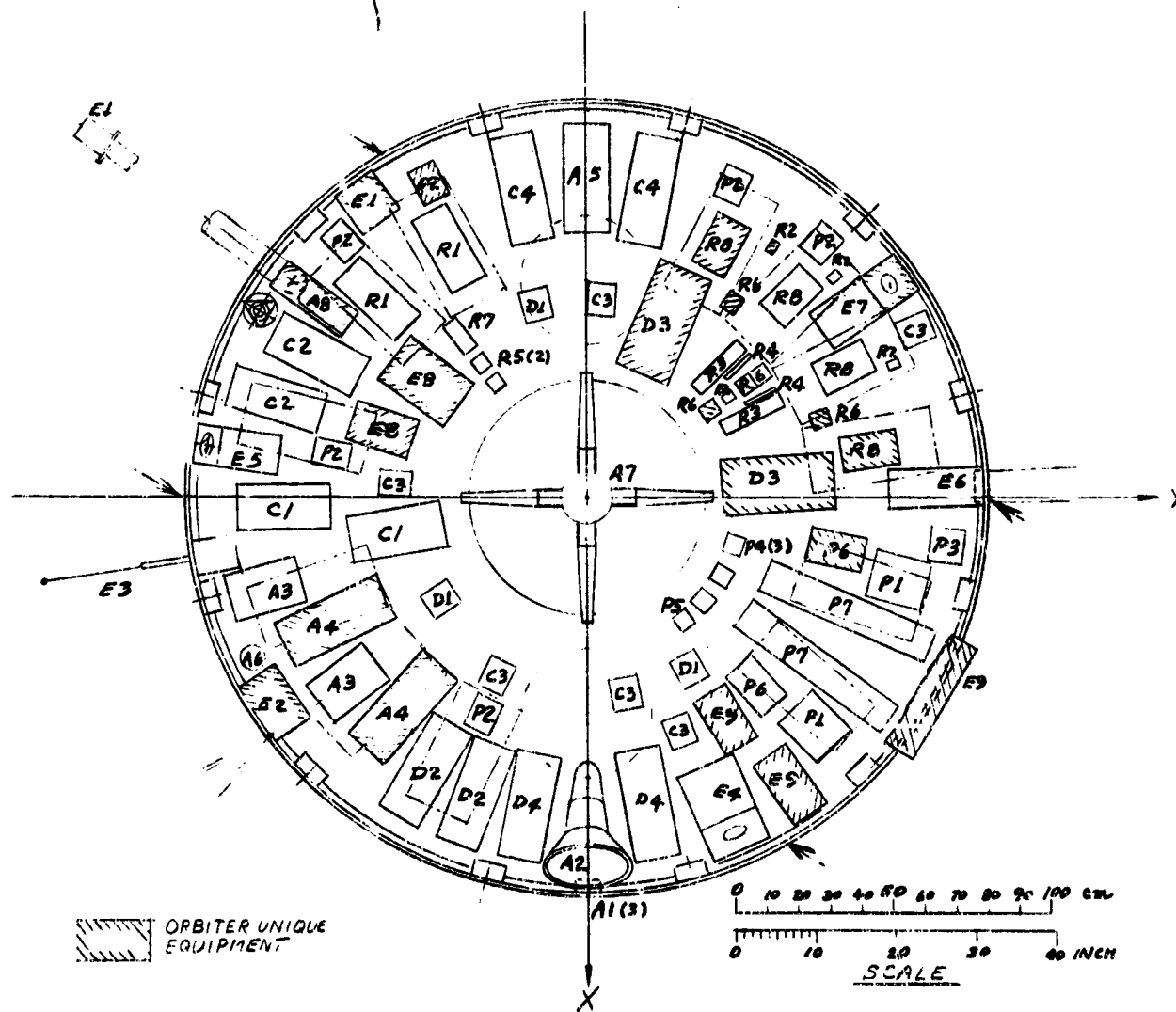
30163-848(U)

CODE	NOMENCLATURE	NO. REQUIRED
E 1	MAGNETOMETER	
2	SOLAR WIND ANALYZER	
3	ELECTRON TEMPERATURE PROBE	1
4	NEUTRAL MASS SPECTROMETER	1
5	ION MASS SPECTROMETER	1
6	UV SPECTROMETER	1
7	IR RADIOMETER	
8	X-BAND OCCULTATION	
9	RADAR ALTIMETER	
E 10	RETARDING POTENTIAL ANALYZER	1
R 1	TRANSPONDER	1
2	HYBRID	2
3	FILTER, Tx BP	2
4	FILTER, HARMONIC	2
5	CIRCULATOR	2
6	SPDT SWITCH	3
7	TRANSFER SWITCH	3
R 8	POWER AMPLIFIER	2
D 1	DUAL REMOTE MULTIPLEXER	3
2	TM PROCESSOR	2
3	DATA STORAGE	
D 4	PCM ENCODER	2
C 1	COMMAND DEMODULATOR	2
2	CENTRAL DECODER	2
3	REMOTE DECODER	6
C 4	PYRO CONTROL UNIT	2
A 1	SUN SENSOR ASSEMBLY	2
2	STAR SENSOR	1
3	ATTITUDE DATA PROCESSOR	2
4	DESPIN CONTROL ELECTRONICS	
5	SOLENOID DRIVER	1
6	NUTATION DAMPER	1
7	BAPTA	
A 8	MAGNETOMETER DEPLOY ASSEMBLY	
P 1	CHARGE/DISCHARGE CONTROLLER	2
2	BUS LIMITER	6
3	UNDERVOLTAGE SWITCH	1
4	CURRENT SENSOR	3
5	HEATER SWITCH	1
6	POWER INTERFACE UNIT	1
7	BATTERY	2
P 8	PROBE BATTERY CHARGER	1



NT

FOLDOUT FRAME



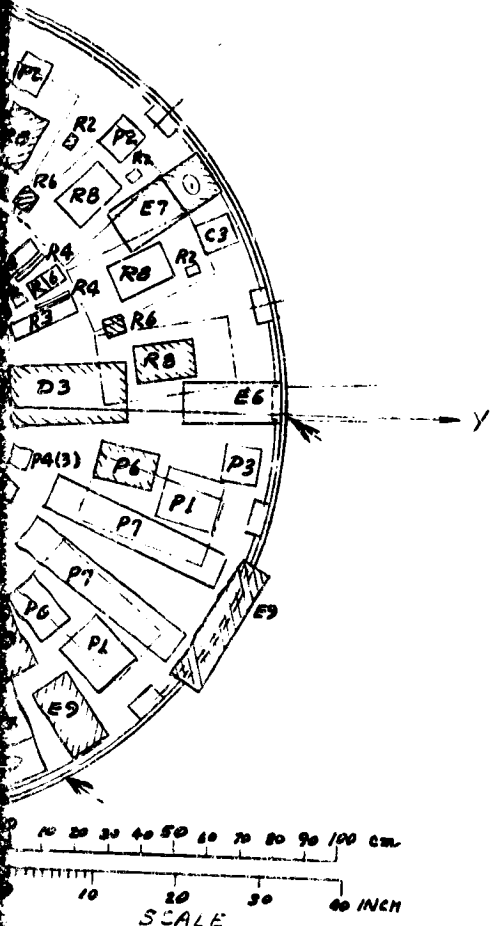
CODE	NOM
E 1	MAGNETOMET
2	SOLAR WIND A
3	ELECTRON TEL
4	NEUTRAL MAS
5	ION MASS SPEC
6	UV SPECTROM
7	IR RADIOMET
8	X-RAND OCCU
9	RADAR ALTIM
E 10	RETARDING P
R 1	TRANSPONDE
2	HYBRID
3	FILTER, Tx BP
4	FILTER, HARM
5	CIRCULATOR
6	SPDT SWITCH
7	TRANSFER SW
R 8	POWER AMPLI
D 1	DUAL REMOT
2	TM PROCESS
3	DATA STORA
D 4	PCM ENCODE
C 1	COMMAND DE
2	CENTRAL DE
3	REMOTE DE
C 4	PYRO CONTR
A 1	SUN SENSOR
2	STAR SENSOR
3	ATTITUDE DA
4	DESPIN CONT
5	SOLENOID D
6	NUTATION D
7	BAPTA
A 8	MAGNETOME
P 1	CHARGE/DIS
2	BUS LIMITER
3	UNDERVOLT
4	CURRENT SE
5	HEATER SWI
6	POWER INTE
7	BATTERY
P 8	PROBE BATT

FIGURE 3-19. ORBITER SHELF ARRANGEMENT

REPRODUCIBILITY OF THE ORIGINAL PAGE IS POOR.

WITHOUT FRAME

10163-849(U)



CODE	NOMENCLATURE	NO. REQUIRED
E 1	MAGNETOMETER	1
2	SOLAR WIND ANALYZER	1
3	ELECTRON TEMPERATURE PROBE	1
4	NEUTRAL MASS SPECTROMETER	1
5	ION MASS SPECTROMETER	1
6	UV SPECTROMETER	1
7	IR RADIOMETER	1
8	X-BAND OCCULTATION	1
9	RADAR ALTIMETER	1
E 10	RETARDING POTENTIAL ANALYZER	1
R 1	TRANSPONDER	2
2	HYBRID	4
3	FILTER, Tx BP	2
4	FILTER, HARMONIC	2
5	CIRCULATOR	2
6	SPDT SWITCH	2
7	TRANSFER SWITCH	6
R 8	POWER AMPLIFIER	4
D 1	DUAL REMOTE MULTIPLEXER	3
2	TM PROCESSOR	2
3	DATA STORAGE	2
D 4	PCM ENCODER	2
C 1	COMMAND DEMODULATOR	2
2	CENTRAL DECODER	2
3	REMOTE DECODER	6
C 4	PYRO CONTROL UNIT	2
A 1	SUN SENSOR ASSEMBLY	2
2	STAR SENSOR	1
3	ATTITUDE DATA PROCESSOR	2
4	DESPIN CONTROL ELECTRONICS	2
5	SOLENOID DRIVER	1
6	NUTATION DAMPER	1
7	BAPTA	1
A 8	MAGNETOMETER DEPLOY ASSEMBLY	1
P 1	CHARGE/DISCHARGE CONTROLLER	2
2	BUS LIMITER	6
3	UNDERVOLTAGE SWITCH	1
4	CURRENT SENSOR	3
5	HEATER SWITCH	1
6	POWER INTERFACE UNIT	2
7	BATTERY	2
P 8	PROBE BATTERY CHARGER	1

ANGEMENT



TABLE 3-21. DETAIL MASS STATEMENT PROBE SPACECRAFT  
ATLAS/CENTAUR BASELINE

Description	Mass	
	kg	lb
Communications subsystem	<u>14.24</u>	<u>31.4</u>
Transponder (2)	3.99	8.8
Hybrid (2)	0.05	0.1
Filter - TxBP (2)	0.91	2.0
Filter - harmonic (2)	0.09	0.2
Circulator - isolator (2)	0.23	0.5
SPDT switch (3)	0.36	0.8
Transfer switch (3)	0.95	2.1
Power amplifier (2)	1.72	3.8
Coax	1.13	2.5
Bicone antenna	3.45	7.6
Medium gain antenna	0.71	2.0
Omni (wide beam)	0.27	0.6
Omni (narrow beam)	0.18	0.4
Data handling subsystem	<u>7.80</u>	<u>17.2</u>
Remote multiplexers (3)	1.09	2.4
Telemetry Processor (2)	3.63	8.0
PCM encoder (2)	3.08	6.8
Command subsystem	<u>9.84</u>	<u>21.7</u>
Command demodulator (2)	2.54	5.6
Central decoder (2)	4.26	9.4
Remote decoder (6)	1.91	4.2
Pyro control unit (2)	1.13	2.5
Controls subsystem	<u>11.89</u>	<u>26.2</u>
Sun sensor assembly (2)	0.32	0.7
Star sensor	2.49	5.5
Attitude data processor (2)	3.27	7.2
Solenoid driver	1.04	2.3
Nutation damper	1.36	3.0
Separation switch (2)	0.45	1.0
Louver (10)	2.95	6.5

TABLE 3-21 (Continued)

Description	Mass	
	kg	lb
Structure and harness subsystem	<u>106.68</u>	<u>235.2</u>
Equipment shelf	21.09	46.5
Shelf support struts	1.95	4.3
Strut fittings	1.54	3.4
Thrust tube	14.47	31.9
Large probe attach structure	13.83	30.5
Omni boom (2)	0.18	0.4
Medium gain antenna bracketry	1.36	3.0
Bicone antenna support structure	1.36	3.0
Cylindrical substrate	13.83	30.5
Small probe attach structure	4.58	10.1
Propellant tank support	1.77	3.9
Thruster support	2.72	6.0
Balance weight	2.72	6.0
Miscellaneous hardware	1.81	4.0
Thermal blankets	11.43	25.2
Shelf doublers	2.27	5.0
Thermal coatings	0.91	2.0
Temperature sensors	0.09	0.2
Wire harness	8.75	19.3
Power subsystem	<u>29.44</u>	<u>64.9</u>
Battery (2)	11.16	24.6
Undervoltage switch	0.77	1.7
Charge/discharge controllers (2)	3.36	7.4
Bus limiter (5)	3.13	6.9
Solar array (excludes substrate)	7.57	16.7
Power interface unit	0.68	1.5
Current sensors (3)	0.50	1.1
Probe battery charger	1.81	4.0
Heater switch unit (2)	0.45	1.0

TABLE 3-21 (Continued)

Description	Mass	
	kg	lb
Propulsion Subsystem (dry)	<u>11.57</u>	<u>25.5</u>
Propellant tanks (2)	5.35	11.8
Thrusters (6)	1.63	3.6
Propellant valve (6)	1.36	3.0
Latch valve (4)	0.54	1.2
Fill valve	0.14	0.3
Filter (4)	0.54	1.2
Pressure transducer	0.23	0.5
Tubing	0.32	0.7
Fittings	45	1.0
Thruster valve heaters (6)	0.05	0.1
Thruster insulation (6)	0.45	1.0
Temperature sensors (8)	0.09	0.2
Propellant plenums (2)	0.14	0.3
Propellant tank heater (2)	0.27	0.6
Bus total (dry)	<u>191.46</u>	<u>422.1</u>
Large probe	245.12	540.4
Deceleration module	<u>92.62</u>	<u>204.2</u>
Heat shield subsystem	(35.52)	(78.3)
Heat shield	35.52	78.3
Structure subsystem	(47.99)	(105.8)
Acroshell structure	15.47	34.1
Internal structure	23.68	52.2
Ballast	1.36	3.0
Aft cover structure	7.48	16.5
Aft cover insulation	-	-
Instrumentation and harness subsystem	(1.91)	(4.2)
Ablation sensor	0.14	0.3
Temperature sensors (3)	0.05	0.1
Wire harness	1.72	3.8

TABLE 3-21 (Continued)

Description	Mass	
	kg	lb
Parachute subsystem	(4.72)	(10.4)
Main parachute	3.27	7.2
Pilot chute	0.50	1.1
Motor	0.45	1.0
Explosive nut assembly (3)	0.50	1.1
Separation subsystem	(2.49)	(5.5)
Bus separation explosive nut assembly (3)	.45	1.0
Bus separation spring assembly (2)	0.77	1.7
In-flight disconnect	0.59	1.3
Pressure vessel separation explosive Nut assembly (3)	-	-
	0.68	1.5
Pressure Vessel Module	<u>152.50</u>	<u>336.2</u>
Communications subsystem	(5.99)	(13.2)
Transponder	2.00	4.4
Filter, TxBP	0.45	1.0
Filter, harmonic	0.05	0.1
Circulator	0.09	0.2
Output amplifier (4)	2.18	4.8
Driver	0.23	0.5
Isolator (2)	0.23	0.5
Three-way summer/divider (2)	0.18	0.4
Coaxial	0.32	0.8
Hemispheric omni antenna	0.27	0.5
Command and data handling subsystem	(3.54)	(7.8)
Command/data unit	1.95	4.3
Pyro control unit	1.18	2.6
Acceleration switch (2)	0.23	0.5
Pressure switch (2)	0.18	0.4
Power subsystem	(12.93)	(28.5)
Battery	10.52	23.2
Power interface unit	2.22	4.9
Current sensor	0.18	0.4

TABLE 3-21 (Continued)

Description	Mass	
	kg	lb
Structure and harness subsystem	(98.43)	(217.0)
Aerodynamic fairing	4.03	9.0
Pressure vessel shell	47.36	104.4
Insulating retainer	2.27	5.0
Shelves (2) (includes heat sink)	23.68	52.2
Shelf interconnect	3.36	7.4
Adapter	3.90	8.6
Flanges (2)	8.80	19.4
Main, pressure seal	-	-
Pressure gauge	0.18	0.4
Strain gauges (3)	0.27	0.6
Wire harness, external	0.14	0.3
Wire harness, internal	0.73	1.6
Cable cutter assembly	0.18	0.4
Penetrations	(1.27)	(2.8)
Electrical feed throughs (5)	0.09	.2
Ports (5)	0.45	1.0
Windows (3)	0.73	1.6
Insulation	1.13	2.5
Temperature sensors (5)	0.05	0.1
Heaters (air)	0.14	0.3
Miscellaneous hardware	0.91	2.0
Scientific instruments	(31.62)	(69.7)
Temperature gauge	.36	0.8
Pressure gauge	.45	1.0
Accelerometers	1.32	2.9
Neutral mass spectrometer	10.43	23.0
Cloud particle size analyzer	4.17	9.2
Solar radiometer	2.63	5.8
Gas chromatograph	4.45	9.8
Wind altitude radar	4.58	10.1
Hygrometer	0.59	1.3
IR flux radiometer	2.63	0.8
Small probe (3)	<u>190.78</u>	<u>420.6</u>
Small probe (1)	<u>63.59</u>	<u>140.2</u>

TABLE 3-21 (Continued)

Description	Mass	
	kg	lb
Deceleration module	<u>25.17</u>	<u>55.5</u>
Heat shield subsystem	(10.02)	(22.1)
Heat shield	10.02	22.1
Structure subsystem	(13.61)	(30.0)
Aeroshell structure	7.48	16.5
Internal structure	5.35	11.8
Fins (4)	0.32	0.7
Pressure port adapter	0.09	0.2
Ballast	0.36	0.8
Harness subsystem	(0.18)	(0.4)
Wire harness	0.18	0.4
Separation/design subsystem	(1.36)	(3.0)
Spin rockets (2)	0.18	0.4
Bolt thruster	0.18	0.4
Hinge arm and open latch	0.41	0.9
In-flight disconnect	0.59	1.3
Pressure vessel module	<u>38.42</u>	<u>84.7</u>
Communications subsystem	(1.86)	(4.1)
Exciter	0.64	1.4
Stable oscillator (see scientific instruments)	-	-
Output amplifier	0.54	1.2
Isolator	0.14	0.3
Driver	0.18	0.4
Coaxial	0.14	0.3
Hemispheric omni antenna	0.23	0.5
Command and data handling subsystem	(2.68)	(5.9)
Command/data unit	1.54	3.4
Regulator unit	0.18	0.4
Pyro control unit	0.54	1.2
Acceleration switch (2)	0.23	0.5
Pressure switch (2)	0.18	0.4
Power subsystem	(5.17)	(11.4)
Battery	3.63	8.0
Power interface unit	1.36	3.0
Current sensor	0.18	0.4

TABLE 3-21 (Continued)

Description	Mass	
	kg	lb
Structure and harness subsystem	(26.08)	(57.5)
Pressure vessel shell	10.07	22.2
External insulation (ESM)	0.18	0.4
Insulation retainer	1.04	2.3
Shelves (2) (includes heat sink)	8.26	18.2
Shelf interconnect	1.32	2.9
Flanges (2)	2.31	5.1
Main pressure seal	-	-
Pressure gauge	0.18	0.4
Antenna cover	0.05	0.1
Fin adapters (4)	0.09	0.2
Temperature gauge support arm	0.23	0.5
Temperature gauge release mech	0.14	0.3
IR flux detector arm	0.23	0.5
IR flux detector release mech	0.14	0.3
Wiring harness, external }	0.27	0.6
Wiring harness, internal }		
Penetrations	(0.41)	(0.9)
Electrical feed throughs (3)	0.05	0.1
Ports (3)	0.09	0.2
Windows (2)	0.27	0.6
Temperature sensors (4)	0.05	0.1
Miscellaneous hardware	0.68	1.5
Internal insulation	0.36	0.8
Heaters (air)	0.09	0.2
Scientific instruments	(2.63)	(5.8)
Temperature gauge	0.36	0.8
Pressure gauge	0.45	1.0
Nephelometer	0.54	1.2
Accelerometer	0.23	0.5
IR flux detector	0.64	1.4
Stable oscillator	0.41	0.9
Spacecraft subtotal	627.36	1383.1
Contingency	<u>149.59</u>	<u>329.8</u>

TABLE 3-21 (Continued)

Description	Mass	
	kg	lb
Experiments (bus)	<u>13.74</u>	<u>30.3</u>
Neutral mass spectrometer	6.26	13.8
Ion mass spectrometer	1.81	4.0
Electron temperature probe	1.13	2.5
UV spectrometer	3.13	6.9
Retarding potential analyzer	1.41	3.1
Spacecraft total (dry)	790.70	1743.2
Propellant	22.23	49.0
Pressurant	0.18	0.4
Spacecraft total (wet)	813.11	1792.6
Spacecraft attach fitting	31.30	69.0
Launch vehicle payload	844.41	1861.6



TABLE 3-22. DETAIL MASS STATEMENT ORBITER  
MISSION -- ATLAS/CENTAUR BASELINE

Description	Mass	
	kg	lb
Communications subsystem	<u>12.84</u>	<u>28.3</u>
Transponder (2)	3.99	8.8
Hybrid (4)	0.09	0.2
Filter - TxBP (2)	0.91	2.0
Filter - harmonic (2)	0.09	0.2
Circulator - isolator (2)	0.23	0.5
SPDT switch (6)	0.68	1.5
Transfer switch	0.32	0.7
Power amplifier (4)	3.45	7.6
Coax cables	1.22	2.7
High gain antenna	1.41	3.1
Omni (widebeam)	0.27	0.6
Omni (narrowbeam)	0.18	0.4
Data handling subsystem	<u>16.87</u>	<u>37.2</u>
Remote multiplexers (3)	1.09	2.4
Telemetry processor (2)	3.63	8.0
Data storage unit (2)	9.07	20.0
PCM encoder (2)	3.08	6.8
Command subsystem	<u>9.84</u>	<u>21.7</u>
Command demodulator (2)	2.54	5.6
Central decoder (2)	4.26	9.4
Remote decoder (6)	1.90	4.2
Pyro control unit (2)	1.13	2.5
Control Subsystem	<u>26.26</u>	<u>57.9</u>
Sun sensor assembly (2)	0.32	0.7
Star sensor	2.49	5.5
Attitude data processor (2)	3.27	7.2
Despin control electronics (2)	3.90	8.6
Solenoid driver	1.04	2.3
Nutation damper	1.36	3.0
BAPTA	6.62	14.6
Magnetometer deployment mechanism	3.27	7.2
Separation switch (2)	0.45	1.0
Louver (12)	3.54	7.8

TABLE 3-22. (Continued)

Description	Mass	
	kg	lb
Structure subsystem	<u>96.03</u>	<u>211.7</u>
Equipment shelf	21.09	46.5
Shelf support struts	1.95	4.3
Strut fittings	1.54	3.4
Thrust tube	14.47	31.9
BAPTA support	2.22	4.9
High gain antenna mast	2.59	5.7
Omni and X-band mast (2)	0.32	0.7
Cylindrical substrate	13.83	30.5
Propellant tank supports (2)	1.77	3.9
Thruster supports (7)	2.95	6.5
Motor attach ring	2.22	4.9
Balance weights	2.72	6.0
RF altimeter support	0.68	1.5
Miscellaneous hardware	1.81	4.0
Thermal blanket	10.52	23.2
Shelf doubler	2.27	5.0
Thermal coating	0.91	2.0
Temperature sensor (21)	0.14	0.3
Wire harness	12.02	26.5
Power subsystem	<u>30.89</u>	<u>68.1</u>
Battery (2)	11.16	24.6
Undervoltage switch	0.77	1.7
Solar array (excludes substrate)	8.39	18.5
Bus limiter (6)	3.76	8.3
Charge/discharge controller (2)	3.36	7.4
Overload control unit (2)	2.72	6.0
Current sensors (3)	0.50	1.1
Heater switch unit	0.23	0.5
Propulsion subsystem (dry)	<u>12.29</u>	<u>27.1</u>
Propellant tanks (2)	5.35	11.8
Thrusters (7)	1.91	4.2
Propellant valve (7)	1.59	3.5
Latching valve (2)	0.54	1.2
Fill valve	0.14	0.3
Filter (4)	0.54	1.2
Pressure transducer	0.23	0.5
Tubing	0.45	1.0
Fittings	0.45	1.0
Thruster valve heaters (7)	0.05	0.1

TABLE 3-22 (Continued)

Description	Mass	
	kg	lb
Thruster insulation (7)	0.54	1.2
Temperature sensors (9)	0.09	0.2
Propellant plenum	0.14	0.3
Propellant tank heaters (2)	0.27	0.6
Orbit insertion motor case	<u>12.58</u>	<u>27.7</u>
Motor case (burned out)	12.52	27.6
Nozzle heater	0.04	0.1
Temperature sensor (2)	0.02	0.0
Bus total (dry)	217.59	479.7
Spacecraft subtotal	217.59	479.7
Contingency	25.31	55.8
Experiments (bus only)	<u>47.54</u>	<u>104.8</u>
Magnetometer	4.04	8.9
Solar wind analyzer	5.76	12.7
Electron temperature probe	1.59	3.5
Neutral mass spectrometer	6.26	13.8
Ion mass spectrometer	1.68	3.7
Ultraviolet spectrometer	6.26	13.8
IR radiometer	6.26	13.8
Radar altimeter	10.43	23.0
X-band occultation	(5.26)	(11.6)
X-band driver	1.36	3.0
X-band TWTA	2.27	5.0
Isolator	0.05	0.1
Rotary joint	0.41	0.9
Coax	0.27	0.6
Antenna	0.23	0.5
Contingency (15 percent)	0.68	1.5
Spacecraft total (dry)	<u>290.44</u>	<u>640.3</u>
Propellant	<u>26.76</u>	<u>59.0</u>
Pressurant	<u>0.20</u>	<u>0.4</u>
Orbit insertion motor expendables	<u>143.36</u>	<u>316.0</u>
Spacecraft total (wet)	<u>460.70</u>	<u>1015.7</u>
Spacecraft attach fitting	31.30	69.0
Launch vehicle payload	<u>492.00</u>	<u>1084.7</u>

TABLE 3-23. VENUS MASS PROPERTIES ANALYSIS  
ATLAS/CENTAUR BASELINE MISSION PROFILE

CONDITION	MASS		CENTER OF GRAVITY		I <sub>X</sub>			I <sub>Y</sub>			I <sub>Z</sub>		I <sub>R</sub> /I <sub>T</sub>
	Kg	Lb	X	Y	Kg-ft <sup>2</sup>	Kg-ft <sup>2</sup>	Kg-ft <sup>2</sup>	Kg-ft <sup>2</sup>	Kg-ft <sup>2</sup>	Kg-ft <sup>2</sup>	Slug-ft <sup>2</sup>	Slug-ft <sup>2</sup>	
<u>MULTIPROBE SPACECRAFT</u>													
At Launch	813.11	1797	.135	53.0	398.1	293.6	409.7	302.2	511.3	377.1	1.26		
After Large Probe Separation	486.75	1073.1	1.15	45.4	311.7	229.9	318.3	234.8	467.6	344.9	1.48		
After Sma'1 Probe Separation	237.27	523.1	.636	32.9	134.5	99.20	139.9	103.2	219.2	161.7	1.60		
Spent Spacecraft	230.52	506.2	.846	33.3	133.4	98.42	135.8	100.2	216.1	159.4	1.60		
<u>ORBITER SPACECRAFT</u>													
At Launch, Boom Retracted	460.70	1015.7	.653	25.7	204.5	150.8	220.9	162.9	285.8	210.8	1.34		
At Launch, Boom Extended	460.70	1015.7	.653	25.7	238.5	175.9	236.3	174.3	335.4	247.4	1.41		
Before Venus Orbit Insertion	454.40	1001.8	.655	25.8	238.1	175.6	233.2	172.0	332.6	245.3	1.41		
In Venus Orbit	311.07	685.8	.823	32.6	199.8	147.4	195.1	143.9	329.2	242.8	1.67		
Spent Spacecraft	290.44	640.3	.855	33.6	196.7	145.1	182.8	134.8	319.4	235.6	1.68		

## Probe Bus

In launch configuration the probe bus has a mass of 813.1 kg (1792.6 lb) with c.m. located 134.6 cm (53 in.) above the separation plane from the launch vehicle. The roll to transverse inertia ratio varies from a minimum value of 1.26 at launch to 1.60 after release of all probes. This inertia ratio range assures adequate spin stability. A maximum diameter of 254 cm (100 in.) and an overall length of 287 cm (113 in.) when in launch configuration allows for generous radial and longitudinal clearances from the allowable payload dynamic envelope.

An Intelsat IV spacecraft attach fitting was selected for use on the launch vehicle. The interface diameter of 112 cm (44.2 in.) permits a larger view factor from the spacecraft aft end than the Mariner 140 cm (55 in.) diameter and permits a larger spacecraft mass than that allowed if the Delta spin table and 3731 fitting are used.

The basic arrangement is composed of the following primary elements. A right conical frustum forms the central thrust tube. The large diameter mates to the Intelsat IV launch vehicle spacecraft adapter. A circular shelf for the mounting of subsystem units and science instruments is positioned at the upper end of the thrust tube. Twelve equally spaced support struts are attached at the shelf perimeter and extend radially to the thrust tube lower end. A cylindrical substrate surrounds the shelf and is positioned so as to provide an enclosed volume for housing equipment above and below the shelf. The substrate extends sufficiently below the shelf to permit the solar array to be mounted entirely in that area, except for patching above the shelf line, to accommodate cutouts in the panel for radial thrusters. The length below the shelf is sized for the larger array required on the orbiter mission and is kept the same for the probe bus for commonality. This also allows the upper substrate area to have apertures, etc., wherever required without interfering with the array.

Located beneath the shelf and supported from the thrust tube are two hydrazine propellant tanks positioned diametrically opposite each other and between struts. This arrangement facilitates assembly of the shelf and thrust tube without disturbing the tank installation. Also, by being below the shelf the upper shelf surface and compartment volume are entirely available for mounting and positioning of subsystem units and science instruments. This basic arrangement of thrust tube, shelf, etc. is identical for probe and orbiter spacecraft.

An inverted right conical frustum adapter installed at the upper end of the thrust tube provides for support and installation of the large probe. The mechanical interface with the probe occurs at three attach fittings equally spaced at the upper end of the adapter. The three smaller probes are positioned symmetrically around the adapter and are supported by structural elements extending radially from the adapter and vertically to the shelf.

Separation of the large probe is in an axial direction with a small  $\Delta V$  being applied from springs located at each attach fitting. After large

probe separation the three smaller probe are released simultaneously. They separate in a tangential direction to the spacecraft with a  $\Delta V$  due to the spacecraft spin. As they leave in the lateral direction they trace a spiral path, in spacecraft coordinates, and opposite in direction to the spacecraft spin, over the upper surface of the spacecraft. Therefore, this region is kept free of protuberances above the forward plane of the substrate.

Three of the bus science instruments, the ion and neutral mass spectrometers, and the retarding potential analyzer (RPA), require an unobstructed conical field of view in the direction of the velocity vector and parallel to the spin axis, after probe release. These instruments are positioned to look between the small probes such that clearance with probe support structure and other spacecraft appendages is ensured. The ultraviolet spectrometer has a small pointing angle forward off the spin axis and the electron temperature probe is 90 deg to the spin axis and are positioned at the shelf outer edge.

The other subsystem units are arranged on the shelf in a manner that provides for functional grouping and balanced mass and thermal distribution. Sufficient space exists on the shelf to permit units to be repositioned if their thermal or mass distributions should change. Ten thermal control louvers are attached to the lower surface of the shelf and will control the thermal radiation out of the aft cavity. Units that tend to dissipate large amounts of energy are located over, or near as possible, to the locations of the louvers to minimize the amount of conductive material required to be added to the shelf. Identical shelf locations are maintained for the majority of those units, and thermal control louvers that are common to both probe and orbiter spacecraft. This feature can be seen by comparison of Figures 3-18 and 3-19.

A dual bicone antenna, with a 360 deg beam in a plane normal to the spin axis and 30 deg in elevation, and a wide beam omni antenna (220 deg beam), are positioned on the spacecraft centerline aft of the thrust tube. The Intelsat IV spacecraft adapter has sufficient usable internal diameter and length to permit the antennas to be mounted on a nondeployable support structure at a distance from the end of the spacecraft thrust tube sufficient to provide them with an unobstructed rf beam field. Adequate clearance between the antennas and the attach fitting exists to provide for separation tipoff conditions.

A medium gain horn antenna, with a 45.7 cm (18.0 in.) aperture and a conical beam angle of 20 deg, is attached at the shelf aft side and pointed parallel with the spacecraft centerline. The antenna is placed in the same sector as one of the hydrazine tanks to minimize potential partial blockage of a louver view.

The star sensor line of sight required is 58 deg from the spin axis on the forward end of the spacecraft and has a 25 deg field of view. By placing it midway between two of the small probes and at the outer perimeter of the shelf possible reflections off the spacecraft are prevented from entering the sunshield. Three sun sensors, with a combined field of view of 150 deg in a plane containing the spin axis and centered about a normal to the axis, are located at the outer perimeter of the substrate, in a location free of extensions, to prevent false readings due to spacecraft reflections.

## Orbiter Spacecraft

The orbiter spacecraft in launch configuration has a total mass of 460.7 kg (1015.7 lb) with a center of mass located at 65.3 cm (25.7 in.) above the separation plane from the launch vehicle. The spin to transverse inertia ratio varies from a minimum value of 1.34 to a maximum of 1.68 at end of life. Like the probe bus, the orbiter spacecraft inertia ratio range assures adequate spin stability throughout the mission. A maximum diameter of 254.0 cm (100.0 in.) and an overall length of 325 cm (128 in.) provides for generous radial and longitudinal clearances from the allowable payload dynamic envelope.

The basic arrangement primary elements, i. e., thrust tube, equipment shelf, struts, substrate, and hydrazine tanks, as previously noted are identical to the probe bus.

An existing quadripod structure from the Telesat design is installed at the upper end of the thrust tube and provides for support and installation of the bearing and power transfer assembly (BAPTA). The high gain antenna (HGA) mast is attached to the despun flange of the BAPTA and positions the centerline of the HGA 97.8 cm (38.5 in.) above the forward plane of the substrate.

Of the nine specified experiments, four are similar to those specified for the probe bus. These are the electron temperature probes, Ultraviolet spectrometer, and the ion and neutral mass spectrometers. They will be at the same shelf positions as for the probe bus but with different pointing angles, except for the electron temperature probe which remains the same. The ion and neutral mass spectrometers are pointed nominally 56 deg from the spin axis in a forward direction and are near the outer edge of the shelf. This provides clearance from the HGA for their required conical field of view. The ultraviolet spectrometer and solar wind instruments have pointing angles 90 deg to the spin axis thus are located at the shelf outer edge and are provided with apertures through the substrate. The magnetometer is deployed by a three link articulated boom to a distance of 5.64 m (18.5 ft) from the spacecraft centerline in a plane just forward of the substrate. For launch the boom is folded and stowed above the substrate at a location that is free of instruments having forward pointing angles. Thus, if the boom should fail to deploy it would not cause blockage to any of the science instruments.

The pointing angle for the radar altimeter antenna is determined by the periapsis latitude. For the Atlas/Centaur baseline (56° S nominal periapsis latitude) the angle is 34 deg from the spin axis in the forward direction. To maintain radar beam (~104 deg in elevation) clearance with the HGA the radar antenna is located at the outer edge of the spacecraft and mainly above the forward plane of the solar panel cylindrical substrate. A reduction in periapsis latitude requires a corresponding increase in the radar antenna pointing angle. The HGA is positioned such that clearance between the HGA beam and the radar antenna is maintained when the latter is positioned for a periapsis latitude of 13 deg. Thus, if it should become desirable to lower the periapsis latitude from the selected 56 deg to one as low as 13 deg only a repositioning of the radar antenna to the new pointing angle is required.

For the rf occultation experiment an X band transmitter and a 20 deg beamwidth X band transmitter is located on the equipment shelf and the antenna is positioned above the HGA on the despun mast. This antenna location will provide clearance between the 20 deg beam and the magnetometer and boom.

The subsystem unit shelf arrangement for the probe bus was developed to maintain commonality of location for units for probe and orbiter wherever possible, and also permit the orbiter additional science instruments to be added without requiring a major rearrangement of the equipment. The additional equipment increases the thermal load on the shelf from that of the probe bus and two additional thermal control louver modules are added to the shelf lower surface to accommodate the increase.

For the baseline type II transit trajectory, the Thiokol modified TE-M-521 solid propellant motor is selected to provide orbit insertion. A motor attach ring is added internally to the thrust tube to provide for installation of the 44.5 cm (17.5 in.) by ~114 cm (45 in.) long motor.

For the alternate type I transit trajectory the candidate insertion motor is the Thiokol TE-M-616 solid propellant motor. This motor is somewhat larger, 69.3 cm (27.3 in.) diameter by 123.7 cm (48.7 in.) long, but can also be accommodated by merely changing motor attach rings.



#### 4. STRUCTURE SUBSYSTEM

The spacecraft structural design criteria and dynamic loads analysis performed for the Thor/Delta booster are discussed in subsection 4.1. The design criteria provide a set of design conditions, requirements and objectives, which when implemented will insure structural integrity. Loads and design conditions are established for the launch phase which is most critical with regard to structural integrity.

In order to verify compliance with structural subsystem design requirements, such as strength and stiffness, a dynamic analysis was performed for the Thor/Delta launch multiprobe and orbiter spacecraft. This analysis consisted of mathematically representing the probe and orbiter vehicles with 39 and 42 mass point models, respectively. These mass points were connected by 87 and 85 structural elements respectively, which represent the stiffness characteristics of the spacecraft structure. From these mathematical models, analyses were then performed to determine internal loads and spacecraft resonant frequencies. The loads were subsequently used in the vehicle stress analysis to insure adequate structural capability. Fundamental vehicle resonances were determined to occur at 23 Hz laterally and 64 Hz axially for the probe spacecraft and at 12 Hz laterally and 65 Hz axially for the orbiter spacecraft. These compare with minimum design goals of 20 Hz laterally and 35 Hz axially. Thus the orbiter lateral resonance at 12 Hz does not meet the design goal. However, it is felt that this is not a serious problem since the 12 Hz resonance results from antenna boom bending and compares with a 12.5 Hz fundamental resonance for the similar Hughes Telesat spacecraft which has experienced no structural difficulties.

The use of beryllium is considered for application on the probe bus and orbiter spacecraft for the Thor/Delta configuration only. The Thor/Delta configuration is weight critical whereas the Atlas/Centaur version is more concerned with economic considerations. Beryllium structural elements are employed on the Thor/Delta spacecraft in areas where Hughes Aircraft's experience with beryllium shows that such elements could be reliably manufactured and assembled. Application of beryllium resulted in a mass savings of 4.8 kg (10.6 lb) on the probe bus spacecraft and 2.5 kg (5.5 lb) on the orbiter spacecraft. Respective cost increases of \$163,800 and \$40,300 for four spacecraft was associated with the use of beryllium.

The descriptions of the Thor/Delta (subsection 4.3) and Atlas/Centaur baseline (subsection 4.4) structural configurations emphasize the fundamental effort to achieve a high degree of commonality between the probe bus and orbiter spacecraft. This is successfully achieved with a design which makes use of a common thrust tube, equipment shelf, shelf support struts, propulsion support structure, solar panel substrate and support fittings. It is estimated that an \$1,040,000 cost savings will be realized for the overall program requirements in the structural subsystem area as a direct result of the employment of these common structural elements for the probe bus and orbiter spacecraft. This estimate applies to either the Thor/Delta or Atlas/Centaur configurations.

#### 4.1 STRUCTURAL SUBSYSTEM REQUIREMENTS

The structural subsystem is required to meet the critical condition of launch and provide a suitable environment for the equipment mounted to it. This section includes the basic structural design requirements for the structural subsystem, and a summary of the preliminary dynamic analyses performed for the Thor/Delta spacecraft together with spacecraft quasi-static and dynamic load requirements for both the Thor/Delta and Atlas/Centaur boost vehicles. Structural design requirements for the probes are presented in Volume 5.

##### Structural Design Requirements

The structure shall possess sufficient strength, rigidity, and other necessary characteristics required to survive the critical loading conditions which exist within the envelope of mission requirements and it shall be designed to achieve minimum weight wherever possible.

The design load environment for the Thor/Delta and Atlas/Centaur spacecraft are shown in Tables 4-1 and 4-2.

The uniform quasi-static loads factors to which the vehicle will be subjected are shown in Table 4-1. These loads are based upon critical flight conditions and are ultimate factors.

In addition to the above uniform quasi-static load condition, nonuniform lateral quasi-static conditions will be used in the vehicle design. These nonuniform conditions represent the first mode flexibility and mode shape which is normally excited at liftoff. Typically these nonuniform lateral loads take the form of a parabolic curve extending from a maximum level at the uppermost point of the spacecraft and decreasing to a minimum value at the base of the adapter.

The design qualification dynamic load environment for both the Thor/Delta and Atlas/Centaur spacecraft are presented in Table 4-2. These consist of unnotched sinusoidal and random test levels applied at the base of the booster adapter. The load conditions of Table 4-2 are intended to simulate

TABLE 4-1. QUASI-STATIC UNIFORM ULTIMATE LOAD FACTORS

Condition	Axis	Acceleration, g
<b>Thor/Delta-Probe Spacecraft</b>		
Liftoff	Thrust	-4.35, +1.5*
	Lateral	3.45
MECO/POGO	Thrust	-21
	Lateral	+1.15
Spin:	Radial	0.164R** (0.416R)
	Radial	0.059R (0.150R)
	Radial	0.0037R (0.0094R)
	Radial	0.0835R (0.212R)
<b>Orbiter</b>		
Liftoff	Thrust	-4.35, +1.5
	Lateral	4.5
MECO/POGO	Thrust	-25
	Lateral	+1.5
Insertion motor burn	Thrust	-13.2
	Lateral	0.5
Spin:	Radial	0.164R (0.416R)
	Radial	0.059R (0.150R)
	Radial	0.0148R (0.0375R)
<b>Atlas/Centaur-Both Vehicles</b>		
Boost	Thrust	-9.6, +4.0
	Lateral	3.0
Insertion burn**	Thrust	-10.0
	Lateral	0.5

TABLE 4-1 (continued)

Condition	Axis	Acceleration, g
Spin: (probe spacecraft)		
Separation (0 rpm)	—	—
Transit (25 rpm)	Radial	0.0106R (0.0268R)
Large probe release (15 rpm)	Radial	0.0037R (0.0094R)
Small probe release (47.5 rpm)	Radial	0.037R (0.094R)
Spin: (orbiter)		
Separation (0 rpm)	—	0
Transit (25 rpm)	Radial	0.0106R (0.0268R)
Orbit (5 rpm)	Radial	0.00039R (0.0010R)

\* See Figures 4-1 and 4-2 for sign convention

\*\* Where R is the radial distance in centimeters and (inches) from the point in question to the spin axis

\*\*\* Orbiter only

TABLE 4.2. UNNOTCHED QUALIFICATION VIBRATION LEVELS

Thor Delta			
Sinusoidal Vibration - Sweep Rate = 2 oct/min			
Thrust Axis		Lateral Axes	
Frequency, Hz	Acceleration, g (0 peak)	Frequency, Hz	Acceleration, g (0 peak)
5-15	2.3	5-14	2.3*
15-21	6.8	14-250	1.5
21-250	2.3	250-400	4.5
250-400	4.5	400-2000	7.5
400-2000	7.5	*3.0 for orbiter spacecraft	
Random Vibration - Time = 2 min/axis			
Thrust and Lateral Axes			
Frequency	PSD $g^2/Hz$	g rms	
20-300	+3 dB/oct	--	
300-2000	0.045	9.2	
Atlas Centaur			
Sinusoidal Vibration - Sweep Rate = 2 oct/min			
Thrust Axis		Lateral Axes	
Frequency, Hz	Acceleration, g (0 peak)	Frequency, Hz	Acceleration, g (0 peak)
5-8.5	1.5 cm dia	5-8	1.1 cm dia
8.5-200	2.3	8-200	1.5
Random Vibration - Time = 4 min/axis			
Thrust and Lateral Axes			
Frequency	PSD $g^2/Hz$	g rms	
20-150	+6 dB/oct	9.3	
150-2000	0.045	-	

conditions more severe than those actually expected from ground handling, launch and orbit insertion in order to provide assurance of discovering any design deficiencies which might exist. They are not intended to exceed design safety margins and care is taken not to introduce unrealistic modes of failure primarily by reducing or "notching" the input levels if required. The qualification levels of Table 4-2 have applied a factor of 1.5 over the expected flight or acceptance levels and would be used in analyses or tests for structural qualification or in determination of unit qualification levels. Protoflight spacecraft test requirements may not necessarily specify these levels and durations.

It is a common practice in spacecraft design to notch (reduce) vibration test input levels when the spacecraft and/or booster adapter will otherwise experience unrealistically high load levels compared with maximum expected flight load levels. Notching is based on consideration of load levels at critical structural locations, such as the booster adapter, and input vibration levels are notched in frequency bands in which major spacecraft resonances are excited.

At the lower frequencies, some compensation must be made for the fact that the rigid seismic mass of the shaker head does not simulate the long, flexible launch vehicle. This compensation is in the form of a reduction of vibration input in the frequency ranges of the fundamental spacecraft resonances. This reduction of input levels is controlled automatically such that the readings at the control strain gauge bridges do not exceed the ultimate strain determined from the structural model static loads test. It will be determined during this test whether parallel notch control based on maximum response acceleration will be required. Acceleration notch control shall be implemented if the maximum response acceleration during the low level tests indicates that the qualification response will exceed the levels derived from a booster/spacecraft dynamic analysis.

The load levels to which the spacecraft is notched are developed from a coupled booster-spacecraft dynamic analysis. This analysis is accomplished in part by the booster contractor and in part by the spacecraft contractor. A detailed analysis accounting for the dynamic characteristics of the spacecraft and launch vehicle is conducted by the booster contractor. This analysis includes consideration of liftoff, staging, and maximum aerodynamic pressure flight events. The results of this analysis are then used by the spacecraft contractor to develop detailed internal loads. As a result of these internal loads, notch levels are obtained for critical areas of the spacecraft.

Unit qualification sinusoidal vibration test levels are presented in Tables 4-3 and 4-4 for the Thor/Delta and Atlas/Centaur, respectively. The levels are intended to approximate ultimate design conditions experienced by the unit when mounted on the spacecraft. These load levels are obtained from a dynamic loads analysis of the spacecraft as described later in this subsection. In general, units and unit support structure will be designed to the peak unit load levels shown in combination with the associated number of stress cycles.

TABLE 4-3. UNIT QUALIFICATION VIBRATION TEST LEVELS - SINUSOIDAL  
SWEEP FREQUENCY (THOR/DELTA)

Axis	Probe Bus and Orbiter Units										Probe Units		
	Acceleration, g, 0-peak										Acceleration, g, 0-peak		
	Frequency, (1) Hz	Large Probe and Pressure Vessel	Small Probe and Pressure Vessel	Shelf Mounted Items (2)	Fuel Tanks	Bicone/ Omni Attachment to Thrust Tube	Bicone/ Omni Antenna (3)	Frequency (1) Hz	Large Probe Shelf Mounted Items (4)	Small Probe Shelf Mounted Items (4)			
Thrust axis	5-14	2.3	2.3	2.9	2.3	2.3	2.3	5-15	2.3	2.3			
	15-21	8.0	8.0	10.0	8.0	8.0	8.0	15-21	8.0	8.0			
	21-55	4.0	5.0	5.0	4.0	4.0	4.0	21-55	4.0	5.0			
	55-85	4.0	25.0	40.0	15.0	6.0	7.5	55-80	4.0	25.0			
	85-150	6.0	4.5	10.0	5.5	10.0	11.5	80-150	20.0	25.0			
	150-400	4.5	4.5	4.5	4.5	4.5	4.5	150-400	4.5	4.5			
Lateral axes	400-2000	7.5	7.5	7.5	7.5	7.5	7.5	400-2000	7.5	7.5			
	5-13	2.5	2.5	4.5	2.5	2.5	2.5	5-13	2.5	2.5			
	13-25	5.5	5.5	5.0	4.0	5.5	8.0	13-25	5.5	5.5			
	25-55	1.8	1.5	1.5	1.7	1.6	2.7	25-55	1.8	1.5			
	55-150	4.0	10.5	8.0	20.0	10.5	17.0	55-80	4.0	10.5			
	150-400	4.5	4.5	4.5	4.5	4.5	4.5	80-150	20.0	35.0			
400-2000	7.5	7.5	7.5	7.5	7.5	7.5	150-400	4.5	4.5				
							400-2000	7.5	7.5				

NOTES: (1) Sweep rate = 2 oct/min.

(2) Inputs for shelf-mounted items are at the shelf attach points.

(3) High gain antenna, horn and narrow beam omni levels to be supplied.

(4) Fundamental frequencies of large and small probe shelf-mounted items, including the shelves, shall be greater than 80 Hz.

TABLE 4-4. UNIT QUALIFICATION VIBRATION TEST LEVELS - SINUSOIDAL SWEPT FREQUENCY (ATLAS/CENTAUR)

Axis	Probe Bus and Orbiter Units										Probe Units		
	Frequency (5) Hz	Large Probe and Pressure Vessel	Small Probe and Pressure Vessel	Thrusters and Shelf Mounted Items (1)	Fuel Tanks	Bicone Omni Attachment to Thrust Tube	Bicone/ Wide Beam Omni Antenna (2)	Frequency (5) Hz	Orbit Insertion Motor (3)	Frequency (5) Hz	Large Probe Shelf Mounted Items (4)	Small Probe Shelf Mounted Items (4)	
Thrust axis	5-15	2.3	2.3	2.7	2.3	2.3	2.3	5-8.5	1.5 cm (0.6 in) double amplitude (d.a.)	5-15	2.3	2.3	
	15-20	10	10	10	8	4	8	8.5-250	2.3	15-20	10	10	
	20-30	8	8	20	10	6	8	250-400	3.75	20-40	8	8	
	30-40	6	40	55	20	10	12	400-2000	7.5	40-50	8	40	
	40-80	6	15	20	10	10	10			80-150	20	25	
	80-150	5	5	10	8	10	12			150-400	3.75	3.75	
	150-400	3.75	3.75	3.75	3.75	3.75	3.75			400-2000	7.5	7.5	
	400-2000	7.5	7.5	7.5	7.5	7.5	7.5						
	Lateral axes	5-13	2.5	2.5	2.5	2.5	2.5	2.5	5-8	1.1 cm (0.45 in) d.a.	5-13	2.5	2.5
		13-20	8	8	7	6	8	12	8-250	1.5	13-20	5	5
20-40		4	4	4	4	4	6	250-400	3.0	20-40	4	4	
40-150		8	12	12	25	15	25	400-2000	7.5	40-150	30	40	
150-400		3.75	3.75	3.75	3.75	3.75	3.75			150-400	3.75	3.75	
400-2000		7.5	7.5	7.5	7.5	7.5	7.5			400-2000	7.5	7.5	

NOTES: (1) Inputs for shelf-mounted items are at the shelf attach points.  
 (2) High gain antenna, horn and narrow beam omni levels to be supplied.  
 (3) Levels at base of spacecraft lower cone. Levels will be notched at motor attachment plane. Values will be obtained from spacecraft dynamics analysis. Random levels are from Table  
 (4) Fundamental frequencies of large and small probe shelf-mounted items, including the sheives, shall be greater than 80 Hz.  
 (5) Sweep rate - 2 oct/min.

REPRODUCIBILITY OF THE ORIGINAL PAGE IS POOR.



## Design Criteria

The following factors of safety are applied to all load levels derived from analysis or test.

	<u>Limit</u>	<u>Proof</u>	<u>Ultimate</u>	<u>Burst</u>
1) Flight loads	1.00	-	1.50	-
2) Nonflight loads, dangerous to personnel	1.00	-	1.50	0
3) Nonflight loads, remote to personnel	1.00	-	1.50	-
4) Pressure loads, dangerous	1.00	1.50	-	-
Tanks	-	-	-	2.00
Lines and other components	-	-	4.00	-
5) Pressure loads, remote to personnel	1.00	1.15	1.25	-

The structural subsystem is designed to withstand, without degradation, simultaneous application of loads, temperatures, and other accompanying environmental phenomena. No factor of safety is applied to any environmental phenomena except loads.

The structural design is such that comparison of the applied load (or stress) to the allowable load (or stress) shall result in a positive margin of safety, MS.

$$MS = \frac{\text{Allowable Load}}{\text{Applied Load}} - 1$$

The effects of combined loads or stresses (interaction) shall be included in the detailed stress analysis. For minimum weight, the structural design shall strive for the smallest permissible margins of safety, which shall be zero, except in certain specific instances where specified finite values may be required.

Material strengths and other mechanical and physical properties shall be selected from authorized sources of reference, such as MIL-HDBK-5B and MIL-HDBK-17, and from Hughes test values when appropriate. Strength allowables and other mechanical properties used shall be appropriate to the loading conditions, design environments, and stress states for each structural member.

Allowable material strengths used in design reflect the effects of temperature and time associated with the design environment. Allowable properties are as follows:

- 1) For single load path structures, the minimum guaranteed values (A values in MIL-HDBK-5B) are to be used
- 2) For multiple load path structures, the 90 percent probability values (B values in MIL-HDBK-5B) are to be used

In designing for fatigue environments, the allowable stress corresponding to the lower edge of the scatter band of test results is used where sufficient data is available. In the event insufficient data is available to define a scatter band, the required number of cycles is increased by a factor of 4 and the mean value fatigue curve used. When multiple fatigue environments exist, the combined effect is determined by the use of Miner's rule or other acceptable methods such as the Method of Universal Slopes.

In addition to meeting strength requirements, the spacecraft structure must also be designed to provide the proper stiffness to comply with structural frequency requirements. Natural frequency requirements are imposed upon the vehicle for the following reasons:

- 1) To avoid dynamic interaction with the booster control system
- 2) To avoid a resonant condition induced by the spinning section when the vehicle is in flight
- 3) To ensure predictable dynamic loads
- 4) To limit deflections

The following are spacecraft design frequency goals:

- |   |               |
|---|---------------|
| 1) Total structure without adapter - lateral: | 20 Hz minimum |
| 2) Total structure without adapter - axial:   | 35 Hz minimum |
| 3) Bracket mounted components:                | 80 Hz minimum |

### Dynamic Loads Analysis

A preliminary dynamic analysis has been performed on the Pioneer Venus probe and orbiter spacecraft. These analyses have been performed for the Thor/Delta spacecraft weighing approximately 384 kg (847 lb) and 293 kg (646 lb), respectively. A summary of these analysis are included herein. Representation of the Atlas/Centaur spacecraft weighing up to 815 kg (1800 lb) would involve a similar type of analysis and modeling. Each spacecraft was subjected to several quasi-static load conditions and also to sinusoidal and random vibration. Each load condition was applied separately, and corresponding loads and accelerations determined. The complete results of this analysis are contained in Study Task VI-4, Dynamic Loads Analysis.

The loads analysis was performed for spacecraft constructed of aluminum. The effect of changing the material of the primary structural elements to beryllium would be to in general increase the stiffness and raise the natural frequency of the structure. This effect should, if anything, lower design loads. Thus, the loads predicted for the aluminum structure are considered acceptable for design of a beryllium structure.

## Mathematic Models

The Hughes matrix analysis routine for structures (MARS) computer program was used to perform the structure analysis under Task No. VI-4.

Probe Spacecraft Model. The probe spacecraft model including the booster adapter, has 39 mass stations which are distributed as shown in Figure 4-1. Due to the preliminary nature of the analysis, some simplifying assumptions were used on constructing the model. For example, the large probe is modeled as a single mass and the weight of shelf mounted equipment is assumed to be uniformly distributed over the shelf surface, and is lumped at 15 mass stations.

A total of 87 structural elements are used to connect the mass stations. The probe spacecraft model utilizes only three element types of the five types which can be modeled in the MARS computer program. The thrust tube, solar panel, antennas, equipment shelf support struts and propellant tank supports comprise 49 thin walled conical and cylindrical element. Supports for the small probes, the propellant tank upper support T-sections and the booster adapter comprise 22 beam elements. The equipment shelf is represented by 16 plate elements.

The first 45 natural frequencies were calculated and used in the loads analysis. The first 10 modes are tabulated and briefly described in Table 4-5. In the spacecraft-without-booster adapter configuration, the fundamental lateral and axial structural frequencies were 23.2 Hz and 64.0 Hz, respectively. These compare with design goals of 20 Hz and 35 Hz, respectively.

Orbiter Spacecraft Model. The orbiter spacecraft model, including the booster adapter, has 42 mass stations which are distributed as shown in Figure 4-2. The thrust tube, adapter, equipment shelf supports, solar panel and fuel tanks and supports are structurally identical to the multiprobe spacecraft structure. The weight of equipment on the shelf is assumed uniformly distributed over the shelf surface at 24 mass stations.

A total of 85 structural elements are used to connect the mass stations. The orbiter spacecraft model utilizes four of the five types which can be modeled in the MARS computer program. Two stiffness matrices are used to represent the bearing and power transfer assembly (BAPTA). The thrust tube, solar panel, antennas, equipment shelf support struts, omni-antenna tie bars, thruster supports and propellant tank supports comprise 50 thin-walled conical and cylindrical elements. The propellant tank upper support T-sections, the orbit insertion motor supports and the booster adapter comprise 9 beam elements. The equipment shelf is represented by 24 plate elements.

The first 40 natural frequencies were calculated and used in the loads analysis. The first 10 modes are tabulated and briefly described in Table 4-6. In the spacecraft without booster adapter configuration, the fundamental lateral and axial structural frequencies were 12 Hz and 62 Hz, respectively.

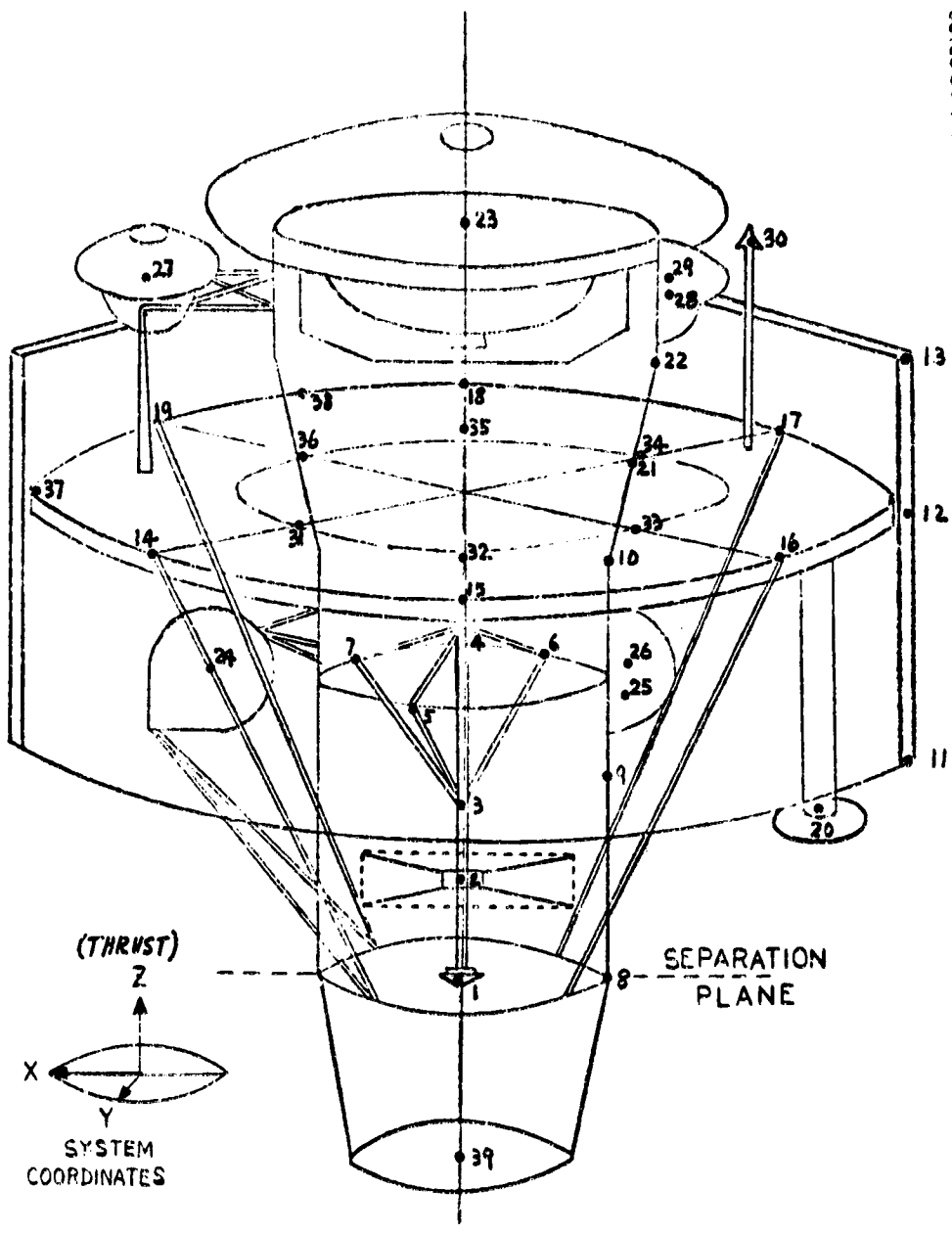


FIGURE 4-1. PROBE SPACECRAFT MATHEMATICAL MODEL

30163-345(U)

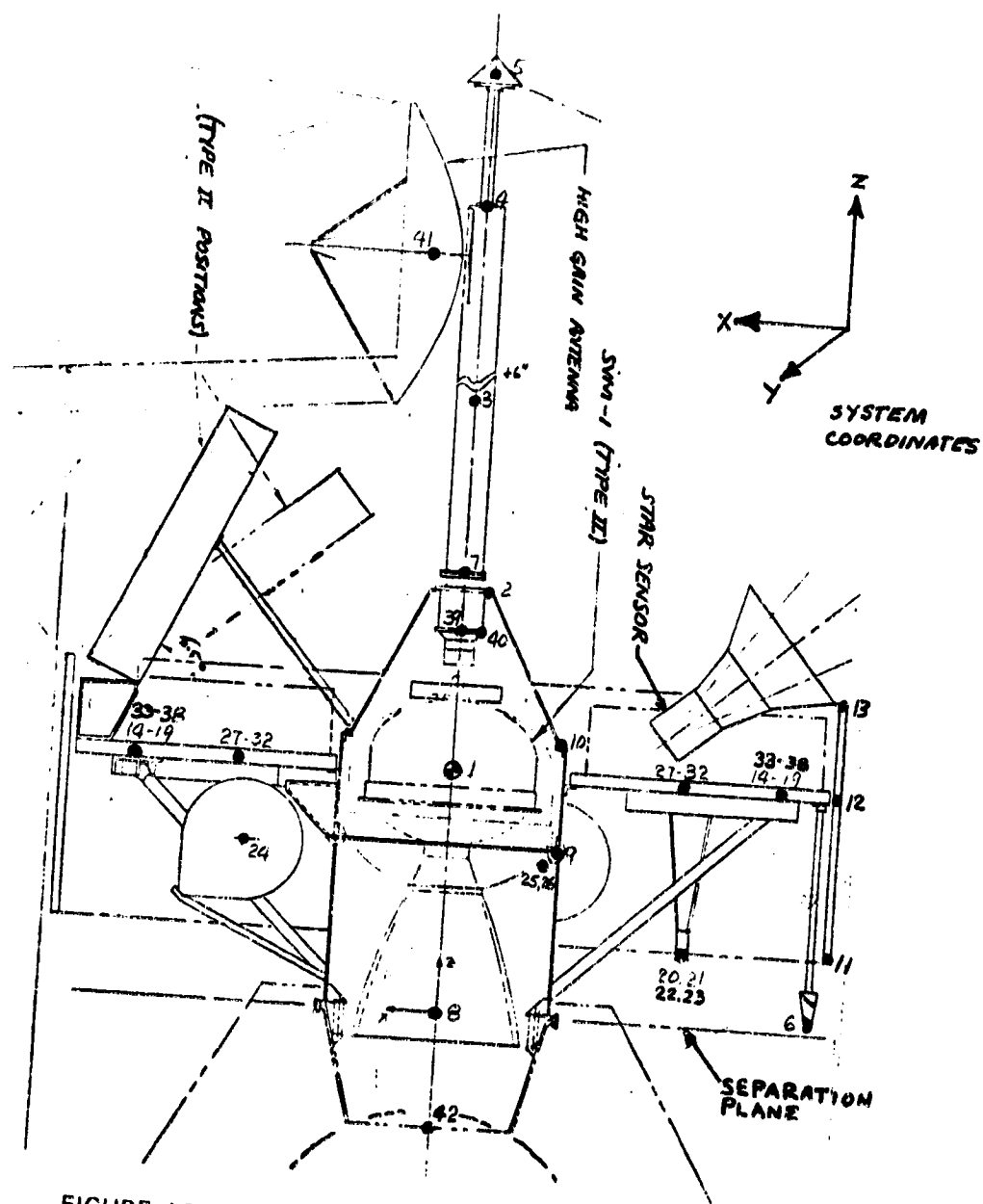


FIGURE 4.2. ORBITER SPACECRAFT MATHEMATICAL MODEL

REPRODUCIBILITY OF THE ORIGINAL PAGE IS POOR

TABLE 4-5. FIRST TEN MULTIPROBE SPACECRAFT  
NATURAL MODES

Mode Number	Frequency, Hz	Description of Mode
1	20.4	Large probe lateral (X)
2	20.4	Large probe lateral (Y)
3	29.8	Small probe lateral (2 in X, 1 in Y)
4	35.7	Bicone/omni antenna (Y)
5	35.7	Bicone/omni antenna (X)
6	61.5	Small probe and shelf (Z) fundamental axial mode
7	65.8	Small probe (Z, X)
8	66.4	Small probe (Z, X)
9	66.9	End fire antenna, small probe (Y)
10	69.3	End fire antenna (Y)

TABLE 4-6. FIRST TEN ORBITER SPACECRAFT  
NATURAL MODES

Mode Number	Frequency, Hz	Description of Mode
1	12.0	High gain antenna (Y)
2	12.1	High gain antenna (X)
3	32.8	Omni antenna (Y)
4	34.4	Omni antenna (X)
5	35.5	Equipment shelf torsion
6	36.1	Motor (Y), shelf (Y, Z)
7	36.4	Spacecraft (X)
8	61.6	Shelf (Z) - fundamental axial mode
9	64.1	Shelf (Z); thrusters (X)
10	66.5	Shelf (Z); thrusters (Y)

These compare with design goals of 20 Hz and 35 Hz, respectively. The 12 Hz lateral mode results from antenna boom bending, and compares with a 12.5 Hz fundamental mode on the Hughes Telesat spacecraft due to antenna distortion. It presents no problem from the spacecraft structural design viewpoint. The first lateral mode which involves bending motion of the adapter and thrust tube occurs at 38.06 Hz.

## 4.2 TRADES

### Beryllium Weight/Cost Considerations

To reduce the structural weight on the Thor/Delta configured probe bus and orbiter spacecraft, a study was conducted to establish the ramifications of employing beryllium in the manufacture of various spacecraft structures. Spacecraft stiffness requirements largely eliminated consideration of other materials.

Hughes Aircraft's 7 years of experience in the application of beryllium structures to spacecraft indicates that the use of beryllium on the Pioneer Venus is practical. Hughes has delivered beryllium flight hardware, on three programs, including spin arm assemblies, cone skin assemblies, complete despin platform assemblies and antenna tubes. Figure 4-3 illustrates several flight proven structural assemblies which have been designed, manufactured, and assembled at Hughes' own facilities. To date the use of beryllium on spacecraft structures has proven to be very successful. Hughes maintains active beryllium manufacturing and laboratory facilities and is engaged in a continuing company-funded effort to enhance the state of the art and reduce costs.

The Thor/Delta spacecraft substituted beryllium for aluminum on the thrust tube and shelf supports. The design of the probe bus readily lent itself to the use of beryllium in the large and small probe support structures. Beryllium was also selected for the BAPTA support on the orbiter vehicle. It is noted that the BAPTA housing and shaft will also be made of beryllium since this has already been accomplished on other programs (see Figure 4-3). A comparison of the estimated weights for the aluminum and beryllium structure indicated a 4.8 kg (10.6 lb) mass savings on the probe bus spacecraft and a 2.5 kg (5.5 lb) mass savings on the orbiter spacecraft. Table 4-7 and Figure 4-4 document and illustrate the mass savings using beryllium.

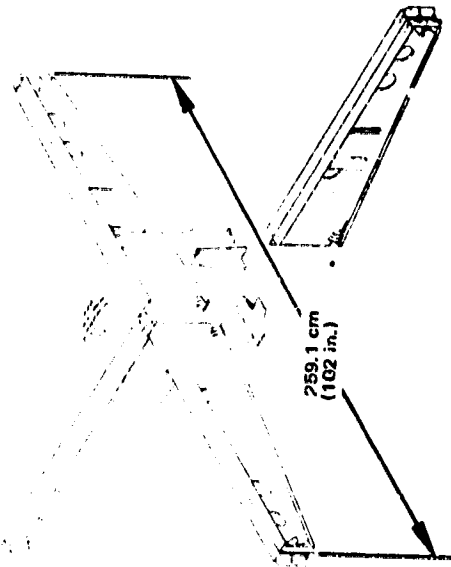
It is concluded that by employing beryllium, the mass reduction of approximately 4.8 kg (10.6 lb) achieved on the probe bus would result in a cost increase of approximately \$163,800 for four spacecraft. Likewise, the mass reduction of approximately 2.5 kg (5.5 lb) would be achieved on the orbiter at an approximate additional cost of \$40,300 for four spacecraft.

30163-346(U)



25.4 cm  
(10 in.)

BAPTA HOUSING SHAFT



259.1 cm  
(102 in.)

SPIN ARM ASSEMBLY



CO. F SKEL ASSEMBLY

FIGURE 4.3. BERYLLIUM FLIGHT HARDWARE AT HUGHES

REPRODUCIBILITY OF THE ORIGINAL PAGE IS POOR



**SMALL  
PROBE SUPPORTS**  
1.0 kg (2.2 lb)

( ) = MASS SAVINGS USING BERYLLIUM

**LARGE  
PROBE SUPPORT**  
1.8 kg (3.9 lb)

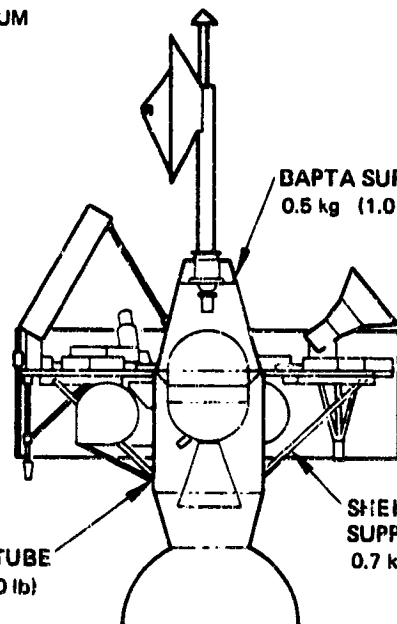
**SHELF  
SUPPORTS**  
0.7 kg (1.5 lb)

**THRUST TUBE**  
1.4 kg (3.0 lb)

STRUCTURE: 41.3 kg (91.0 lb) Al  
36.5 kg (80.4 lb) Be

TOTAL REDUCTION 4.8 kg (10.6 lb)

**MULTIPROBE SPACECRAFT**



**BAPTA SUPPORT**  
0.5 kg (1.0 lb)

**SHELF  
SUPPORTS**  
0.7 kg (1.5 lb)

**THRUST TUBE**  
1.4 kg (3.0 lb)

STRUCTURE: 36.0 kg (77.2 lb) Al  
32.5 kg (71.7 lb) Be

TOTAL REDUCTION 2.6 kg (5.5 lb)

**ORBITER SPACECRAFT**

30153-347(U)

FIGURE 4.4. STRUCTURAL MASS REDUCTION USING BERYLLIUM

TABLE 4-7. ALUMINUM VERSUS BERYLLIUM MASS COMPARISONS

Item:	Probe				Orbiter			
	Estimated Mass		Savings kg (lb)	Estimated Mass		Savings kg (lb)		
	Al	Be		Al	Be			
Thrust tube	5.0 (11.0)	3.6 (8.0)	1.4 ( 3.0)	5.0 (11.0)	3.6 (8.0)	1.4 (3.0)		
Shelf supports	2.0 ( 4.5)	1.4 (3.0)	0.6 ( 1.5)	2.0 ( 4.5)	1.4 (3.0)	0.6 (1.5)		
Large probe support*	5.6 (12.3)	3.8 (8.4)	1.8 ( 3.9)					
Small probe support	3.0 ( 6.6)	2.0 (4.4)	1.0 ( 2.2)					
BAPTA support				1.3 ( 2.8)	0.8 (1.8)	0.5 (1.0)		
			4.8 (10.6)			2.5 (5.5)		

\* Includes support longerons

## Stress Analysis

The primary purpose of the stress analysis is to substantiate the structural integrity of the principal structural elements of the spacecraft. The design conditions and loads used in the analysis are described in subsection 4.1 of this report. The appendix which presents a condensed stress analysis performed for the aluminum version is concerned with only those structural elements which will be made of beryllium. Hughes experience in the machining, drilling, and handling of beryllium indicates a minimum material thickness of 0.076 cm (0.030 in.) should be used to assure the development of practical structures having a large degree of reliability.

The thrust tube and the shelf support struts are identical for both the probe and orbiter spacecraft. Investigation of the design loads shows that the probe spacecraft loads are critical for the thrust tube and shelf support struts. The BAPTA support appears only on the orbiter spacecraft, while the large and small probe supports are only included on the probe spacecraft. For a detailed description of the probe bus and orbiter spacecraft, refer to subsection 3.4 and 4.4. The critical analysis parameter for each item is the elastic stability requirements due to buckling load environments. Stress levels produced in the structural elements are readily satisfied by the allowable strength properties of both materials. The equations used in this analysis to obtain allowable buckling loads are either generally accepted industry standards or have been verified by Hughes structural tests. Accordingly, a minimum margin of safety of 15 percent is maintained for thin shell buckling to account for scatter in test data.

### 4.3 THOR/DELTA BASELINE DESCRIPTION

The structural design approach employed in the Thor/Delta probe bus and orbiter spacecraft was derived from the Hughes built Canadian Domestic Satellite (Telesat - see Table 4-8). A primary consideration in the overall spacecraft structural design was to attain a high degree of commonality between the probe bus and orbiter spacecraft and the use of structure common to, or similar to, spacecraft developed to date. This approach results in a significant cost reduction. Commonality of structure reduced the overall engineering, design, tooling, manufacturing and ground support equipment costs by an estimated \$1,040,000 for the overall program requirements in the structural subsystem area.

The thrust tube, equipment shelf, shelf support struts, propulsion support structure, solar panel substrate and support fittings are the same on both the probe bus and orbiter spacecraft. The primary structural member is a cylindrical thrust tube onto which is mounted the 205.7 cm (81 in.) diameter equipment shelf and six shelf support struts. A cylindrical solar panel substrate is supported by attach fittings at the equipment shelf and thrust tube. Two hydrazine propellant tanks are supported by struts which originate at the thrust tube.

TABLE 4-8. SPACECRAFT STRUCTURAL HARDWARE DERIVATION

Item	Probe Bus	Orbiter
Equipment shelf	Telesat type 205.7 cm (81 in.) dia., Al	Telesat type 205.7 cm (81 in.) dia., Al
Shelf support struts	New (6, Be)	New (6, Be)
Thrust tube	New 61.0 cm (24 in.) dia., Be	New 61.0 cm (24 in.) dia., Be
Solar panel cylinder	Telesat type 213.4 cm (84 in.) dia.	Telesat type 213.4 cm (84 in.) dia.
Large/small probe attach structure	New (Be)	New (Be)
BAPTA support	-	New (Be)
HGA	-	New (Al)

A large probe support structure, an inverted conical frustum, is mechanically fastened to a ring frame on the thrust tube shelf on the probe bus spacecraft. A joint at the shelf facilitates ease of probe support structure assembly. The support structure for each of the three small probes is attached to both the inverted conical frustum supporting the large probe and the equipment shelf. On the orbiter spacecraft a mechanically despun antenna (MDA) is supported on a BAPTA fitting which is in turn supported by a conical frustum structure. This support structure is mechanically fastened to a ring frame on the thrust tube.

In order to minimize structural weight, thrust tube skins, large probe and small probe support structure and BAPTA support structure, will be constructed of formed 0.076 cm (0.030 in.) thick, cross rolled beryllium sheet. The wall thickness of the extruded equipment shelf support struts will be 0.076 cm (0.030 in.). Hughes' experience in the machining, drilling and handling of beryllium dictates a minimum material thickness of 0.076 cm (0.030 in.) to assure the development of practical structures having a large degree of reliability. Rings and separation interfaces in the thrust tube and

large probe support structures will be made of aluminum. A 3.81 cm (1.5 in.) thick sandwich construction, consisting of 0.025 cm (0.010 in.) thick aluminum face sheets with an aluminum honeycomb core, will be used for the equipment shelf. A 1.27 cm (0.5 in.) diameter extruded aluminum tubing will be used for the propellant tank supports. The cylindrical substrate is constructed from a 1.9 cm (0.75 in.) thick sandwich construction consisting of an aluminum honeycomb core and bonded fiberglass facesheets.

Based upon the above discussed material designations for the respective structural parts, an estimated mass of 36.4 kg (80.4 lb) was established for the probe bus spacecraft and 32.3 kg (71.7 lb) was established for the orbiter spacecraft. Table 4-9 documents a detailed mass breakdown of the structural subsystem elements. The analysis in subsection 4.2 confirms that these estimates are conservative by approximately 0.6 kg (1.5 lb) since the beryllium structure mass estimates presented herein were based upon the relative densities of the beryllium and aluminum with no consideration given to the reduction in material thicknesses of the beryllium. It is noted that earlier requirements for the use of longerons on the large probe structure have been removed as a result of better loads definition. The deletion of the longerons from the design enhances the confirmation that the estimate presented herein is conservative.

TABLE 4-9. STRUCTURAL SUBSYSTEM MASS STATEMENT  
THOR/DELTA CONFIGURATION

	Estimated Weight	
	kg	lbs
<b>Multiprobe Spacecraft</b>		
Equipment shelf	11.3	24.9
Shelf support struts (Be)	1.0	2.3
Shelf support brackets (Be)	0.2	0.5
Shelf support doublers (Be)	0.1	0.3
Thrust tube (Be)	3.6	8.0
Large probe attach structure (Be)	3.0	6.5
Large probe structure longerons (6) (Be)	0.9	1.9
Omni boom mounting	0.2	0.4
Medium gain antenna bracketry	0.1	0.2
Bicone deployment support	0.4	0.8
Substrate	8.0	17.7
Small probe attach structure (Be)	2.0	4.4
Propellant tank supports	1.5	3.4
Thruster supports	1.4	3.1
Balance weights	1.8	4.0
Miscellaneous hardware	0.9	2.0
<b>Total</b>	<b>36.4</b>	<b>80.4</b>
<b>Orbiter Spacecraft</b>		
Equipment shelf	11.3	24.9
Shelf support struts (Be)	1.0	2.3
Shelf support brackets (Be)	0.2	0.5
Shelf support doublers (Be)	0.1	0.3
Thrust tube (Be)	3.6	8.0
BAPTA support (Be)	0.8	1.8
HGA boom	1.0	2.2
Omni booms (2)	0.2	0.4
Substrate	8.0	17.7
Propellant tank supports (2)	1.0	2.3
Thruster supports (8)	1.5	3.3
Motor attach ring	0.5	1.2
Balance weights	1.8	4.0
RF altimeter support	0.4	0.8
Miscellaneous hardware	0.9	2.0
<b>Total</b>	<b>32.5</b>	<b>71.7</b>

#### 4.4 ATLAS/CENTAUR BASELINE DESCRIPTION

The structural design employed in the probe bus and orbiter spacecraft was derived from the Hughes built Canadian Domestic Satellite (Telesat - see Table 4-10). As was the case in the Thor/Delta configuration, the primary consideration in the overall spacecraft structural design for the Atlas/Centaur configuration was the attainment of a high degree of commonality between the probe bus and orbiter spacecraft. This approach has significant cost impact and is in accordance with the objective of reducing program costs. Commonality of structure will reduce the overall engineering, design, tooling, manufacturing, and ground support equipment costs by an estimated \$1,040,000 for the overall program requirements in the structural subsystem area.

The result of this effort is the development of a probe bus and orbiter spacecraft that makes use of the same basic structure. The thrust tube, equipment shelf, shelf support struts, propulsion support structure, solar panel cylindrical substrate, and support fittings are the same on both the probe bus and orbiter spacecraft. The primary structural member is a conical frustum onto which is mounted the 247.7 cm (97.5 in) diameter equipment shelf and 12 shelf support struts. A cylindrical solar panel substrate is supported by attach fittings at the equipment shelf. Two hydrazine propellant tanks are supported by struts that originate at the thrust tube.

A large probe support structure, an inverted conical frustum, is mechanically fastened to the equipment shelf on the probe bus spacecraft. A joint at the shelf facilitates ease of probe support structure assembly. The support structure for each of the three small probes is attached to both the inverted conical frustum supporting the large probe and the equipment shelf. On the orbiter spacecraft a mechanically despun antenna (MDA) is supported on a BAPTA fitting, which is in turn supported by a pedestal structure. This pedestal structure is mechanically fastened to a ring frame on the thrust tube and is identical to the Telesat pedestal support structure.

All of the primary structural elements will be made of aluminum. The thrust tube skins will be made from 0.170 cm (0.068 in.) 2024-T3 Aluminum, and the large probe support structure will be constructed from 0.102 cm (0.040 in.) thick 2024-T3 aluminum. 3.18 cm. (1.25 in.) diameter extruded aluminum tubing will be used for the 12 equipment shelf support struts. A 6.4 cm (2.5 in.) thick sandwich construction, consisting of 0.025 cm (0.010 in.) thick aluminum facesheets with an aluminum honeycomb core, will be used for the equipment shelf. 1.91 cm (0.75 in.) diameter extruded aluminum tubing will be used for the propellant tank supports. The cylindrical substrate will be constructed from a 1.9 cm (0.75 in.) thick sandwich construction consisting of an aluminum honeycomb core and bonded fiberglass facesheets.

TABLE 4-10. SPACECRAFT STRUCTURAL HARDWARE DERIVATION

ITEM	PROBE BUS	ORBITER
	Equipment shelf	Telesat type 247.7 cm (97.5 in) dia, Al
Shelf Support Struts	New, Al (12 struts)	→
Thrust tube	New, Frustum, Al 71.1 cm (28 in) and 112.4 cm (44.25 in) dia	→
Solar panel cylinder	Telesat Type 254.0 cm (100 in) dia	→
Large/small probe Attach structure	New, Al	--
BAPTA support		Telesat
HGA support		New, Al



Based upon the above discussed material designations for the respective structural parts, an estimated weight of 83.8 kg (183.5 lbs) was established for the probe bus spacecraft and 70.2 kg (154.7 lbs) was established for the orbiter spacecraft. Table 4-11 documents a detailed weight breakdown of the structural subsystem (excluding the thermal elements listed in section 5.4).

The design loads used in the stress analysis included in Appendix B were derived from the dynamic loads analysis performed for the Thor/Delta configurations. The loads used for sizing the primary structural elements were obtained by applying the ratios of the weight and C.G. height of components on the Atlas/Centaur configuration to the Thor/Delta loads presented in Appendix A. For example the bending moment at the separation plane is:

$$M_{A/C} = M_{T/D} \left[ \frac{(WGT.) A/C}{(WGT.) T/D} \right] \left[ \frac{(C.G. HEIGHT) A/C}{(C.G. HEIGHT) T/D} \right] \quad (1.30)$$

In addition, a safety factor of 1.30 has been applied to the design loads for Atlas/Centaur to provide increased confidence in the structural design and consideration of deletion of a structural test model. Since this 1.30 safety factor is applied to all Atlas/Centaur loads, the requirement for a minimum margin of safety of 0.15 on buckling stability (normally used to account for scatter in test data) has been deleted.

TABLE 4-11. STRUCTURE SUBSYSTEM MASS STATEMENT  
(EXCLUDING THERMAL ELEMENTS)

	Estimated Mass	
	Kg	Lbs
<u>Multiprobe spacecraft</u>		
Equipment shelf	21.1	46.5
Shelf support struts (12)	2.0	4.3
Strut fittings	1.5	3.4
Thrust tube	14.5	31.9
Large probe attach structure	13.8	30.5
Omni boom mounting	0.2	0.4
Medium gain antenna bracketry	1.4	3.0
Bicone support structure	1.4	3.0
Cylindrical substrate	13.8	30.5
Small probe attach structure	4.6	10.1
Propellant tank supports (2)	1.8	3.9
Thruster supports (6)	2.7	6.0
Balance weights	2.7	6.0
Miscellaneous hardware	1.8	4.0
	<hr/>	<hr/>
TOTAL	83.8	183.5
<u>Orbiter spacecraft</u>		
Equipment shelf	21.1	46.5
Shelf support struts (12)	2.0	4.3
Strut fittings	1.5	3.4
Thrust tube	14.5	31.9
BAPTA support	2.2	4.9
HGA mast	2.6	5.7
Omni and X-band mast	0.3	0.7
Cylindrical substrate	13.8	30.5
Propellant tank supports (2)	1.8	3.9
Thruster Supports (7)	3.0	6.5
Motor attach ring	2.2	4.9
Balance weights	2.7	6.0
Radar altimeter support	0.7	1.5
Miscellaneous hardware	1.8	4.0
	<hr/>	<hr/>
TOTAL	70.2	154.7

## 5. THERMAL CONTROL

This section describes the design studies performed which have led to the selection of the probe bus and orbiter thermal designs and presents baseline designs and performance for both the Thor/Delta and Atlas/Centaur launch vehicles. Also included in this section is a discussion of probe pre-entry thermal design; i. e., for the mission from launch to entry.

The emphasis in these design studies has been directed toward the Thor/Delta configuration. However, where Atlas/Centaur configuration differences significantly affect these results, this is indicated in the Atlas/Centaur baseline description (subsection 5.4).

The thermal designs selected for probe bus and orbiter spacecraft are identical in concept and utilize thermal louvers and superinsulation to control shelf-mounted science and spacecraft equipment; insulation and electrical heaters to control critical propulsion subsystem temperatures, and passive finishes on less thermally sensitive elements such as antennas and support structure.

Differences exist between the two spacecraft thermal designs only where required by configuration differences. The principal difference is the addition of the probes on the probe bus and the deletion of the despun high gain antenna and the orbit insertion motor. However, the probe bus is thermally independent of probes. Louver arrangement is common to both spacecraft with additional louvers utilized on the orbiter to accommodate higher shelf power. There is a corresponding similarity between the Thor/Delta designs and those for the Atlas/Centaur.

The principal thermal control elements are the thermal louvers which are utilized to control shelf temperatures over a wide range of electrical dissipations, nearly independent of the even greater variations in solar heating during the mission.

Since the shelf mounted science and spacecraft equipment is insulated from the environment except at the louvered surfaces, thermal control of the equipment is relatively insensitive to spacecraft orientation with respect to the sun, assuming minimum solar panel or battery power is available. However, solar illumination of the louvers can seriously decrease their capability to dissipate shelf power. Therefore, mission sun angle histories are important design considerations.



The thermal designs of the probes for the mission phases up to entry are passive augmented with heater power supplied by the probe bus early in the transit mission. The important design points are the initial temperatures at entry (critical to the descent thermal designs), temperatures at probe separation from the bus, and minimum temperatures during the initial phase of the mission near earth. The critical phase is the 20 day period between separation and entry when the probes must be controlled independently of the bus while experiencing continuously varying sun angles and increasing solar intensity. The interfaces between the probe bus and the probes are designed to provide thermal isolation so that the probe bus thermal behavior is minimally affected by probe separation.

The results of the design studies have led to the following important conclusions:

- 1) Spacecraft spin axis orientation normal to ecliptic plane results in the simplest thermal control design. The alternate axis orientation along the spacecraft-earth line can be accommodated with substantial increase in weight and complexity.
- 2) Substitution of thermal barriers or finishes for certain insulation blankets to reduce weight and cost generally result in significant performance penalties.
- 3) It is not weight effective to use doublers to provide conductance for equipment shelf arrangements requiring the transport of any significant amount of thermal energy laterally along the shelf. This is best done by heat pipes. However, shelf arrangements have been achieved whereby the placement of moderate to high power units directly over louver modules virtually eliminates the need to provide this conductance.
- 4) Experimental measurements indicate that solar illumination of louver modules will be significant enough to require constraints on the time spent at certain spin axis attitudes off the ecliptic plane normal.
- 5) Rocket exhaust plume heating requires the insulation blankets in the vicinity of the orbit insertion motor to be made of Kapton.
- 6) Minimum weight is required if the probe preentry thermal designs are passive during the post-separation period and the resulting uncertainty in initial temperature at entry is accounted for in the descent phase thermal design.

## 5.1 REQUIREMENTS

The spacecraft thermal designs have been selected to maintain equipment mounting surface temperatures within the limits given in Table 5-1 under all environmental and operational conditions of the multiprobe and orbiter missions. Mounting surface temperatures are specified rather than

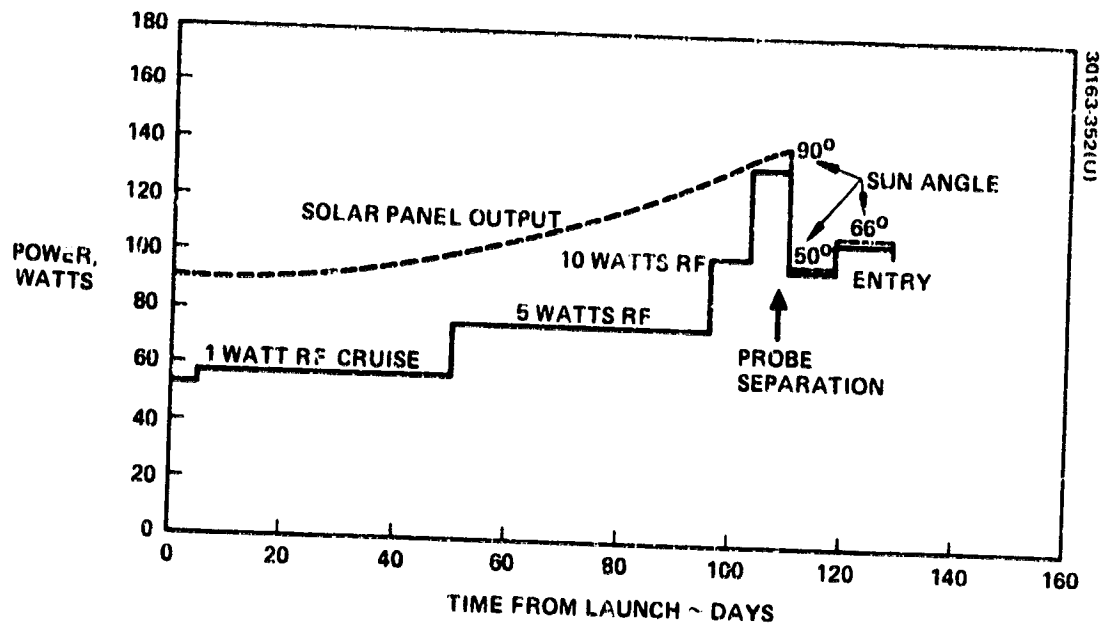


FIGURE 5-1. PROBE BUS POWER HISTOGRAM

unit temperatures because the latter are dependent upon unit thermal design detail and power distribution which are not normally considered at the spacecraft level thermal design. As noted, some of these limits apply to the units themselves rather than mounting surfaces. The science instruments on the equipment shelf will have mounting surface temperatures controlled within the range of 4 to 38°C (40 to 100°F). Steady-state unit power requirements at 28 volts are shown in Table 5-2. The science instrument power requirements shown for the Atlas/Centaur spacecraft configurations are the nominal values with 20 percent margin added.

Total spacecraft power demand histograms at 28 volts are shown in Figures 5-1 and 5-2 for the Thor/Delta spacecraft configurations. The details of unit dissipation for each of the many operational modes are given in Volume 6, Power Subsystem Trades. Because the spacecraft power buses are unregulated with regulation done at each unit using dissipative regulators, actual unit dissipation is a function of bus voltage. The solar array power output/voltage characteristics are dependent upon array temperature, solar intensity, and efficiency degradation induced by solar flare activity. These characteristics are shown in Figure 5-3 for the Thor/Delta orbiter and probe bus spacecraft. Array output is shown for two mission points: 1) at the beginning of the mission near earth, and 2) at Venus. These conditions generally represent the cases of minimum and maximum spacecraft power, respectively. Because array degradation resulting from solar activity can occur at any time during the mission, the thermally worst case is assumed. Maximum degradation is applied to the near earth condition to give minimum power, and the undegraded array output is used at Venus for the maximum power case.

The solar array designs are optimized to satisfy the spacecraft requirements shown in Figures 5-1 and 5-2 for minimum weight. However, maximum array output is typically only utilized for short periods during the mission. When spacecraft demand falls below panel output, bus voltage increases until a balance is achieved or until the bus voltage limiters are activated. At this point, the bus is held at 33 V and any excess panel output is dissipated in the limiter resistors.

The spacecraft thermal designs rely on isolation from the environment and, therefore, are relatively insensitive to solar orientation. However, the internal power is dissipated from louvered radiators, which cannot be efficiently designed for conditions of steady direct solar illumination. Normally, the spacecraft are oriented with spin axis normal to the ecliptic plane and radiator placement has been selected consistent with this. However, some deviation from this orientation is necessary at certain times in the missions. A summary of sun angle conditions for the Thor/Delta missions is given in Table 5-3. Sun angles are measured from the probe end of the probe bus and the high gain antenna end of the orbiter. As indicated, no steady state orientations are required with the sun illuminating the aft end of the spacecraft ( $\gamma > 90$  deg) where the louvered radiators are located. The critical condition exists for the orbiter spacecraft at the time of orbit insertion motor firing when thrust vector orientation requires aft end illumination.

30163 353(U)

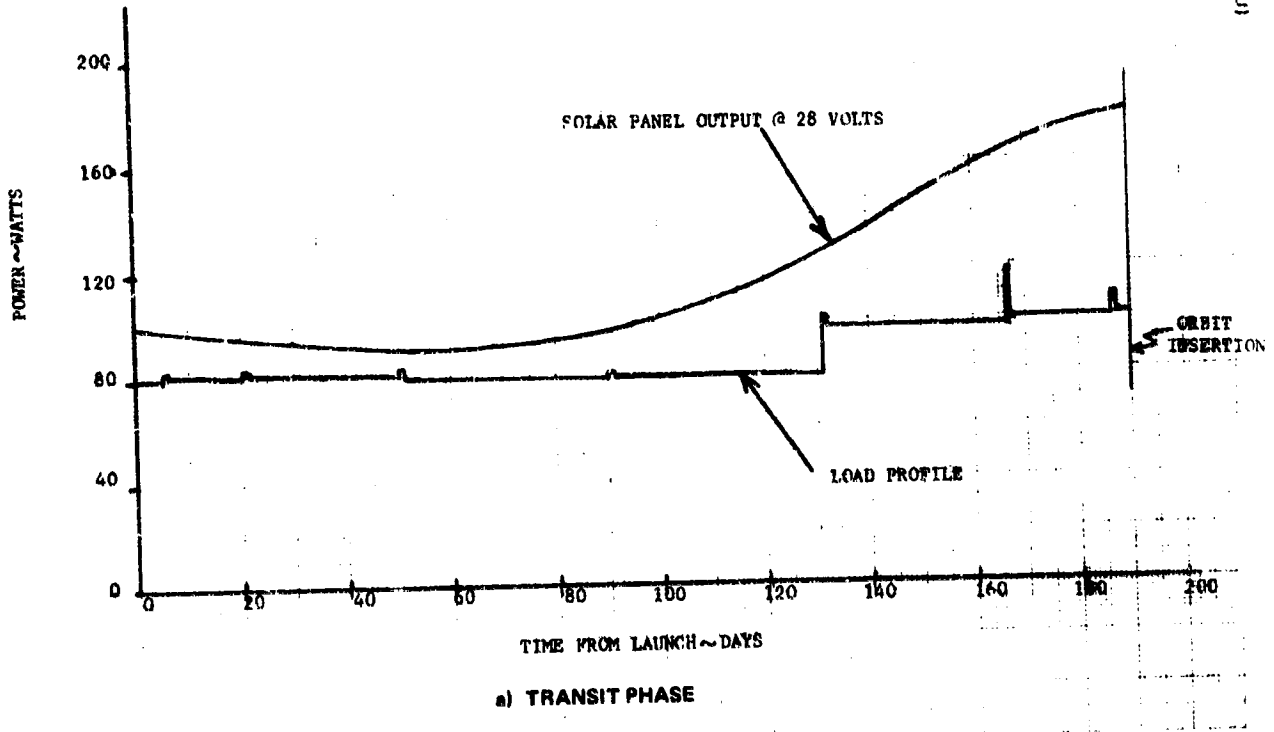


FIGURE 5-2. THOR/DELTA ORBITER POWER HISTOGRAM



30163-354(U)

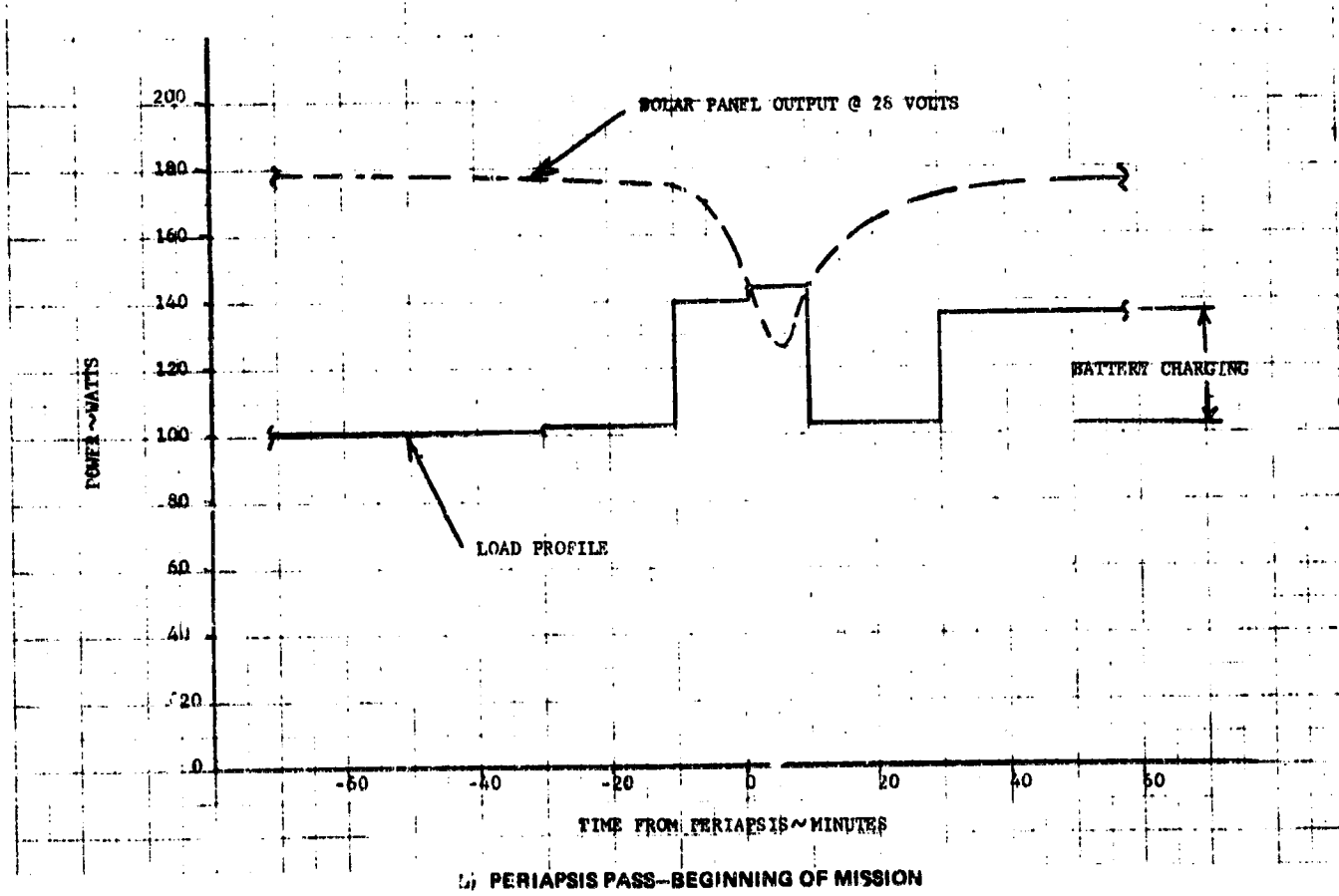


FIGURE 5-2 (CONTINUED). THOR/DELTA ORBITER POWER HISTOGRAM

30153-355(U)

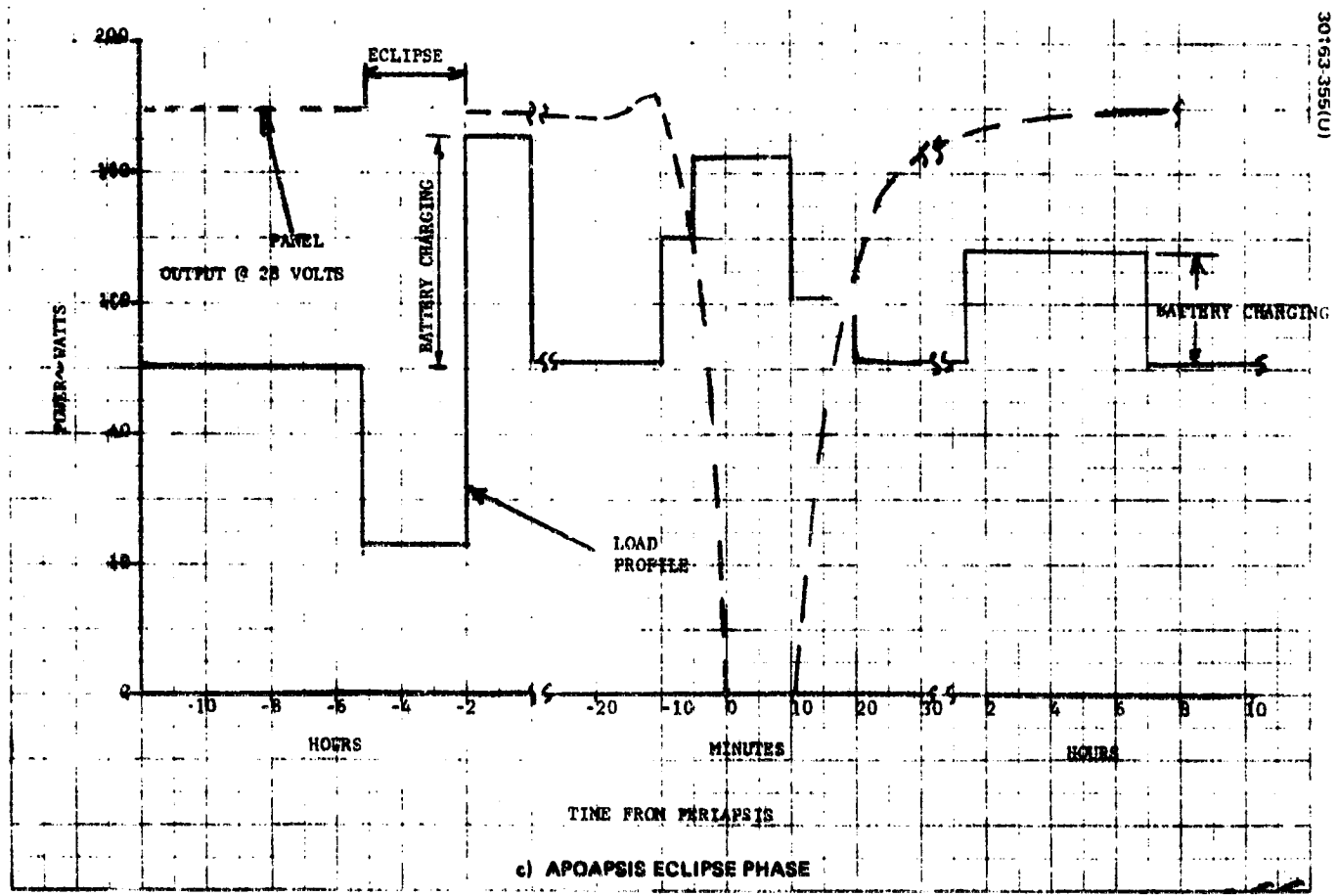


FIGURE 5-2 (CONTINUED). THOR/DELTA ORBITER POWER HISTOGRAM

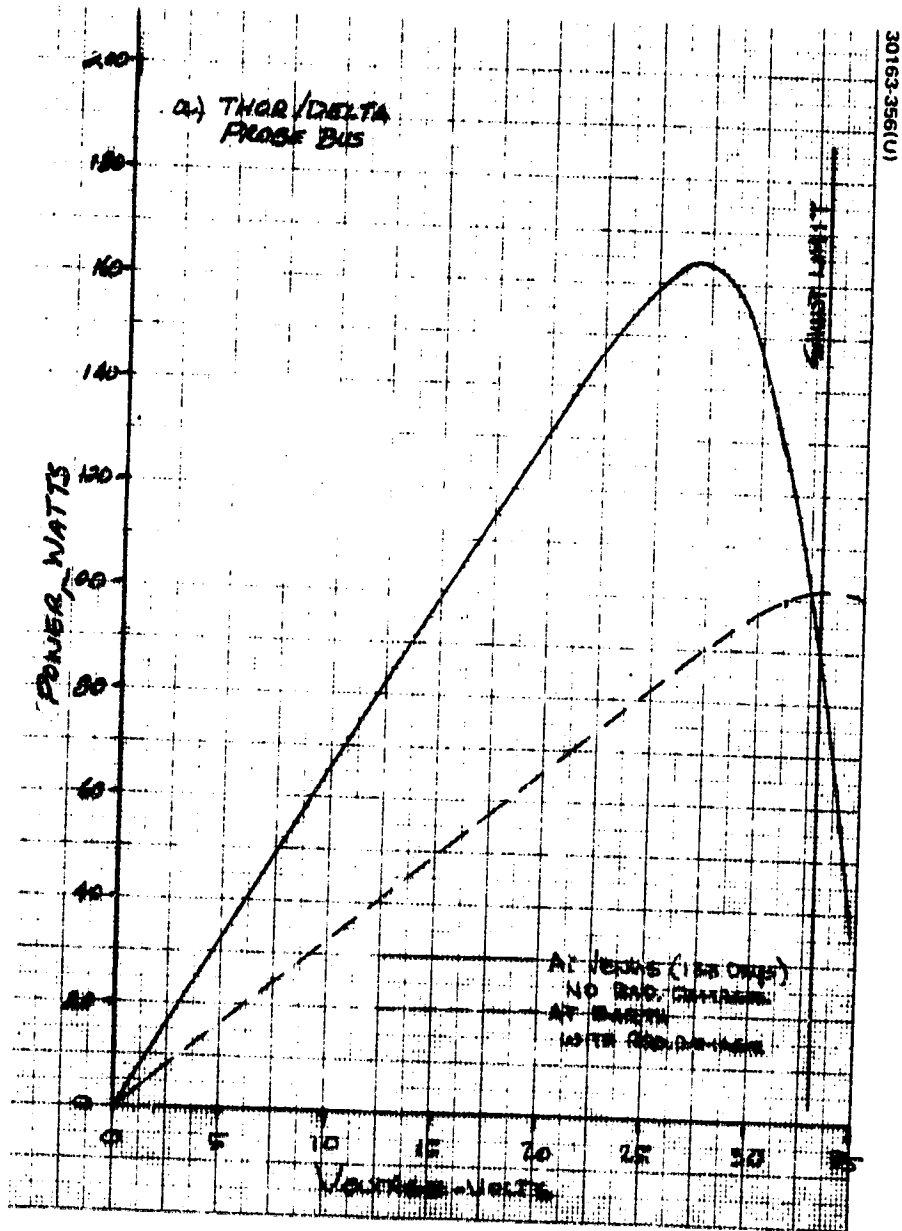


FIGURE 5-3. SOLAR ARRAY PERFORMANCE



TABLE 5-2. UNIT POWER REQUIREMENTS

Subsystem	Power, W at 28 V			
	Thor/Delta		Atlas/Centaur	
	Probe Bus	Orbiter	Probe Bus	Orbiter
<u>Science</u>				
Neutral mass spectrometer	12.0	12.0	14.4	14.4
Ion mass spectrometer	1.0	1.0	3.0	3.0
Electron temperature probe	2.0	2.0	3.6	3.6
Retarding potential analyzer	—	—	—	—
Magnetometer	3.0	3.0	—	4.8
Solar wind analyzer	—	4.0	—	6.0
IR radiometer	—	6.0	—	7.2
X-band occultation	—	—	—	14.4
Radar altimeter	—	17.0	—	20.4
UV fluorescence	—	—	—	—
UV spectrometer	8.0	8.0	1.8	7.2
<u>Communication</u>				
Power amplifier driver				
5 W mode	25.2	25.2	37.8	37.8
10 W mode	50.4	50.4	72.8	72.8
Receiver	6.0	6.0	6.0	6.0
Exciter	4.0	4.0	4.0	4.0
Switches	0.6	0.6	0.7	0.7
<u>Command and Data Handling</u>				
Remote multiplexer	0.4	0.4	0.4	0.4
PCM encoder	2.7	2.7	2.6	2.6
Format generator	5.7	5.7	5.7	5.7
Demodulator	3.0	3.0	3.0	3.0
Data storage	—	0.2	—	3.0
Decoder/memory	1.8	1.8	3.6	3.6
Remotes	0.3	0.3	0.3	0.3
<u>Attitude Control</u>				
Star sensor	1.0	1.0	1.0	1.0
ADP	3.5	3.5	4.0	4.0
DCE	—	5.0	—	6.0
BAPTA motor	—	1.0	—	2.0
JCE	0.5	0.5	0.5	0.5
<u>Propulsion</u>				
Thruster heaters	4.5	5.75	4.5	5.75
Orbit insertion	—	—	—	9.0
Motor heater	—	5.0	10.0	10.0
Tank heaters	—	—	—	—

TABLE 5-3 THOR/DELTA DESIGN SUN ANGLE AND ECLIPSE SUMMARY

Event	Mission	Sun Angle deg*	Duration	Time of Occurrence (After Launch)
Launch/ascent	Probe Orbiter Probe	20 to 35 80 Eclipse	1.5 h 30 min	- -
Cruise	Probe Orbiter	90 ±3	Continuous	0 to 20 days before entry 0 to orbit insertion
First TCM	Both	10 to 170	00 min	5 days
Second TCM	Both	45 to 135	40 min	20 days
Subsequent TCM	Both	90	-	-
Orbit insertion motor firing	Orbiter	103.5	2 h	Encounter
Orbit	Orbiter Orbiter	90 ±3 Eclipse	Continuous {23 min (max) 190 min (max)}	- 80 days in orbit 180 days in orbit
Large probe separation	Probe	45	3 h	20 days before entry
Small probe separation	Probe	37	4.5 h	20 days before entry
Bus targeting	Probe	38	1 h	18 days before entry
Preentry cruise 1	Probe	45 to 58	Continuous variation	10 to 18 days before entry
Preentry cruise 2	Probe	50 to 66	Continuous variation	10 days to entry

\*Measured from spin axis, probe/HGA end

The resulting solar heating limits the time spent in this attitude. Detailed discussion of the effects of solar illumination on louvers is given in subsections 5.2, 5.3, and 5.4 of this volume.

Eclipse times are also shown in Table 5-3. These are important only if internal power is curtailed to minimize battery weight, as is the case during the long eclipse occurring near apoapsis in Venus orbit.

Because the probes are inactive during transit to Venus, much broader temperatures are applied during this period, as indicated in Table 5-1. The most sensitive pressure vessel module unit is the battery. It sets the minimum pressure vessel temperature ( $-40^{\circ}\text{C}$ ). Because the pressure vessel descent thermal design relies on heat capacity to limit maximum temperature at impact, it is important that initial temperatures at entry be as low as possible. Here, again, the battery sets the limit ( $-1^{\circ}\text{C}$  ( $30^{\circ}\text{F}$ )).

Because the probes are thermally independent of the spacecraft bus, particularly during the 20-day period between separation and entry, sun angle variation during the mission is quite important to the thermal design selection. Probe sun angle data is given in Table 5-3.

## 5.2 TRADES

The following trade/design studies were performed to support the selection of the baseline thermal designs.

### Spin Axis Orientation

A system level trade study (Task EX12; see also subsection 3.3, Volume 4) has been performed comparing the advantages of the baseline spin axis orientation normal to the ecliptic with those of an alternate design having the spin axis aligned parallel to the earthline. In support of the study, the effect of this alternate approach on the spacecraft thermal design was examined and a configuration developed to accommodate the resulting differences. The principal effect is the large variation of sun angle with respect to the spin axis. The variation is shown in Figure 5-4 for type I trajectories during the 1976-77 launch opportunity.

The thermal design of the orbiter with the spin axis earth-pointing is adversely affected because every side of the vehicle is exposed to direct solar radiation during the course of the mission. The louvers, which do not provide efficient radiator surfaces when subjected to significant solar illumination as they do when the earth is behind the sun, must be shielded, which also reduces their efficiency. Furthermore, since solar panels must be mounted on the ends of the spacecraft to provide sufficient power when the sunline approaches the spin axis, the minimum attainable average shield solar absorptance to emittance ratio ( $\alpha/\epsilon$ ) is limited. As a result excessive shield temperatures in sunlight near Venus require placing louvers on both sides of the equipment shelf to enable viewing a suitable sink temperature at all times. These effects result in nearly three times more required louver

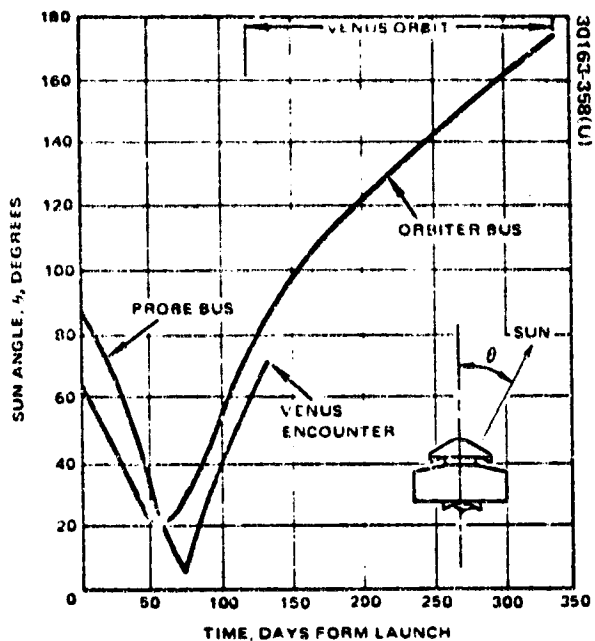


FIGURE 5-4. SUN ANGLES - EARTH POINTING SPIN AXIS DESIGN

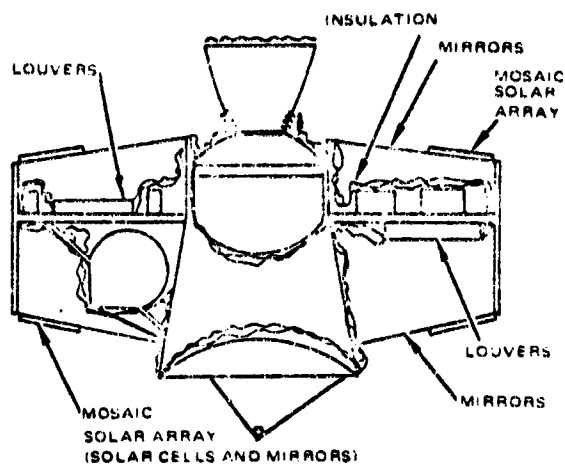


FIGURE 5-5. ALTERNATE ORBITER CONFIGURATION

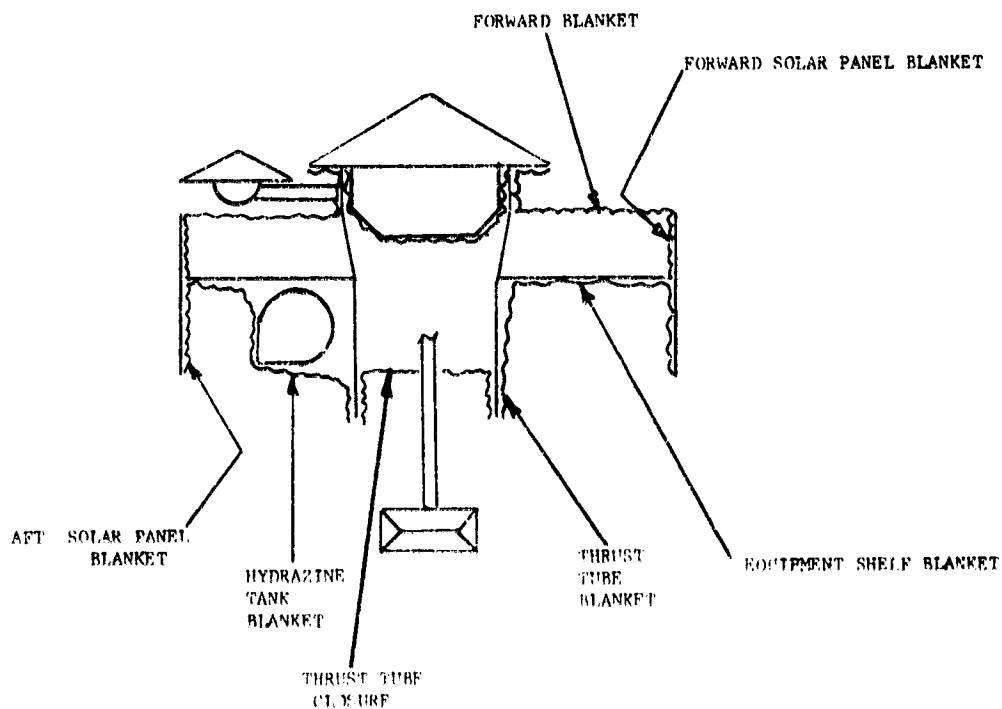


FIGURE 5-6. THOR/DELTA PROBE BUS INSULATION BLANKET ARRANGEMENT



area with a weight increase of 4.5 kg (10 lb). These changes to the baseline design are shown in Figure 5-5.

The louver arrangement not only complicates equipment arrangement but also increases required lateral conductance, leading to the possible need for heat pipes to minimize weight. The end panel must be designed to keep temperatures below the desired solar panel operating point. End array temperatures may be limited by utilizing a mosaic of solar cells and second surface mirrors, minimizing substrate weight required for lateral conduction. Mosaics with cell to mirror area ratios of 1 and 0.5 can limit forward and aft panels, respectively, to maximum average temperatures near 60°C (158°F).

Because direct sunlight is never incident on the antenna end of the spacecraft for the probe mission, the probe bus allows retention of the baseline louver arrangement with louvers mounted on the antenna side of the equipment shelf. However, the probe end solar panel exhibits the design complexities of the ends panels of the orbiter. The general conclusion of this study was that many disadvantages exist for the alternate spin axis orientation, only one of which was a much more complex thermal design.

#### Candidate Thermal Designs

This study examined elements of the baseline spacecraft thermal design to determine if alternate approaches were more advantageous from a cost or weight standpoint.

The principal design concept, utilization of variable emittance (louvered) radiators, is required because of the combination of large changes in solar intensity, relatively large power variation during the mission, and, in the case of the orbiter, long eclipses at minimum power. In addition, the louvered design provides substantially more predictability than does a completely passive design.

However, because this approach also included the isolation of the controlled volume (equipment shelf) from the environment, large insulation blanket weights were involved. Cost was also a consideration. Therefore, examination was made into the possibility of replacement of some of these blankets with lighter, less expensive finishes. Two areas were reviewed: the forward blanket used to enclose the equipment shelf and the blanket covering the inner solar panel surface, decoupling it from the louvers mounted on shelf. These areas are illustrated in Figure 5-6.

On the Thor/Delta spacecraft configurations, approximately 2.3 kg (5.1 lb) of insulation could be removed if the aft solar panel blanket were replaced by a low emittance VDA (vapor deposited aluminum) finish. An examination of this alternative, using the bulk spacecraft thermal nodal model, has shown slightly higher shelf temperature results. A comparison of bulk shelf temperatures are shown in Table 5-4 for the baseline and this design modification. Also considered were the effects of replacing the forward insulation blanket with a single layer barrier, which would save about 1.5 kg (3.2 lb). The blanket was assumed to have an effective inside to outside emittance

TABLE 5-4. EFFECTS OF ALTERNATE  
BLANKET ARRANGEMENTS

Blanket Configuration	Bulk Shelf Temperatures					
	Design Conditions					
	Near Earth Cruise		Venus Encounter, Sun Normal to Spin Axis		Venus Encounter, Sun 30 deg Off Normal	
	°C	°F	°C	°F	°C	°F
Baseline	19	66	28	83	-	-
Aft solar panel blanket replaced by vapor deposited aluminum finish	20	68	29	85	31	87
Vapor deposited aluminum on aft panel and forward blanket replaced by barrier	16	60	25	77	31	87

of 0.02 and the barrier to be 0.0025 cm (0.001 in.) Kapton with an external solar absorptance of 0.4, an emittance of 0.7, and an interior surface emittance of 0.05. As shown in Table 5-4, this additional modification tends to depress shelf temperatures significantly during conditions when the sun is normal to the spin axis. However, this trend disappears when even moderate sun angles are experienced as indicated by the case of the sun 30 deg off normal (toward the probe end of the spacecraft).

The shelf temperature increase caused by the VDA solar panel finish appears to be a minor effect. However, as will be discussed later in this section, interreflections in the cavity formed by the solar panel, equipment shelf, and thrust tube, produce significant solar loading on the louvers. Since much of this results from reflection off the solar panel insulation, it is estimated that a VDA finish, being much more reflective, would tend to aggravate this problem.

The effects of using the forward barrier indicate a significantly greater shelf temperature range could be expected on the probe bus, comparing near earth performance to near Venus entry when large off-normal sun angles exist. This effect is even more important when considering the uncertainty of the solar absorptance for so large a barrier. Furthermore, the use of this barrier on the orbiter would increase losses during the critical 190 min apoapsis eclipse.

It was concluded that these two alternatives to insulation blankets were detrimental to the overall design performance and they were not incorporated into the baseline design.

### Probe Preentry Design Trades

This study examined the thermal control design of the Pioneer Venus entry probes during the transit mission to Venus. In particular, the feasibility of a passive design was considered along with heater power requirements associated with active control. Design conditions were for a pre-midterm Thor/Delta design. The performance uncertainties of the passive design were examined along with two approaches for compensation:

- 1) Additional pressure vessel insulation
- 2) Active heating prior to entry

A comparison of weight requirements show the additional insulation to be the lightest approach.

Passive thermal control of the entry probes during the portion of the mission from launch to the beginning of entry into the Venus atmosphere is influenced by the following:

- 1) Increase in solar intensity by a factor of 1.92 from Earth to Venus
- 2) Sun angle variation during the period from separation to entry
- 3) Differences in the extent of solar illumination in the pre- and post-separation conditions
- 4) Duration of post-separation phase

The large variation in solar intensity during the mission can be designed for if relatively broad temperature limits can be tolerated. Fortunately, during the transit period the probes are inactive and the survival temperature limits shown in Table 5-1 apply. As indicated, the batteries are the limiting units in the pressure vessel; in the deceleration module, the heat shield/aeroshell bond line temperature is the important parameter. At the time of entry, when the probes are powered up, a more restrictive minimum battery temperature is shown.

Except for a brief systems checkout at separation and just prior to entry, no power is dissipated within the probes during the preentry phase.

As shown in Figure 5-7, the nominal spacecraft orientation during cruise results in a sunline normal to the probe axis of symmetry. Transiently, during midcourse corrections, the sunline can approach 0 or 180 deg relative to the axis. The maximum maneuver period was assumed to be 0.9h.

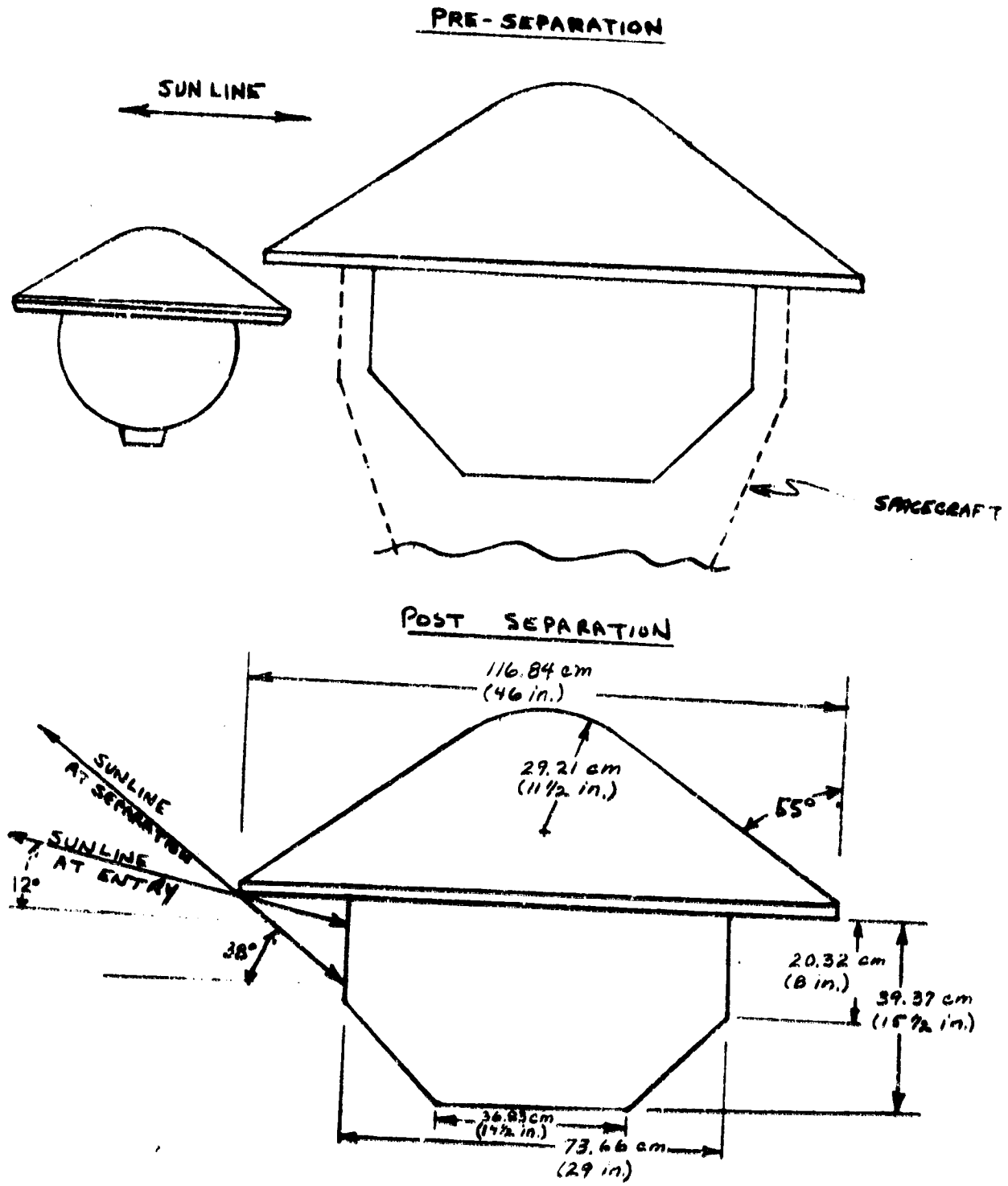


FIGURE 5-7. PROBE CONFIGURATION AND SUN ANGLES

To achieve the desired targeting of the probes, the spacecraft is reoriented just prior to separation. During the 20 day period between probe separation and entry, a gradual change in sun angle occurs. The resulting sun angles assumed for the large probe are shown in Figure 5-7. The effect of sun angle variation is to change the projected area relative to the sun line, hence total incident solar heat load. Figure 5-8 illustrates the variation in the ratio of projected area to surface area with sun angle for the conical heat shield of the large probe.

Also indicated in Figure 5-7 is the installation of the probes on the spacecraft. Significant differences in both illuminated and radiating area are experienced at large probe separation. Most important is the exposure of the aft side of the probe. For the separation and entry sun angles considered, the aft cover receives direct solar illumination. In addition, some minor shadowing of the large probe by the small probes during the preseparation condition is indicated.

The finishes selected for the large probe are shown in Figure 5-9 along with their associated properties.

At separation, the increased radiating area provided by the aft cover tends to somewhat offset the higher solar loading resulting from the higher sun angle on the heat shield. However, it is necessary to minimize solar loading on the aft cover. Therefore, 2-mil silvered Teflon was selected as the finish on cylindrical and conical portions of the aft cover. This is a relatively straightforward means for achieving a stable low  $\alpha/\epsilon$  surface with a moderately high emittance. To maximize the aft end emittance, the heat shield base and the end of the aft cover are painted black. This is compatible with the transparency requirement for the latter surface.

To achieve the desired pressure vessel entry temperature a striping of black paint and aluminized Teflon was selected for the heat shield finish. Aluminized Teflon was selected for this application rather than silvered Teflon to minimize cost since the lower  $\alpha/\epsilon$  is not required. As indicated, a 0.04 increase in solar absorptance is expected during the cruise solar (UV) exposure.

Since the pressure vessel descent (post entry) thermal design is heat capacity dependent, it is desirable to begin the entry phase with the minimum allowable pressure vessel temperature. The constraining limit is the minimum battery operating temperature which was initially assumed to be 4°C (40°F).

To determine the heat shield striping pattern required to nominally achieve the 4°C (40°F) pressure vessel entry temperature, a simple steady state thermal math model of the large probe was developed. The three node model depicted the heat shield/aeroshell, the pressure vessel, and the aft cover with radiation and conduction coupling. Iterative solution of this model indicated a striping of 45 percent Teflon/55 percent black paint yields the nominal 4°C (40°F) entry temperature. Adjusting this model for the pre-separation configuration, solar intensity at earth, and small probe shading

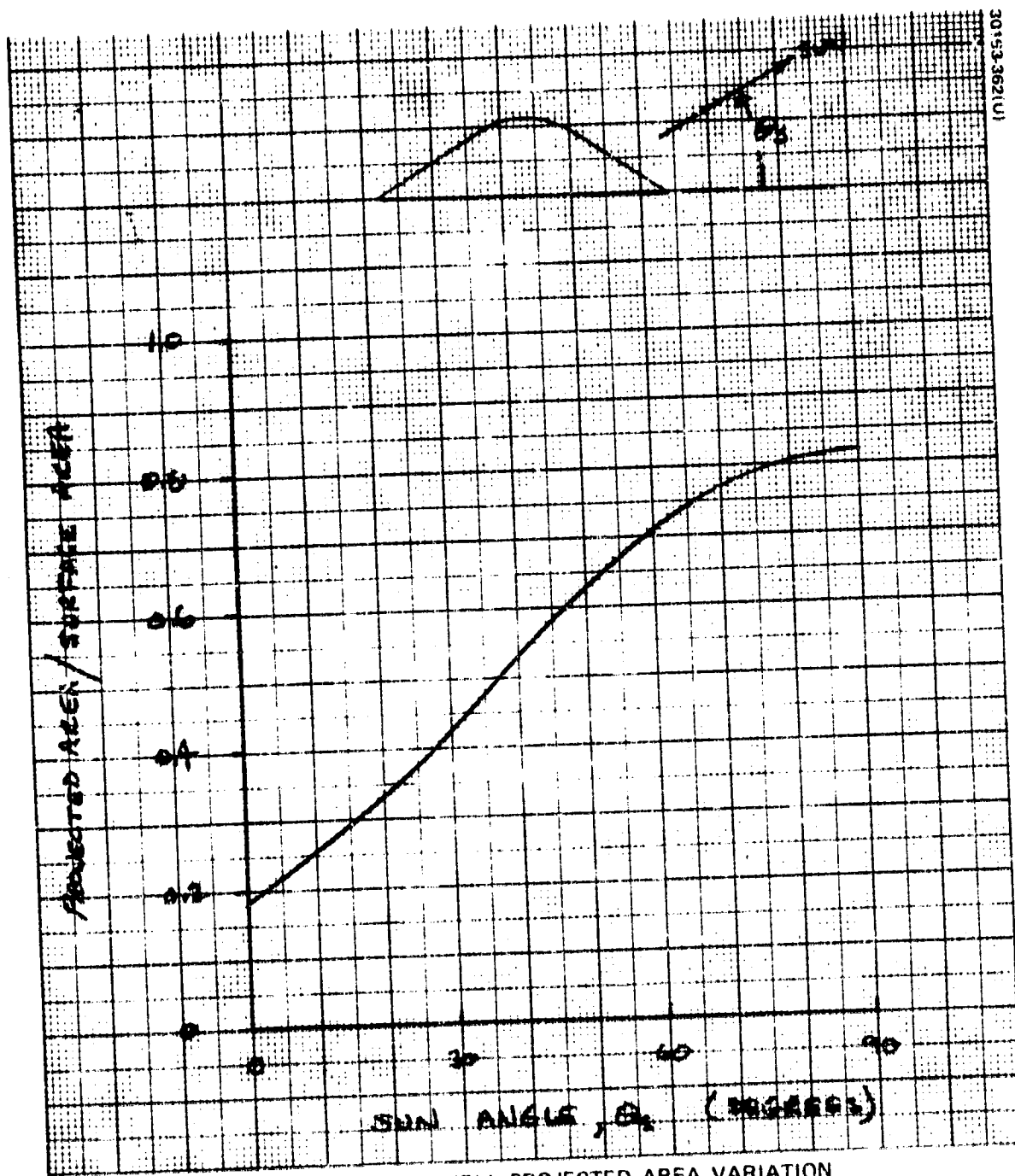


FIGURE 58. AEROSHELL PROJECTED AREA VARIATION

20153-362(U)

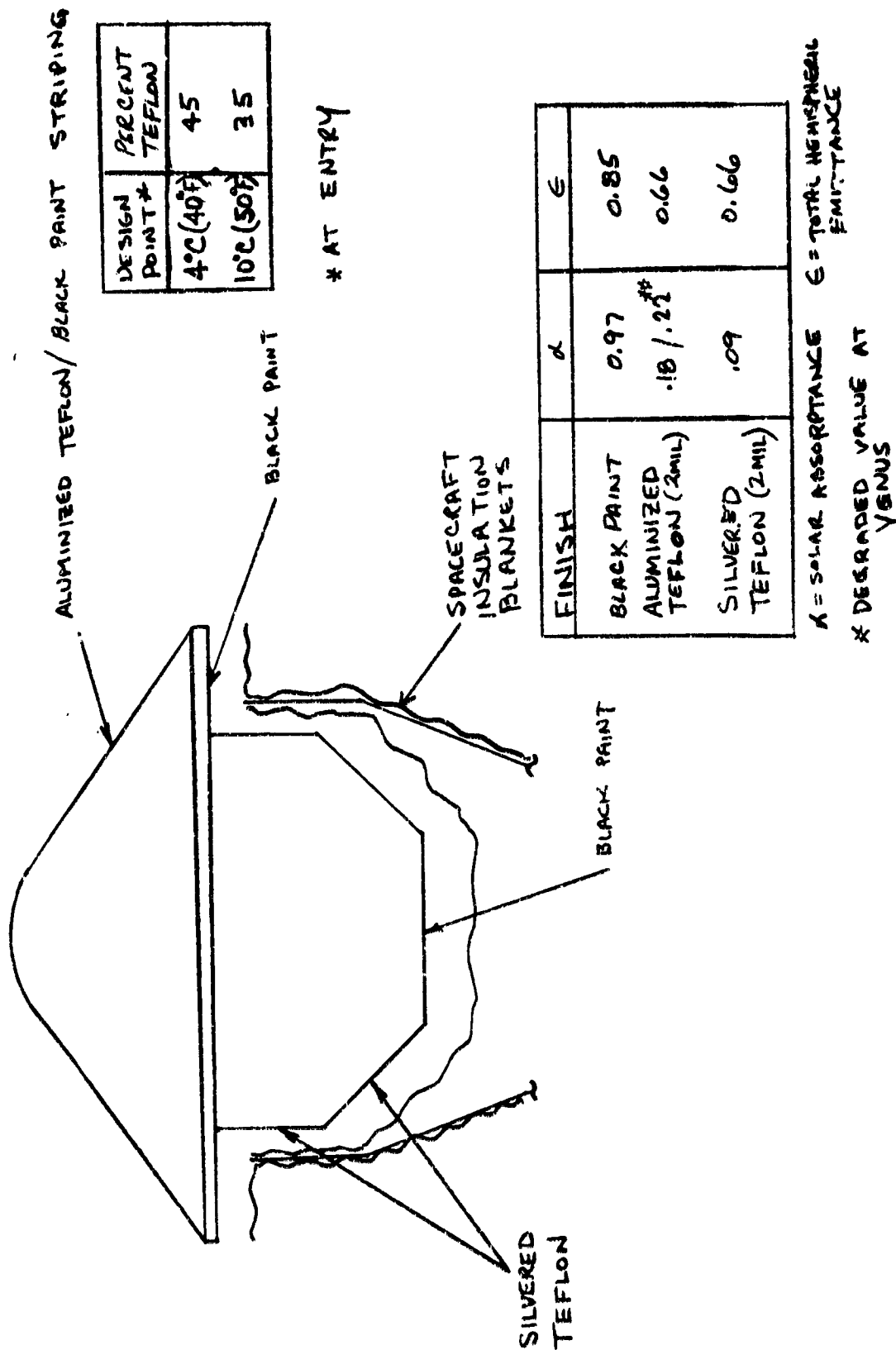


FIGURE 5-9. LARGE PROBE THERMAL FINISHES

4°C (40°F) ENTRY DESIGN POINT

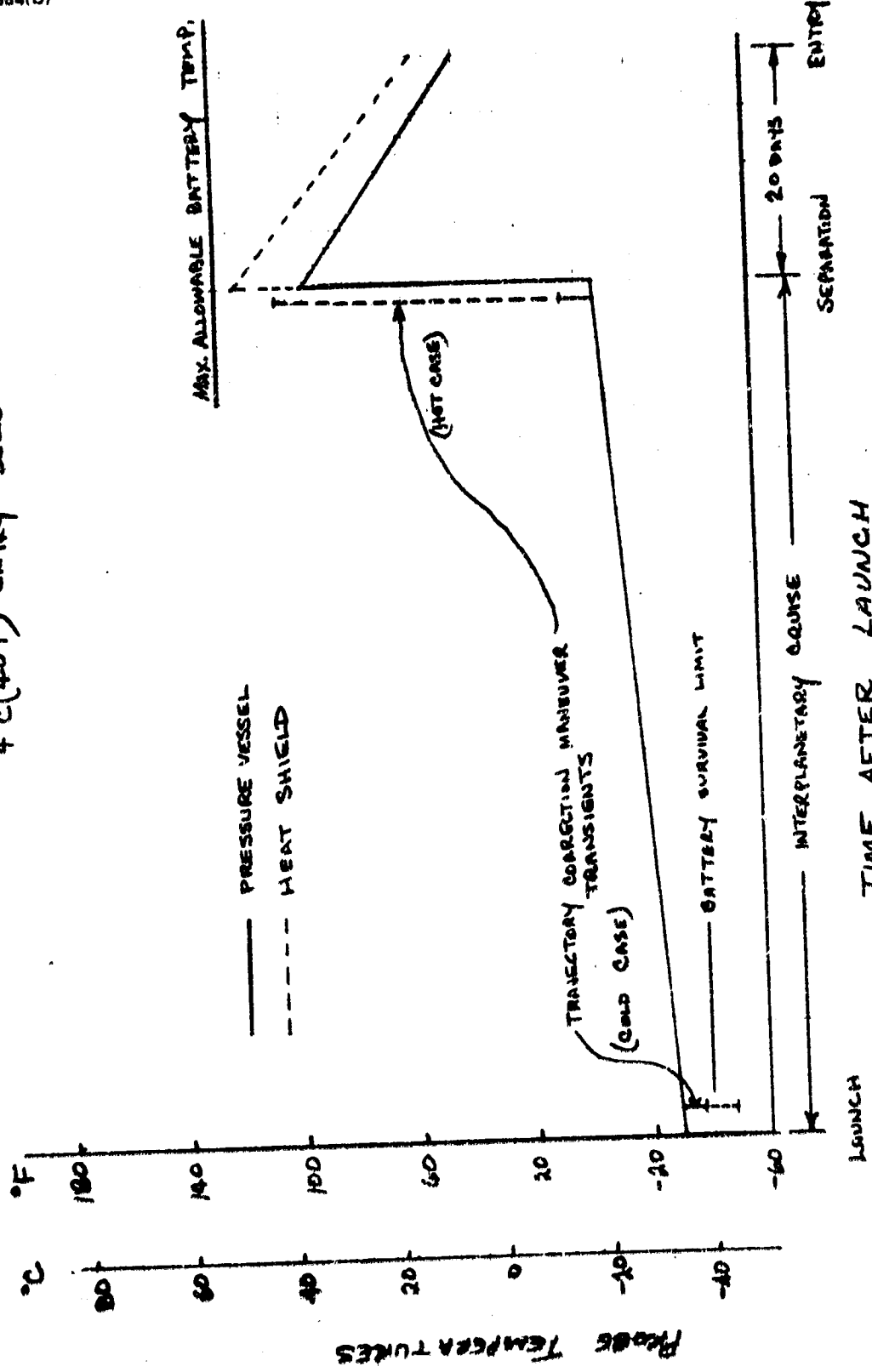


FIGURE 5-10. NOMINAL LARGE PROBE PREENTRY TEMPERATURE HISTORY



(10 percent), the temperatures indicated at the beginning of the interplanetary cruise were shown to be below the minimum battery survival limit ( $-40^{\circ}\text{C}$ ).

By blocking radiation off the aeroshell base with an insulated shield supported by the spacecraft, these temperatures were computed to be about  $-34^{\circ}\text{C}$  ( $-30^{\circ}\text{F}$ ). A solution of this model at the separation conditions indicates temperatures near the maximum allowable. The mission variation of probe temperatures is shown in Figure 5-10. A transient math model was developed for the large probe utilizing single nodes for the heat shield/aeroshell and the aft cover. The Min-K insulation, the pressure vessel shell, and the payload were represented by separate nodes. This model was used to compute response to the off nominal sunline orientation during trajectory corrections (one near earth and one near separation, durations of  $\sim 0.9$  h). These results are also indicated in Figure 5-10 for the cases of sun directly along the cone axis (hot case) and  $180$  deg opposite this (cold case). Temperatures remain within limits for these conditions.

It is concluded, therefore, that the selected passive design nominally satisfies the probe temperature requirements up to entry into the Venus atmosphere.

A brief examination was made of the uncertainty associated with the large probe passive design. Typically spacecraft thermal performance can be predicted within  $5^{\circ}$  to  $8^{\circ}\text{C}$  ( $10^{\circ}$  to  $15^{\circ}\text{F}$ ) for this kind of design. If adequate development testing is undertaken much of this uncertainty could be eliminated. The remaining elements of uncertainty include sun angle dispersions, finish degradation, variations in contact conductances at interfaces, and deviations in test simulation from actual flight conditions and hardware.

The first three elements were examined for some assumed dispersions. For example, 20 percent variation in conductance yielded less than  $0.5^{\circ}\text{C}$  change in the pressure vessel temperature predicted by the probe math model. Similar sensitivities were  $\sim 2^{\circ}\text{C}$  for a 0.02 variation in solar absorptance of aluminized Teflon and  $1^{\circ}\text{C}$  for a 1 deg variation in sun angle. The rss'ed uncertainty is about  $3^{\circ}\text{C}$ . For the purposes of evaluating the effect on probe design, a  $5^{\circ}\text{C}$  ( $10^{\circ}\text{F}$ ) uncertainty in pressure vessel temperature was assumed.

Nominally, no active control (electrical heating) of the probes is indicated by the analysis discussed above. However, consideration of the passive design uncertainty and how it can best be treated in the overall thermal design leads to the possibility of utilizing active heating to condition the probe batteries just prior to entry. The alternative is to bias the nominal design temperature at entry to provide margin for this uncertainty, i. e.,  $10^{\circ}\text{C}$  ( $50^{\circ}\text{F}$ ) instead of  $4^{\circ}\text{C}$  ( $40^{\circ}\text{F}$ ). This approach tends to increase the nominal pressure vessel insulation thickness.

Active heating, depending upon its implementation, can require substantial battery weight since the probes are separated 20 days prior to entry and, therefore, cannot utilize spacecraft power. The least electrical energy is required if a thermostatically controlled heater were activated just prior

30163 365(U)

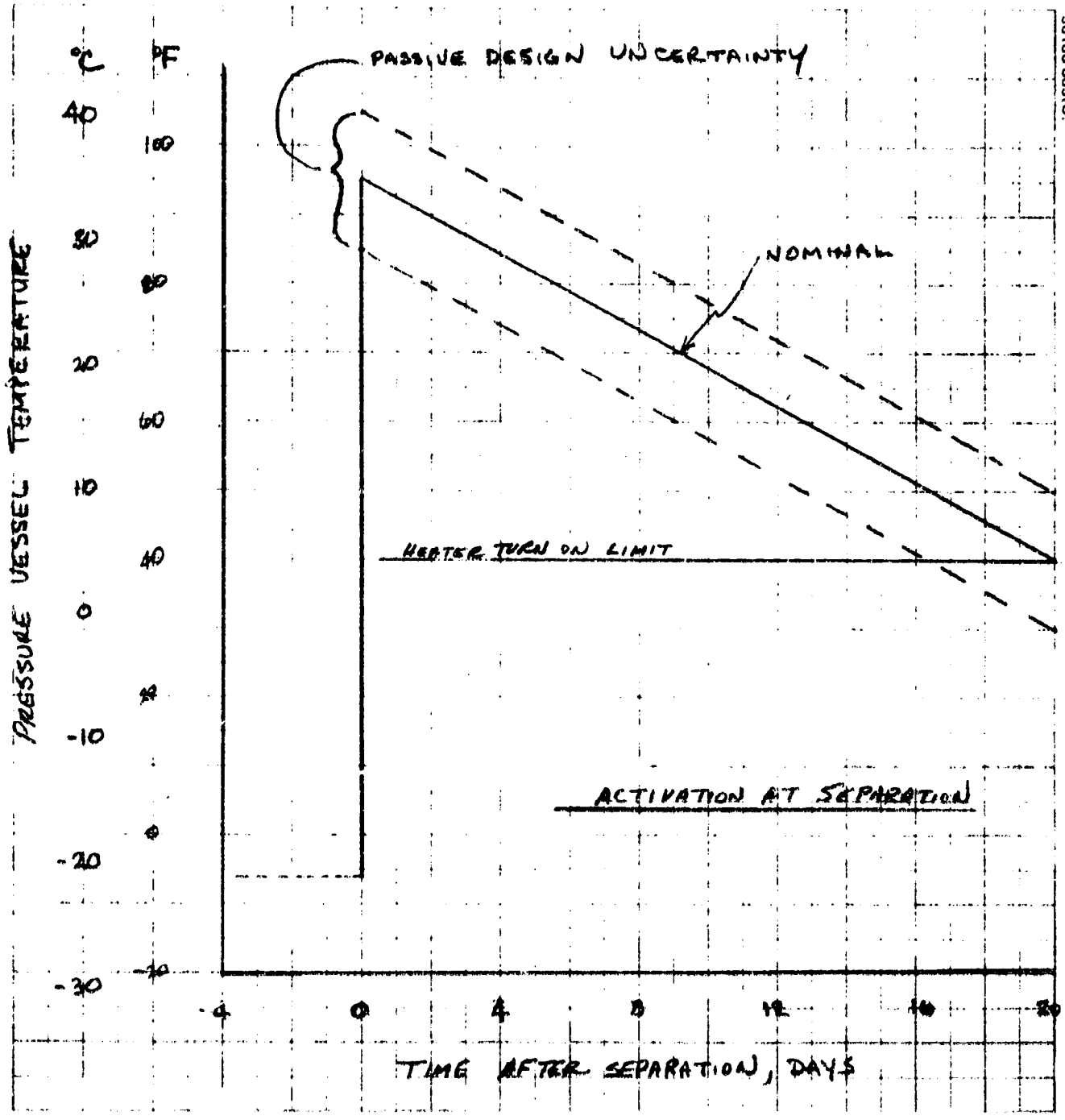


FIGURE 5-11. PRESSURE VESSEL HEATER OPERATING REQUIREMENTS

to entry, bringing battery temperature up to the required minimum. This, however, is somewhat contradictory since the battery itself is the source of heater power and its use violates the limit being controlled. The penalty associated with battery discharge at low temperature is loss in capacity. Therefore, if battery operation below its desired minimum temperature is allowed, it would seem more appropriate to account for this in battery margin rather than adding capacity for heating. If the battery limit is strictly observed, heater control activation would be required at separation.

The weight requirements associated with both heating approaches has been evaluated using the probe math models to compute heater requirements, both steady and transient, to maintain the pressure vessel at 4°C (40°F) at entry assuming the passive design performance were 5°C (10°F) below the nominal.

Figure 5-11 illustrates the effect of uniformly decreasing the nominally calculated pressure vessel temperature during the separation to entry period by 5°C (10°F). This shows heater turn-on at approximately 3.5 days prior to entry. Assuming a linear temperature and heater power variation, the 20 W heater shown to be required at the entry condition results in the battery capacity and weight requirements shown in Table 5-5.

Figure 5-12 shows the energy requirements for the transient warm-up technique as a function of heater power. The associated battery weight also shown in Table 5-5 for a reasonable heater size includes a 30 percent penalty because of low temperature discharge.

A comparison of these weights, which neglect heater weight and any pressure vessel shell increase, with the estimated insulation weight increase associated with a 50°F (10°C) entry temperature show the latter to be minimum. Subsequent to this study, the minimum battery temperature was lowered to -1°C (30°F), making the nominal 4°C (40°F) entry acceptable.

TABLE 5-5. WEIGHTS REQUIRED FOR COMPENSATING  
5°C (10°F DESIGN UNCERTAINTY)

Approach	Required Battery Capacity, (W-hr)	Weight	
		kg	lb
Passive - increased insulation (Min-K TE 1400)	--	1.0	2.3
Active heating:			
Activation at separation (20 W maximum)	860	18.6*	41.0*
Activation at entry	87	2.5*	5.4*

\*Neglects weight for increased pressure vessel volume.

30163-366(U)

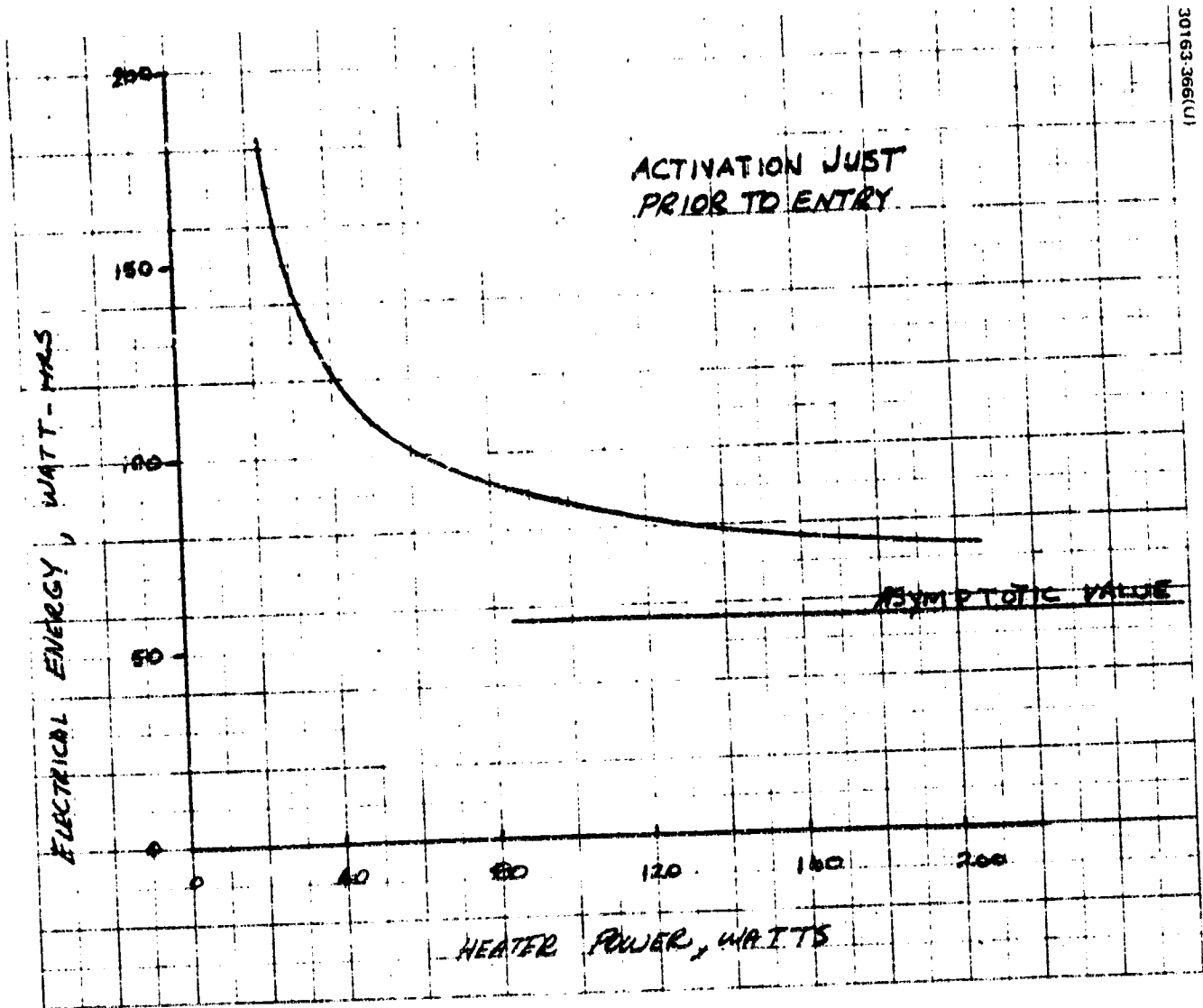


FIGURE 5-12. PRESSURE VESSEL WARMUP HEATING REQUIREMENTS

The passive thermal control of the large probe during the preentry phase appears to be feasible and the desired approach.

The present baseline for the small probes is also a passive design.

#### Aft Cavity Solar Interreflection Test Evaluation

Hughes Aircraft Company has been conducting IR&D studies to develop spacecraft thermal control systems for many years. In a recent IR&D test\* solar interreflection measurements were made at Hughes, using a one-third scale model of the aft cavity geometry representative of the Pioneer Venus orbiter spacecraft. The purpose of these tests was to provide estimates of the solar loading on the thermal control louvers mounted within this cavity. Although the spacecraft will be nominally oriented with its spin axis normal to the sunline, there will be periods (trajectory correction maneuvers, orbit insertion motor firing) when the aft end of the spacecraft receives direct solar illumination. The measurements were taken, using the sun as the illumination source, at elevation angles of 0, 10, 20, 30, 60 and 80 deg out of the spin plane. Figure 5-13 shows a sketch of the model and the solar orientation geometry; Figure 5-14 is a photograph of the model. At a given solar elevation, measurements were taken at azimuth positions from 0 to 180 deg in increments of 30 deg. These results were then integrated to obtain spin-averaged loads. They are summarized in this report and some general observations made concerning the importance of these results to the spacecraft design. Detailed analysis of the effects of these data on the spacecraft thermal performance is discussed in subsections 5.3 and 5.4. The results obtained indicate the need to constrain the solar elevation angle as the spacecraft approaches Venus to avoid louver blade overheating. Also, the duration of significant cavity illumination, even near earth, should be limited to transient conditions to avoid overheating the spacecraft equipment platform.

#### Module Average Solar Loads

The photometer measurements were taken on each of the three simulated louver modules grouped as shown in Figure 5-13. The data reduction was performed in two different ways. First, to evaluate the effect on louver heat rejection capability, the data was averaged over all modules at a given solar elevation to obtain variation with azimuth angle. Typical results are shown in Figure 5-15. As shown, maximum module solar illumination occurs at an azimuth angle of 180 deg. In or near this position, incoming solar energy incident on the outboard edge of the concave surface of the solar panel cylinder tends to be focused down into the bottom of the cavity.

At lower solar elevations, the minimum intensity appears to be near 90 deg azimuth where shadowing from direct illumination still exists and incident reflections are minimum. However, at higher elevations, direct

\*R. W. Fehr, "Planetary Spacecraft Solar Interreflection Tests," Hughes TIC 4112.12/481, dated 30 January 1973. (See Appendix)

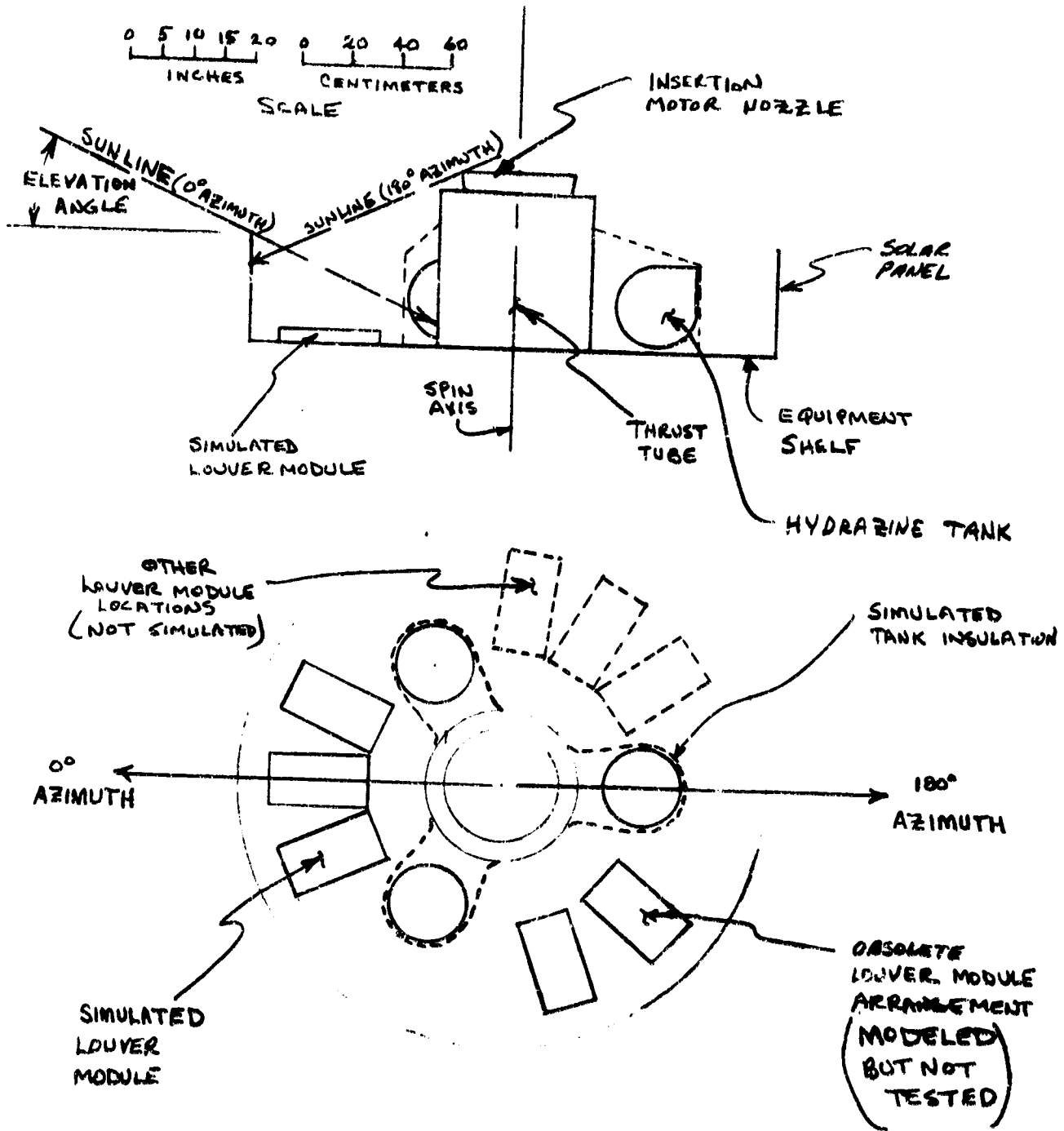


FIGURE 5-13. MODEL AND SOLAR GEOMETRIES

REPRODUCIBILITY OF THE ORIGINAL PAGE IS POOR.

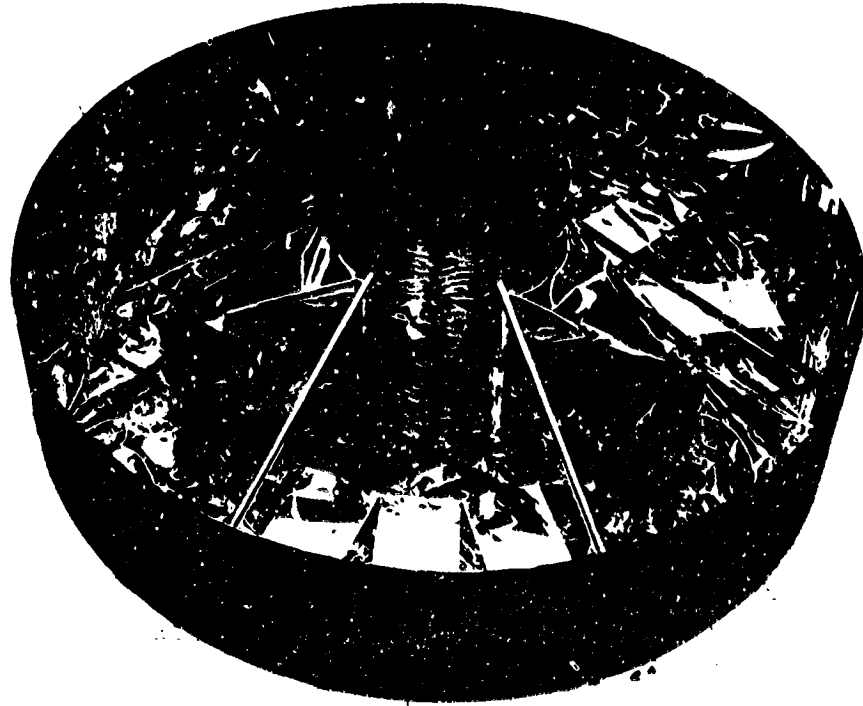
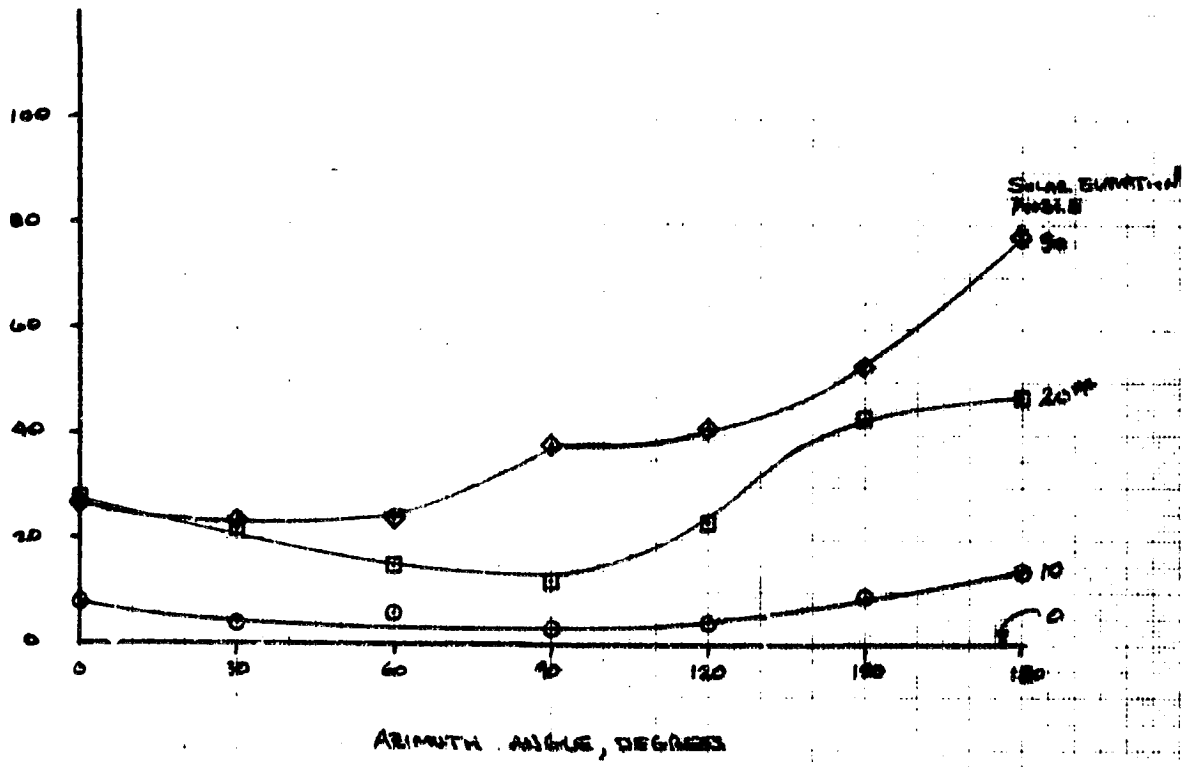


FIGURE 5-14 TEST MODEL (PHOTO 30163-368)

REPRODUCIBILITY OF THE ORIGINAL PAGE IS POOR.

INTENSITY, PER CENT OF SOLAR INTENSITY



30163-369(1)

# 6 POINT, 11-10 AVERAGE MEASUREMENTS; ALL OTHERS, 30 POINT MEASUREMENTS

FIGURE 5-15. AVERAGE MEASURED INCIDENT LOUVER MODULE SOLAR LOADS



illumination occurs. Indirect illumination at the 0 deg azimuth tends to increase with elevation angle. The measurements at 0 deg solar elevation were within the background noise and the repeatability of a typical measurement.

A similar data reduction was performed averaging the measurements on the center louver module separately from the two outer modules. This tends to show a small difference between modules.

The azimuth distribution of measured intensities were integrated to determine the spin-averaged intensity variation with elevation angle as shown in Figure 5-16. Results for the three module average intensity are compared with the average values for the right and left-hand (R/L) outer modules, which tended to be higher than those for the center module. Considering the uncertainties of the technique, these values are very little different. The initial test program was conducted for solar elevation angles up to 30 deg. Subsequent testing was done at 60 and 80 deg.

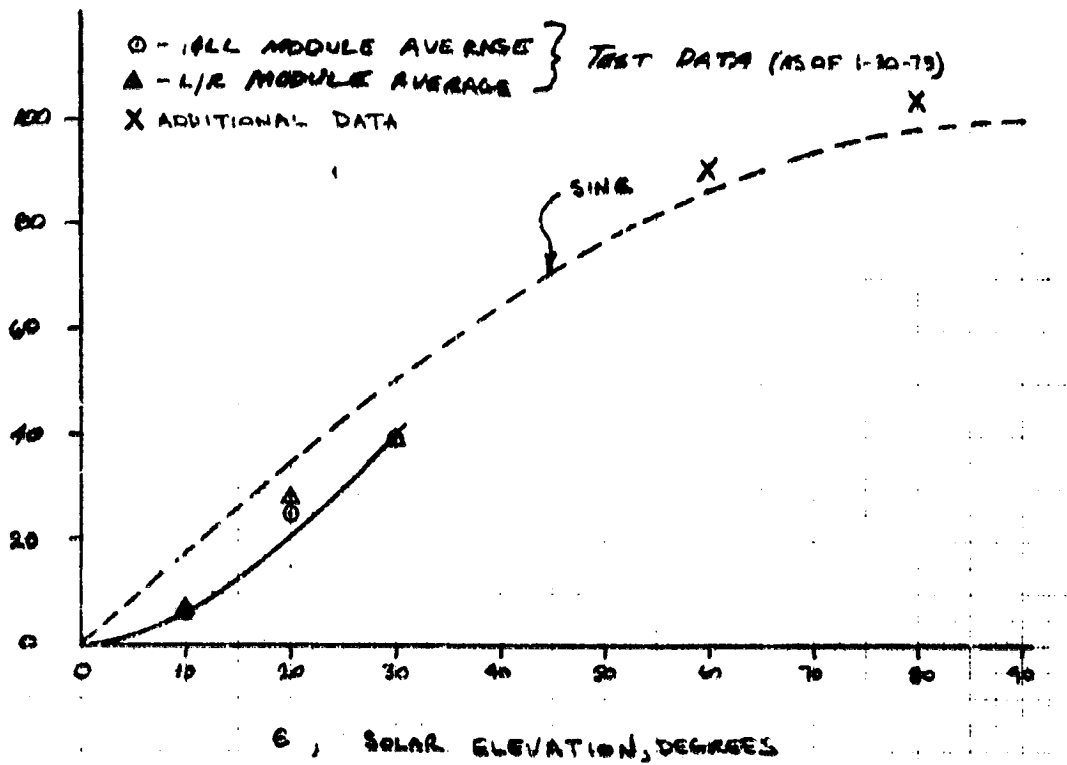
As a comparison, a plot of  $\sin \epsilon$  is also shown. This quantity corresponds to the direct solar load if there were not interreflections or shading in the cavity. This simple correlation matches the data rather closely.

#### Average Louver Blade Solar Loads

Of principal concern is the heating of the louver blades themselves during periods of direct or reflected solar illumination. Because the blades have a high ratio of solar absorptance to emittance ( $\sim 0.20/0.05$ ) and are thermally isolated from the module frame and the mounting surface, very high blade temperatures can result if significant solar loading is experienced. Moreover, because of its low heat capacity each  $5.1 \times 40.7$  cm ( $2 \times 16$  in.) blade weighs only 22.7 gm (0.06 lb), the blade time constant is on the order of minutes. To assess the magnitude of local blade solar loads during cavity illumination, a somewhat different data reduction method was used. Measurements along a given blade location were integrated with respect to azimuth angle to obtain intensity distributions along blade length. Left and right hand louver module distributions were averaged together since symmetry should make these loads nearly the same over 360 deg of azimuth. The maximum local spin-averaged blade solar flux is shown in Figure 5-17 as a function of solar elevation angle. Again, the quantity  $\sin \epsilon$ , where  $\epsilon$  is the solar elevation angle, is shown for comparison. As would be expected, the maximum local solar loading is somewhat higher than the louver module averages. A representative example of intensity variation along a blade is shown in Figure 5-18.

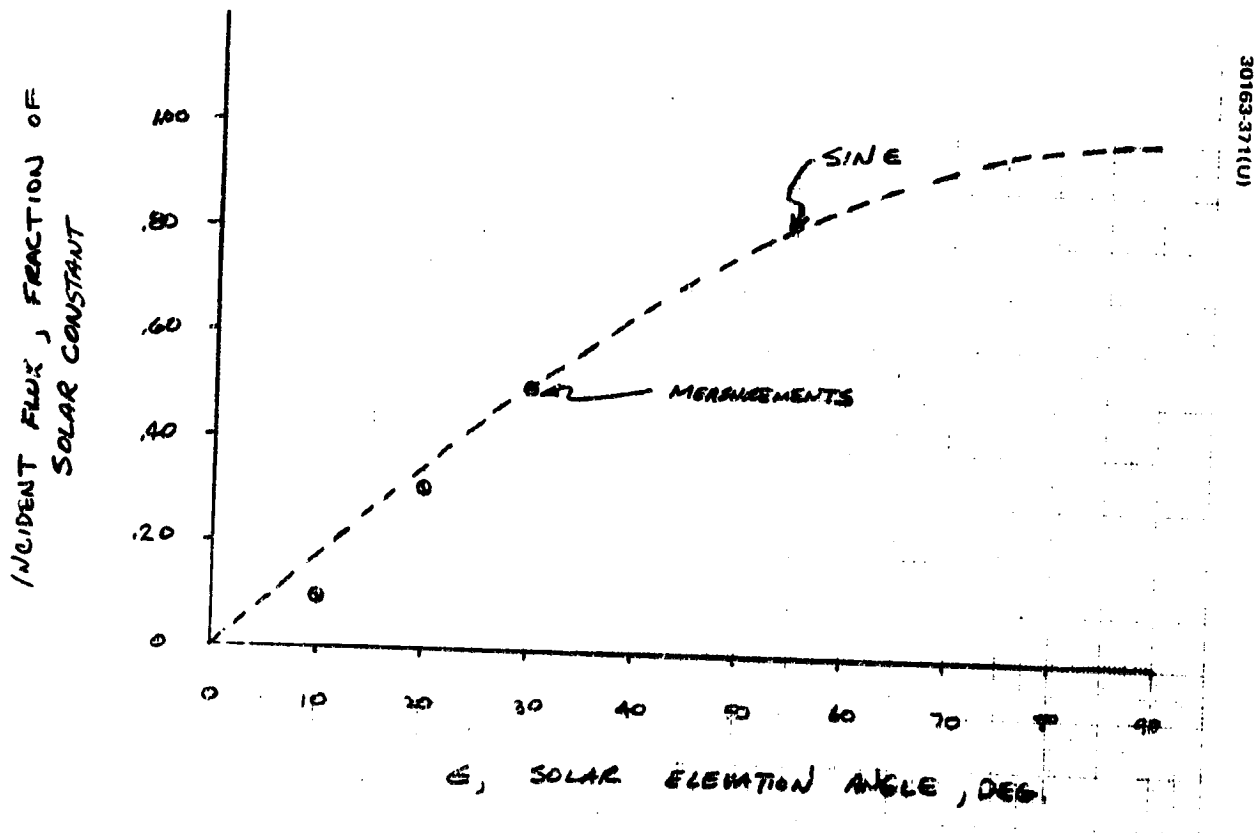
The overall results of this test program indicate that significant solar loading will be experienced by the louvers even at moderate sun angles. This is particularly important at Venus where solar intensity is nearly doubled. Detailed analysis of spacecraft and louver blade response to this heating is presented in subsections 5.3 and 5.4 of this volume.

IRRADIANT INTENSITY, PERCENT OF SOLAR INTENSITY



30163-370(U)

FIGURE 5-16. SPIN AVERAGED MEASURED LOUVER MODULE SOLAR LOADS



30163-371(U)

FIGURE 5-17 SPIN AVERAGED MAXIMUM LOCAL LOUVER BLADE SOLAR FLUXES

30163-372(U)

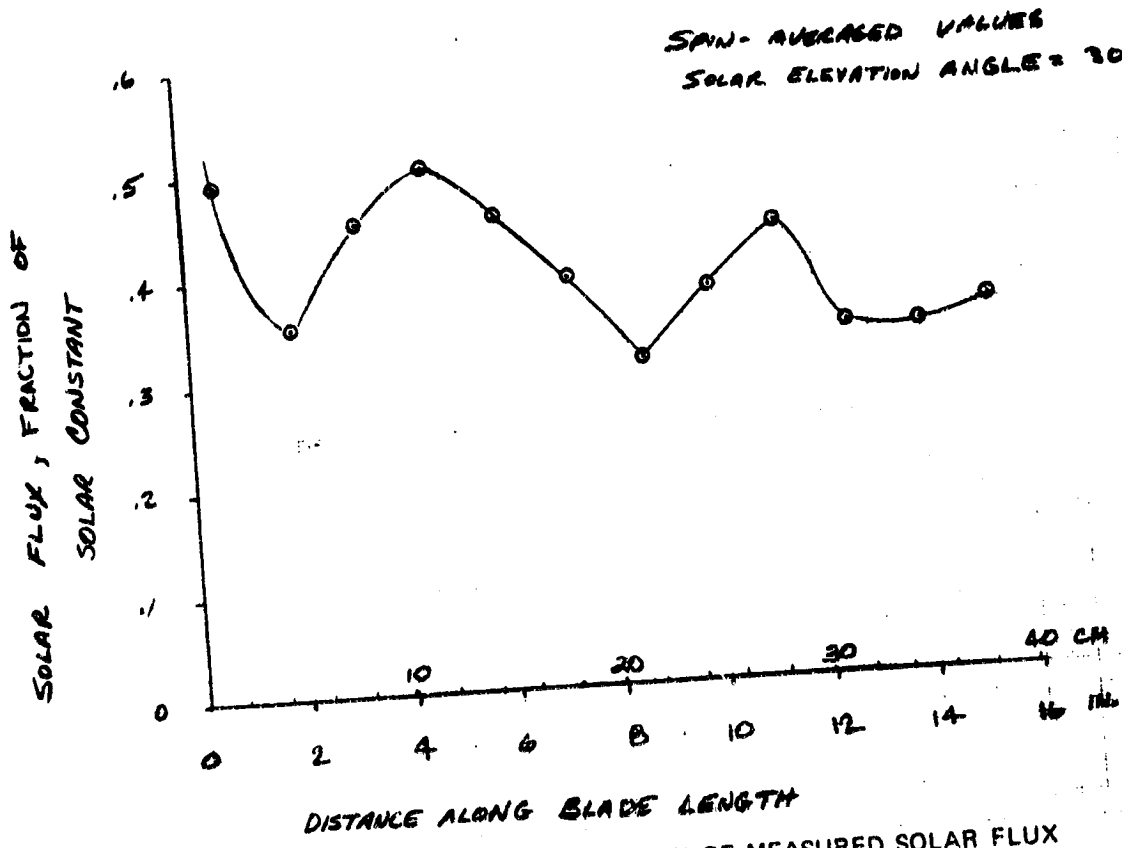


FIGURE 5-18. TYPICAL DISTRIBUTION OF MEASURED SOLAR FLUX ALONG LOUVER BLADE

## Rocket Exhaust Plume Impingement Study

This study examined the effects of rocket exhaust plume heating resulting from the orbit insertion motor and Delta third stage (TE-364-4) firings. Convective heating rates for the orbit insertion motor were based on computed plume flow field while radiative heating was scaled from experimental measurements made during a TE-364-1 (Surveyor retro motor) qualification firing. Heating of the Kapton superinsulation blankets and the blades of the thermal control louvers was of primary concern because of their low thermal capacity. Response of spacecraft antenna located near the plumes was also examined.

The results of this study influence the spacecraft design as follows:

- 1) Selection of Kapton as the insulation material because of its high temperature capability
- 2) Insulation blanket outer layer thickness increased from 1 to 5 mils over local areas to provide desired margin
- 3) Stainless steel foil barrier used instead of Kapton blankets for closure between thrust tube and insertion motor nozzle because of high local heating
- 4) Aft omni antenna structure minimum wall thickness constrained by plume heating

The heating resulting from the orbit injection motor plume has been shown to be more severe than that specified for the Delta third stage firing.

Figure 5-19 illustrates the location of the orbit insertion motor in the Thor/Delta orbiter spacecraft configuration and those spacecraft surfaces which are anticipated to experience significant plume convective and radiative heating. Also indicated in the location of the Delta third stage motor (TE-364-4) nozzle exit plane relative to these surfaces. The following discussion presents the bases for the predicted plume heating rates and the associated spacecraft thermal response.

### Orbit Insertion Motor

When this study was initiated, the orbiter spacecraft was being designed for a type I interplanetary trajectory and the insertion motor selected was the Aerojet SVM-2 (modified). However, subsequent to the generation of a plume flow field based on SVM-2 properties, the spacecraft design was modified for a type II trajectory and the insertion motor changed to the Thiokol TE-M-521 (modified). To determine the applicability of the SVM-2 plume to the TE-M-521, two parameters were compared: nozzle area (expansion) ratio and chamber pressure. Generally, higher expansion ratio means: 1) higher exit plane Mach number, hence decreased flow expansion, and 2) lower exit plane density. These effects decrease local density and, hence, convective heating rates. Higher chamber pressure tends to have the

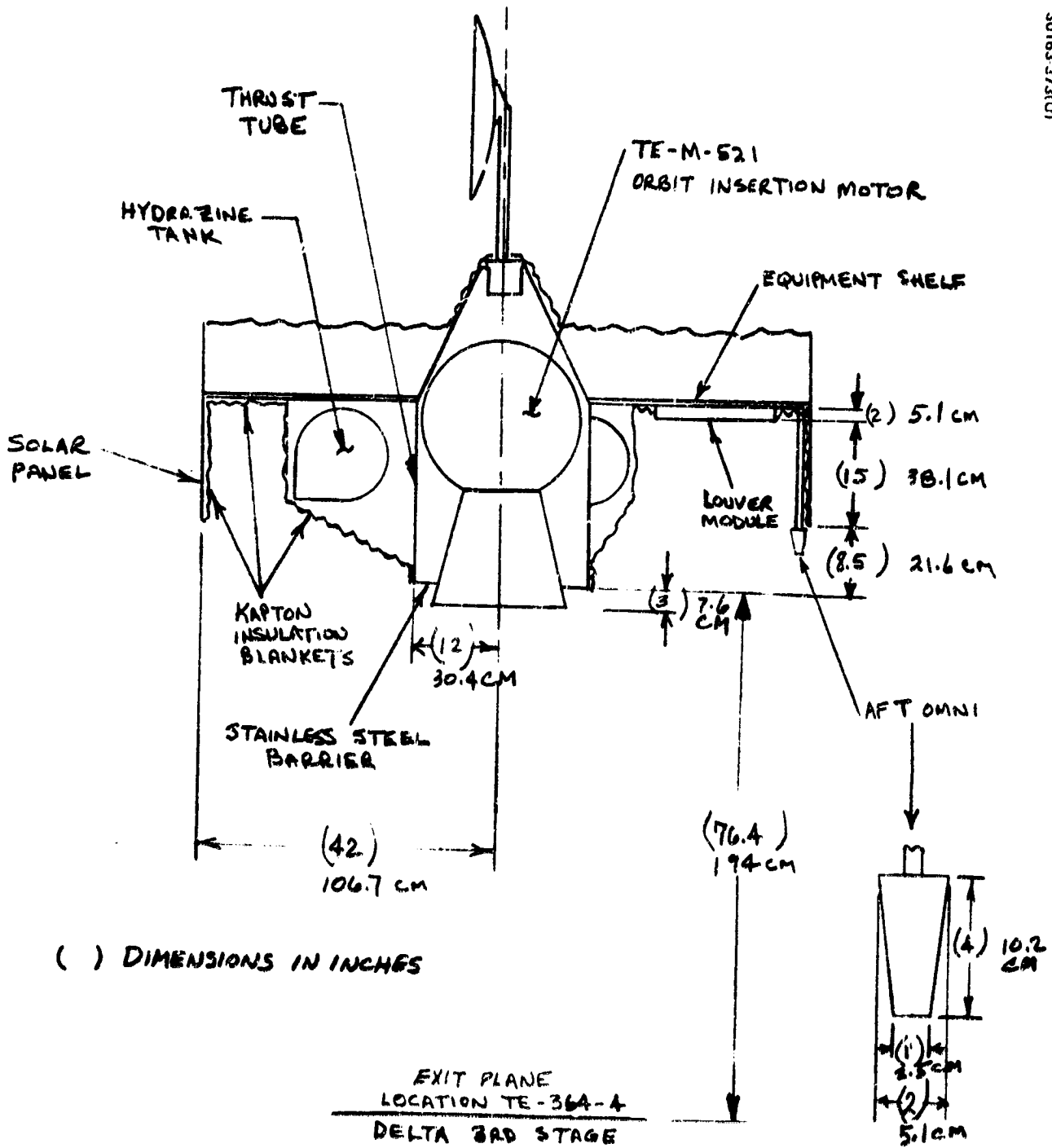


FIGURE 5-19. THOR/DELTA ORBITER AFT CAVITY GEOMETRY

opposite effect, i. e., higher exit plane density. The expansion ratios and chamber pressures assumed for these two motors are given in Table 5-6. As indicated, the modified SVM-2 has lower values for both these parameters; therefore, a qualitative plume comparison could not be made. However, a plume flow field computed for the UTC FW-5 apogee motor used on the HS-333 (Telesat) was available for comparison. As also shown in Table 5-6, the FW-5 motor has approximately the same expansion ratio (60:1) as the TE-M-521 (58:1) and a higher chamber pressure. A comparison was made of the convective heating rates obtained for the orbiter spacecraft using the SVM-2 plume with corresponding heating rates using the FW-5 plume. The SVM-2 heating rates were slightly higher; therefore, it was decided to use the SVM-2 plume to evaluate the TE-M-521 heating rates. Flow field properties are defined for radial and axial coordinates normalized to nozzle exit plane radius. Of course, the TE-M-521 nozzle radius was used to evaluate local plume properties.

### Heating Rates

As discussed above, the SVM-2 (modified) plume was used to compute the convective heating rates on several surfaces of the orbiter spacecraft. This plume was computed by an axisymmetric method of characteristics program using the exit plane properties given in Table 5-6. Included in the nozzle expansion are the effects of the low Mach number nozzle boundary layer, which tends to substantially increase the flow expansion back into the region of interest, i. e., the spacecraft aft cavity. The principal feature of this technique is the replacement of the subsonic portion of the boundary layer with an equivalent layer which is assumed to become slightly supersonic ( $M \sim 1.05$ ) immediately at the exit plane with no flow turning associated with this sudden transition.

The plume flow field is defined by lines of constant density and flow direction as shown in Figure 5-20. The aft geometry of the orbiter spacecraft is superimposed to illustrate the local variation of these quantities. These curves are shown for radial and axial position relative to an origin along the nozzle centerline at the exit plane, with coordinates normalized to nozzle exit plane radius. The TE-M-521 nozzle radius was used to construct the superimposed spacecraft geometry.

The complex flow geometries combined with rarefaction effects makes accurate prediction of plume heating rates quite difficult. Bounding calculations can be made by assuming a simple free molecule flow model with perfect accommodation.

However, there are many cases where this assumption results in highly conservative heating rates which penalize the spacecraft design. For certain surfaces, reasonable boundary layer heating rates can be estimated from conventional aerodynamic heating formulations. However, most of the surfaces of concern in this study do not generally fall into this category.

These surfaces, such as the solar panel, are large relative to the extent of the flow field, and as such represent a geometry similar to those

TABLE 5-6. ROCKET MOTOR CHARACTERISTICS

Parameter	Motor Designation						
	SVM-20	TE-M-5210	TE-M-616	TE-364-4	FW-5	SVM-40	TE-361-
Chamber pressure (N. O. 25 basis)	$1.4 \times 10^3$ ( 297 )	$3.5 \times 10^3$ (735 )	$2.3 \times 10^3$ (475 )	-	$3.9 \times 10^3$ ( 800 )	$3.1 \times 10^3$ ( 630 )	$2.4 \times 10^3$ ( 500 )
V ratio	40	57.9	41.9	-	60	40	53.5
Portions, sec	27.6	13.6	35.0	41.4	40.5	-	44
Exit plane diameter, mm.	33.2 ( 17.4)	35.8 ( 14.1)	50.2 ( 19.77)	62.2 (24.5)	40.2 ( 15.8)	59.7 ( 23.5)	61.0 ( 24 )
Exit plane velocity, m/sec	2980 (91.7 )	-	-	-	3740 (12294 )	2940 (9639 )	2720 (9050 )
N. O. 25 muls. dia.	11.8	-	-	13	19	-	18
Evilant mass flow, kg and (lb/sec)	5.2 ( 11.4)	5.6 ( 14.4)	9.4 ( 20.7 )	25.2 ( 55.4)	6.8 ( 14.9)	-	13.6 ( 30 )
Percentage of aluminum content, by weight	-	16	16	-	16.4	-	15

M in mm

REPRODUCIBILITY OF THE ORIGINAL PAGE IS POOR.



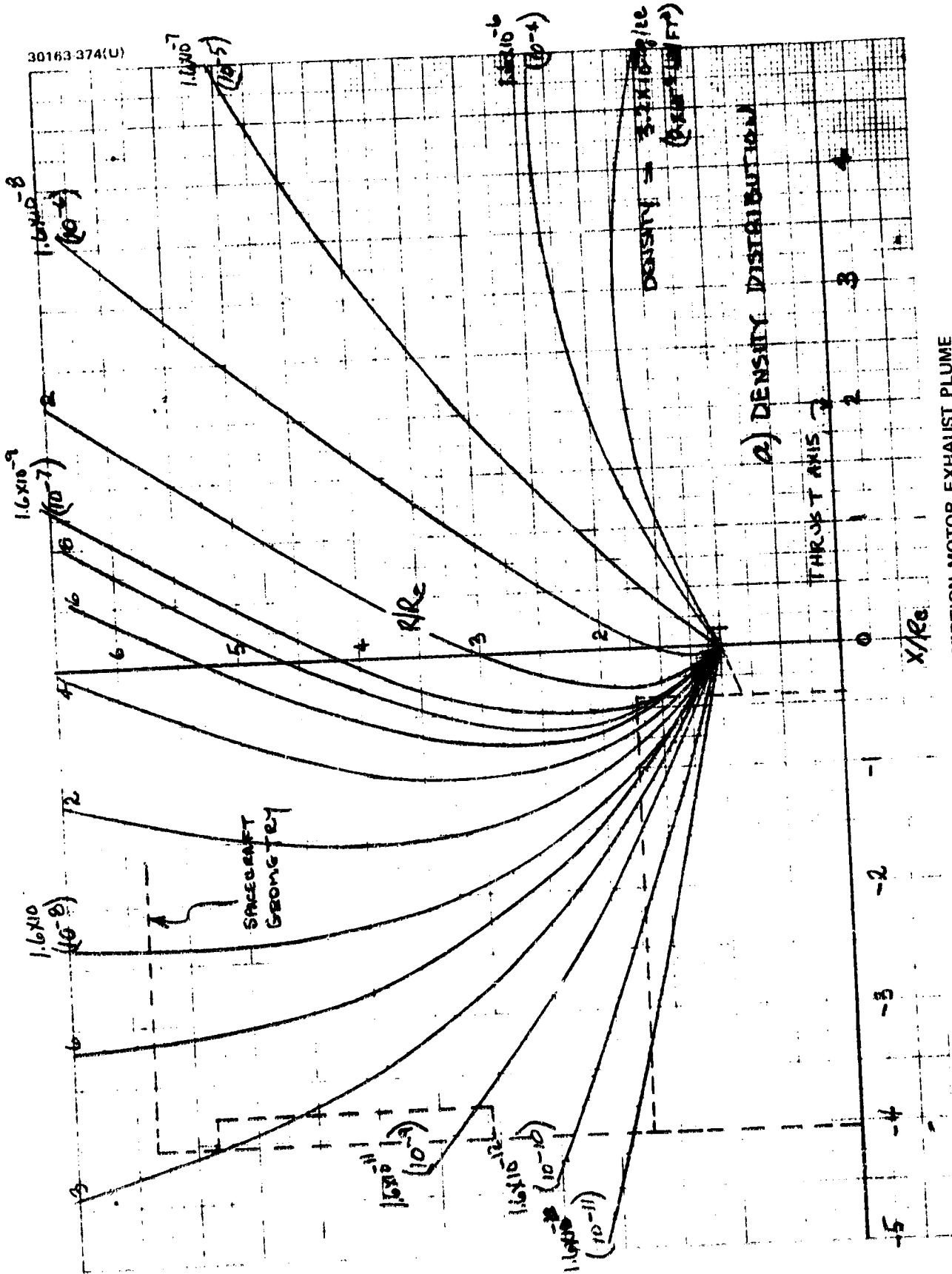


FIGURE 5-20. TE-M-521 ORBIT INSERTION MOTOR EXHAUST PLUME

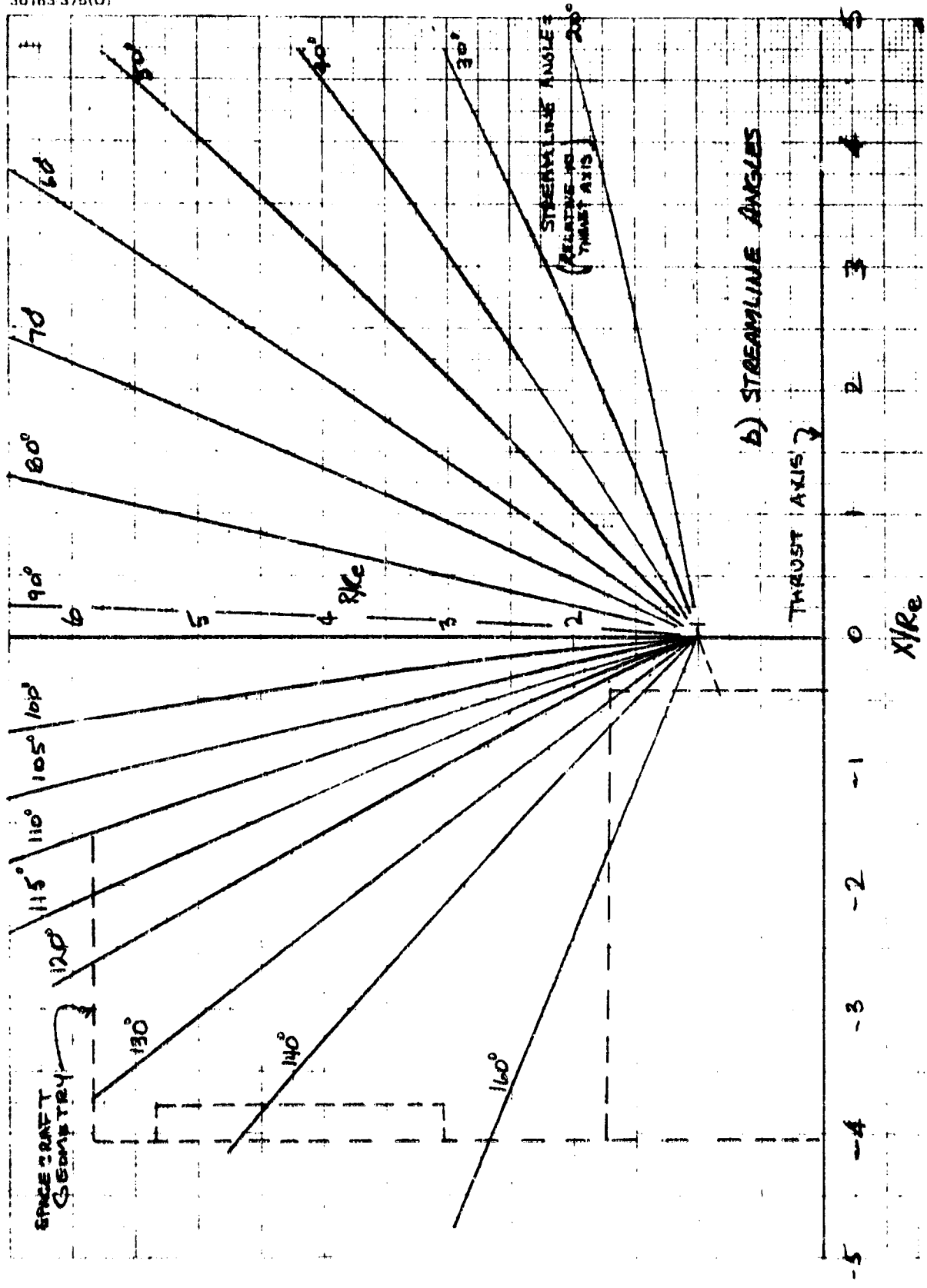


FIGURE 5-20 (Continued). TE-M-521 ORBIT INSERTION MOTOR EXHAUST PLUME

experimentally studied by Peisik, Koppang, and Simkin.\* In these studies convective heating rates caused by plume impingement on large flat plates were measured and correlation equations developed.

Plume heating rates were calculated along the solar panel, thrust tube closure, and louver modules using these correlations and the free molecule flow formulation.

Radiation from the condensed aluminum oxide in the solid propellant motor exhaust plume is estimated by scaling plume radiosity from test measurements of the TE-364-1 (Surveyor Retro) qualification firings.\*\* From this test an exit plane radiosity of  $0.73 \text{ W/m}^2$  ( $6.5 \text{ Btu/ft}^2\text{-sec}$ ) was derived.

Based on these data the TE-M-521 plume exit plane radiosity is estimated to be approximately  $0.52 \text{ W/m}^2$  ( $5.0 \text{ Btu/ft}^2\text{-sec}$ ). Plume radiosity is assumed to be inversely proportional to distance from the nozzle exit plane.

#### Spacecraft Thermal Response

The response of the spacecraft surfaces exposed to plume heating were computed from the combined convective and radiative heating rates. Where differences between free molecule flow and continuum heating rates were important, both were used and the results compared. Figure 5-21 shows the distribution of temperature along the solar panel insulation for both free molecular and continuum heating. Also shown is the effect of increasing outer sheet thickness to 0.013 cm (5 mils) for the assumption of near continuum flow heating rates. Based on these results, the decision was made to use the 0.013 cm (5 mil) cover sheet on the outer 12.7 cm (5 in.) of panel length to provide additional temperature margin. This results in a weight increase of approximately 0.14 kg (0.3 lb).

Combined heating rates predicted on the closure between the thrust tube on the orbit injection motor nozzle clearly exceed the capability of Kapton. Instead, a stainless steel barrier was selected to provide the necessary closure. This barrier, similar to one flown on the HS-333 spacecraft, consists of a 0.0076 cm (3 mil) stainless steel foil, coated with a high temperature black finish (Bo-Chem Black Oxide) on the outboard surface and Hanovia gold deposition on the inboard surface to provide the desired thermal isolation. Figure 5-22 shows the response at the outboard radial edge of the barrier where heating rates are maximum. Temperatures are shown for the assumptions of free molecule flow, oblique shock, and normal shock heating. As indicated even free molecule flow heating results in temperatures just exceeding the HS-333 limit. It is felt that sufficient margin exists to allow for heating rate uncertainty. If necessary, barrier temperature limits can be increased to  $980^\circ\text{C}$  ( $1800^\circ\text{F}$ ) by revising the gold deposition process.

\* E. T. Peisik, R. R. Koppang, D. J. Simkin, "Rocket-Exhaust Impingement on a Flat Plate at High Vacuum," AIAA Paper No. 66-46, January 1966.

\*\* R. P. Bobco, et al, "Surveyor Exhaust Plume Heating: October 1961 to August 1964," Hughes Aircraft Company, SR5 649, 23 October 1964.

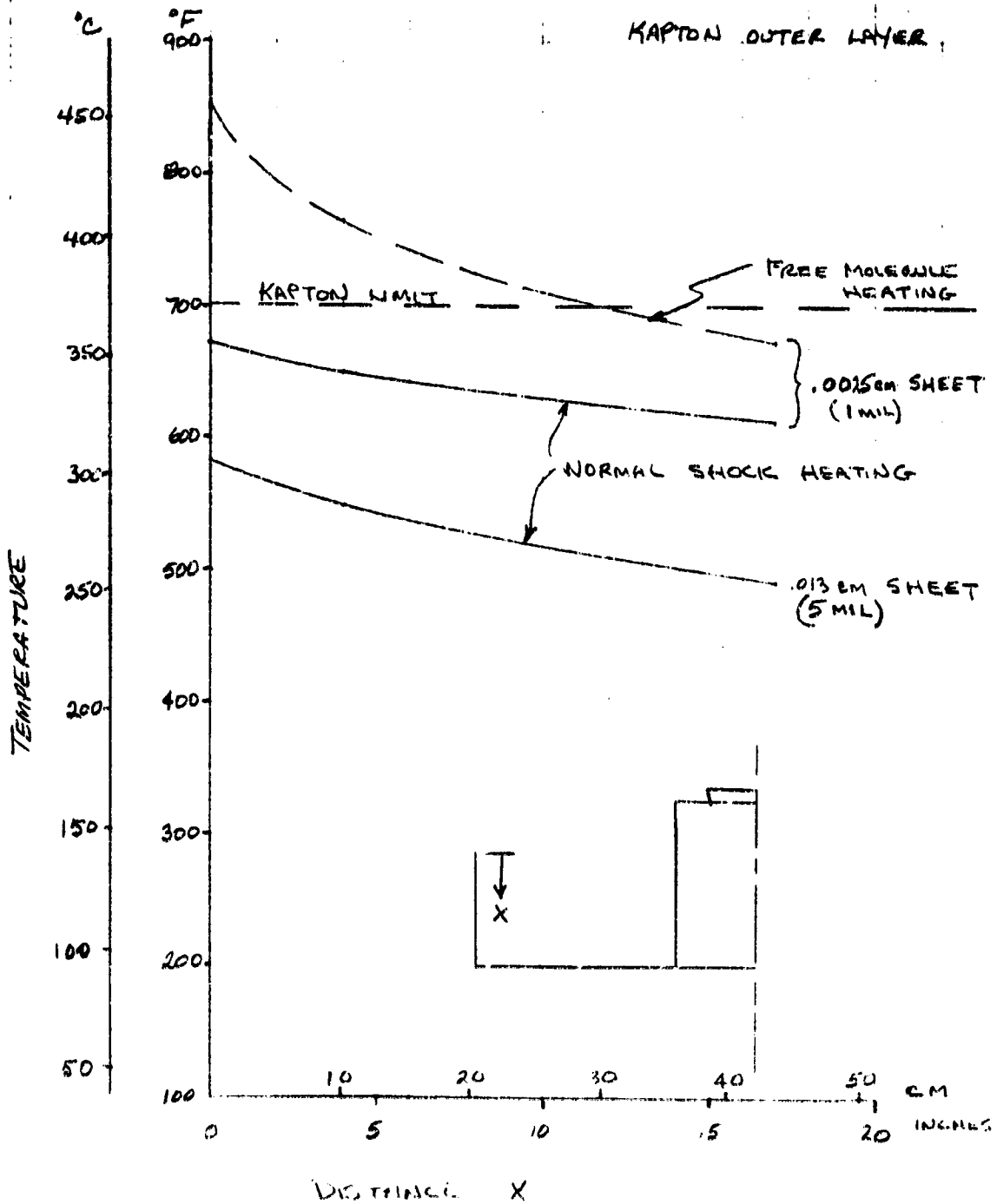


FIGURE 5-21. ORBITER SOLAR PANEL INSULATION TEMPERATURES AT TE-M-521 BURNOUT

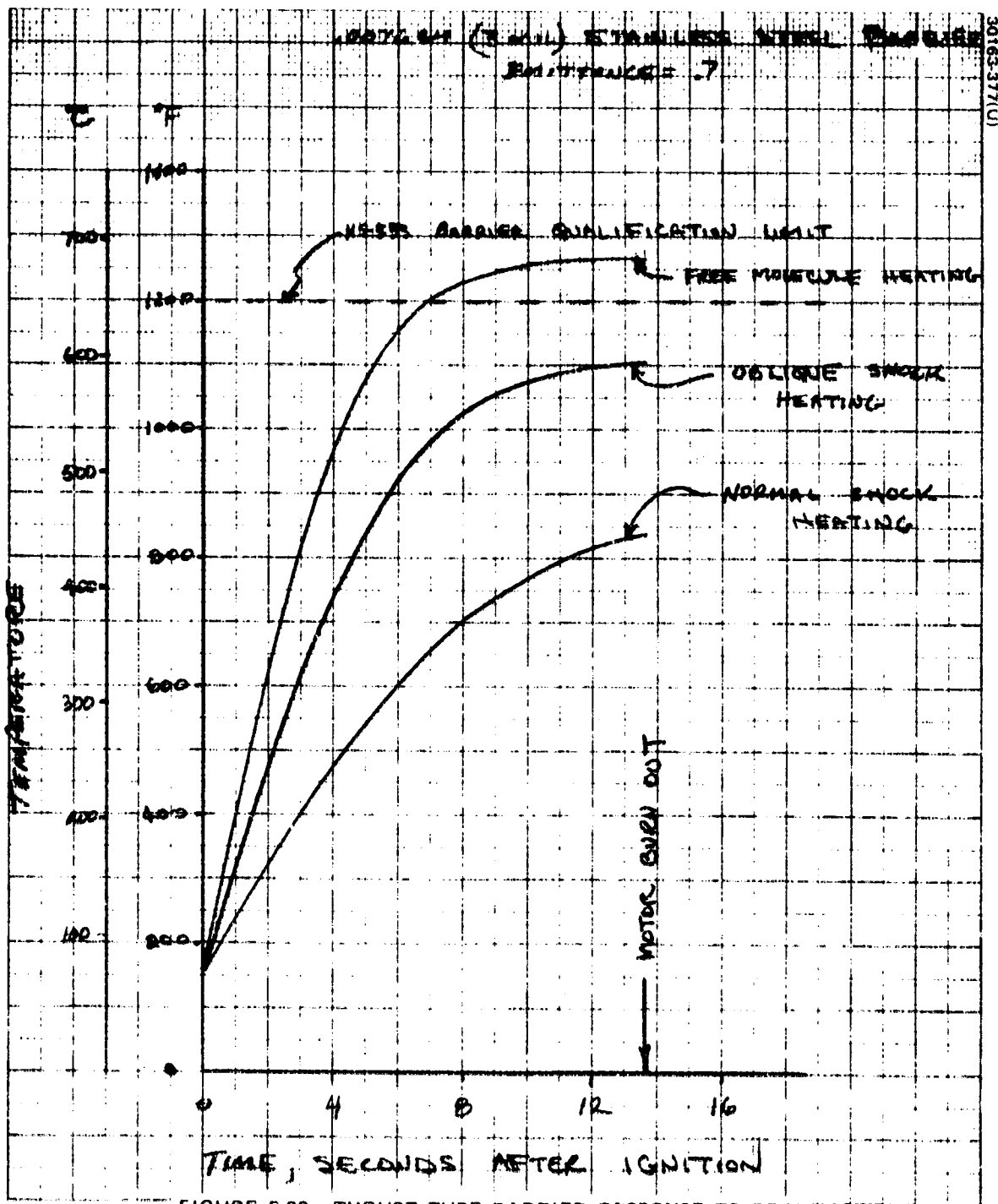


FIGURE 5-22. THRUST TUBE BARRIER RESPONSE TO TE-M-521 PLUME HEATING

REPRODUCIBILITY OF THE ORIGINAL PAGE IS POOR.

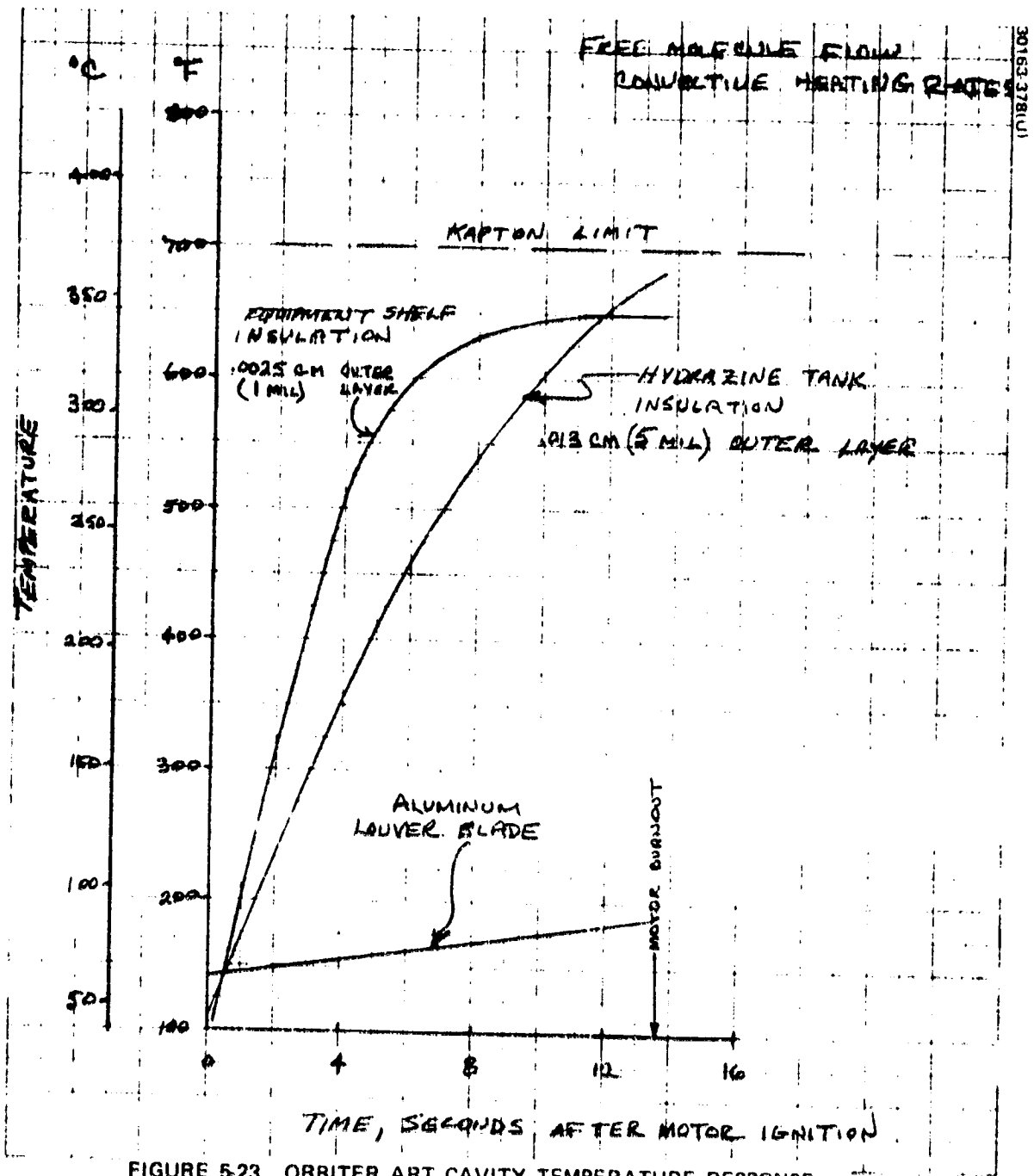


FIGURE 5-23. ORBITER ART CAVITY TEMPERATURE RESPONSE TO TE-M-521 PLUME HEATING

REPRODUCIBILITY OF THE ORIGINAL PAGE IS POOR.

Equipment shelf and hydrazine tank insulation plume heating response is shown in Figure 5-23, along with louver blade temperature. These temperatures assume free molecule flow heating rates. As indicated, shelf insulation and blade temperatures are acceptable, but the 0.0025 cm (1 mil) insulation outer sheet reaches temperatures beyond the Kapton limit. A 0.013 cm (5 mil) cover sheet provides the necessary heat capacity for a weight increment of less than 0.05 kg (0.1 lb).

The temperature response of the aft omni antenna is shown in Figure 5-24 for two wall thicknesses. Preliminary antenna design requirements indicate a 0.076 cm (30 mil) wall is functionally adequate. However, a 0.1 cm (40 mil) thickness has been recommended to provide additional margin with negligible weight penalty. The antenna support will be aluminum with adequate heat capacity to withstand this heating.

#### Delta Third Stage (TE-364-4) Plume Radiation

Ames Research Center\* defines the radiative heating rates to be assumed incident on aft facing spacecraft surfaces. To apply these heating rates to the orbiter and probe bus spacecraft, they were interpreted to be heating rates to surfaces normal to the motor thrust axis. To adjust these rates for different surface orientation, they were multiplied by the ratio of local plume shape factor to shape factor for the aft facing surface. The effective plume radiating surface was defined by the methods described above using the motor characteristics given in Table 5-6.

Temperature responses of the aft cavity surfaces are given in Figure 5-25. These temperatures are generally lower than those predicted for the orbit insertion motor firing. These temperatures apply to the probe bus spacecraft as well as to the orbiter.

Maximum predicted temperatures of the orbiter aft omni antenna are lower for this event than for the orbit insertion firing. The maximum temperature response of the probe bus end fire (medium gain horn) antenna, given in Figure 5-26 for the minimum wall thickness being considered (0.051 cm (20 mils) of aluminum), is acceptable.

---

\*"Requirements for Pioneer Venus Mission Systems Design Study," Ames Research Center Specification 2-17502, Revision 1, 15 September 1972.

MATERIAL: FIBERGLASS  
 POLYIMIDE RESIN

TEMPERATURE LIMIT: 260 to 316°C  
 (500 to 600°F)

FINISH: BLACK PRINT  
 $\epsilon = .95$

( ) DIMENSIONS IN INCHES

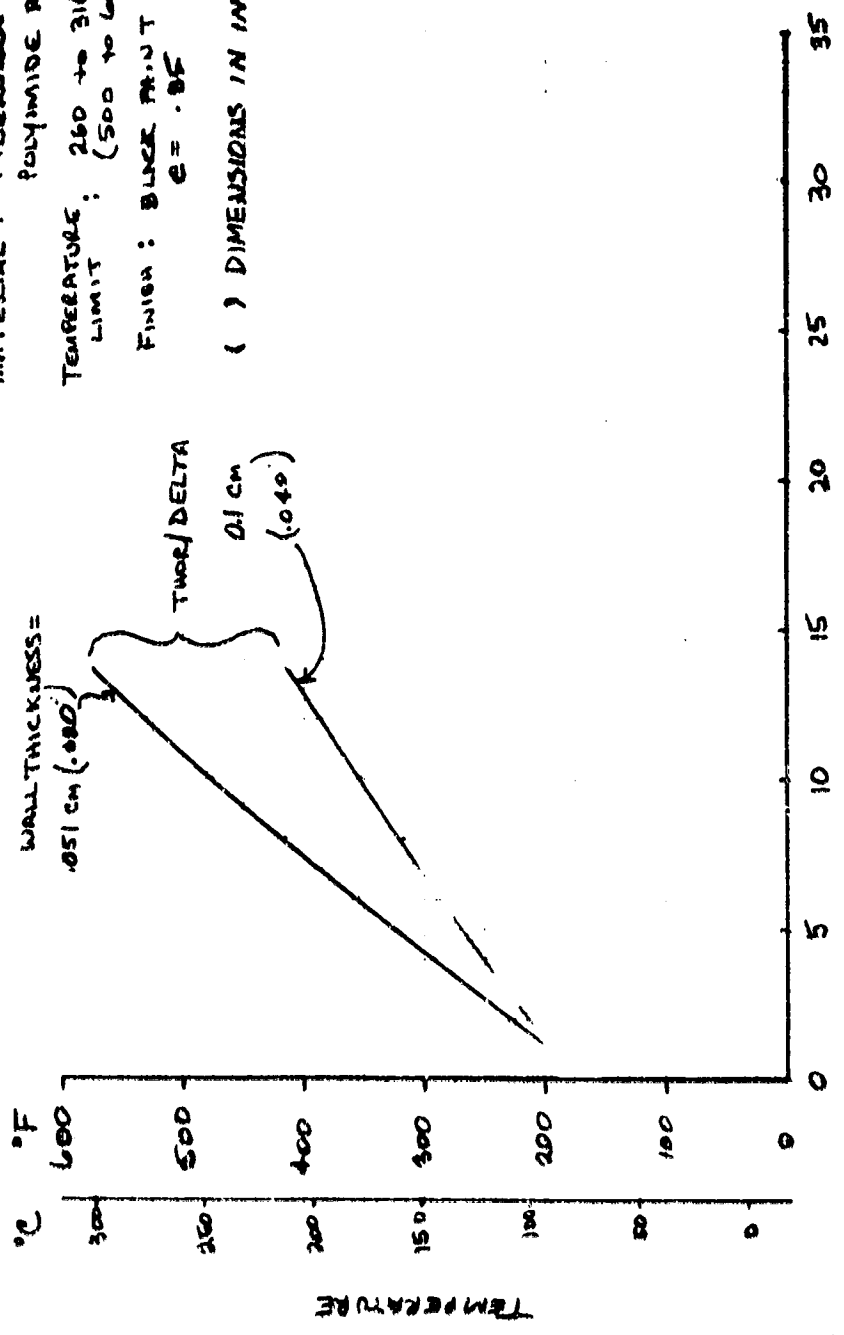


FIGURE 5-24. PIONEER VENUS AFT OMNI RESPONSE TO PLUME HEATING

REPRODUCIBILITY OF THE ORIGINAL PAGE IS POOR.



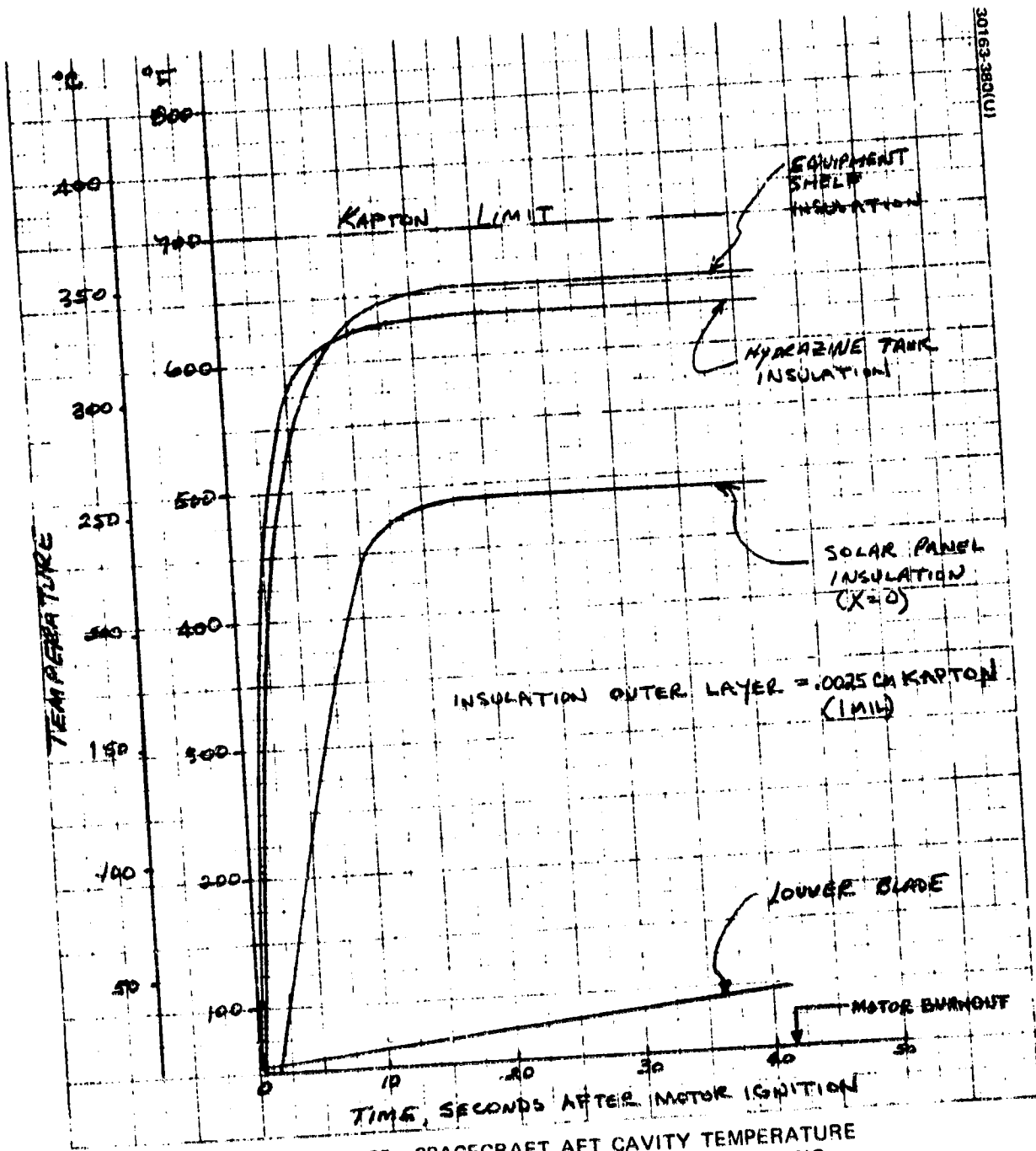


FIGURE 5-25. SPACECRAFT AFT CAVITY TEMPERATURE RESPONSE TO DELTA THIRD STAGE PLUME HEATING

REPRODUCIBILITY OF THE ORIGINAL PAGE IS POOR.

30163-381(U)

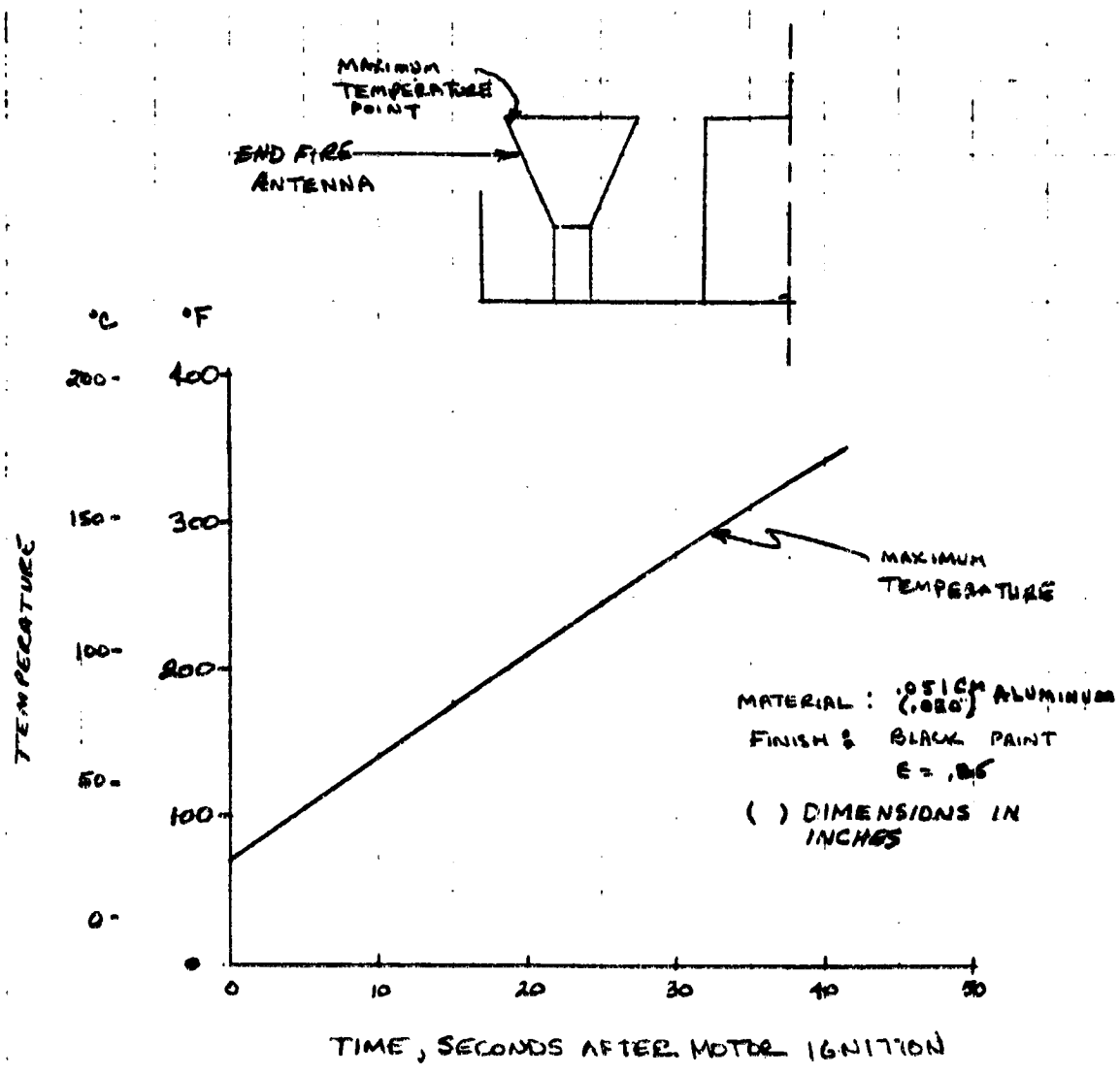


FIGURE 5-26. PROBE BUS END FIRE ANTENNA RESPONSE TO DELTA THIRD STAGE PLUME HEATING

REPRODUCIBILITY OF THE ORIGINAL PAGE IS POOR.

### 5.3 THOR/DELTA BASELINE DESCRIPTION

#### Spacecraft Design

##### Equipment Shelf

The thermal designs of the Thor/Delta probe bus and orbiter spacecraft are illustrated in Figure 5-27. As discussed in subsection 5.2, the design approach selected for both spacecraft is to isolate the equipment shelf from the environment and control temperatures by dissipating unit power from variable emittance radiators. Radiator emittance is controlled by thermally actuated louvers mounted on the outboard side of the equipment shelf. Those units which dissipate 5<sup>W</sup> or more are mounted on the shelf directly opposite louver modules to minimize the need to provide lateral conductance along the honeycomb shelf.

The shelf is 3.8 cm (1.5 in.) thick, 0.48 cm (3/16 in.) cell aluminum honeycomb, 0.0018 cm (0.0007 in.) ribbon with 0.025 cm (0.019 in.) aluminum face sheets.

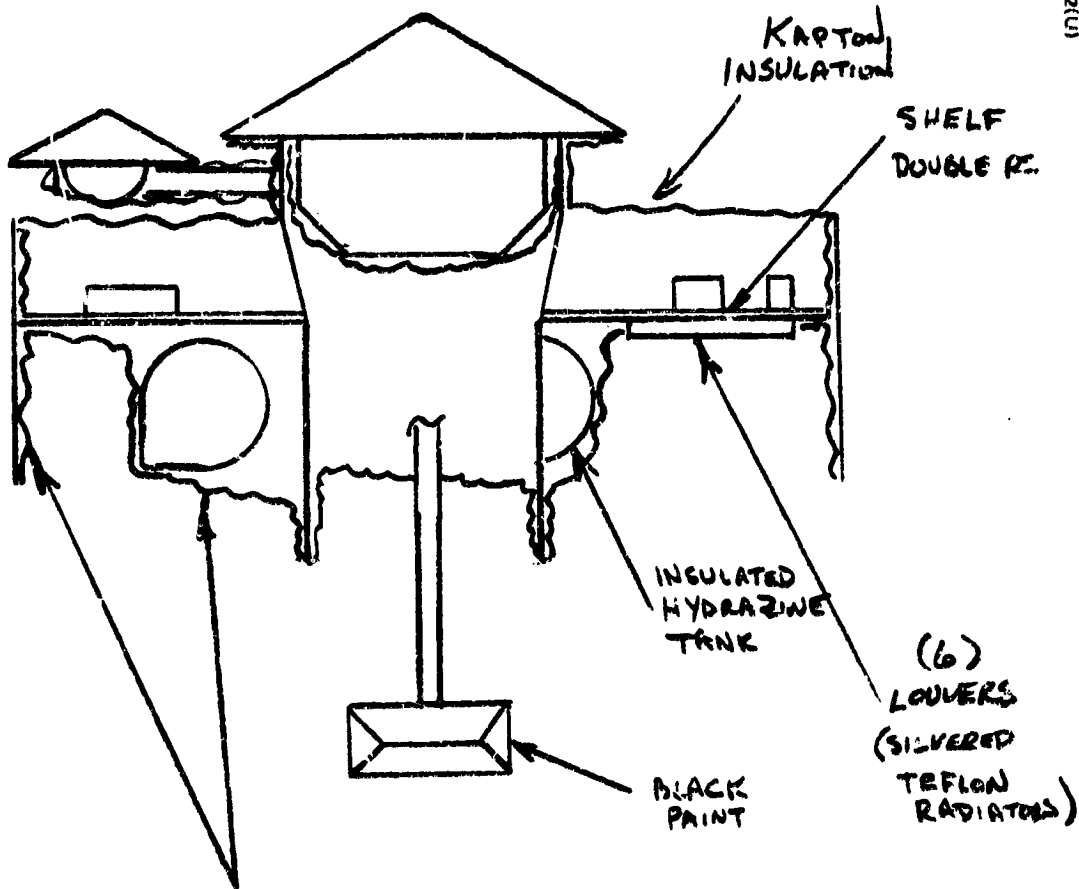
For the maximum shelf power design conditions, eight louver modules are required to maintain shelf temperature limits on the orbiter spacecraft. The lower powered probe bus requires six modules.

The louvers used in this design are shown in Figure 5-28. Rotation of the louver blades is performed by conversion of heat energy into mechanical motion by use of a bimetallic actuator. The bimetallic actuator is wound so that the strip of material with the greatest coefficient of expansion forms the outer surface of the spring. This construction causes the actuator to contract or close when heated sufficiently and expand or open when sufficiently cooled. The actuators are keyed to their respective louver blade so that the louver rotates with the actuator movement. Each louver blade set (two blades) is individually actuated with a bimetal element. The fully closed to fully open position occurs over a fixed temperature range of 14°C (25°F). However, the opening set point can be adjusted. For the Pioneer Venus application, the initial opening temperature is 13°C (55°F), the fully open set point is 27°C (80°F). Unit test and flight experience have shown that the effective emittance of these louvers fully open is 0.69 and about 0.1 when closed.

The radiator surface directly beneath the louvers is covered with an 0.013 cm (0.005 in.) layer of silvered teflon. This surface acts as a second surface mirror reflecting a large percentage of any solar energy reaching the louvers, while efficiently radiating the shelf equipment dissipation. The measured solar reflectance and total hemispherical emittance for this material is 0.08 and 0.80, respectively. However, because of interreflections off the polished louver blades and housing surfaces, a significantly higher net effective solar absorptance can be expected. These effects have been theoretically

a) THOR/DELTA PROBE BUS

30163-382(U)



KAPTON INSULATION BLANKETS

- HYDRAZINE THRUSTER VALVE & CATALYST BED HEATERS (NOT SHOWN)

FIGURE 5-27. THERMAL DESIGN

b) THOR/DELTA ORBITER

30163-383(U)

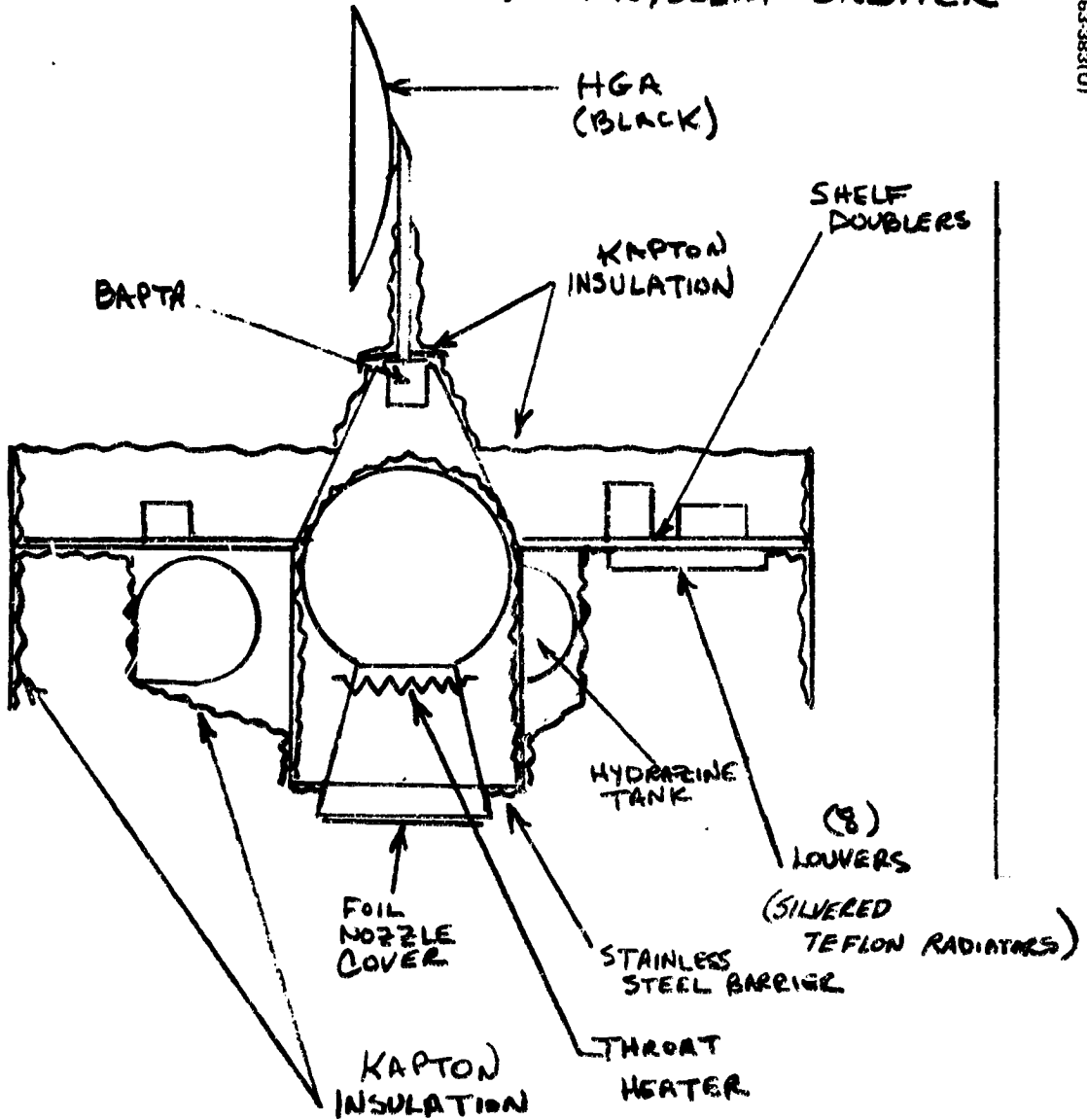


FIGURE 5-27 (continued). THERMAL DESIGN

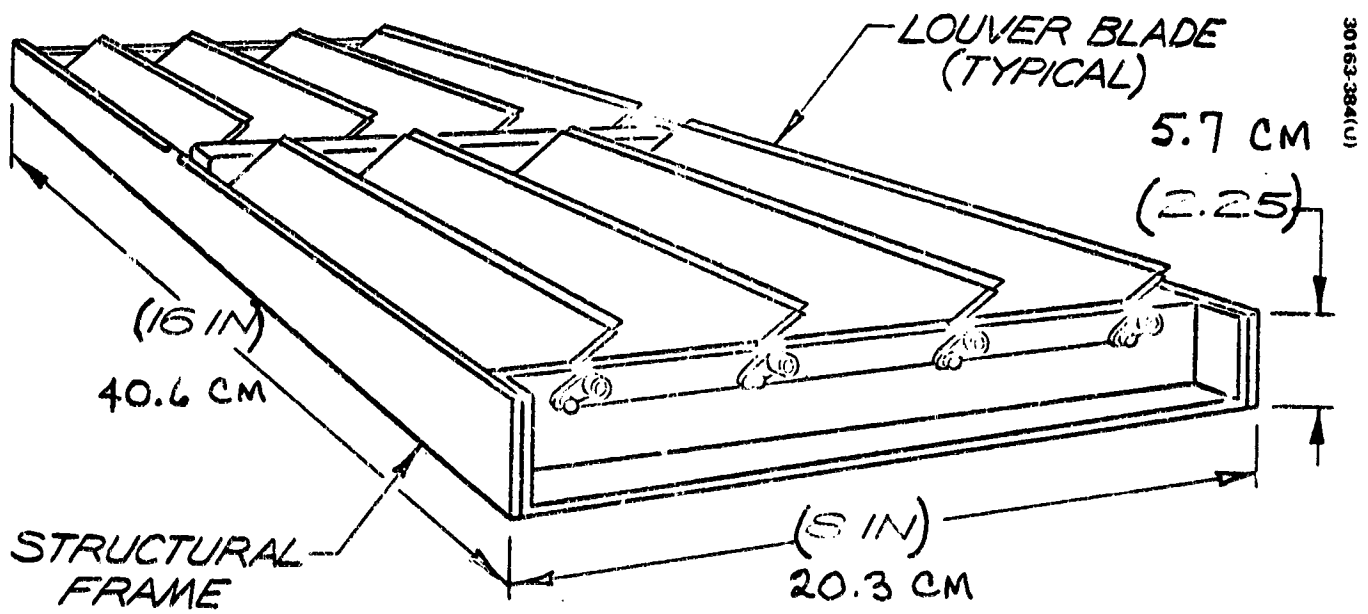


FIGURE 5-28. THERMAL CONTROL LOUVER DESIGN

predicted and experimentally measured by Michalek\*, et al. Radiator solar absorptance was found to vary substantially with blade opening angle and solar elevation angle, measured in a plane normal to the blade axis of rotation. Typical results of this study are reproduced in Figure 5-29, which compares measured and theoretical louver absorptance. Based on these data, an effective solar absorptance of 0.22 has been assumed.

The inboard surface of the shelf and mounted equipment are painted black (emittance  $\sim 0.85$ ).

Beryllium doublers are utilized to distribute the dissipation from a few high power density units on the shelf to prevent local hot spots.

### Insulation

The exposed outboard surface of the equipment shelf is covered by a superinsulation blanket except over those areas directly adjacent to the two hydrazine propellant tanks. Here insulation blankets form an enclosure around each tank blending into the shelf blanket and a blanket covering the central thrust tube. This arrangement provides a direct view from the tanks to the shelf. These insulation blankets consist of 15 layers of crinkled 0.00064 cm (0.00025 in.) aluminized Kapton covered by an outer layer of 0.0025 cm (0.001 in.) aluminized Kapton (Kapton side out). Kapton was selected as the insulation material to withstand the rocket exhaust plume heating described in subsection 5.2.

To decouple the louvered radiators from the hot solar panel, a Kapton blanket is also placed on the inner panel surface. Because of high exhaust plume heating rates, the blanket outer layer is increased to 0.013 cm (0.005 in.) on the outboard 12.8 cm (5 in.) of the panel. A similar local increase is made on the end surfaces of the tank insulation.

Kapton blankets are also placed in the inside surface of the forward solar panel substrate to further isolate the equipment shelf. Finally, a blanket is supported across the forward end of each spacecraft to complete the shelf enclosure. For the probe bus, additional blankets are required on the probe support structure and between the large probe and the spacecraft. This is required to maintain spacecraft temperatures following probe separation. On the orbiter spacecraft, the high gain antenna mast is also superinsulated to maintain the required BAPTA temperatures.

All superinsulation blankets have an effective inside to outside emittance of 0.02.

---

\* T. J. Michalek, E. A. Stipandic, and M. J. Coyle, "Analytical and Experimental Studies of an All Specular Thermal Control Louver System in a Solar Vacuum Environment," Paper No. 72-268, AIAA 7th Thermophysics Conference, San Antonio, Texas, April 1972.

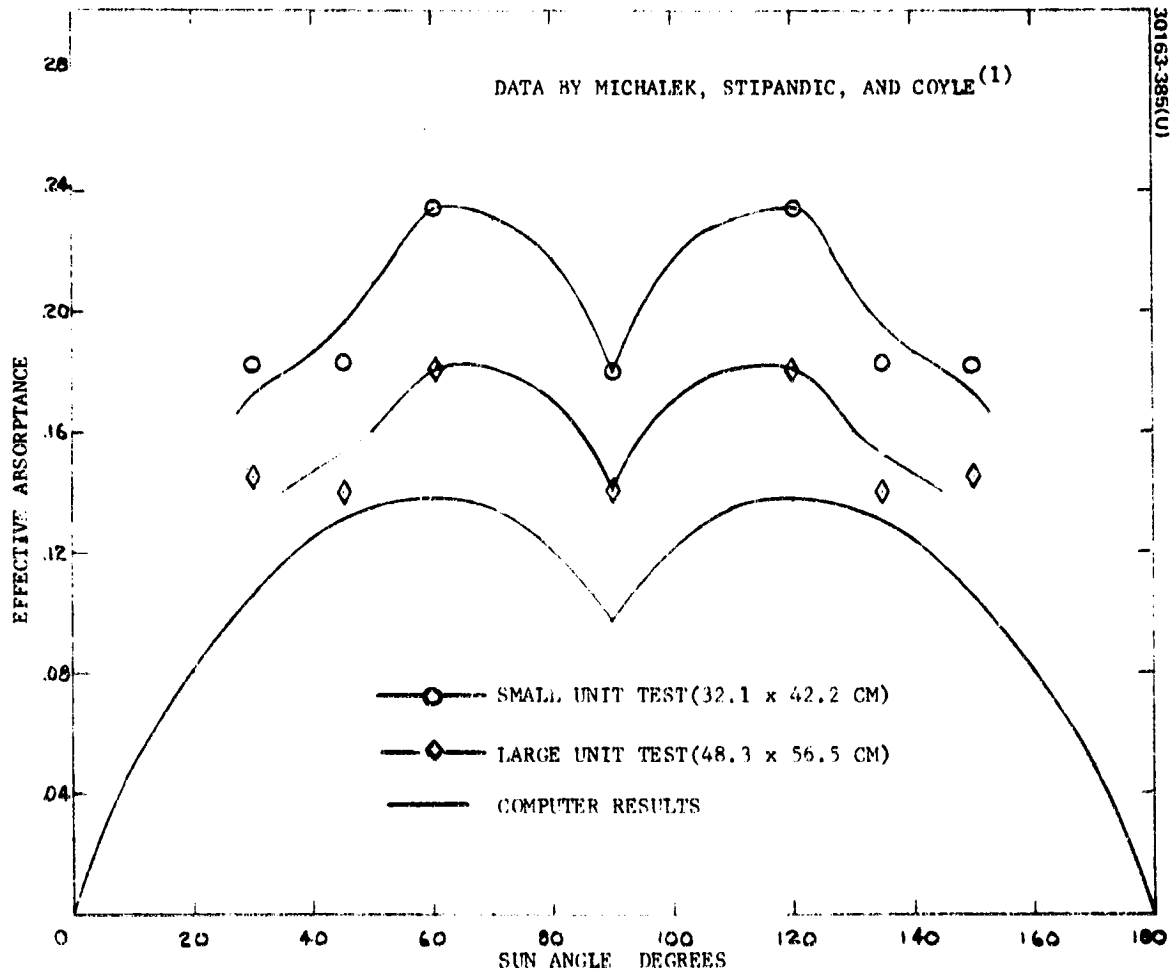


FIGURE 5-29. EFFECTIVE LOUVER SOLAR ABSORPTANCE -  
BLADE ANGLE = 90 DEG



The aft end of the probe bus thrust tube is closed by a blanket. On the orbiter spacecraft, this closure is a stainless steel barrier, 0.0076 cm (0.003 in.) thick, required to withstand the orbit insertion motor exhaust plume heating. The outer surface of the barrier is finished with a high temperature black oxide coating having a total emittance of 0.63. The inside surface of the barrier has a Hanovia gold finish, emittance of 0.05.

### Propulsion

As indicated in Figure 5-30, axial thrusters are mounted on support structures attached to the equipment shelf. The forward axial thrusters are enclosed by the forward insulation blanket which provides necessary isolation of thruster valve and propellant line from the environment. The aft thrusters are mounted to the opposite side of the shelf in a similar manner.

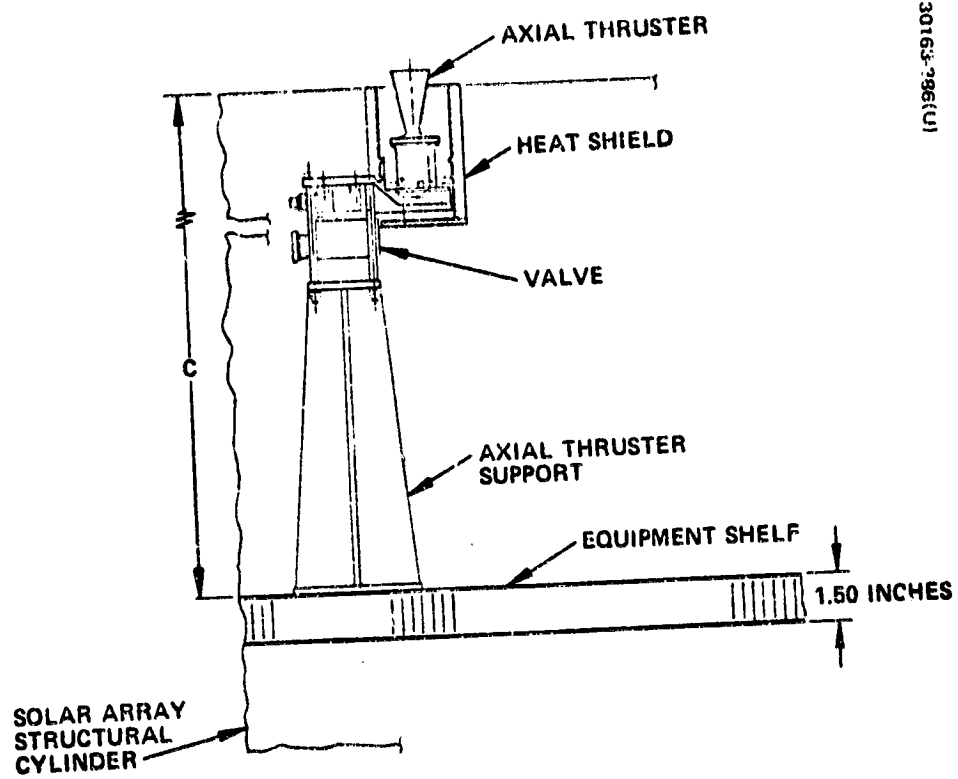
However, since this end of the spacecraft is open, an insulation blanket must be added to enclose the support structure providing a coupling to the shelf.

Figure 5-31 illustrates alternate installations of the radial thrusters. The first is used for the probe bus thrusters fired prior to probe separation. After the probes are released, the axial shift in c. g. requires use of a second set of thrusters mounted in the manner shown in Figure 5-31b. In this second installation, shown mounted on the aft shelf surface, the shelf blanket encloses the thruster and bracket. In all thruster installations, a multilayer stainless steel radiation heat shield is placed around the catalyst bed and nozzle to protect surrounding surfaces from high temperatures during thruster firing.

To maintain thruster valves above propellant freezing point and catalyst beds at minimum firing temperatures, electrical heating is required. To maintain temperatures near earth and during eclipses, 0.25 W heaters are provided for each radial thruster valve and each catalyst bed. When not illuminated by the sun, the axial thrusters require 0.5 W heaters on the valves, 0.75 W on the catalyst beds.

All heaters are commandable. The axial thruster heaters are separately switched, forward and aft, because when one end of the spacecraft is illuminated by the sun near Venus, heaters must be off to prevent overheating while the heaters must be on for the opposite thrusters. The radial heaters can remain on continuously, but are capable of being commanded off through a single (redundant) switch.

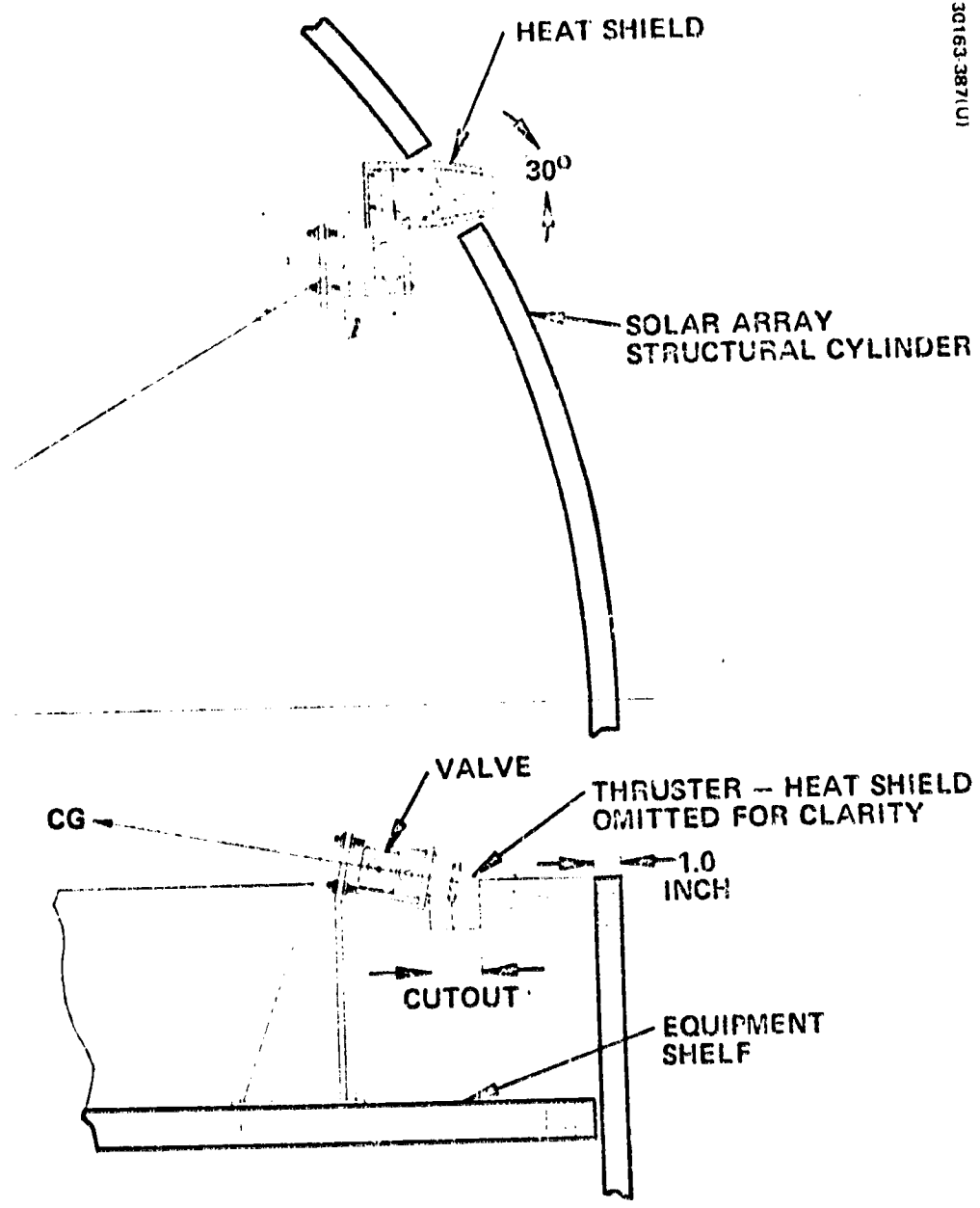
The enclosed propellant lines and insulated tanks require no heating. The tank manifold lines must be mounted to the shelf under the insulation blanket to efficiently control their temperature. If located outside this blanket, they would require several watts of heater power since they are difficult to insulate separately and would overheat during periods of solar illumination if covered with a simple low emittance aluminum foil.



30163-196(U)

FIGURE 5-30. TYPICAL AXIAL THRUSTER INSTALLATION

30163-387(U)



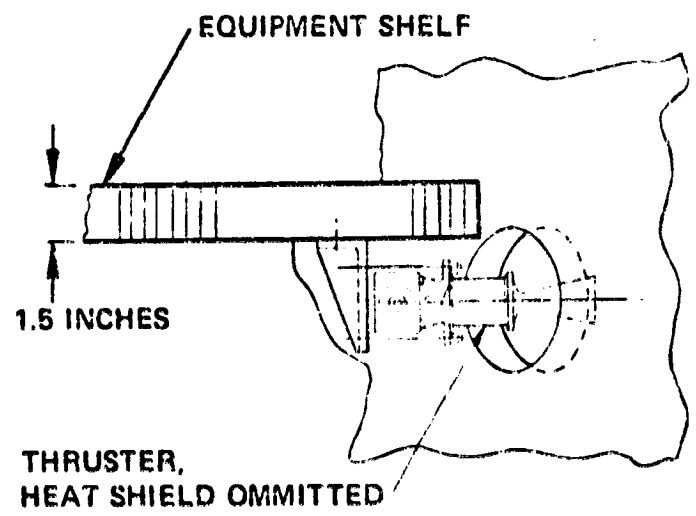
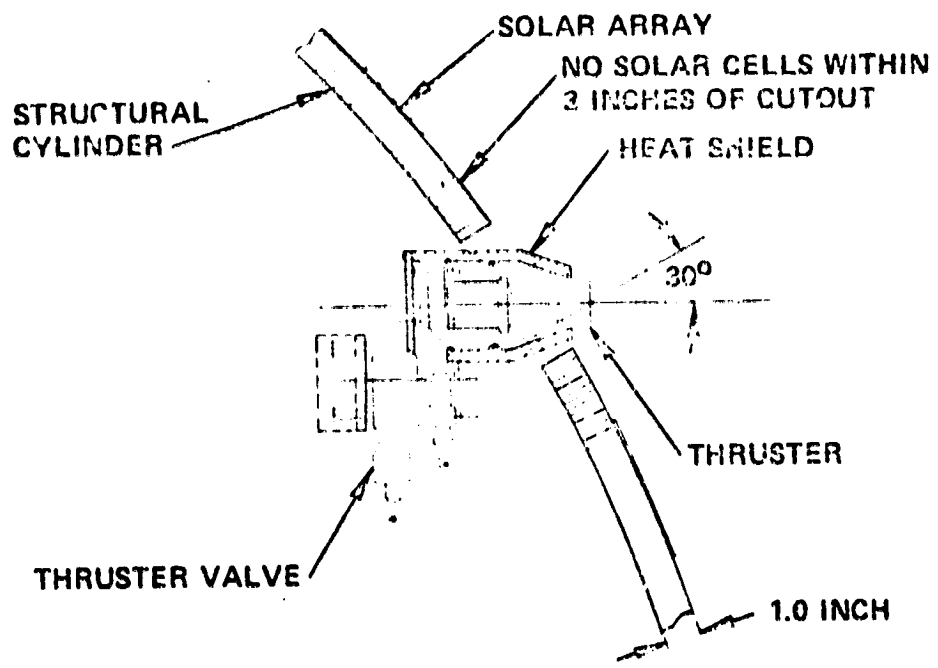
a) NEAR TOP OF SOLAR ARRAY STRUCTURAL CYLINDER

FIGURE 5-31. RADIAL THRUSTER INSTALLATION

REPRODUCIBILITY OF THE ORIGINAL PAGE IS POOR

REPRODUCIBILITY OF THE ORIGINAL

30163 388(U)



b) THROUGH SOLAR ARRAY STRUCTURAL CYLINDER

FIGURE 5-31 (Continued). RADIAL THRUSTER INSTALLATION

The orbit insertion motor is isolated from the spacecraft to minimize post firing heat soak back and heat losses during the long apoapsis eclipse. To provide the required maximum propellant temperature just prior to firing at Venus encounter, the exposed nozzle is covered with 0.0025 cm (0.001 in.) aluminized teflon. To provide the required minimum propellant temperatures near earth, a nozzle throat heater is utilized, requiring 5.0 W of power. The heater is commandable and is switched off near Venus.

### Other Finishes

The antenna surfaces are generally black (emittance  $\sim 0.85$ , solar absorptance  $\sim 0.95$ ) to preclude solar reflections into star sensors, etc. The portion of the solar panel substrate not supporting solar cells, will be carbon black impregnated to prevent solar energy transmission.

### Probe Preentry Design

As indicated in subsection 5.2, a passive design approach has been utilized to provide thermal control of the probes during the period from launch to just prior to entry. Control is achieved by applying passive finishes to the deceleration module heat shield and aft cover. The finishes selected for the probes are shown in Table 5-7. Thermal coupling at the interfaces between probes and spacecraft is minimized to make the thermal designs independent.

TABLE 5-7. PROBE THERMAL FINISHES

Surface	Large Probe	Small Probe
Heat shield	45 percent aluminized teflon 55 percent black paint	Aluminized Kapton
Aft cover	Silvered teflon	
Sides		66 percent black paint 34 percent aluminum foil
Rear	Black paint	Aluminum foil

TABLE 5-8. THOR/DELTA SPACECRAFT THERMAL CONTROL MASS AND POWER SUMMARY

	Probe Bus			Orbiter		
	Mass		Power, W	Mass		Power, W
	kg	lb		kg	lb	
Louvers	1.7	3.9	-	2.3	5.2	-
Blankets	6.5	14.2	-	6.5	14.2	-
Shelf doublers	1.5	3.3	-	1.9	4.2	-
Coatings	0.5	1.0	-	0.5	1.0	-
Temperature sensors	0.1	0.2	-	0.1	0.3	-
Thruster heaters	*	*	4.5	*	*	5.8
Orbit insertion motor heater	-	-	-	*	*	5.0
<b>Totals</b>	<b>10.3</b>	<b>22.6</b>	<b>4.5</b>	<b>11.3</b>	<b>24.9</b>	<b>10.8</b>

\* Weight in propulsion subsystem

TABLE 5-9. THERMAL CONTROL HARDWARE DERIVATION

Element	Hardware Derivation
Louvers	Procured from Northrop Corp. for classified spacecraft program
Silvered teflon radiator	Classified program
Thruster heaters	Intelsat IV
Orbit insertion motor heater	Intelsat IV
Kapton insulation blankets	Intelsat IV
Stainless steel thrust tube barrier	HS-333
Coatings	Intelsat II, IV, TACSAT, ATS, OSO

## Mass and Power Summary and Hardware Derivation

The spacecraft thermal control mass summary is shown in Table 5-8, along with heater power requirements. Heater mass is reported by the propulsion subsystem. The derivation of the subsystem hardware is shown in Table 5-9. As indicated, thermal control utilizes hardware elements proven on flight spacecraft.

## Spacecraft Design Performance

### Bulk Temperatures

To determine the basic design approach and provide boundary conditions to more detailed thermal models, bulk spacecraft thermal nodal models were devised for the probe bus and orbiter spacecraft. These networks, shown in Figure 5-32, include the equipment shelf, the louvered radiators, hydrazine tanks, the aft cavity surfaces, solar panel, thrust tube, orbit insertion motor, and forward blanket.

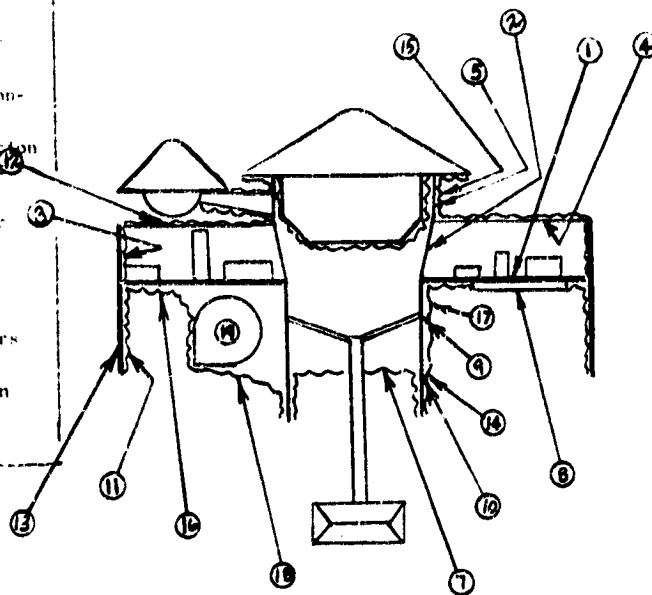
The principal steady state design conditions for the probe bus include near earth cruise, near Venus cruise, and post probe separation. Table 5-10 summarizes the bulk temperatures for these conditions along with assumed shelf power based on the requirements and solar array characteristics given in subsection 5.1. Similar results are shown in Table 5-11 for the orbiter. In this case, the nearly steady condition of near apoapsis operation in Venus orbit is shown for the maximum temperature condition along with the effect of a 3 deg off normal sun angle.

These temperatures generally indicate the required limits are met with satisfactory margin. However, several transient conditions must be examined. Using the orbiter bulk model, the following mission events were analyzed:

- 1) Trajectory correction maneuver near earth, sun angle = 170 deg
- 2) Orbit insertion, sun angle =  $103.5 \pm 5$  deg
- 3) Periapsis heating
- 4) Near apoapsis eclipse

The near earth TCM case applies to either spacecraft and was based on the worst case orientation. The solar interreflection data discussed in subsection 5.2 were used to determine the solar loads on the louvers. Shelf and louver blade overheating are of concern during this event. The results, shown in Figure 5-33, indicate neither occurs during the maximum allotted maneuver time of one hour. The louver blade temperature equilibrates rather rapidly while shelf temperature is still increasing. This suggests that extending the maneuver could cause shelf overheating. It also indicates that this extreme sun angle would certainly cause louver blade overheating if required near Venus.

NODE NO.	LOCATION
1	Equip. Shelf
2	Probe Support Structure - Lower
3	Upper Solar Panel Insulation - Inside Surface
4	Forward Insulation Blanket Support
5	Probe Support Structure - Upper
6	(Not Assigned)
7	Thrust Tube Closure
8	Louver Radiators
9	Thrust Tube - Forward Section
10	Thrust Tube - AFT Section

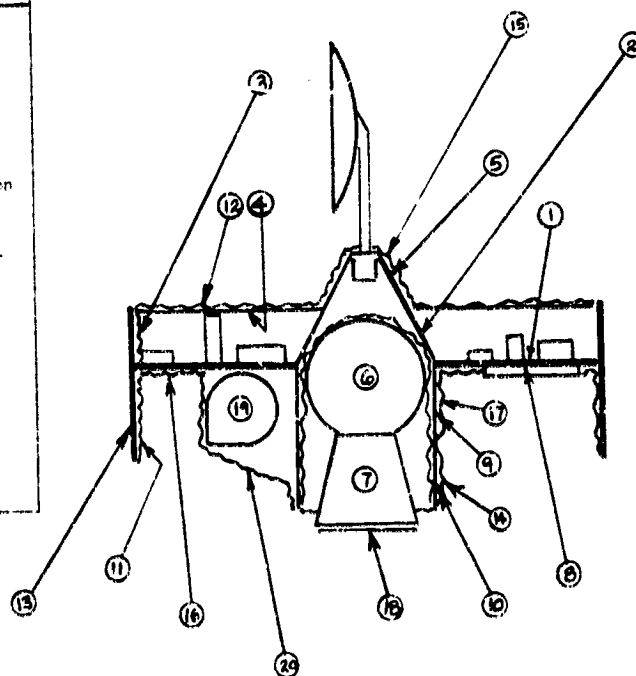


a) THOR/DELTA PROBE BUS

NODE NO.	LOCATION
11	AFT Solar Panel Insulation
12	Forward Insulation Blanket
13	Solar Panel
14	Thrust Tube Insulation - AFT
15	Probe Support Structure Insulation
16	Shelf Blanket
17	Thrust Tube Insulation - Forward
18	Hydrazine Tank Insulation
19	Hydrazine Tanks

30163-390(U)

NODE NO.	LOCATION
1	Equip. Shelf
2	Bapta Support Structure - Lower
3	Upper Solar Panel Insulation - Inside Surface
4	Forward Insulation Blanket Support
5	Bapta Support Structure - Upper
6	Orbit Insertion Motor Case
7	Orbit Insertion Motor Nozzle
8	Louver Radiators
9	Thrust Tube - Forward Section
10	Thrust Tube - AFT Section



b) THOR/DELTA ORBITER

NODE NO.	LOCATION
11	AFT Solar Panel Insulation
12	Forward Insulation Blanket
13	Solar Panel
14	Thrust Tube Insulation - AFT
15	BAPTA Support Structure Insulation
16	Shelf Blanket
17	Thrust Tube Insulation - Forward
18	Nozzle Closure
19	Hydrazine Tanks
20	Hydrazine Tank Insulation

30163-390(U)

FIGURE 5-32. BULK THERMAL NODAL MODEL



TABLE 5-10. THOR/DELTA PROBE BUS STEADY STATE BULK TEMPERATURES

Location	Temperature Limits		Temperature °C (°F)		
			Design Conditions		
	°C	°F	Near Earth Cruise	Near Encounter	Post Probe Separation*
Louver radiators	-	-	14 (57)	17 ( 63)	21 (69)
Equipment shelf	4 to 49	40 to 120	16 (61)	21 ( 69)	25 (77)
Hydrazine tanks	4 to 38	40 to 100	7 (44)	11 ( 51)	12 (54)
Solar panel	-100 to 72	-148 to 162	24 (75)	67 (152)	36 (97)

\* 45 deg sun angle

TABLE 5-11. THOR/DELTA ORBITER STEADY STATE BULK TEMPERATURES

Location	Temperature Limits		Temperature °C (°F)			
			Design Conditions			
	°C	°F	Near Earth Cruise	Near Orbit Insertion	Orbit Operation	In Orbit 3 Deg Off Normal
Louver radiators	-	-	15 (59)	18 ( 65)	18 ( 65)	21 ( 70)
Equipment shelf	4 to 49	40 to 120	18 (64)	22 ( 72)	22 ( 72)	25 ( 77)
Orbit motor case	-7 to 32	20 to 90	4*(40)	25 ( 77)	-	-
Hydrazine tanks	4 to 38	40 to 100	9 (48)	15 ( 59)	12 ( 53)	16 ( 61)
Solar panel	-160 to 135	-256 to 275	20 (68)	72 (162)	72 (162)	72 (162)

\* With 5 W heater

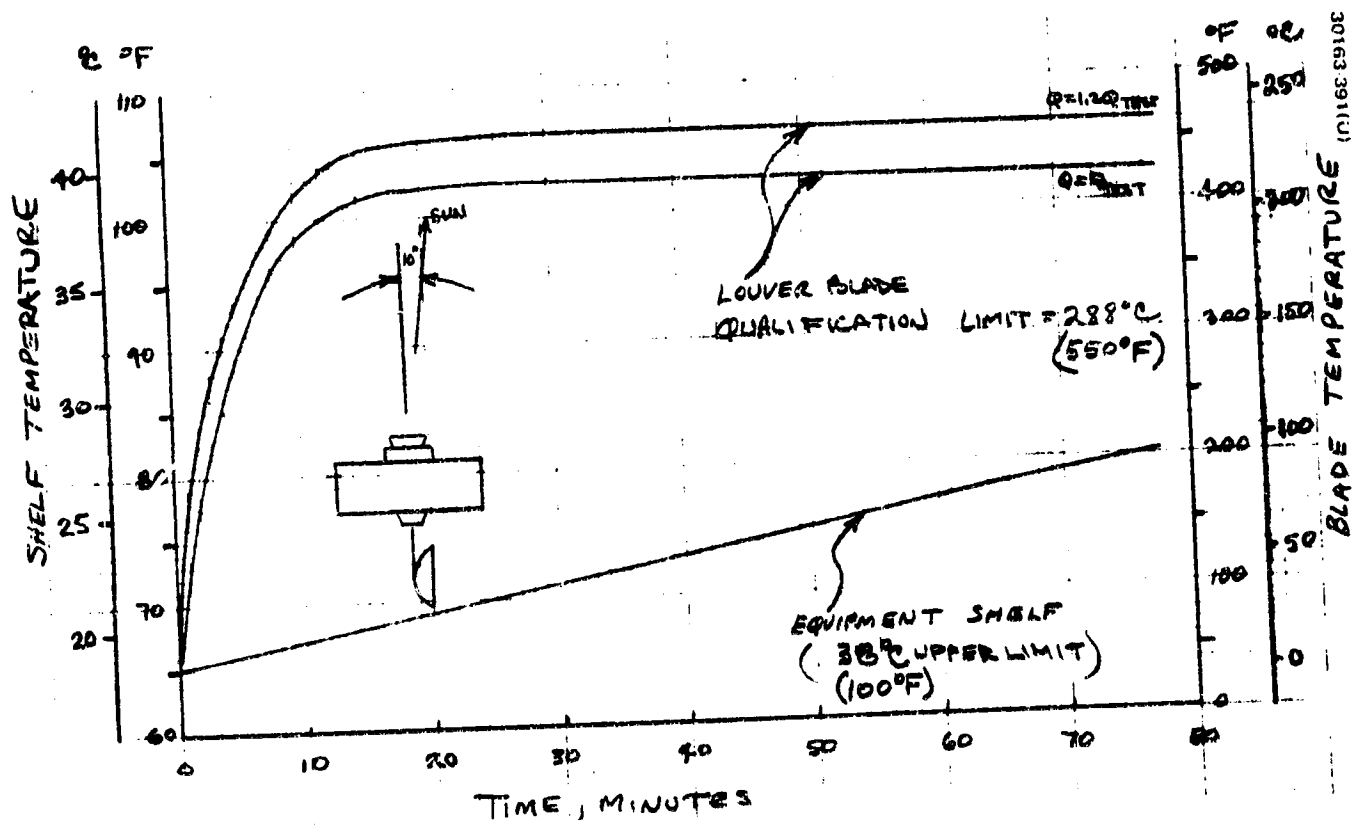


FIGURE 5-33. AFT CAVITY HEATING EFFECTS DURING FIRST TCM

A similar condition exists for the orbiter during the orbit insertion sequence. For the Type II transit trajectory, the sun angle for the firing is  $103.5 \pm 5$  deg. Again, using the data obtained in the interreflection tests, the response of the shelf was analyzed to determine the allowable time at this attitude. The results are shown in Figure 5-34. The nominal shelf temperature of  $49^{\circ}\text{C}$  ( $120^{\circ}\text{F}$ ) is reached within about 4 h for the maximum sun angle. Allowing  $5^{\circ}\text{C}$  ( $10^{\circ}\text{F}$ ) design margin, these data show that this attitude can be maintained for about 2.5 h for the maximum sun angle, about 6 h for the nominal angle, and indefinitely at the minimum angle. The louver blades would reach equilibrium temperatures for this case somewhat lower than those shown for the near earth TCM.

The response of the orbiter shelf temperature during the maximum periapsis planetary heating condition was analyzed. The spacecraft/orbital/sun geometry assumed is shown in Figure 5-35. The minimum periapsis latitude of  $21^{\circ}\text{N}$  was assumed to maximize the albedo load. The planetary loads on the louvers, computed assuming a 150 km periapsis altitude, were bounded by assuming that no blockage occurs and that all the energy incident on the disk representing the solar panel diameter is absorbed by the spacecraft aft cavity. The variation of these loads with time from periapsis is shown in Figure 5-36. The shelf response to this transient is small as shown in Figure 5-37.

The eclipse response for both spacecraft is bounded by the orbiter transient during the 190 min near-apoapsis eclipse. During this period, internal power is minimum (40 W), whereas during the shorter ( $\sim 23$  min) periapsis eclipses the spacecraft is at full power. The probe bus experiences a single eclipse of about 30 min at launch.

Bulk orbiter eclipse response is shown in Figure 5-38 for the shelf and the hydrazine tanks with propellant mass is a parameter. As shown, minimum shelf temperature is quite acceptable. For an 0.68 kg (1.5 lb) minimum propellant mass remaining at this point (180 days in orbit), the hydrazine temperature limits are satisfied.

#### Solar Array Temperatures

The mission profile of solar array temperatures for the probe bus (Type I trajectory) and the orbiter (Type II) are shown in Figure 5-39. These temperatures are nominal values assuming spin axis normal to the ecliptic plane and zero array electrical efficiency. The incremental temperature effect of assumed efficiency on array temperature is shown in Figure 5-40, along with temperature prediction uncertainty.

An important condition is experienced by the orbiter solar array during periapsis pass where transient planetary heating occurs. Array response for the worst case sun orientation (which occurs  $\sim 180$  days) is shown in Figure 5-41, along with the response for the periapsis heating at the time of orbit insertion. A significant response is indicated for the worst case and a significantly reduced peak temperature for the more nominal case. As shown, the maximum aerodynamic heating at 150 km periapsis has a small effect.

30163 392(U)

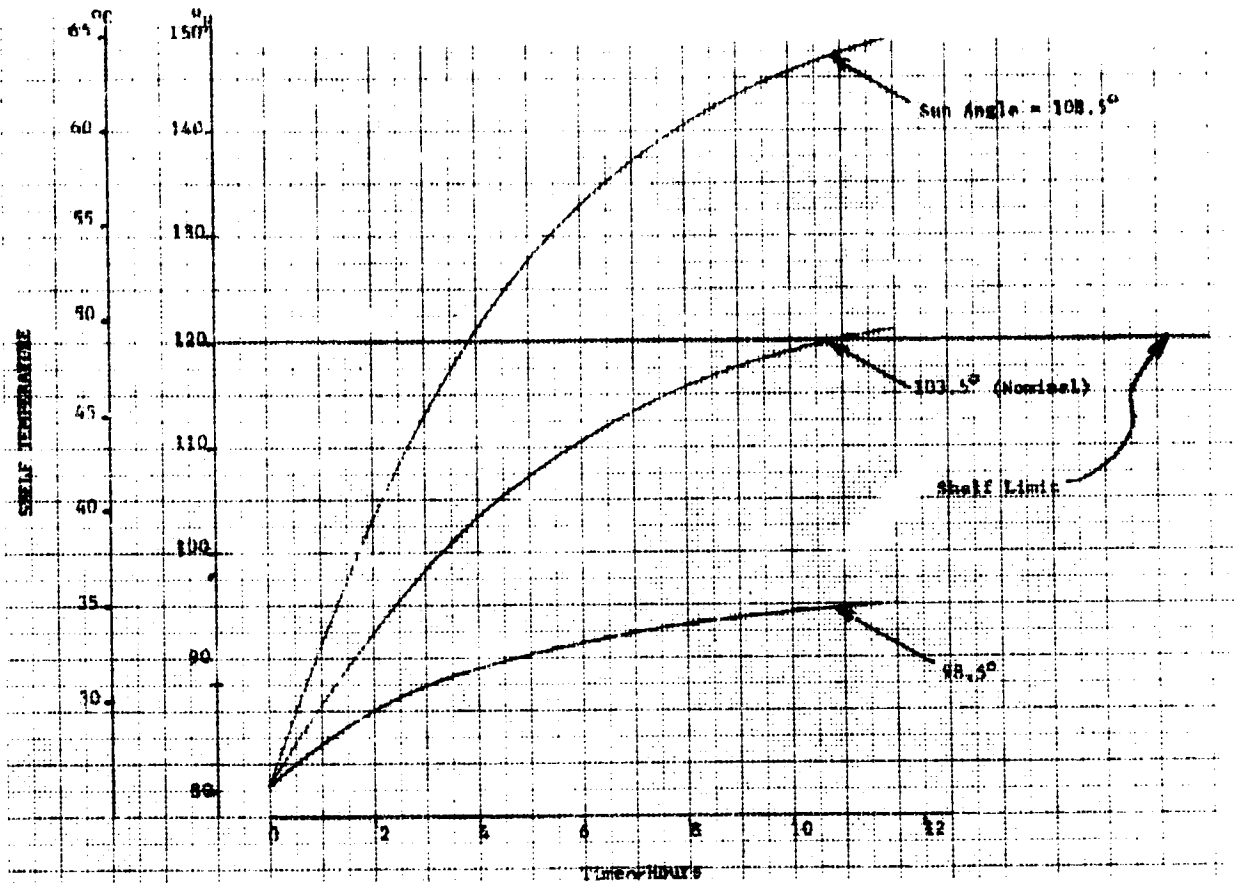


FIGURE 5-34. THOR/DELTA ORBITER SHELF RESPONSE DURING ORBIT INSERTION PHASE

30163 393(U)

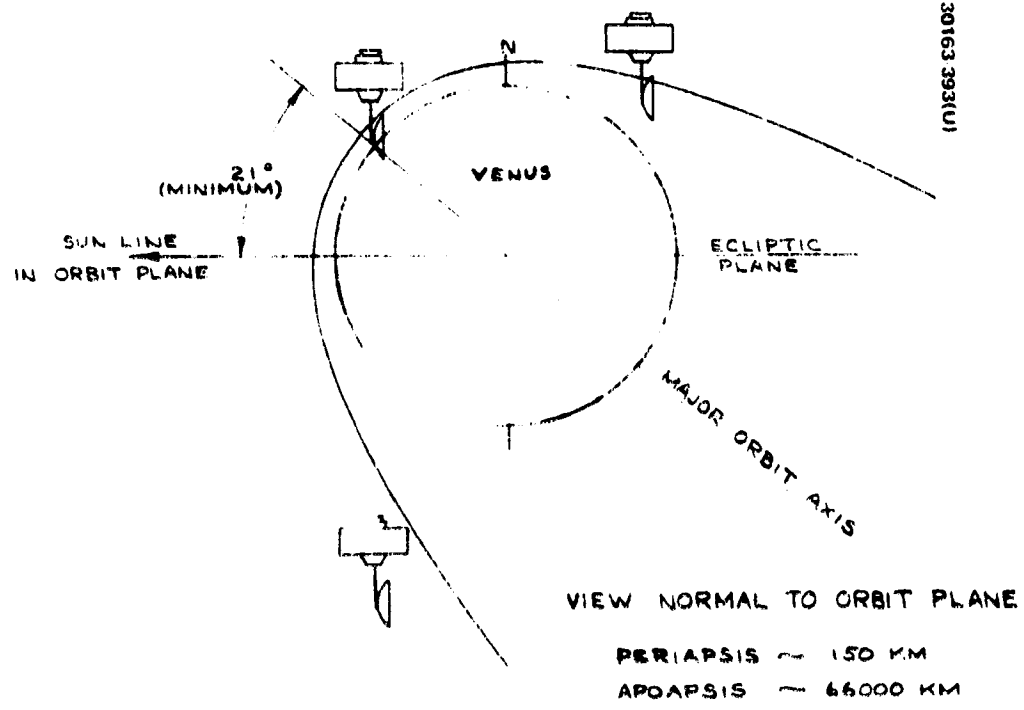


FIGURE 5-35. THOR/DELTA TYPE II ORBIT GEOMETRY

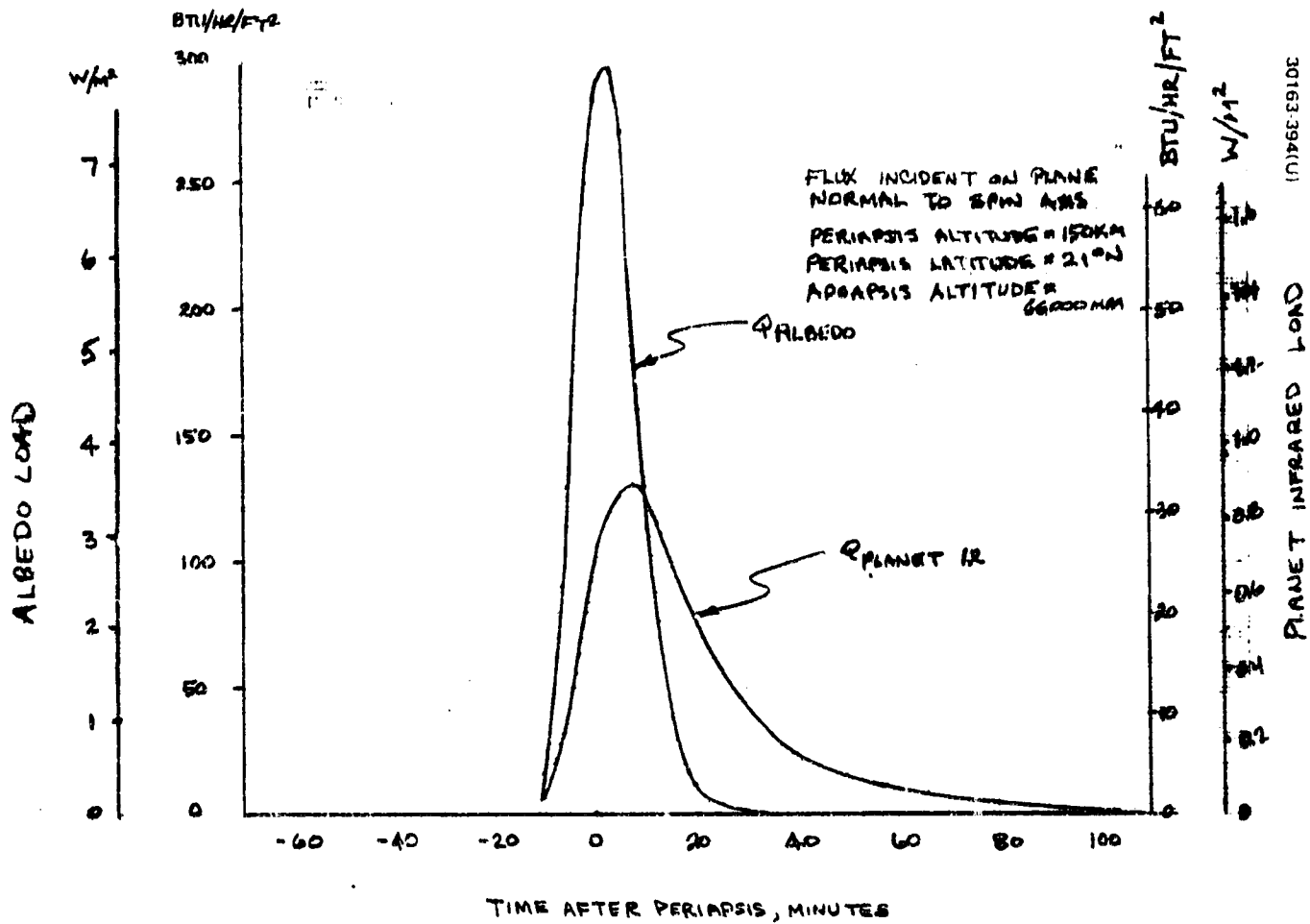


FIGURE 5-36. PLANET HEATING LOADS

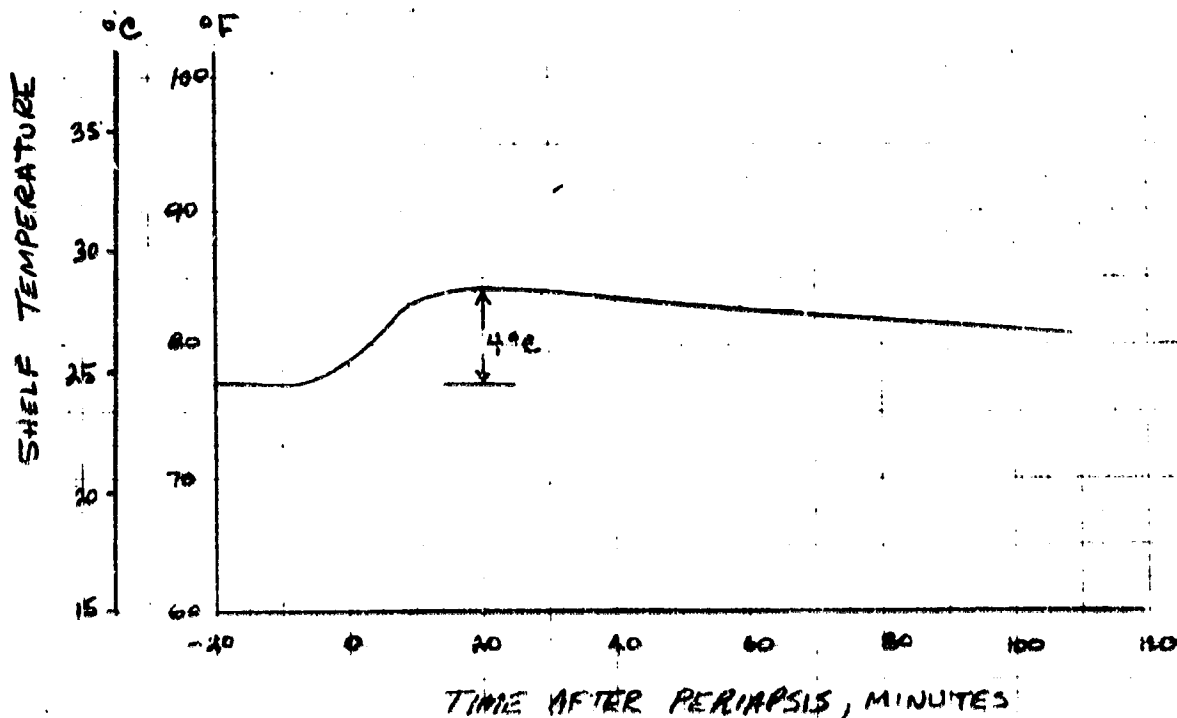


FIGURE 5-37. THOR/Delta ORBITER EQUIPMENT SHELF BULK RESPONSE TO PERIAPSIS HEATING

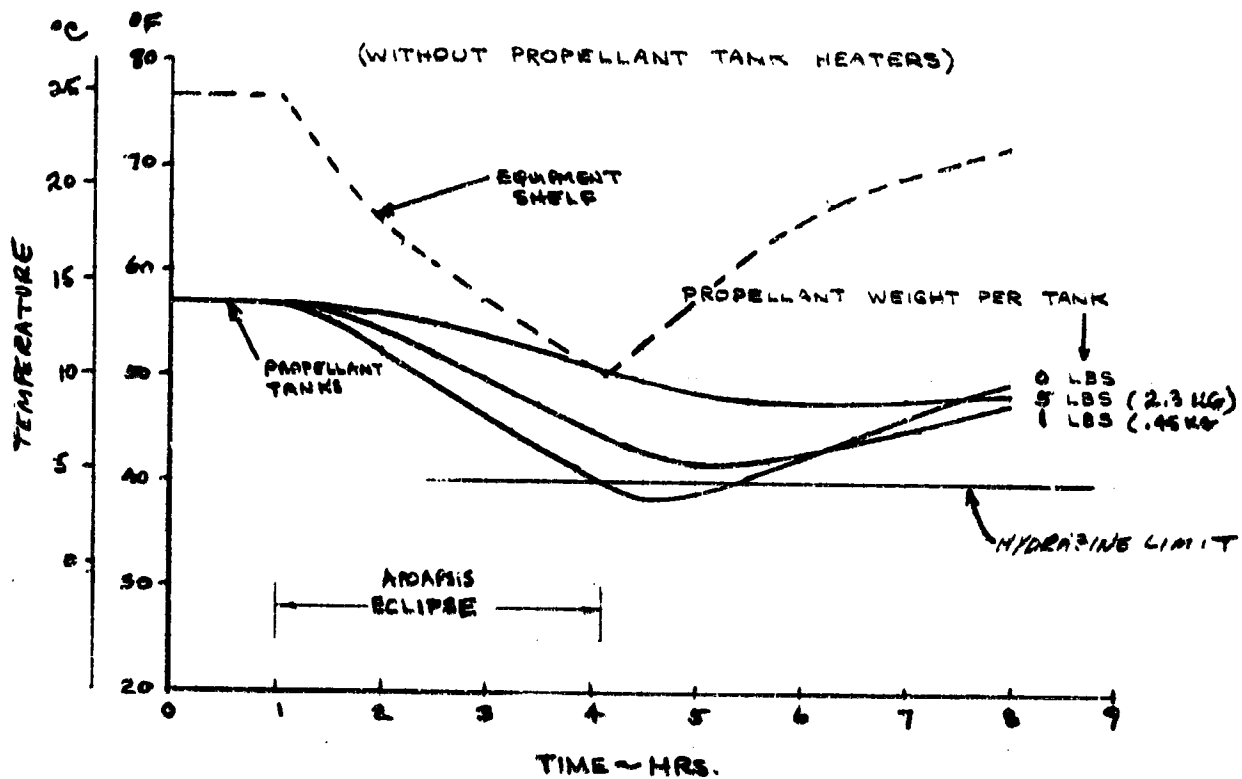
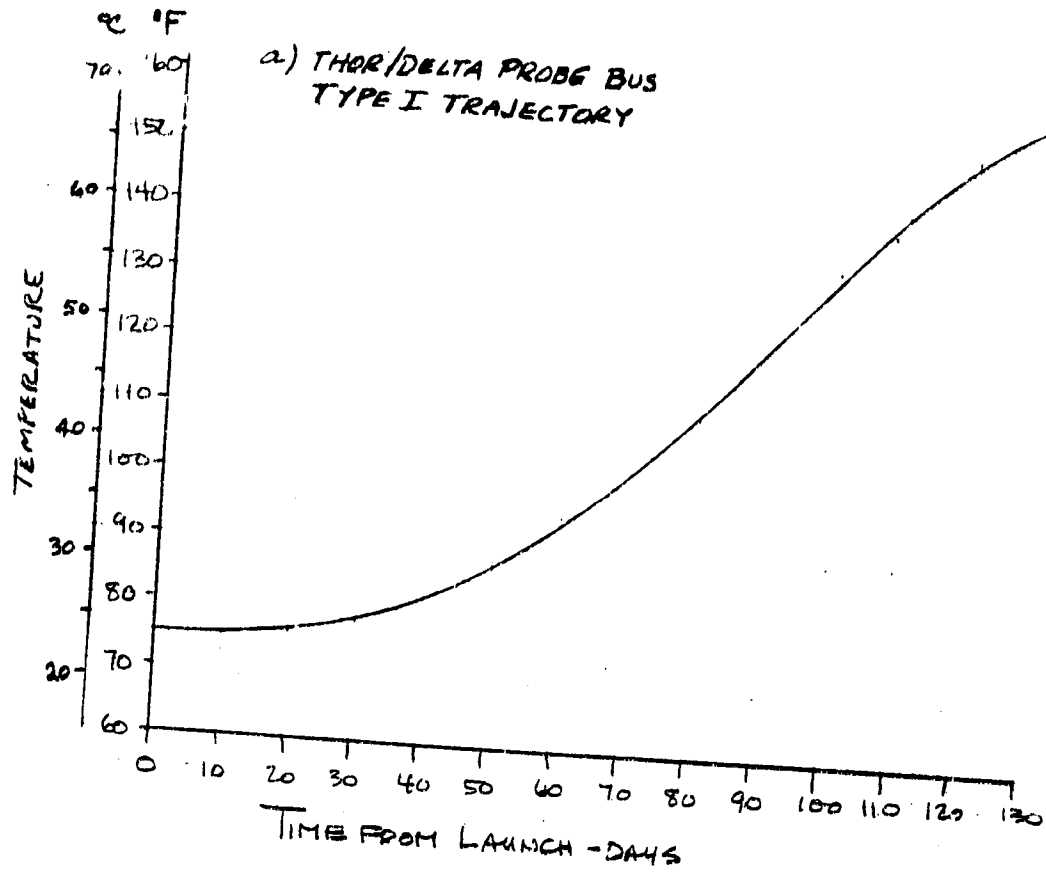
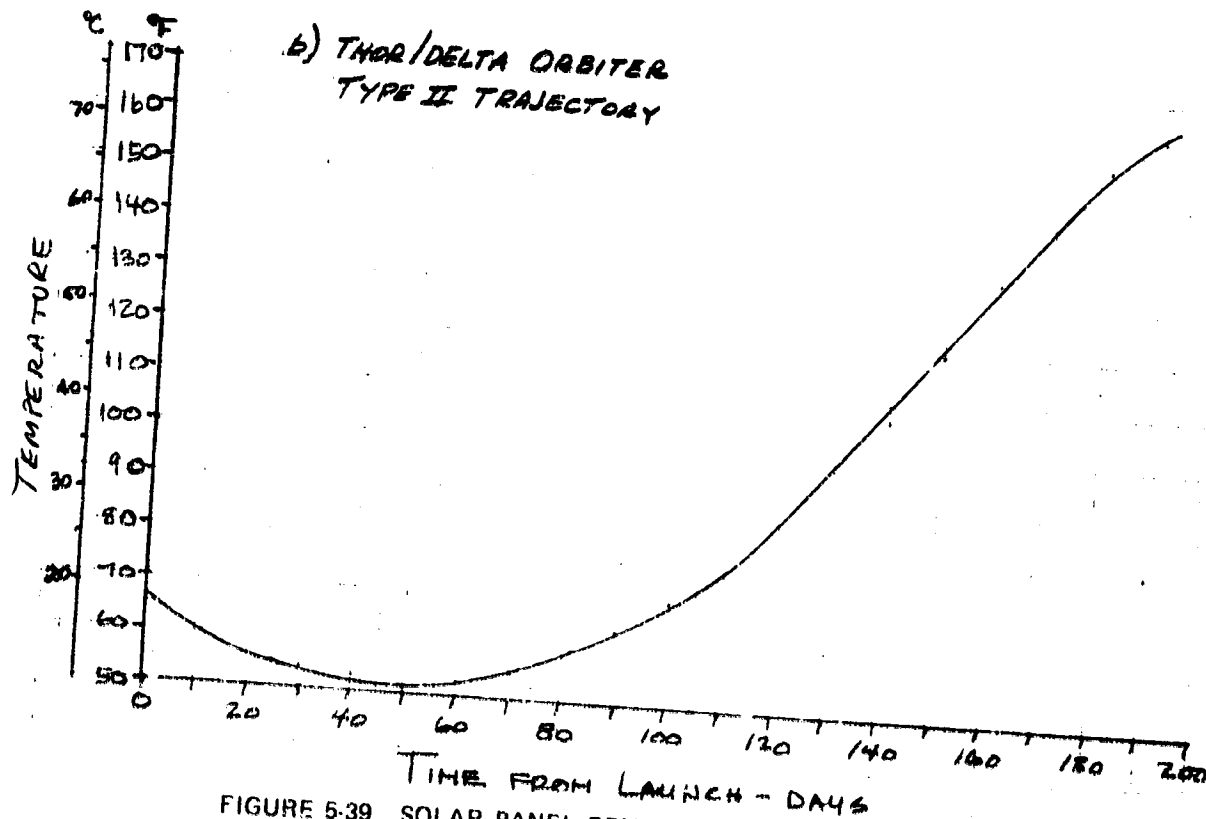


FIGURE 5-38. ORBITER TEMPERATURE RESPONSE DURING ECLIPSE



30163-397(U)



30163-358(U)

FIGURE 5-39 SOLAR PANEL TEMPERATURE VERSUS TIME

... OF THE ORIGINAL PAGE IS POOR

30163 39(11)

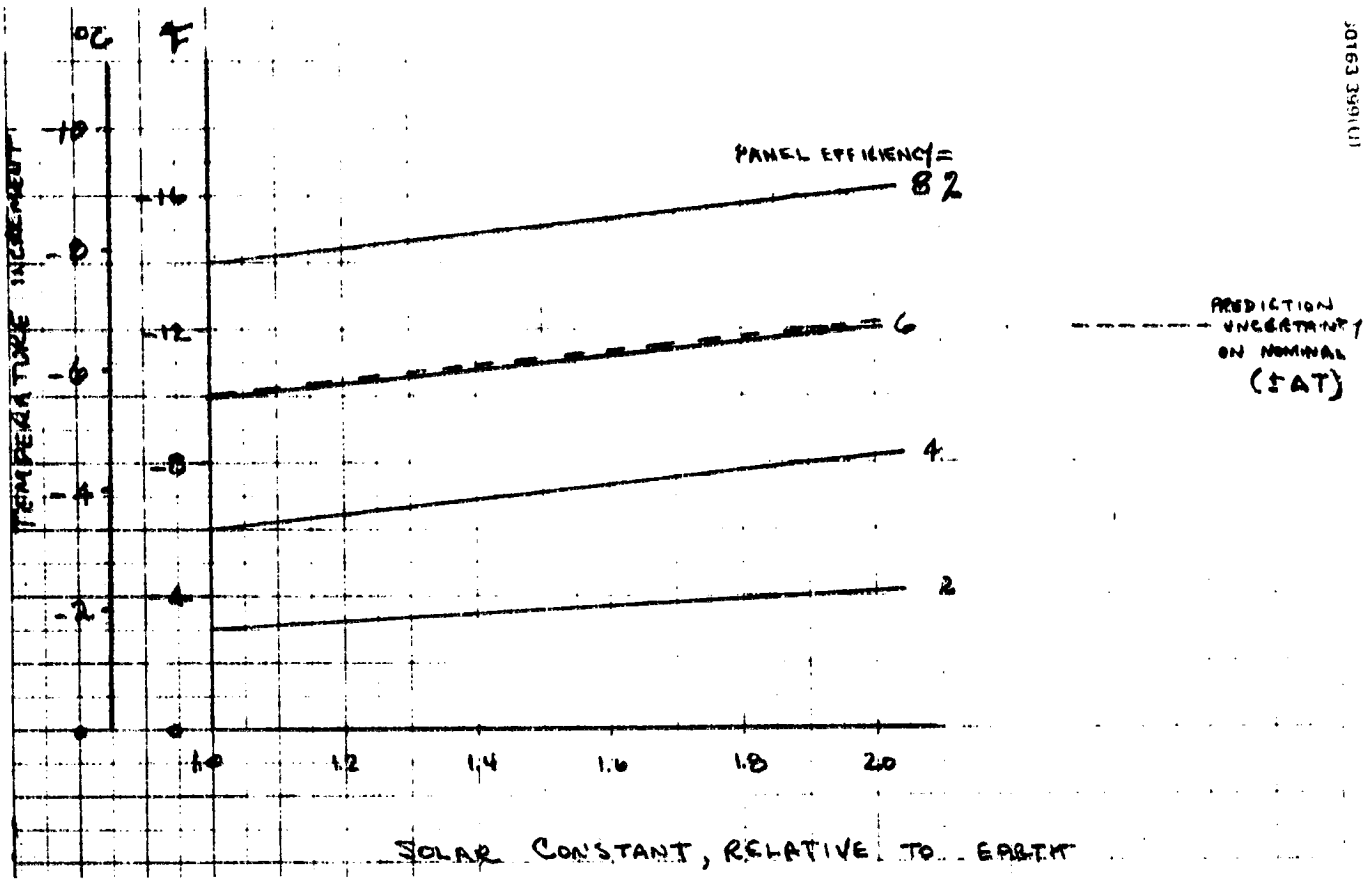


FIGURE 5-40. EFFICIENCY AND UNCERTAINTY EFFECTS ON SOLAR ARRAY TEMPERATURES



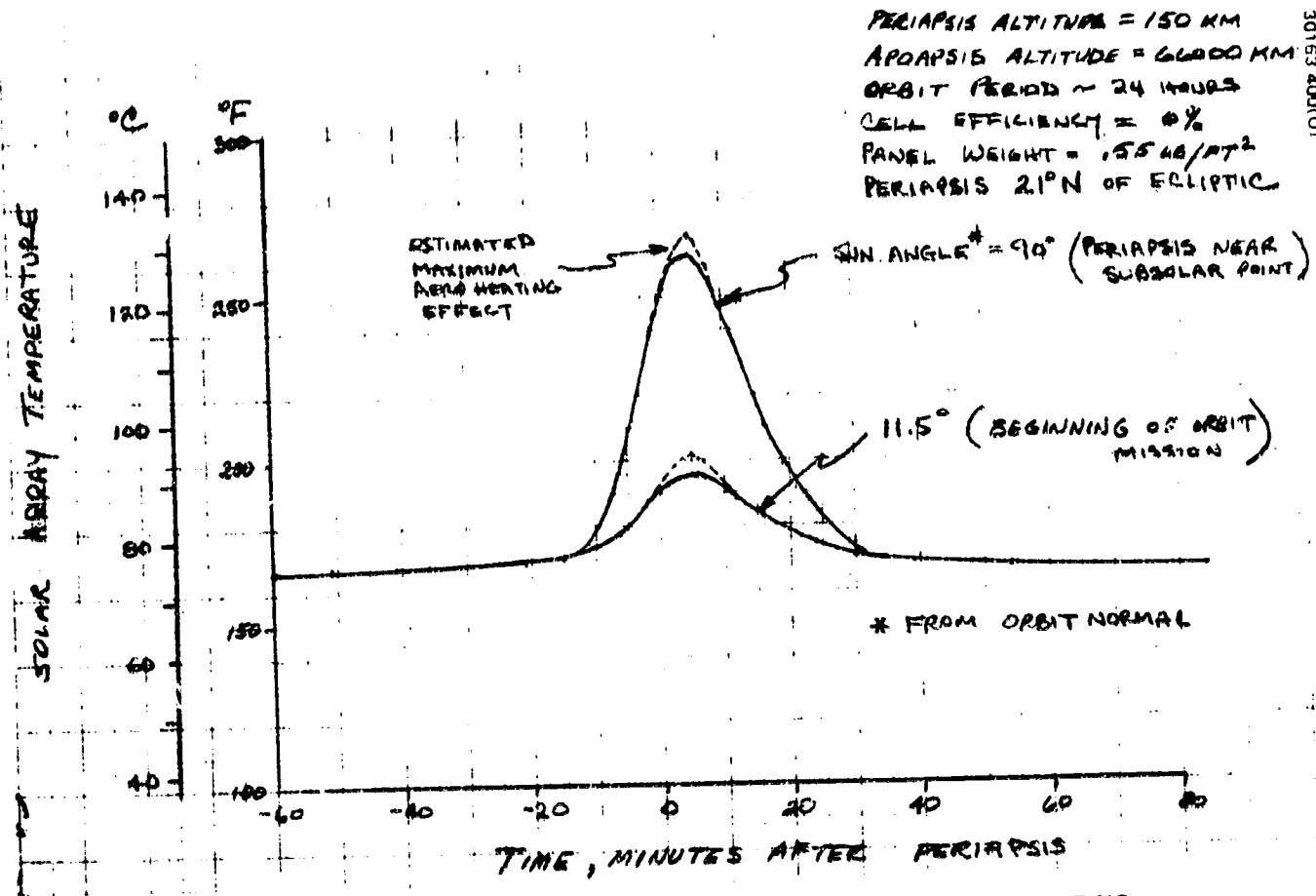


FIGURE 5-41. ORBITER SOLAR ARRAY RESPONSE TO PERIAPSIS HEATING

30163 401(U)

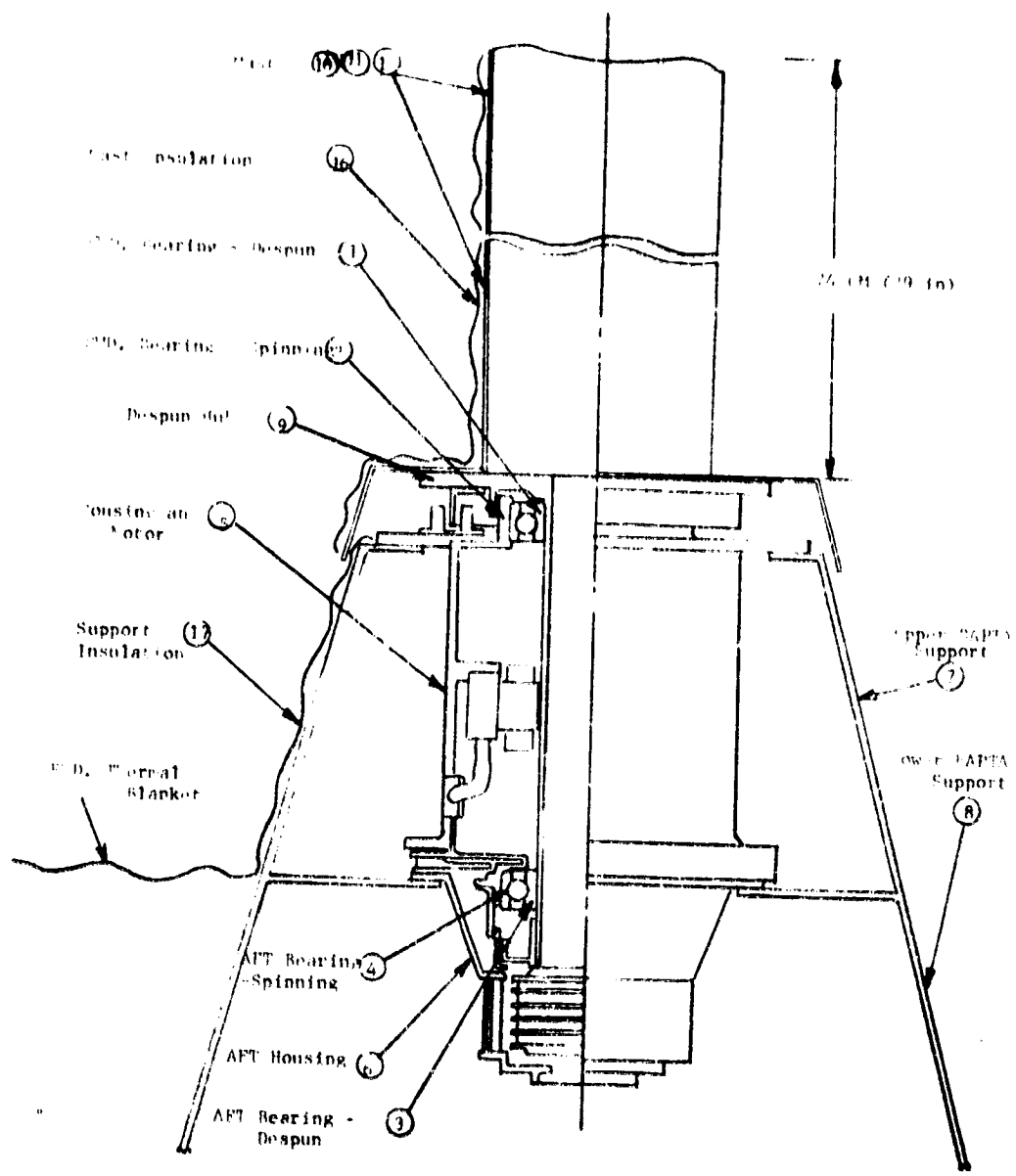


FIGURE 5-42. BAPTA THERMAL NODAL MODEL

### BAPTA Temperatures

The orbiter high gain antenna is despun by the bearing and power transfer assembly (BAPTA). Temperature control of this assembly is important, since bearing torque and loads are dependent upon temperature level and differentials. Detailed temperature distributions were generated from the BAPTA thermal network depicted in Figure 5-42. As indicated, the antenna mast is assumed to be superinsulated to minimize energy conducted to or from the despun side of the bearing. Radiation and conduction boundary temperatures were taken from the spacecraft bulk temperature solutions discussed above. Bearing dissipation was assumed to be 1.0 W maximum, distributed in the manner shown in Figure 5-42.

Two design conditions were examined to determine the range of temperatures occurring within the BAPTA during the mission. Maximum temperatures will exist during Venus orbit operation when environmental loads and boundary temperatures are maximum. Minimum temperature conditions occur during the near apoapsis 190 min eclipse, with the bearing motor off. The predicted steady state nodal temperatures are given in Table 5-12 for the apoapsis power condition. As indicated, the bearing temperatures are well below the upper limit of 38°C (100°F). Maximum bearing temperature difference (at the forward bearing) is approximately 2°C (3.6°F), an acceptable value. The forward and aft bearing response to the near apoapsis eclipse is shown in Figure 5-43. Again, adequate margin above the design limit of 4°C (40°F) is indicated. An examination of the design without the mast insulation showed marginal performance during the steady cruise conditions and minimum forward bearing temperature 5°C (9°F) below the design limit during apoapsis eclipse.

TABLE 5-12. ORBITER BAPTA STEADY STATE TEMPERATURES

Location	Temperature °C (°F)		
	Design Conditions		
	Near Earth, Operating*	Near Earth, Nonoperating	In Orbit Operating*
Bearing - Top			
Spinning side	12.8 (55.1)	11.8 (53.2)	18.4 (65.1)
Despun side	13.0 (55.4)	10.5 (50.8)	20.4 (68.7)
Bearing - Bottom			
Spinning side	14.1 (57.4)	10.8 (51.4)	21.1 (70.0)
Despun side	13.7 (56.6)	10.6 (51.0)	20.9 (69.6)
Motor	13.0 (55.0)	12.0 (53.0)	18.0 (65.0)
Despun Hub	13.0 (55.0)	"	21.0 (69.0)

\* 1 W motor power

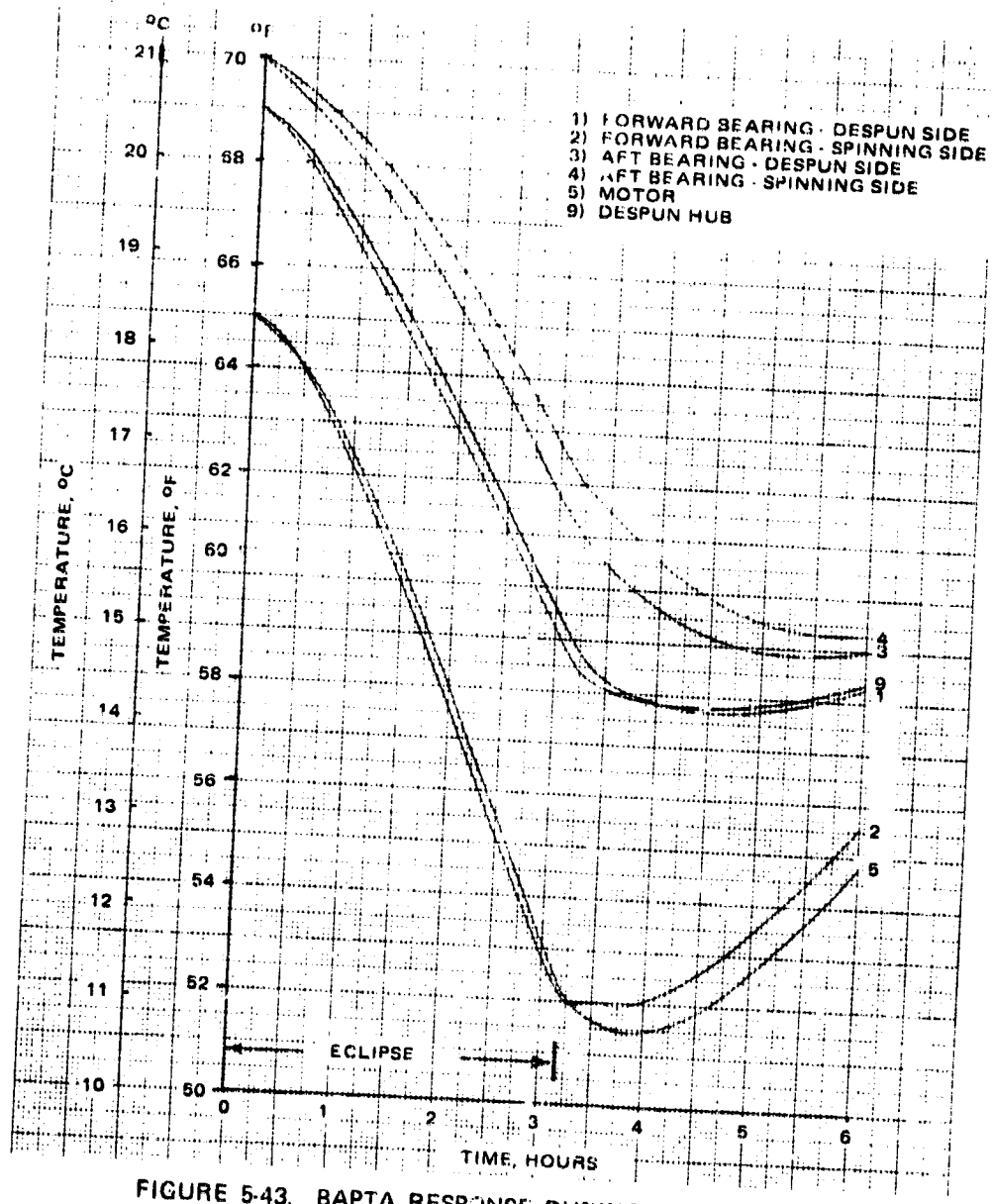


FIGURE 5-43. BAPTA RESPONSE DURING APOAPOSIS ECLIPSE

## Thrusters and Propellant Lines

Conditions leading to maximum and minimum (nonfiring) thruster assembly temperatures are dependent upon the thruster location and spacecraft mission. Thruster valve and catalyst bed heaters are sized for the worst case environmental conditions experienced in either mission by each type of thruster (radial or axial), making the designs common to both spacecraft.

The radial thrusters experience steadily increasing solar heating as the spacecraft approaches Venus with its spin axis normal to the sun line. Some quasi-steady variations are present during the multiprobe mission when the spacecraft spin axis is reoriented for probe release and final atmospheric entry. However, maximum and minimum steady temperatures are determined by solar heating at Venus and earth respectively with the spin axis normal to the sun line. Steady-state radial valve and catalyst bed temperatures are given in Figure 5-44 for these environmental conditions as a function of valve heater size. As shown, no catalyst bed heating is considered. These results indicate that an 0.25 W valve heater is required to maintain valve temperature above its lower limit with sufficient margin during the near earth environment. Maximum temperatures at Venus are acceptable with the valve heater on. Heater sizing is based on a minimum bus voltage of 26 V. The effect of maximum bus voltage (33 V) can be derived from the data given ( $Q_{33} = 1.61 Q_{26}$ ). Adequate maximum temperature margin is shown with this effect considered.

Transient design conditions for the radial thrusters are dominated by the long, infrequently encountered 190 min apoapsis eclipse, which occurs near the end of the Venus orbit mission. Thruster valve and catalyst bed response to this condition is shown in Figure 5-45a, for the 0.25 W valve heater only. As indicated, valve temperature can be satisfactorily maintained but catalyst bed temperature is marginal. Figure 5-45b shows that an 0.25 W heater on the catalyst bed provides substantial margin.

The axial thruster assembly mounted on the aft end of the spacecraft was selected for analysis since its location results in the poorest thermal coupling to the thermally controlled portion of the spacecraft.

Several design conditions exist which can size the axial thruster heaters. The 3 deg tolerance on the nominal spacecraft spin axis orientation normal to the sun line can, in the worst case, result in substantial shading the aft thruster. During probe separation (multiprobe mission) and final entry, even more extensive shading can occur. These conditions can exist for long periods relative to the thruster assembly time constant. There is also the long orbiter apoapsis eclipse transient. It was conservatively assumed that the thruster heaters should be sized for steady shadowing. Figure 5-46 presents thruster and catalyst bed temperatures based on this assumption and minimum (near earth) shelf temperature. Valve temperatures

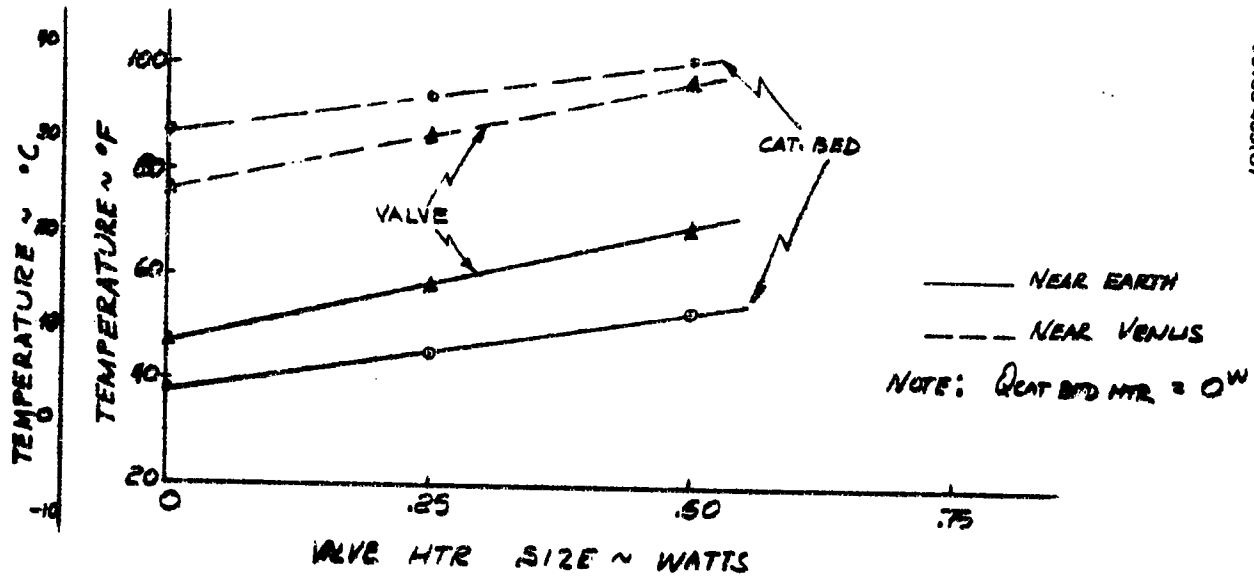


FIGURE 5-44. STEADY STATE RADIAL THRUSTER TEMPERATURES

30163-403(U)

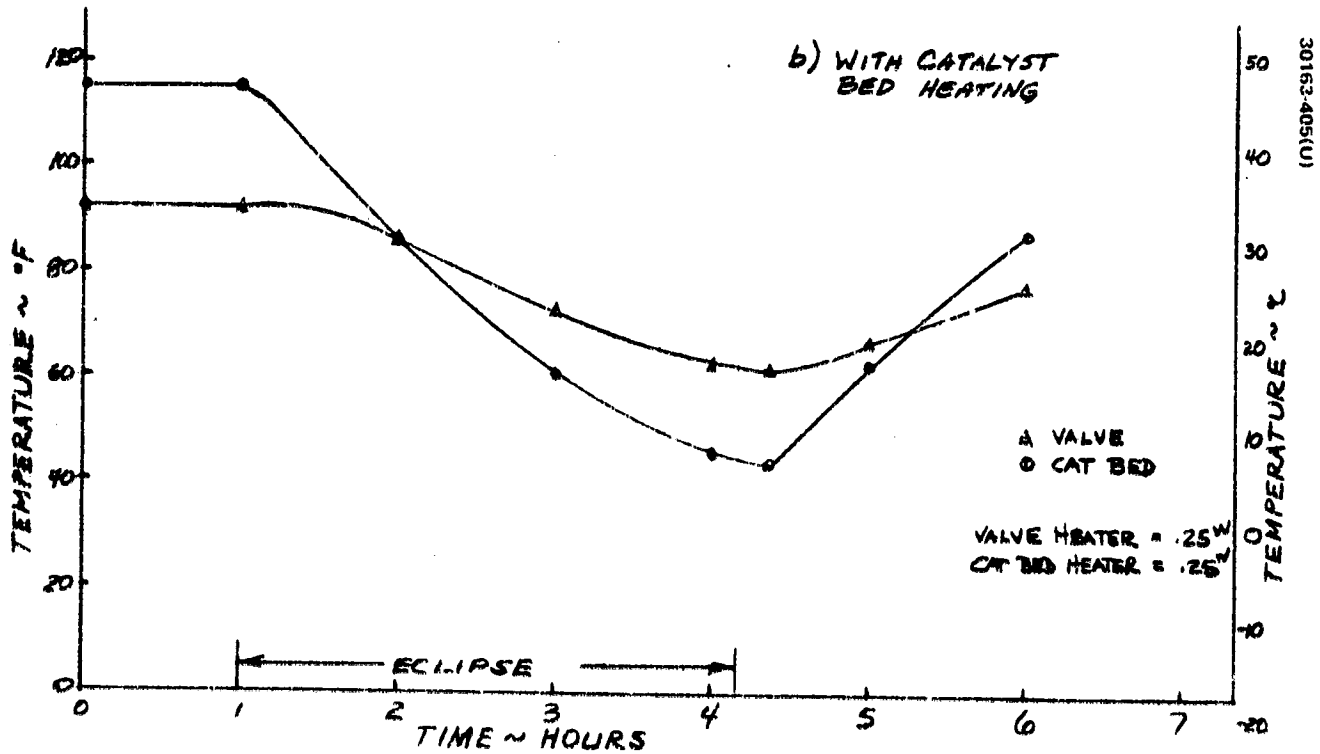
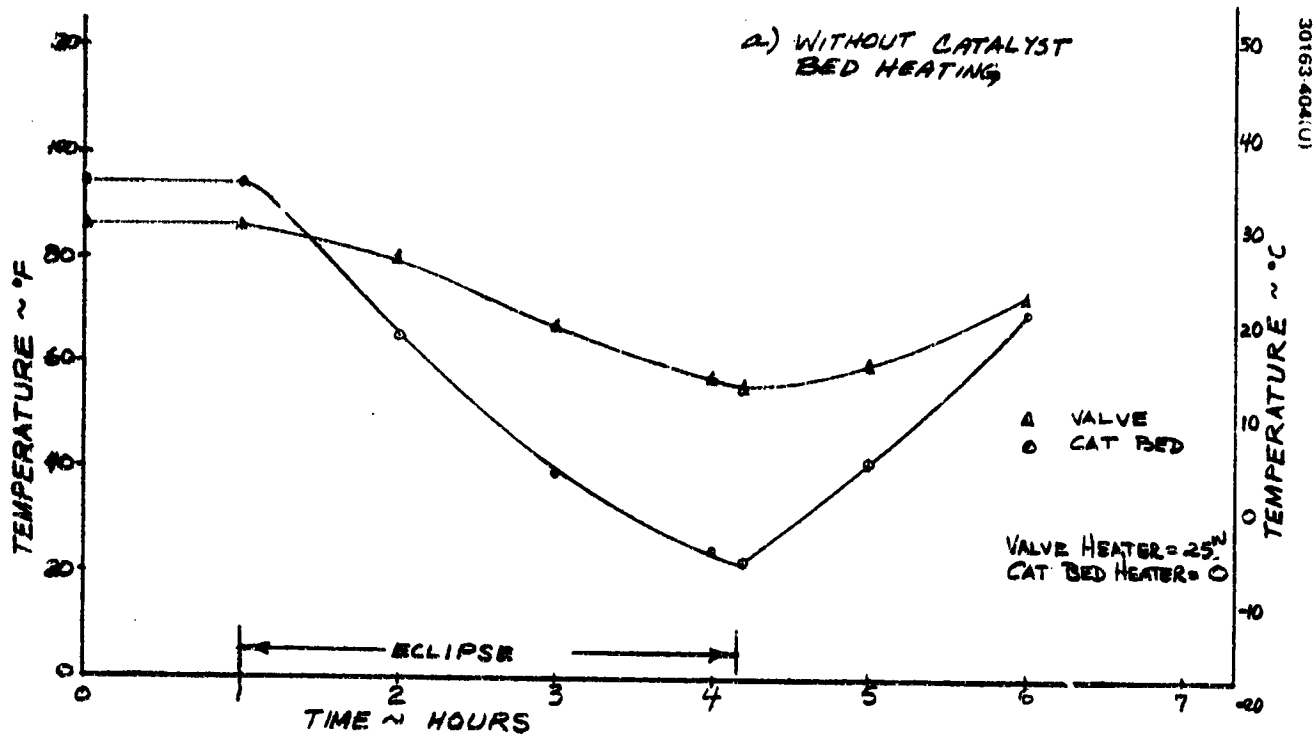


FIGURE 5-45. RADIAL THRUSTER THERMAL RESPONSE DURING ORBITER APOAPSIS ECLIPSE

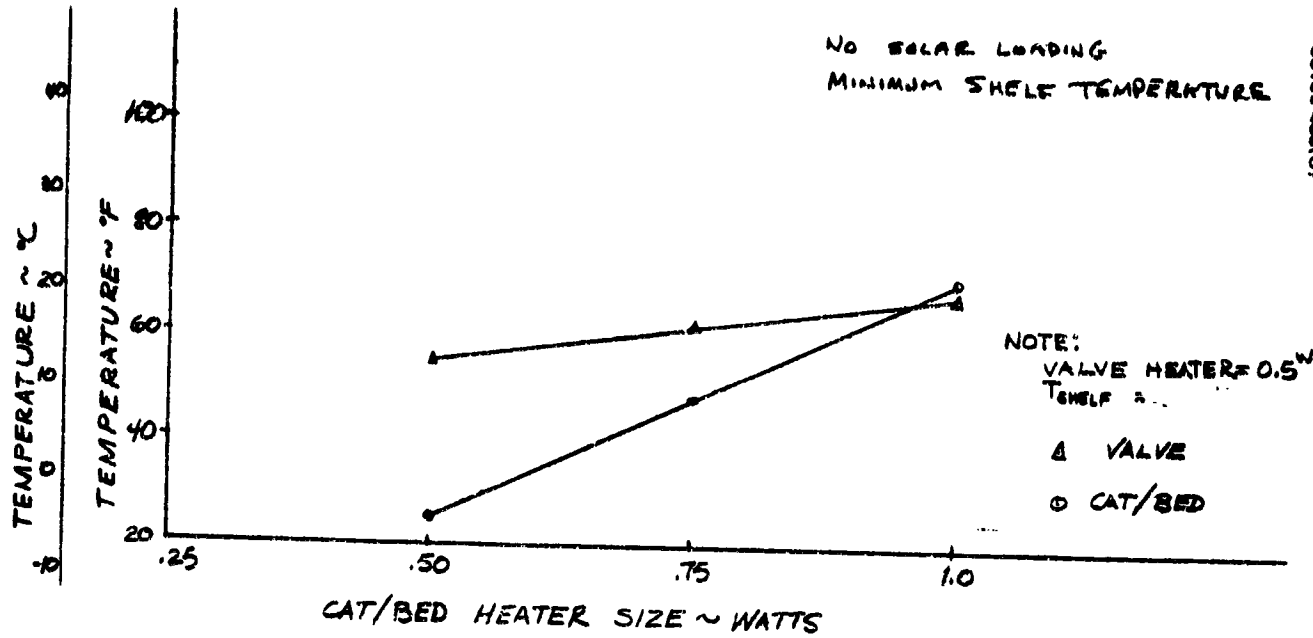


FIGURE 5-46. AXIAL THRUSTER STEADY STATE TEMPERATURES

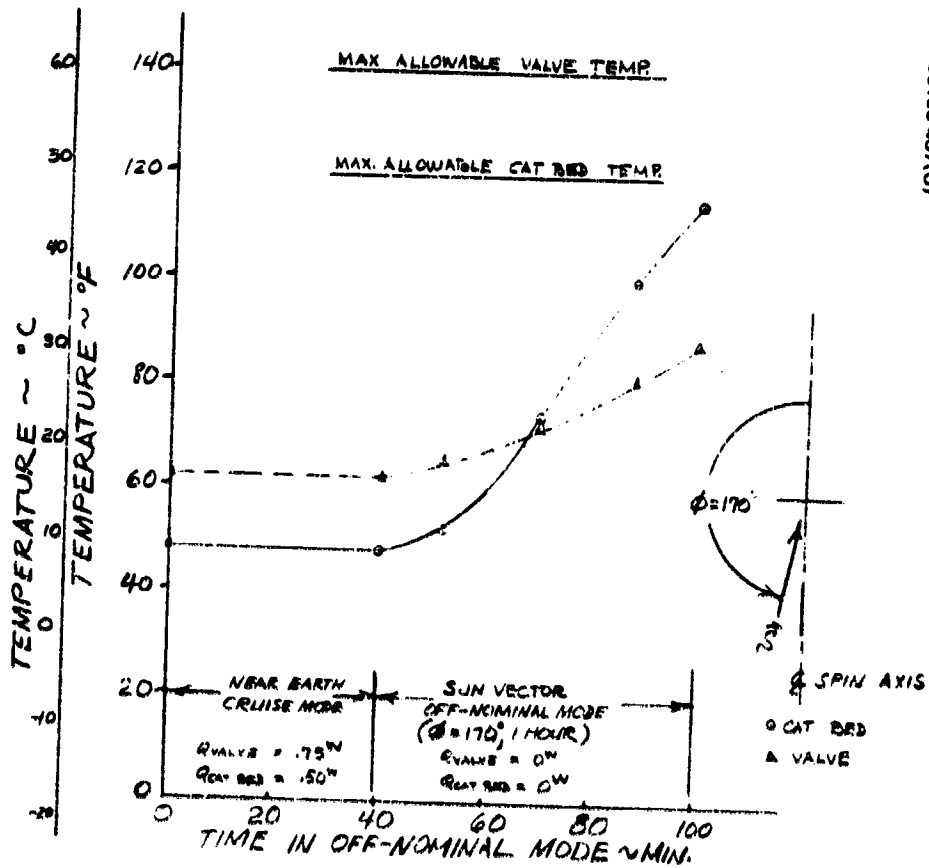


FIGURE 5-47. THERMAL PERFORMANCE OF AXIAL THRUSTER THRUSTERS IN NEAR-EARTH OFF-NOMINAL MODE



are shown to be relatively insensitive to catalyst bed heater so that an 0.5 W valve heater was assumed and the catalyst bed heater varied to find the required combination. As shown, an 0.75 W catalyst bed heater is necessary to maintain satisfactory margin. It was assumed in this study that heater size increment is 0.25 W.

The maximum temperature condition for the axial thrusters occurs during the first TCM if the extreme 170 deg sun angle is assumed to exist for 1 h. Figure 5-47 shows the aft thruster response to this transient. As indicated, temperature limits are maintained if heaters are turned off. A similar condition could exist for the forward axial thrusters if the sun angle were ~ 10 deg. Furthermore, since spacecraft spin axis orientation of the sun line normal tends to produce maximum heating on one set of axial thrusters minimum heating of the axials on the opposite side of the spacecraft, these heaters must be separately switchable. Similarly, the radial thruster heaters must be switched independently from the axials.

#### Orbit Insertion Motor

Table 5-11 presents the orbit insertion motor temperatures and heater power requirement for this design. The design requires that sometime during the transit trajectory from earth to Venus, the throat heater is switched off when it is no longer necessary.

#### Probe Temperatures

Temperature profiles for the large probe during the mission prior to entry are given in subsection 5.2. As indicated, maintaining minimum probe battery temperature above  $-40^{\circ}\text{C}$  near earth while providing initial temperature at entry in the range  $4^{\circ}\text{C} \pm 5^{\circ}\text{C}$  are the primary objectives, which the passive design has been shown to provide.

## 5.4 ATLAS/CENTAUR BASELINE DESCRIPTION

The thermal design concepts utilized for the Atlas/Centaur configurations are nearly identical to those shown for Thor/Delta. Equipment temperature limits and power requirements are given in subsection 5.1 for the Atlas/Centaur designs. The sun angle conditions and eclipse durations are somewhat different for the 1978 Atlas/Centaur Type I multiprobe and Type II orbiter missions. As indicated in the summary given in Table 5-13, notable differences occur in the probe sun angles after separation and the orbiter sun angle at orbit insertion. Also shown is the decreased duration of the apoapsis eclipse from 190 to 108 min.

### Spacecraft Design

The thermal designs of the Atlas/Centaur probe bus and orbiter spacecraft are shown in Figures 5-48 and 5-49. As indicated, these designs are very similar to the Thor/Delta configurations.

### Equipment Shelf

The same approach is used to control shelf temperatures, i. e., isolation from the environment and the use of thermal louvers. Somewhat higher spacecraft power and increased louver blockage by the conical thrust tube has led to increasing the number of louver modules to 10 on the probe bus and to 12 on the orbiter. Furthermore, the use of additional radiator area on the orbiter to generally depress the orbiter temperature level was considered necessary to extend the transient capability of the design during the orbit insertion phase. The shelf honeycomb thickness for the Atlas/Centaur designs has been increased to 6.4 cm (2.5 in.) to reduce the vibration loads predicted for the increased diameter shelf. The adverse effects of the increased temperature difference across this thickness between the equipment mounting surface and the radiators has also required increased radiator area.

The orbiter equipment shelf layout is illustrated in Figure 5-50, showing unit, louver, and doubler placement and doubler thicknesses. The doublers are beryllium sheets placed under those units which have power densities requiring radiating surface areas substantially more than the unit mounting areas, even though they are placed directly over louver modules. The rf power amplifiers are the principal items in this category. Other units that cannot easily be placed over louver modules, but have moderately high power density requiring more lateral conduction than is provided by the shelf, are also placed on doublers. The magnetometer electronics and the solar wind analyzer experiment are such units. The other experiments, being used only transiently, are controlled by heat capacity.

The probe bus shelf arrangement is similar as shown in Figure 5-51 with orbit unique units being replaced by the fewer probe bus unique units. The reduced bus power allows the removal of 2 of the 12 orbiter louver modules. The doublers remain the same.

TABLE 5-13. ATLAS/CENTAUR SUN ANGLE AND ECLIPSE HISTORY

Event	Mission	Sun Angle* deg	Duration	Time of Occurrence
Launch/Ascent	Probe Orbiter	14 67	1.4 hr 1.4 hr	-
Cruise	Probe	Eclipse	25.0 min	-
	Both	90 ±3	Continuous	103 days 199 days
First TCM	Both	90 ±80	1.0 hr	5 days
Subsequent TCM's	Both	90	40.0 min	From 20 days
Orbit insertion	Orbiter	111 ±3	3.5 hr	Encounter
Orbit	Orbiter	90 ±3	Continuous	-
	Orbiter	Eclipse	23.0 min 1.8 hr 3.2 hr	80 days in orbit 180 days in orbit 1980 launch
Large probe Pre-separation Post-separation Entry	Probe	31.8	3.0 hr	100 days
		31.8 60.7	{ Continuous variation	{ 23 day coast
Small probe Pre-separation Post-separation Entry	Probe	30.9	4.0 hr	103 days
		30.9 41.9	{ Continuous variation	{ 20 day coast
Probe bus Post-probe separation Entry	Probe	22.0 66.0	{ Continuous variation	20 days before encounter

\* Measured from axis, probe/HGA end

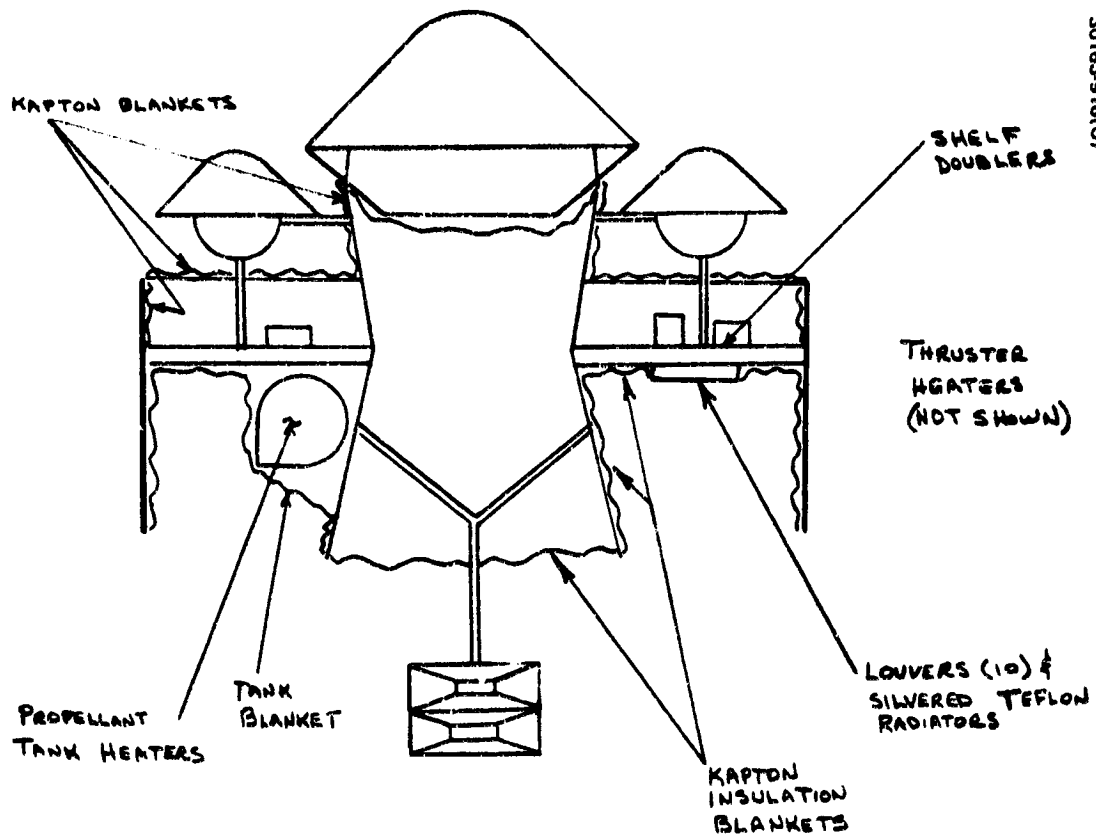


FIGURE 5-48. PROBE BUS THERMAL DESIGN

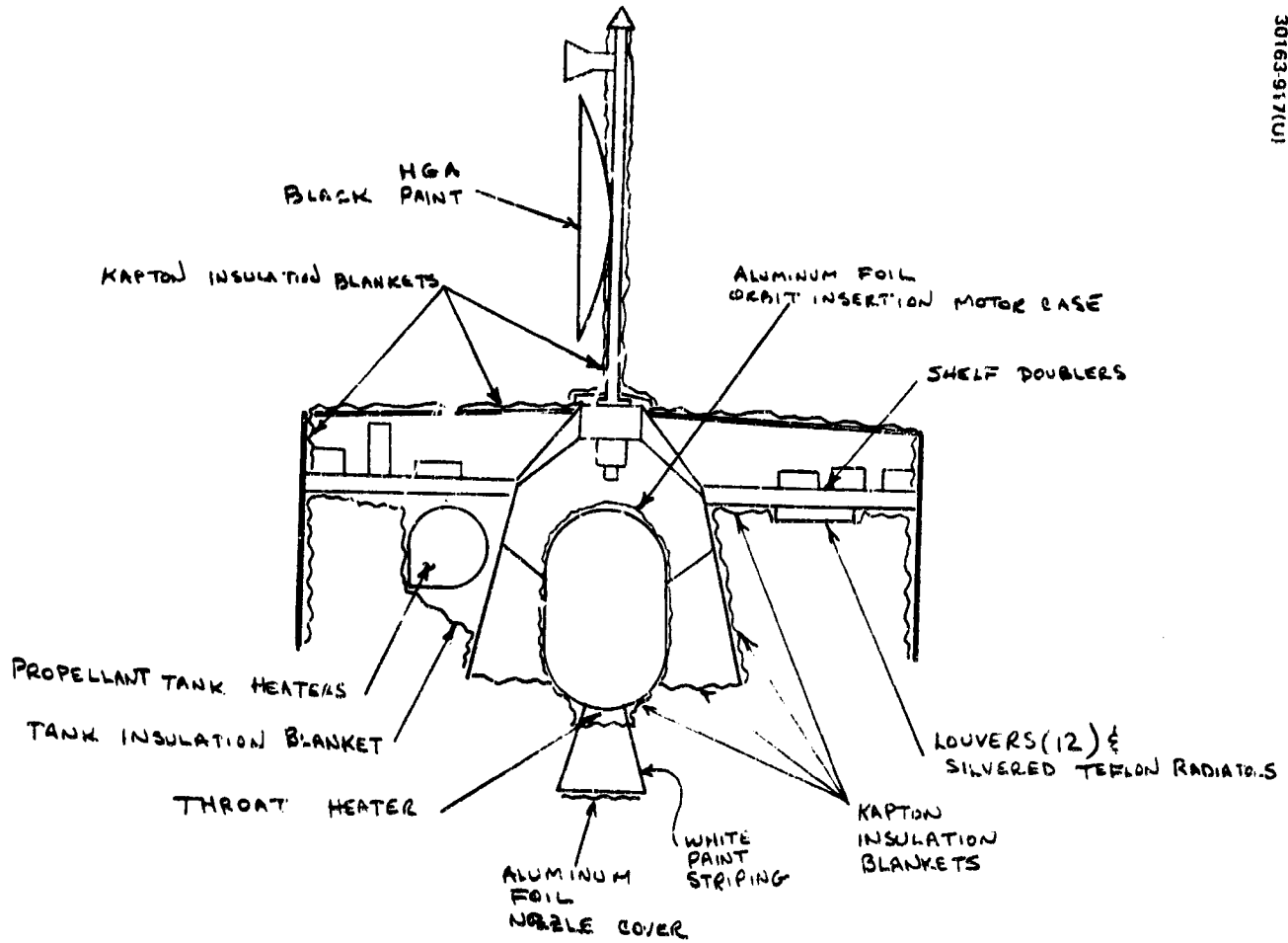


FIGURE 5-49. ORBITER THERMAL DESIGN

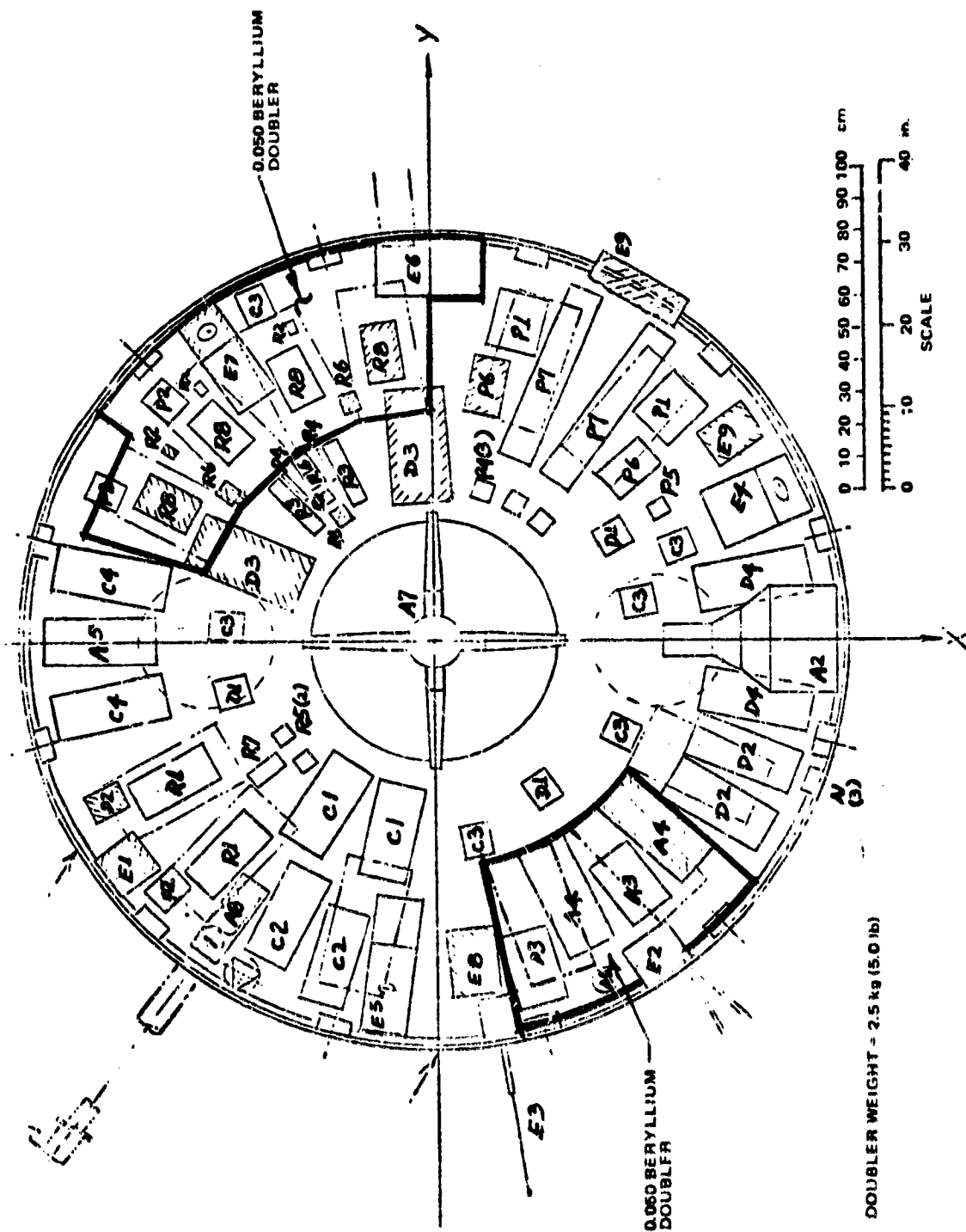


FIGURE 5-50. ORBITER EQUIPMENT SHELF LAYOUT

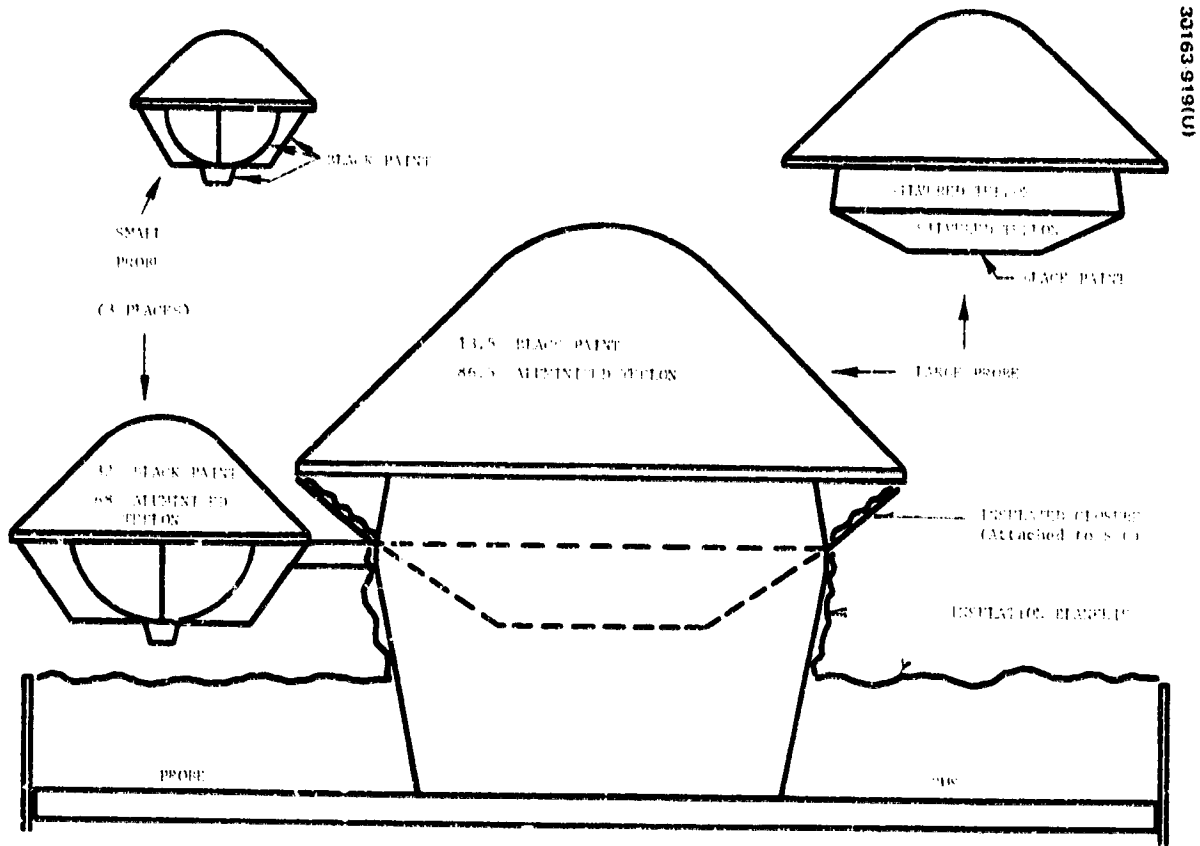


FIGURE 5-51. PROBE PRE-ENTRY THERMAL FINISHES

### Insulation

Multilayer Kapton superinsulation blankets are utilized on the Atlas/Centaur spacecraft in much the same manner as shown for the Thor/Delta design. A notable exception is in the area of the orbit insertion motor on the orbiter configuration. Here, the motor nozzle and a small portion of the case extend outside the thrust tube/launch vehicle separation plane. This increased distance of the motor nozzle exit plane from any thermal barrier closing the area between thrust tube and motor results in greatly reduced exhaust plume heating. Based on the data given in subsection 5.2, the high temperature stainless steel barrier shown for the Thor/Delta design was replaced by a Kapton multilayer blanket. Furthermore, the larger diameter thrust tube results in a larger shape factor between the thrust tube and the cavity between the shelf and the forward blanket. Therefore, to provide better radiant coupling between these two elements, the inner thrust tube surface has a high emittance finish rather than insulation. Motor isolation is provided by covering the case with aluminum foil.

Because exhaust plume heating rates are also lower on the solar panel and propellant tank insulation, the local thickening of insulation outer sheets is not required for the Atlas/Centaur designs.

### Propulsion

Here again, most of the Thor/Delta design concepts are retained. The hydrazine thruster assembly design has been somewhat modified from that considered in the Thor/Delta studies. Thermal isolation between propellant valves and catalyst beds has been reduced to the point where separate catalyst bed heaters are no longer required. Instead, valve heaters have increased to provide the same total heater power, i. e., 1/2 W for each radial thruster valve and 1-1/4 W for each axial valve.

Because orbiter temperature levels have been depressed to increase capability during the orbit insertion phase, propellant temperature during the near earth phase of the mission approaches the lower temperature limit of 4°C (40°F). Therefore, to gain the necessary design margin, tank heaters have been incorporated into the Atlas/Centaur design, requiring 5 W of power per tank.

Control of orbit insertion motor temperatures requires somewhat higher heater power (9 W) because of revised motor temperature limits. The lower limit of -7°C (20°F), previously used for Thor/Delta studies, has been increased to 4°C (40°F). Thermal treatment of the motor is somewhat changed because of installation differences. The nozzle throat heater and igniters are now covered with a Kapton blanket because these items extend outside the thrust tube insulation barrier. Also, the nozzle finish is a striping of inorganic (Hughes HP 135) white paint on the bare nozzle to limit peak propellant temperatures just prior to firing. This paint is highly stable in the solar environment and can withstand the 500°-600°C (1,000°F) nozzle temperatures. Solar absorptance of this paint is expected to increase from 0.18 initially to approximately 0.25 at firing because of solar exposure.



## Probe Preentry Design

The passive thermal control approach utilized for the Thor/Delta probe preentry design has been retained for the Atlas/Centaur designs. However, because the minimum nonoperating temperature of elements, the probe rf subsystem has been increased to  $-23^{\circ}\text{C}$  ( $-10^{\circ}\text{F}$ ) for the Atlas/Centaur design, heater power is required from the probe bus during the early portion of the transit from Earth to Venus.

The range of sun angles experienced by the large probe between separation and entry are shown in Table 5-13. As the large probe approaches Venus, this sun angle variation results in steadily decreasing solar heating despite the increasing solar constant. Therefore, probe temperatures will tend to decrease. However, at sun angles greater than about 52 deg, the aft cover receives illumination. This tends to increase probe temperatures, depending upon the choice of finishes. Since the primary thermal design objective is to provide minimum temperatures at entry, the approach was to use a low solar absorptance on the aft cover. The selection of black paint and aluminized teflon on the heat shield, silvered teflon on the illuminated aft cover surfaces, and black paint on the aeroshell base and on the aft cover rf window is shown in Figure 5-51. To minimize bus heater power required during transit, an insulated enclosure is provided around the aft cover and heat shield base. This is necessary because these surfaces would otherwise absorb little solar energy while dissipating substantial energy during the transit mission when the sun is normal to the probe spin axis.

The small probe thermal finishes are also shown in Figure 5-51. Since the small probes experience less sun angle variation, illumination of the aft surface will not occur. Therefore, these surfaces have a high absorptance (black paint), which tends to minimize bus heater power.

## Mass and Power Summary and Hardware Derivation

A summary of the spacecraft thermal control hardware is shown in Table 5-14, along with heater power requirements. The derivation of this hardware is similar to that shown for the Thor/Delta designs.

## Spacecraft Design Performance

### Bulk Temperatures

The bulk spacecraft temperatures were derived using the thermal nodal models shown in Figures 5-52 and 5-53, which are similar to those used in the Thor/Delta studies.

The bulk temperatures of the probe bus are shown in Table 5-15 for the principal steady state design conditions using equipment shelf power based on the requirements and solar array characteristics given in subsection 5.2. Similar results are shown in Table 5-16 for the orbiter spacecraft. These temperatures indicate the required margins are met with satisfactory margin.

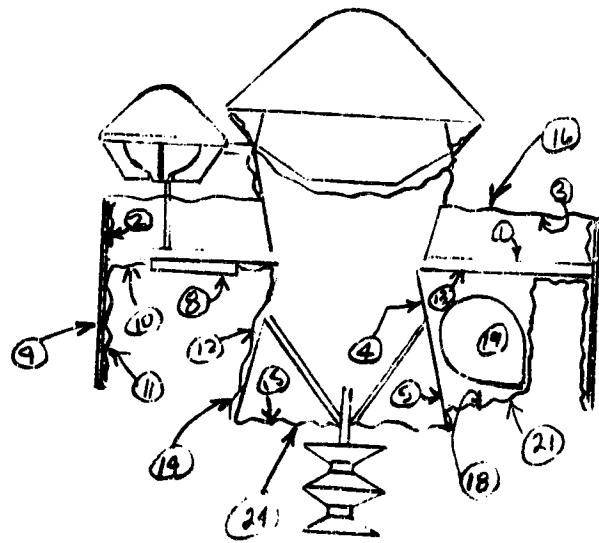
TABLE 5-14. ATLAS/CENTAUR THERMAL CONTROL, MASS AND POWER REQUIREMENTS

	Probe Bus			Orbiter		
	Mass		Power, W	Mass		Power, W
	kg	lb		kg	lb	
Louvers*	( 2.9)	6.5	—	( 3.6)	7.8	—
Blankets/support	11.5	25.2	—	10.6	23.2	—
Shelf doublers	2.3	5.0	—	2.3	5.0	—
Coatings	0.9	2.0	—	0.9	2.0	—
Temperature sensors	0.1	0.2	—	0.1	0.3	—
Thruster heaters**	(0.16)	0.4	4.6	( 0.2)	0.5	5.8
OIM heater	—	—	—	( 0.04)	(0.1)	15.0
Tank heaters**	(0.27)	(0.6)	10.0	( 0.27)	(0.6)	10.0
Totals	14.8	32.4	14.6	13.8	30.5	30.5

\* Mass tabulated in Controls Subsystem.

\*\* Mass tabulated in Propulsion Subsystem.

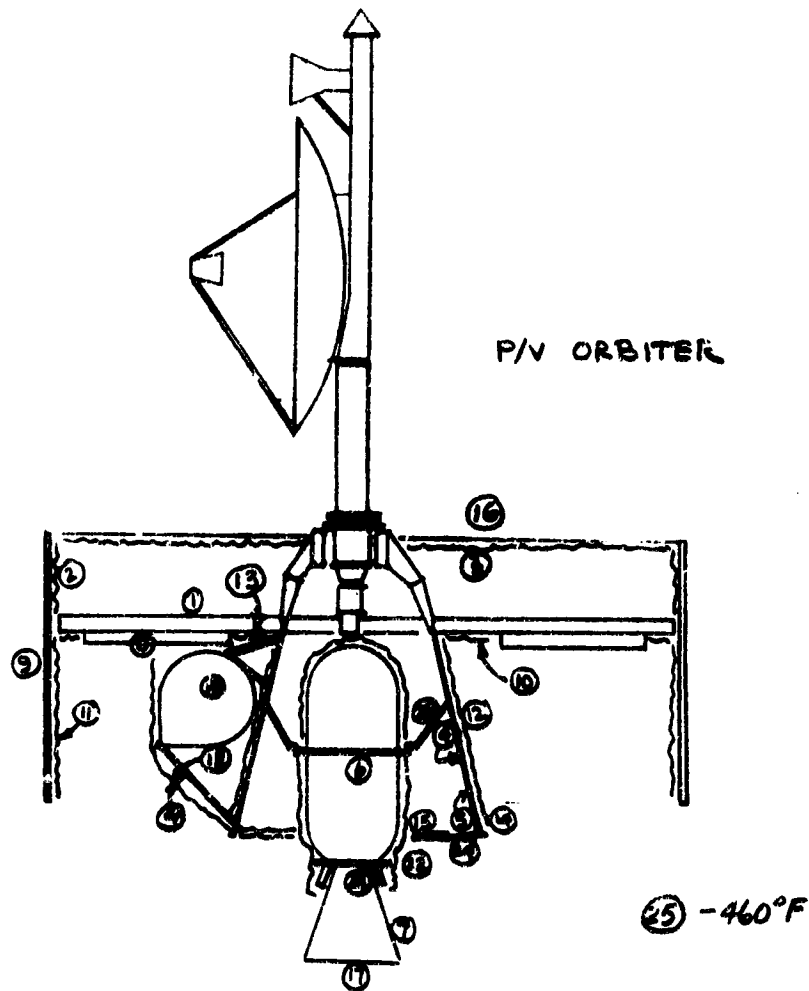
30163-920(U)



NODE ID DESCRIPTION	NODE ID DESCRIPTION
1 EQUIPMENT SHELF	13 EQUIPMENT SHELF
2 INSULATION	14 INSULATION
3 INSULATION	15 INSULATION
4 THRUST CONE	16 INSULATION
5 THRUST CONE	18 TANK INSULATION
8 LOUVERS	19 PROPELLANT TANK
9 SOLAR PANEL	21 INSULATION
10 INSULATION	24 INSULATION
11 INSULATION	
12 INSULATION	

FIGURE 5-52. PROBE BUS NODAL MODEL

30163-921(U)



NODE ID	DESCRIPTION	NODE ID	DESCRIPTION
1	EQUIPMENT SHELF	13	EQUIPMENT SHELF (AFT (VTY. SIDE))
2	INSULATION	14	INSULATION
3	INSULATION	15	INSULATION
4	THRUST CONE	16	FORWARD CLOSURE
5	THRUST CONE	17	NOZZLE CLOSURE
6	OIM	18	INSULATION
7	NOZZLE	19	PROPELLANT TANK
8	LOWERS	20	OIM SUPPORT
9	SOLAR PANEL	21	INSULATION
10	INSULATION	22	INSULATION
11	INSULATION	23	OIM THROAT
12	INSULATION	24	INSULATION
		25	SPACE BOUNDARY

FIGURE 5-53. ORBITER THERMAL NODAL MODEL

TABLE 5-15. PROBE BUS STEADY STATE BULK TEMPERATURES

Location	Temperature Limits		Temperatures, °C (°F)		
	°C	°F	Near Earth Cruise	Design Conditions	
				Near Encounter	Post Probe Separation*
Louver radiators	-	-	11 (51)	13 (59)	21 (70)
Equipment shelf	4 to 49	40 to 120	11 (51)	17 (63)	25 (78)
Hydrazine tanks	4 to 38	40 to 100	9 (48)	12 (53)	12 (54)
Solar panel	-160 to 135	-256 to 275	17 (63)	65 (150)	10 (50)

\*Sun 30° off probe axis.

TABLE 5-16. ATLAS/CENTAUR ORBITER STEADY STATE BULK TEMPERATURES

Location	Limits		Design Conditions					
	°C	°F	Near Earth Cruise (50 Days)		Near Orbit Insertion		Orbit Operation	
			°C	°F	°C	°F		
Louver radiators	-	-	12	54	16	61	17	68
Equipment shelf	4 to 49	40 to 120	13	55	19	67	20	68
Orbit motor case	4 to 32	40 to 90	11*	52	26	78	-	-
Hydrazine tanks	4 to 38	40 to 100	18**	50	13	55	13**	56
Solar panel	-160 to 135	-256 to 275	17	63	72	161	72	161

\* With 9 watt heater

\*\* With 5 watt heater per tank

However, as was the case for the Thor/Delta design, temperature extremes for the orbiter spacecraft will be encountered during transient conditions. Using the orbiter bulk model, the orbit insertion phase was examined to determine maximum time which could be spent in the worst case attitude before the equipment temperature limits were exceeded. As shown by the response given in Figure 5-54, bulk average temperatures of 46°C (115°F) are reached in 3.5 hours for the worst sun angle (114 deg). This satisfies the temperature limits for most equipment operating during this period. However, the high power density rf units, i. e., the transmitter power amplifiers, will sustain local mounting surface temperatures about 11°C (20°F) higher than the bulk average shelf temperature. Therefore, these units require higher temperature limits of 60°C (140°F) to meet this transient condition. Also shown is the response for the nominal sun angle of 111 deg, which results in a shelf bulk temperature of 40°C (104°F). This analysis was based on louver solar loads derived from the interreflectance test given in subsection 5.2. While this data was developed using a model of the Thor/Delta aft cavity geometry, it is considered applicable to the Atlas/Centaur design. Although the conical thrust tube would tend to increase reflected loads, the major source of reflections is the solar panel. Since the proportions of the cavity are similar, no major differences in this latter effect is expected. Furthermore, as indicated in the referenced test report, some conservatism is present in the data because of modeling limitations.

Minimum orbiter temperatures will be experienced during the apoapsis eclipse in Venus orbit. Bulk shelf response is shown in Figure 5-55, along with propellant tank temperature. As indicated, shelf temperature remains well above minimum limits. The propellant tanks are shown to be above their lower limit after the 1.8 hr eclipse duration associated with the 1978 Type II mission.

The alternate 1980 launch results in an eclipse duration of 3.2 hrs. The tank temperature for this eclipse duration is shown to be at the limit. The effect of providing 5 W of heater power per tank is also shown to produce acceptable temperatures for this extended eclipse. However, shelf temperature is approaching its lower limit of 4°C (40°F).

The other transient design conditions, including first TCM and periapsis heating, will have effects similar to those shown for the Thor/Delta designs.

### Shelf Temperatures

Temperatures of shelf units is shown in Table 5-17 for several important orbiter design conditions. The early cruise mode results in steady state temperatures well within the lower bulk shelf limit of 4°C (40°F). The apoapsis operating mode in Venus orbit (no long eclipses) results in temperatures substantially below upper limits. Temperatures for the orbit insertion, and apoapsis eclipse transients are also shown. The orbit insertion transient with maximum solar illumination in the aft cavity results in maximum unit temperatures. As shown for a 3-1/2 h period, the power amplifier temperatures slightly exceed their 60°C (140°F) limits as do the ADP and T/M processor. Because some degree of conservatism exists in the lower solar loads and

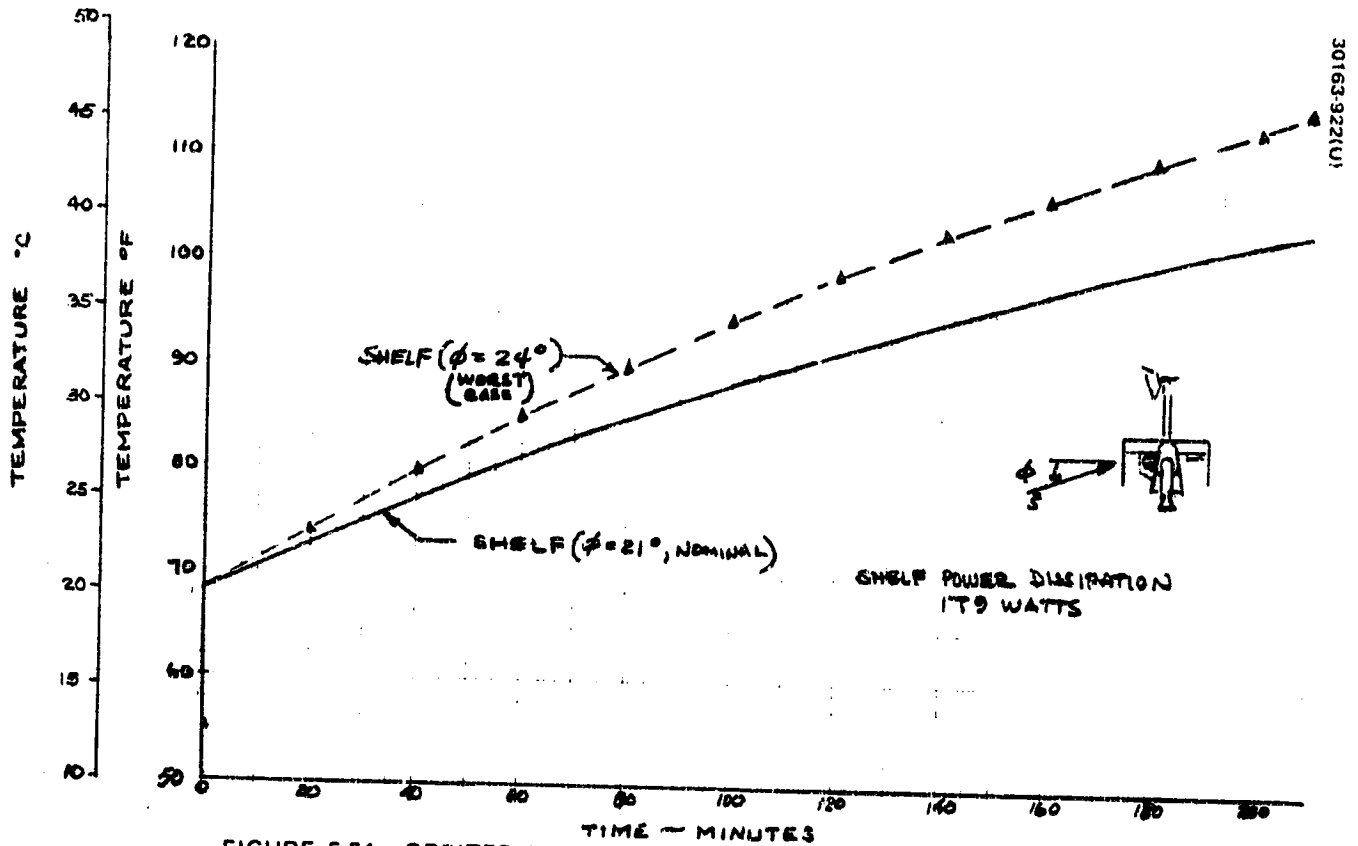


FIGURE 5-54. ORBITER TRANSIENT RESPONSE OF EQUIPMENT SHELF. ORBIT INSERTION

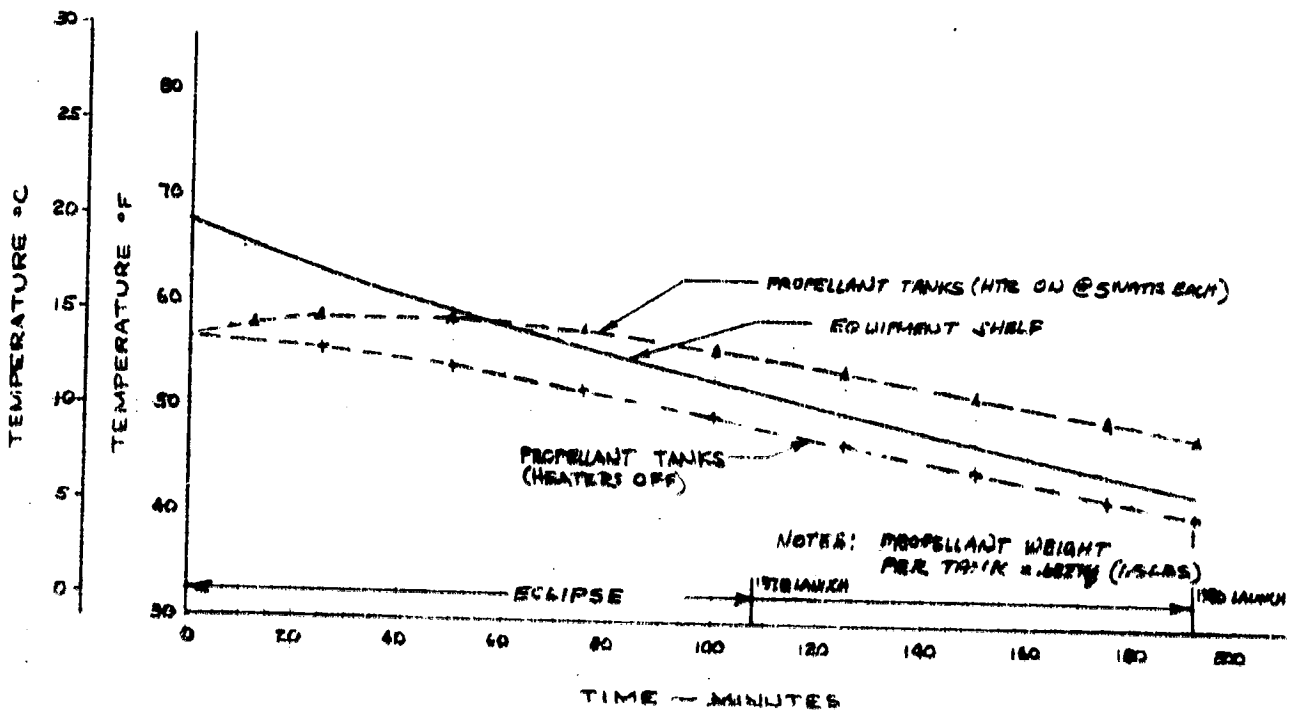


FIGURE 5-55. ORBITER ECLIPSE RESPONSE IN VENUS ORBIT

PERSONNEL CAPABILITY OF THE ORIGINAL PAGE IS POOR



TABLE 5-17. PIONEER VENUS ORBITER SHELF MOUNTED UNITS TEMPERATURES - °C (°F)

Unit Designation	Minimum Steady State (Cruise-10)	Maximum Temperature Steady State (APO-2)	Maximum Temperature Orbit Insertion +3.5 hrs	Minimum Temperature Cruise Cycle Follows		Maximum Temperature at 2000 alt.
				3.2 hr Elapse	1.5 hr Elapse	
E 1 Magnetometer	13 (-8)	ON 29 (83)	47 (116)	ON	13 (55)	23 (74)
E 2 Solar wind analyzer	13 (-8)	ON 29 (83)	47 (116)	ON	14 (55)	21 (70)
E 3 Eled temperature orifice	13 (-8)	22 (72)	42 (108)		10 (50)	17 (63)
E 4 Neutral mass	10 (-15)	ON 66	31 (-8)		15 (59)	27 (81)
E 5 Ion mass spectrometer	13 (-8)	ON 66	45 (113)		3 (43)	32 (90)
E 6 TV spectrometer	22 (-7)	ON 64 (83)	48 (121)	ON	15 (57)	22 (72)
E 7 IR radiometer	14 (-5)	24 (76)	48 (118)		12 (54)	17 (63)
E 8 X-Ray calibration	12 (-10)	19 (66)	37 (99)		12 (54)	17 (63)
E 9 Radar altimeter	19 (-7)	19 (66)	25 (77)		15 (59)	15 (59)
K 1 Transponder	14 (-8)	ON 27 (81)	48 (118)	ON	12 (55)	14 (57)
K 2 Gyro	19 (-7)	25 (82)	45 (113)		6 (43)	13 (55)
R 3 Filter TYGO	13 (-8)	13 (66)	41 (106)		8 (46)	13 (55)
R 4 Filter harmonics	10 (-15)	13 (66)	41 (106)		8 (46)	13 (55)
R 5 Calculator	12 (-10)	14 (66)	42 (108)		9 (45)	13 (55)
R 6 SPT switch	10 (-15)	25 (82)	45 (113)		5 (46)	13 (55)
R 7 Transfer switch	12 (-10)	19 (66)	42 (108)	ON	9 (48)	13 (55)
R 8 Power amplifier	OFF ON 14 29 (55 84)	ON 36 (96)	ON 63 (141)	ON	10 (50)	14 (58)
R 9 Driver	OFF ON 13 27 (54 80)	ON 51 (92)	ON 11 (42)	ON	10 (50)	14 (58)
D 1 Dual remote MUX	10 (-15)	ON 11 (63)	ON 41 (106)	ON	9 (48)	12 (53)
D 2 TM processor	18 (-1)	ON 22 (71)	ON 56 (133)	ON	7 (44)	12 (53)
D 3 Data storage	14 24 (56 76)	32 (89)	59 (138)	ON	10 (50)	14 (58)
D 4 PCM encoder	11 (-12)	ON 24 (75)	ON 46 (115)	ON	8 (47)	13 (55)
C 1 Command demodulator	11 (-12)	ON 23 (72)	ON 44 (111)	ON	9 (48)	13 (55)
C 2 Central decoder	13 (-8)	ON 23 (73)	ON 48 (119)	ON	8 (46)	12 (54)
C 3 Remote decoder	8 (-18)	ON 19 (66)	ON 43 (110)	ON	3 (39)	8 (46)
C 4 Poro control	11 (-12)	25 (77)	48 (119)		8 (46)	11 (51)
A 1 Sun sensor	11 (-12)	22 (72)	46 (115)		8 (47)	13 (55)
A 2 Star sensor	13 (-8)	ON 23 (73)	ON 56 (133)	ON	3 (42)	13 (55)
A 3 Attitude data processor	11 (-12)	ON 24 (75)	ON 51 (130)	ON	9 (48)	13 (55)
A 4 De-spin control	11 (-12)	ON 25 (77)	ON 48 (119)	ON	8 (46)	13 (55)
A 5 Solenoid driver	13 (-8)	24 (75)	ON 49 (121)	ON	11 (51)	14 (58)
A 6 Nutation damper	13 (-8)	23 (73)	46 (115)		8 (47)	12 (54)
A 7 Magnetometer deslow	13 (-8)	23 (73)	46 (115)		8 (47)	12 (54)
B 1 Charge discharge unit	12 (-10)	ON 29 (84)	40 (104)	ON	3 (42)	12 (54)
B 2 Bus limiter	12 (-10)	ON 17 (63)	ON 48 (119)	ON	8 (47)	12 (54)
B 3 Power voltage switch	10 (-15)	ON 17 (63)	ON 42 (107)	ON	10 (50)	13 (55)
B 4 Current sensor	10 (-15)	18 (64)	42 (107)		7 (45)	11 (52)
B 5 Heater switch	10 (-15)	ON 19 (66)	ON 46 (121)	ON	11 (51)	14 (58)
B 6 Power off relay	11 (-12)	ON 17 (62)	ON 42 (108)	ON	8 (46)	11 (51)
B 7 Battery	10 (-15)	19 (66)	38 (101)	ON	10 (50)	12 (54)

ON = ON (no battery)  
 OFF = OFF (no battery)  
 12. All values are shown in orbit and driver

REPRODUCIBILITY OF THE ORIGINAL PAGE IS POOR.

because these temperatures exist only briefly, operating in the region of unit qualification margin ( $\pm 10^{\circ}\text{C}$ ) was considered acceptable. The batteries approach  $38^{\circ}\text{C}$  ( $100^{\circ}\text{F}$ ). However, they are nonoperating during this phase as is the entire experiment complement.

The transient experiment operation at periapsis results in maximum temperatures within limits. Satisfactory minimum battery temperatures are shown for both the 1.8 h and 3.2 h apoapsis eclipses.

#### Solar Array Temperatures

Solar array temperatures, including those during orbiter periapsis passes, will be similar to those shown for the Thor/Delta designs.

#### BAPTA Temperatures

The BAPTA design is similar to that proposed for the Thor/Delta and the thermal integration into the spacecraft will be similar, i. e., BAPTA enclosed in the forward insulation blanket and the high gain antenna mast insulated.

The BAPTA temperature extremes are dependent on the spacecraft boundary temperatures which are similar for the two designs.

#### Thruster Temperatures

The temperatures of thruster assemblies shown for the Thor/Delta design are generally applicable to the Atlas/Centaur configuration.

#### Orbit Insertion Motor

Temperatures and heater power required for the orbit insertion motor are shown in Table 5-16, indicating satisfactory margins.

#### Spacecraft Design Tradeoffs

##### Louver Arrangement

Because the louver actuator senses mounting surface temperature, proper control is achieved when the louvers are mounted to the equipment shelf. As discussed in subsection 5.3, interreflections limit the minimum solar absorptance achievable with a louvered radiator to about 0.22. This requires that the louvers be located so that direct solar illumination occurs only transiently at most. This is particularly important at Venus where solar intensity is nearly double the value at Earth.

As indicated in Table 5-13, probe bus attitude requirements result in extensive steady state solar illumination of the probe end of the spacecraft, while the aft end is illuminated for not more than 1 hr near earth during the first TCM. These attitude requirements, combined with the mounting arrangement of the small probes, makes spacecraft heat rejection from louvers mounted on the probe side of the equipment shelf very difficult. Therefore,

louvers are mounted on the aft side of the shelf and equipment on the forward side. This also satisfies experiment requirements for fields of view forward along the spin axis.

The orbiter spacecraft configuration could accommodate forward radiating louvers, since the HGA represents minimal blockage. Furthermore, the orbiter attitude requirements do not result in any long term solar illumination on the forward end of the spacecraft. Conversely, the orbit insertion attitude causes moderate illumination of the aft cavity for a minimum of 3-1/2 hr. To simplify mission operations, it is desirable to extend this time if possible. This suggests that the optimum orbiter thermal configuration is an arrangement placing equipment on the aft side of the shelf with the louvers radiating out the front end of the spacecraft, as illustrated schematically in Figure 5-56. However, experiments requiring a forward view must also be mounted on the forward side, complicating the forward thermal blanket design and creating some additional louver blockage.

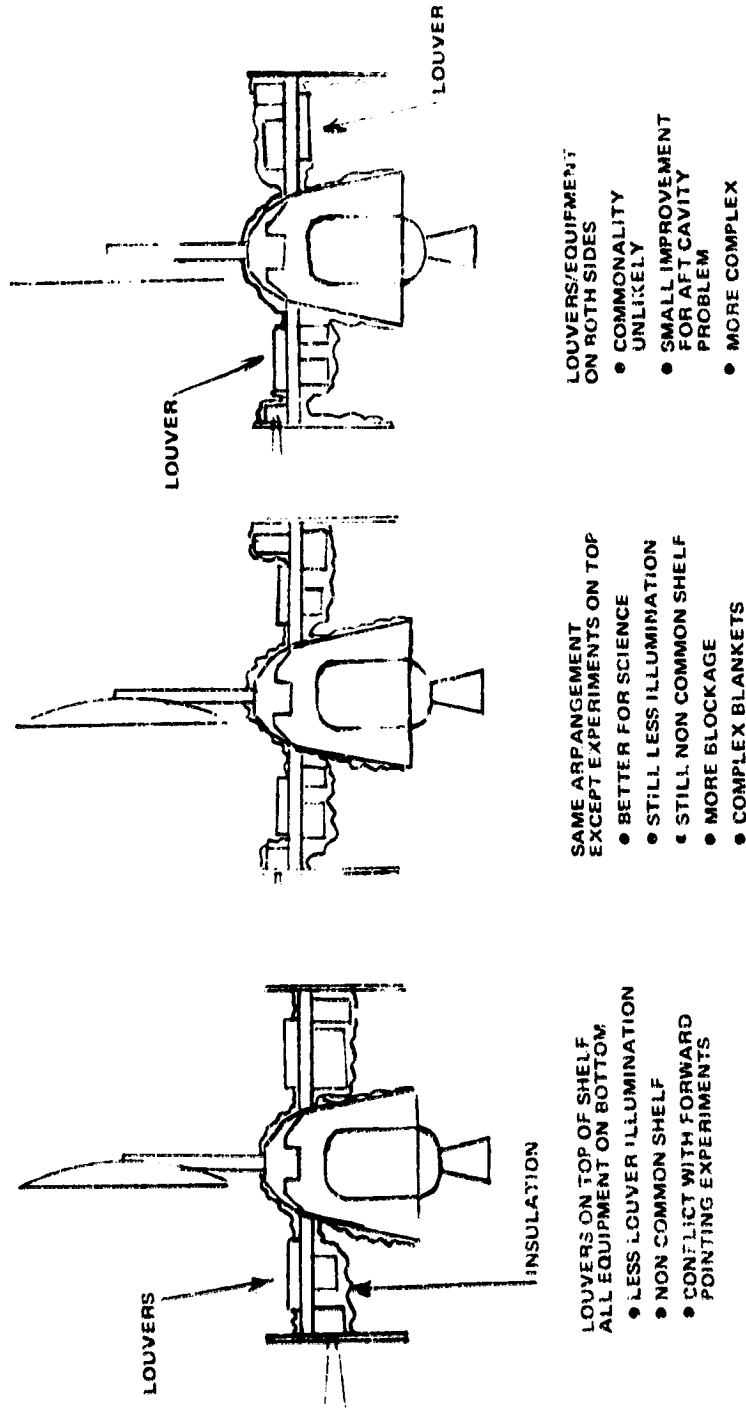
This arrangement, also shown in Figure 5-56, does provide the capability of maintaining the orbit insertion attitude indefinitely without overheating the equipment shelf. The constraint then becomes orbit insertion motor propellant overheating. However, this would not occur for several additional hours, because of the large motor heat capacity. Furthermore, this constraint could be removed if the motor nozzle finish was modified to a lower temperature level. This would, of course, increase heater power required near earth.

A disadvantage of this reversal of lower mounting is loss of shelf design commonality between probe bus and orbiter. As mentioned above, thermal blanket design is substantially more complex because of the need to cover experiments on the forward side of the shelf; access is also impaired. This approach was not selected because the cost of deviation from a common shelf design was deemed unjustified when considering that the selected baseline configuration can provide the 3-1/2 hr minimum time in the orbit insertion attitude.

Consideration of mounting all equipment and louvers on the forward side of the shelf was discarded because of excessive shelf weight required to conduct unit dissipations laterally to the louvered radiator surfaces. This could be reduced by using heat pipes embedded in the shelf at the cost of increased complexity and departure from flight proven design. Furthermore, shelf area is probably insufficient to achieve a workable arrangement.

#### Aft Cavity Design

The thermal finishes selected for the surfaces forming the spacecraft aft cavity strongly influence the solar loads received by the louvered radiators. Because time in the orbit insertion attitude is limited by shelf temperature rise caused by the solar heating of the aft cavity, alternative cavity designs have been studied. The first alternative considered was the removal of the solar panel insulation and painting of the inboard surface of the panel black to reduce solar reflections. This results in a substantial reduction in panel temperature (from 72°C to 32°C) and an estimated 50 percent reduction in



**LOUVERS/EQUIPMENT ON BOTH SIDES**

- COMMONALITY UNLIKELY
- SMALL IMPROVEMENT FOR AFT CAVITY PROBLEM
- MORE COMPLEX

**SAME ARRANGEMENT EXCEPT EXPERIMENTS ON TOP**

- BETTER FOR SCIENCE
- STILL LESS ILLUMINATION
- STILL NON COMMON SHELF
- MORE BLOCKAGE
- COMPLEX BLANKETS

**LOUVERS ON TOP OF SHELF ALL EQUIPMENT ON BOTTOM**

- LESS LOUVER ILLUMINATION
- NON COMMON SHELF
- CONFLICT WITH FORWARD POINTING EXPERIMENTS

FIGURE 5-56. ALTERNATE LOUVER ARRANGEMENTS

solar loads on the louvers. However, the radiation coupling of the louvers to the solar panel, even at this reduced temperature, increases the preorbit insertion shelf temperature level 5°C. The net result is that shelf temperatures after 3-1/2 hr at the orbit insertion attitude are nearly the same as predicted for the baseline design.

Another approach considered was the retention of the solar insulation and the decrease of solar reflectance of all insulated surfaces by some means. This would reduce louver solar heating by about 85 percent. However, the means for achieving a "black" outer surface on the insulation blankets is not obvious. Kapton has been painted black for some applications other than insulation blankets. However, the paints which have been used could not withstand the high temperatures expected from orbit insertion motor exhaust plume heating. High temperature paints tend to be brittle, making them undesirable for application to the flexible insulation blankets. A black fiberglass insulation cover could be used, but its weight would equal that of the insulation. Because of the uncertainties in the implementation of this approach, it was not considered further.

### Shelf Design

The use of heat pipes to provide lateral conduction paths along the equipment shelf was considered as an alternate to doublers. Early studies indicated that for shelf arrangements where units dissipating 5 W or more are located some distance from a louver, no reasonable doubler thickness could provide the necessary conduction path. A limited examination was made to determine a heat pipe arrangement which could provide this path. Such an arrangement is shown in Figure 5-57. The pipes were assumed to be aluminum using ammonia as working fluid. The major consideration is the allowable temperature difference ( $\Delta T$ ) from unit base to the louvered radiator. Excluding drop across the shelf thickness, this  $\Delta T$  was selected as 10°C (18°F), assuming the shelf temperature over the louvers was 20°C (68°F).

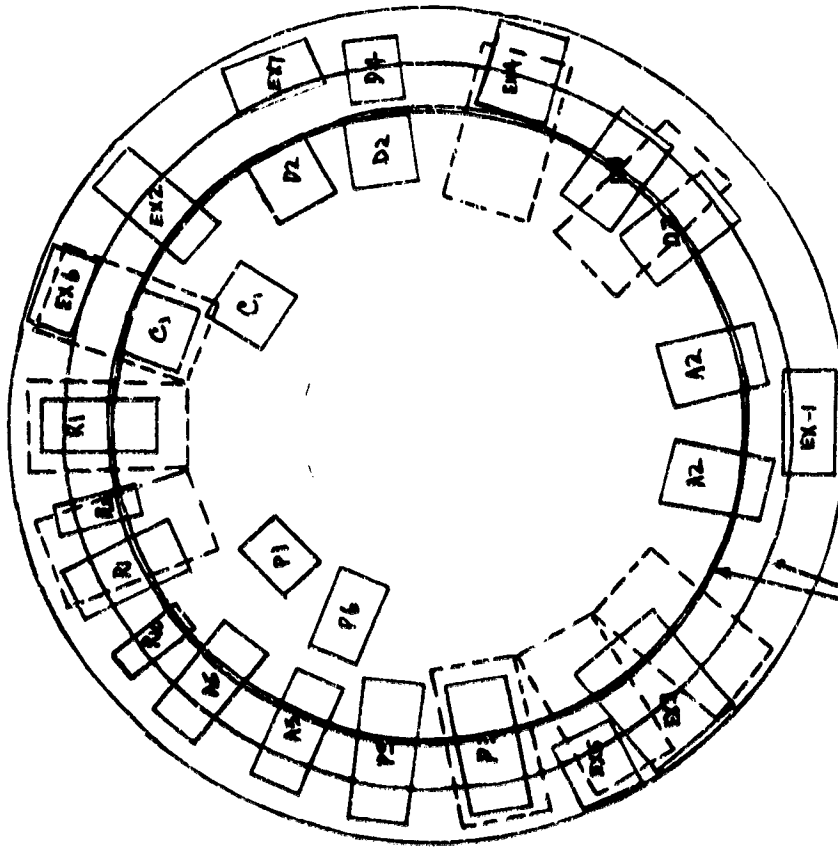
However, it was concluded that careful arrangement of equipment resulting in the location of units dissipating 5 W or more steady state directly over louvers could achieve the same objectives. The use of doublers in this case is more effective since their primary purpose is to limit local power density rather than transport energy laterally along the shelf. As indicated, the baseline doubler weight is comparable to that shown for the heat pipe arrangement. The doubler approach was selected because of its simplicity.

### Probe Design Performance

The large probe temperature histories throughout the preentry mission are shown in Figure 5-58. As indicated, the desired minimum pressure vessel interior temperatures are achieved at entry just prior to the final checkout. The minimum shelf temperatures occur at the beginning of the transit mission. As indicated, to maintain shelf temperatures above -23°C (-10°F), 15 W of probe bus heater power are required. The variation of power required versus minimum shelf temperature is shown in Figure 5-59.

30163 926(U)

SYMBOL	UNIT	POWER WATT
EX1	RADAR ALTIMETER	4
EX2	IR RADIOMETER	1
EX3	UV SPECTROMETER	3
EX4	NEUTRAL MASS SPEC.	1
EX5	ION MASS SPEC.	1
EX6	SOLAR WIND PROBE	4
EXT	MAGNETOMETER	3
R1	RECEIVER/EMITTER	7.4
R10	POWER AMPLIFIER	13
D2	PCM ENCODER	1.9
D3	FORMAT GENERATOR	3
D4	DATA STORAGE	1.2
C1	DEMODULATOR	2.6
A2	ALTITUDE DATA PROC.	3
A5	DESIGN CONTROL ELEC.	5
P1	DISCHARGE REGULATOR	-
P3	BATTERY	-
P6	CHARGE CONTROLLER	-



PIPE WEIGHT = 1.1 Kg (2.5)  
 DOUBLER WEIGHT = 0.9 (2.0)  
 TOTAL WEIGHT = 2.0 Kg (4.5)

TWO AMMONIA PIPES

FIGURE 5-57. EQUIPMENT SHELF WITH HEAT PIPES

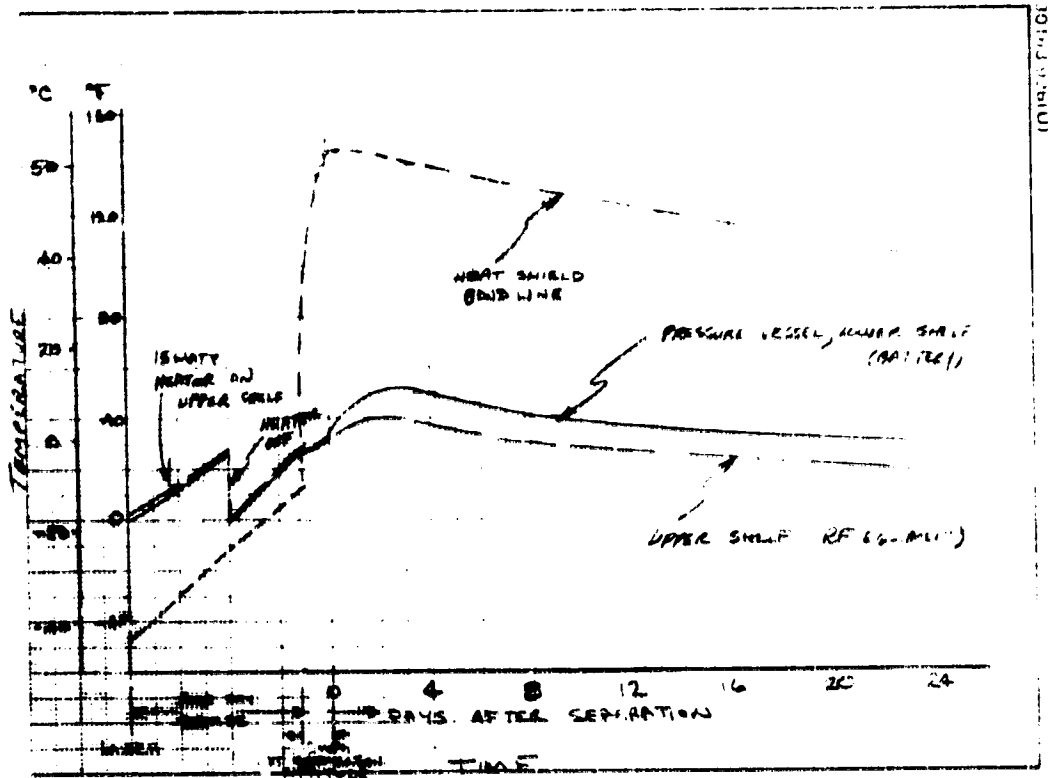


FIGURE 5-58. LARGE PROBE TEMPERATURE HISTORY

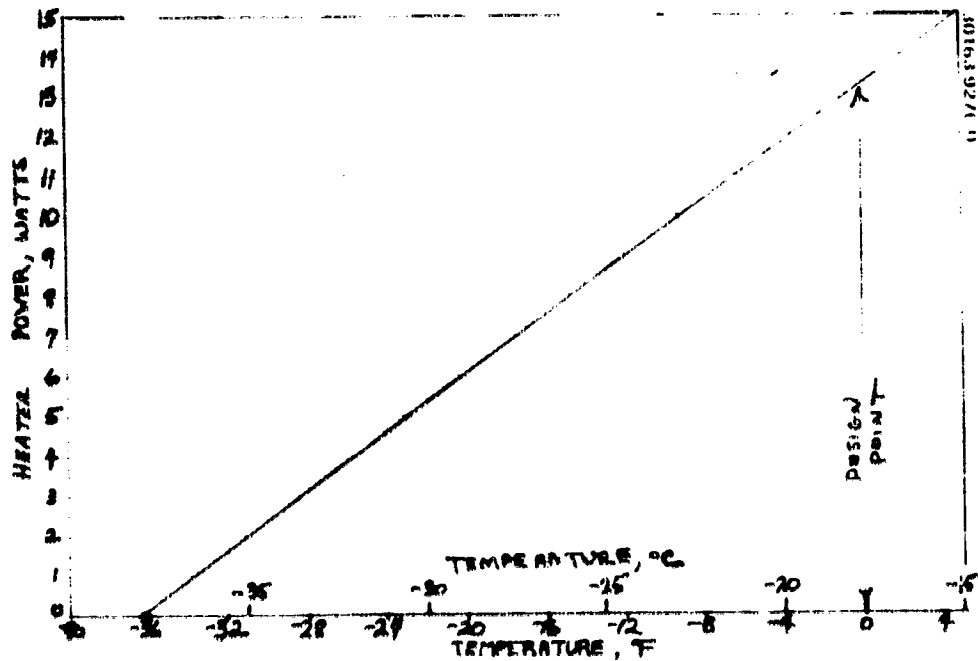


FIGURE 5-59. LARGE PROBE HEATER POWER REQUIREMENTS

REPRODUCIBILITY OF THE ORIGINAL PAGE IS POOR.

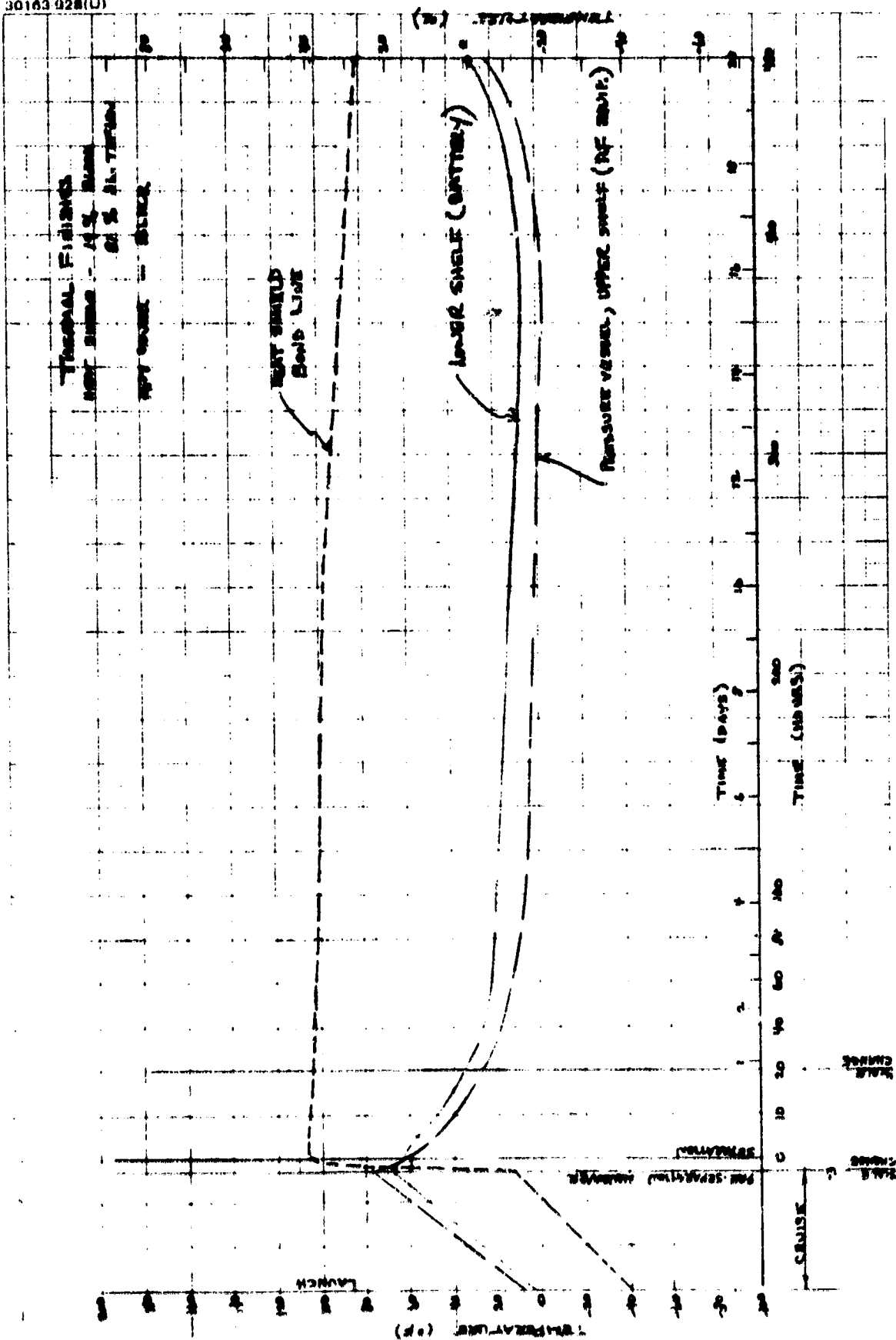


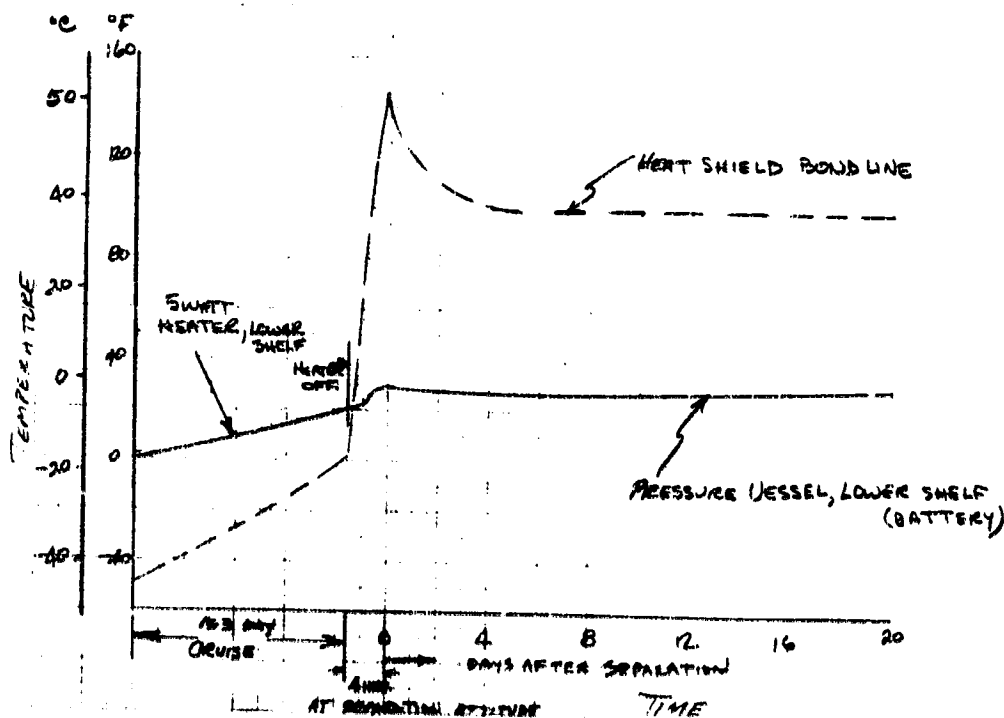
FIGURE 5-60. LARGE PROBE PRE-ENTRY TEMPERATURE HISTORIES

OF THE ORIGINAL PAGE IS POOR.



An alternate design approach was considered which could eliminate this power requirement. By increasing the solar absorptance of the aft cover (i. e., black paint) and making the appropriate change in the heat shield striping, the desired entry temperature can be achieved while increasing the probe temperatures at the beginning of the transit mission. This, of course, also entails the deletion of the insulated barrier enclosing the aft end of the large probe when mounted on the bus. The resulting temperature histories are shown in Figure 5-60, assuming no bus heater power. Unfortunately, this design results in shelf temperatures approaching  $-18^{\circ}\text{C}$  ( $0^{\circ}\text{F}$ ) during the period between separation and entry. It was decided that there was some risk in operating the battery at this temperature even at the low load required during this time. Therefore, the more conservative design approach was selected.

The small probe temperature histories are shown in Figure 5-61. Here again, heater power (5 W) is required to maintain minimum survival temperatures. A somewhat different postseparation temperature history is shown for the small probes in that temperatures increase slightly with time rather than decrease, as shown for the large probe. This is attributed to the smaller variation in sun angle which tends to be more than offset by the increasing solar intensity as the planet is approached. The entry temperature design point of  $-1^{\circ}\text{C}$  ( $30^{\circ}\text{F}$ ) is retained to favor the descent thermal control design. Although the battery minimum temperature margin just after separation is somewhat reduced ( $3^{\circ}\text{C}$  instead of  $5^{\circ}\text{C}$  as provided at entry), the low battery load at this time makes this acceptable.



30163-929(U)

FIGURE 5-61. SMALL PROBE PRE-ENTRY TEMPERATURES

## 6. HARNESS SUBSYSTEM

The harness subsystem for the probe bus and orbiter consists of the harness assemblies, comprised of wire bundles, connectors, and ancillary hardware, mounted on the forward side of the equipment shelf; it provides interconnections for all units of all other subsystems. An evaluation was made of the use of small gage wire (28 AWG) and microminiature connectors in lieu of the more conventional heavier gage wires (24 and 22 AWG) and sub-miniature connectors for weight and volumetric savings (Study Task EP 3). This study was limited to that portion of intercabling served by insulated conductors terminating in multipin connectors; rf circuits requiring waveguide and coax are described in the communication subsystem section.

The tradeoff consists of savings in weight at the expense of reduced reliability and increased cost. Data derived from an experimental harness fabricated with the lighter components was favorable with respect to durability. The estimated cost increment is significant but not excessive.

Weight calculations for conceptual cabling subsystems show savings in excess of 32 percent for both spacecraft.

Since the tradeoff is primarily cost versus weight, the 28 AWG/matrix connector combination was selected for the Thor/Delta baseline to achieve weight improvement. For the Atlas/Centaur baseline, the 24 AWG/matrix connector combination was selected to minimize cost.

### 6.1 REQUIREMENTS

The harness subsystem, including component, process, and material selection, must be designed and fabricated to provide the optimum combination of size, weight, electrical performance, reliability, and environmental protection. These characteristics must be achieved while considering minimum cost and maximum accessibility. This subsystem must also provide appropriate interfaces, both electrical and mechanical, with all other subsystems. Finally, the design must satisfy functional requirements of EMC control, magnetic field suppression, EED safety, and electrical bonding.

For an intercabling system definition, interconnect requirements must be known or assumed. These consist of equipments, equipment configuration, number and sizes of disconnects per equipment, signal list and signal destination per equipment, routing paths and wire lengths. Basic data

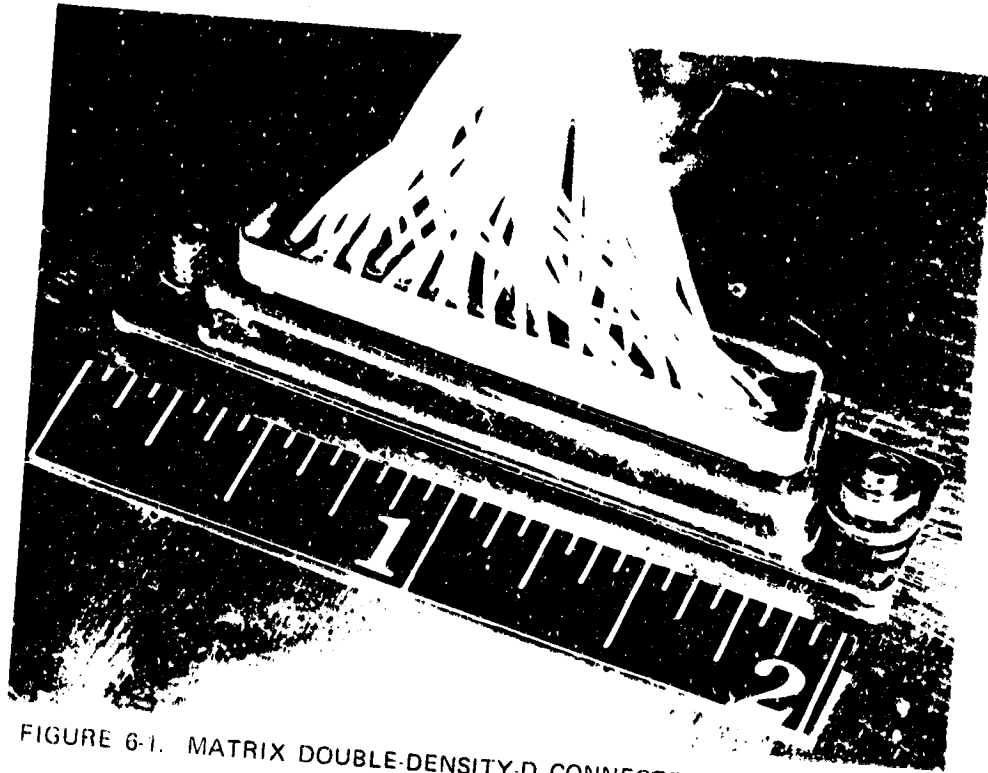


FIGURE 6-1. MATRIX DOUBLE-DENSITY-D CONNECTOR (PHOTO 30163-408)

REPRODUCIBILITY OF THE ORIGINAL PAGE IS POOR.

were derived from preliminary subsystem specifications and design data. Where preliminary requirements were not definitive enough, the assumption was made that the interconnection data would be similar to that of corresponding subsystems on prior space vehicle design.

## 6.2 TRADES

Most of the requirements noted in the preceding subsection are in conflict, such that optimization of any one parameter results in degradation of others. In considering tradeoffs, the one area which seems the most promising with respect to feasibility and improved mission capabilities is in the field of cabling size and weight. Wire and connector size can be reduced from accepted standard practice without compromising electrical performance. In very few circuits is copper size dictated by voltage drop or current carrying capacity considerations. Minimum wire gage and connector size are in most cases selected on the basis of the mechanical strength required to withstand handling.

Conventional Hughes practice on all prior space vehicles has been the use of 24 AWG wire, in high strength copper alloy conductor, as an acceptable minimum, in conjunction with a class of connectors denoted as subminiature. An evaluation was made of the use of small gage wire (28 AWG) and micro-miniature connectors in lieu of the more conventional heavier gage wires (24 and 22 AWG) and subminiature connectors for weight and volumetric savings (Study Task EP 3).

Feasibility of harness fabrication with adequate durability, using these materials for similar intercabling requirements, had previously been demonstrated in a Company-sponsored IR&D program (TIC No. 4114.20/65, dated 14 Mar. 1972: IR&D Summary Report Light Weight Harness Design).

In the connector terminology used herein, which is in agreement with vendor's data sheets, subminiature refers to connectors having number 20 contacts on 0.100 in. centers, and microminiature describes connectors having number 22 or smaller contacts spaced on centers substantially less than this, down to 0.050 in. Typical of the subminiature class is the Cannon DM rectangular; typical of the microminiature class is the Cannon MDM rectangular.

Conclusions from the Company-sponsored program were as follows. The microminiature connector having wire form solder contacts on 0.050 in. centers presented significant assembly problems as compared to another candidate having insertable crimp contacts on 0.075 in. centers. This latter connector, the Matrix Double-Density-D (Figure 6-1), was judged to be an acceptable compromise between the subminiature and microminiature classes of connectors. As its name implies, it provides double the contact density in the same shell size as the corresponding standard subminiature, but can be readily wired using standard assembly and handling techniques. For these reasons, in addition to the fact that the Matrix design has been

30163-409(U)

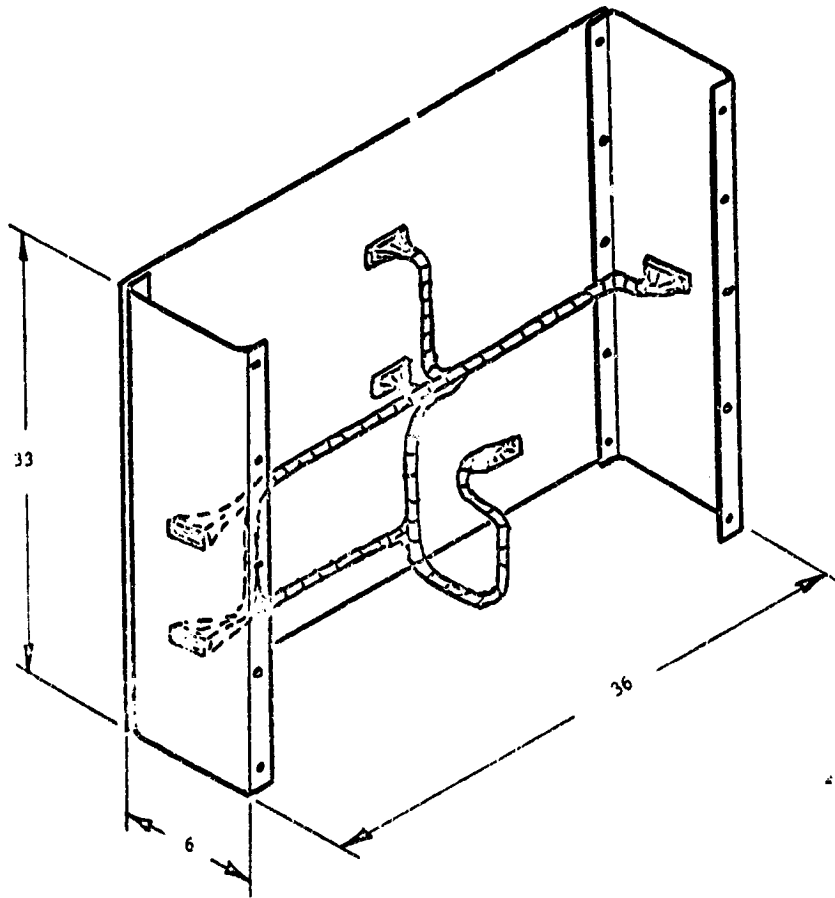


FIGURE 6-2. DEVELOPMENT HARNESS LAYOUT

REPRODUCIBILITY OF THE ORIGINAL PAGE IS POOR.

qualified and slated for use on the OSO program, this connector was selected as the standard for evaluation of wiring techniques in the probe bus and orbiter.

For those few leads where voltage drop considerations might negate 28 AWG, the connector can be provided with contacts as required to accept either 24 or 22 AWG wires.

In the Company-sponsored program, a multiconnector harness having wire runs averaging three feet was constructed employing 28 AWG wire (Figure 6-2). To simulate the most severe handling conditions, the harness was subjected to several rework cycles. The assembly technicians reported no difficulty in working with the small gage wire, either during initial fabrication or rework at the crimp type connectors as proposed for Pioneer Venus, and no failure modes were encountered.

The tradeoff incurs an increase in both design and manufacturing costs, resulting from the development of new processes, procurement of new tools, and greater difficulty in handling and terminating, particularly where shielded wires are involved, which were not evaluated in the experimental harness. Miniaturization implies tighter, hence more costly, tolerances; e. g., the tolerance on crimp indent depth for 24 AWG wire would be unacceptable on 28 AWG wire. The major cost increment is in the area of manufacturing labor costs, estimated to increase by 20 to 30 percent; for the probe bus, the cost delta is approximately \$11,000, and for the orbiter, the delta is approximately \$15,600.

The weight tradeoff, however, is significant; Table 6-1 shows, for 28 AWG, a savings of 2.22 kg (4.9 lb) for the probe bus harness and 3.21 kg (7.0 lb) for the orbiter harness for Thor/Delta.

### 6.3 THOR/DELTA BASELINE DESCRIPTION

Both the probe bus and orbiter harness subsystems are comprised of several major harness subassemblies, mounted on the shelf with breakouts as required to subsystem units. Because of higher equipment density on the orbiter, this cabling subsystem will be larger, more complex, and weigh more than that provided for the probe bus.

A conceptual cabling scheme was devised for the orbiter and probe bus configurations, and weights calculated with the tradeoff being 24 AWG versus 28 AWG. All versions employed the Matrix connector. Results are tabulated in Table 6-1, and the input data was derived using the following assumptions:

- Total number of connectors required reflects the configuration of units as defined at the time of the study
- Average weight per connector was derived from an assumed mix of connector sizes required

- Number of circuits (wires) required was based on schematic data as available at the time of the study
- Average length per wire was based on structure size, equipment placement, and available routing paths
- Wire weight/unit length (kg/km) assumes use of wire having insulation per MIL-W-81044, employing in addition a conventional mix of shielded, unshielded, and multiple constructions

Table 6-1 indicates the weight savings which can be achieved through the use of 28 AWG wire and dictates its selection for the Thor/Delta baseline where weight reduction is of paramount importance.

#### 6.4 ATLAS/CENTAUR BASELINE DESCRIPTION

In a manner similar to the Thor/Delta baseline, as described in the preceding paragraph, the harness subsystem will be arranged on the equipment shelf with appropriate breakout pigtails. Assumptions required to arrive at a weight estimate are as for Thor/Delta, with the following exceptions:

- Minimum wire size is 24 AWG.
- Average length per wire is scaled up by 20 percent to account for the larger diameter equipment shelf, as is wire support provisions.
- The Atlas/Centaur orbiter version includes the following equipment items over and above the Thor/Delta configuration:
  1. Two power amplifiers
  2. An X band transmitter (coaxial included in the communications subsystem)

Table 6-2 summarizes the weight delta for just these items. Table 6-3, based on the foregoing assumptions, summarizes the harness subsystem characteristics and weight estimates.

TABLE 6-1. SPACECRAFT HARNESS WEIGHT

	Wire Size, AWG	Number Of Connectors	Average Connector Mass (Weight), kg (lb)	Total Connector Mass (Weight), kg (lb)	Number Of Circuits (Wires)	Average Wire Length, m (ft)	Total Wire Length, km (ft)	Wire Mass, kg/km (lb/1000 ft)	Total Wire Mass, kg (lb)	Miscellaneous Hardware Mass, kg (lb)	Total Harness Mass, kg (lb)
Probe bus harness	24	126	9.07 (0.02)	1.14 (2.52)	1215	1.22 (4.0)	1.48 (4860)	3.7 (2.5)	5.45 (12.10)	0.23 (0.50)	4.95 (10.95)
Baseline	28	126	9.07 (0.02)	1.14 (2.52)	1215	1.22 (4.0)	1.48 (4860)	2.2 (1.5)	3.26 (7.2)	0.23 (0.50)	4.63 (10.20)
Orbiter harness	24	154	9.07 (0.02)	1.4 (3.08)	1765	1.22 (4.0)	2.15 (7060)	3.7 (2.5)	7.96 (17.60)	0.45 (1.0)	9.81 (21.70)
Baseline	28	154	9.07 (0.02)	1.4 (3.08)	1765	1.22 (4.0)	2.15 (7060)	2.2 (1.5)	4.75 (10.60)	0.45 (1.0)	6.6 (14.70)

TABLE 6-2. HARNESS REQUIREMENTS FOR ADDITIONAL ORBITER UNITS

Item	No. of Connectors	Total Connectors		Average Wire Length, m (ft)	Total Wire Length, m (ft)	Unit Wire Mass (Weight), kg/km (lb/1000 ft)	Total Wire Mass (Weight), kg (lb)	Miscellaneous Support Hardware, kg (lb)	Total, kg (lb)
		Mass (Weight), kg (lb)	Wires						
Power Amplifiers 2 Required	4	0.036 (0.08)	4	1.5 (5)	6.1 (20)	3.7 (2.5)	0.023 (0.05)	0.005 (0.01)	0.064 (0.14)
X band Transmitter	2	0.018 (0.04)	8	1.5 (5)	12.2 (40)	3.7 (2.5)	0.036 (0.08)	0.005 (0.01)	0.060 (0.13)

TABLE 6-3. SPACECRAFT HARNESS CHARACTERISTICS AND MASS

Harness	Wire Size, AWG	No. of Connectors	Average Connector Mass (Weight), kg (lb)		No. of Circuits (Wires)	Average Wire Length, m (ft)	Total Wire Length, km (ft)	Wire Mass (Weight), kg/km (lb/1000 ft)	Total Wire Mass (Weight), kg (lb)	Miscellaneous Hardware Mass (Weight), kg (lb)	Total Harness Mass (Weight), kg (lb)
			Mass (Weight), kg (lb)	Wires							
Atlas Contour Probe Bus Harness	24	126	0.009 (0.02)	1.14 (2.52)	1215	1.52 (5.0)	1.85 (6075)	3.7 (2.5)	6.89 (15.2)	0.27 (0.6)	8.75 (19.3)
Atlas Contour Orbiter Harness	24	162	0.009 (0.02)	1.47 (3.24)	1783	1.52 (5.0)	2.71 (8900)	3.7 (2.5)	10.07 (22.2)	0.54 (1.2)	12.02 (26.5)



APPENDIX A  
THOR/DELTA SPACECRAFT STRESS ANALYSIS

## THRUST TUBE

THE THRUST TUBE IS REQUIRED TO TRANSMIT THE SPACE CRAFT LOADS TO THE LAUNCH VEHICLE ADAPTER

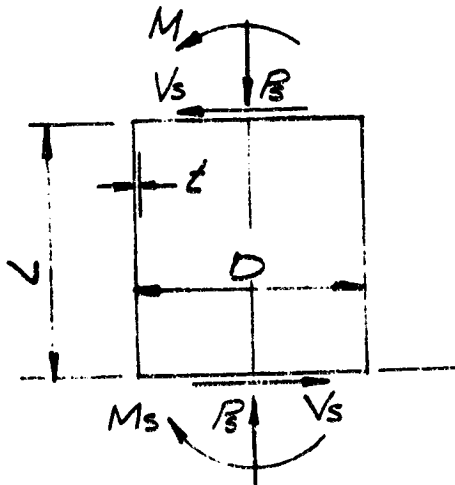
### 1- DESIGN LOADS \*

$$\left. \begin{aligned} V_s &= 22300 \text{ N (5012 LB)} \\ P_s &= 16850 \text{ N (3786 LB)} \\ M_s &= 2530000 \text{ CM}\cdot\text{N (223800 IN}\cdot\text{LB)} \end{aligned} \right\} \begin{array}{l} \text{REF 1, APP I} \\ \text{COND 3, PG 51} \end{array}$$

### 2- CYLINDER INSTABILITY (AL 2024-T3)

$$\left. \begin{aligned} C_1 &= .202 \\ C_2 &= .249 \\ C_3 &= 259 \end{aligned} \right\} \begin{array}{l} \text{BUCKLING COEFF.} \\ \text{FROM TEST DATA} \end{array} \quad \begin{array}{l} t = .044 \text{ IN.} \\ \mu = .33 \text{ (POISSON'S RATIO)} \\ E_c = 10.7 \times 10^6 \text{ LB/IN}^2 \end{array}$$

$$M = M_s - V_s L = 93688 \text{ IN}\cdot\text{LB.}$$



### (a) ALLOWABLE BUCKLING LOADS

$$M_{CR} = C_2 \pi E_c \left(\frac{D}{2}\right) t^2 = 2145000 \text{ CM}\cdot\text{N} \quad (189649 \text{ IN}\cdot\text{LB})$$

$$V_{CR} = \frac{C_3 \pi E_c t^3 \left(\frac{D}{2}\right)}{12 L^2 (1 - \mu^2)} = 52300 \text{ N (11775 LB)}$$

$$P_{CR} = C_1 (2.0) \pi E_c t^2 = 118800 \text{ N (25698 LB)}$$

$$L = 26.0 \text{ IN.}$$

$$D = 24.0 \text{ IN.}$$

### (b) MARGIN OF SAFETY

$$MS = \frac{2}{R_a + R_b + \left[ (R_a + R_b)^2 + 4(R_s)^2 \right]^{1/2}} - 1 \quad (\text{REF. 2})$$

$$R_a = \frac{P_s}{P_{CR}} = .147, \quad R_b = \frac{M}{M_{CR}} = .494, \quad R_s = \frac{V_s}{V_{CR}} = .426$$

$$MS = .172$$

\* N = NEWTONS  
CM = CENTIMETERS

## LARGE PROBE SUPPORT

THE LARGE PROBE SUPPORT TRANSMITS ALL FORCES PRODUCED IN THE LARGE PROBE AND THE LATERAL FORCES PRODUCED IN THE SMALL PROBES TO THE THRUST TUBE.

### 1- DESIGN LOADS

WEIGHT OF SMALL PROBES ( $W_{SP}$ ) = 102 KG. (224.7 LB)  
 SMALL PROBE LAT. LOAD FACTOR ( $M_{SP}$ ) = 7.52 (REF 1, APP. 1)  
 WEIGHT OF LARGE PROBE ( $W_{LP}$ ) = 114.6 KG. (252.6 LB)  
 LARGE PROBE LAT. LOAD FACTOR ( $M_{LP}$ ) = 7.899 (REF. 1, APP. 1)

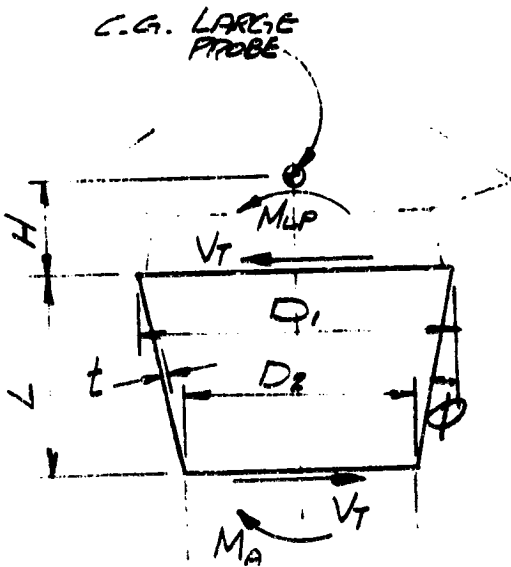
$$V_T = V_{LP} + V_{SP}$$

$$V_{LP} = (W_{LP})(M_{LP}) = 8880 \text{ N (1990 LB)}$$

$$V_{SP} = (W_{SP})(M_{SP}) = 7520 \text{ N (1690 LB)}$$

$$V_T = 16400 \text{ N (3680 LB)}$$

$$M_{LP} = (V_{LP})(H) = 220800 \text{ CM}\cdot\text{N} \\ (19900 \text{ IN}\cdot\text{LB})$$



### 2- CONE INSTABILITY (AL2024-T3)

$$t = .028 \text{ IN.}, E_c = 10.7 \times 10^6 \text{ LB/IN}^2$$

$$C_2 = .249 \quad \left. \begin{array}{l} \text{BUCKLING COEFF.} \\ \text{FROM TEST DATA} \end{array} \right\}$$

$$C_3 = 238$$

$$\mu = .33$$

$$L = 21.2 \text{ IN.}$$

$$H = 10.0 \text{ IN.}$$

$$D_1 = 32.25$$

$$D_2 = 24.0$$

$$D = 28.125$$

$$\phi = 11.01^\circ$$

### (a) ALLOWABLE BUCKLING LOADS

$$M_{CR} = C_2 \pi E_c \left(\frac{D_1}{2}\right) t^2 (\cos \phi)^2$$

$$M_{CR} = 1111000 \text{ CM}\cdot\text{N (98134 IN}\cdot\text{LB.)}$$

$$V_{CR} = \frac{C_3 \pi E_c t^3 \left(\frac{D}{2}\right)}{(12) L^2 (1 - \mu^2)} = 21400 \text{ N (4807 LB.)}$$

### (b) MARGIN OF SAFETY

$$MS = \frac{2}{R_b + [(R_b)^2 + 4(R_s)^2]^{1/2}} - 1 \quad (\text{REF 2})$$

$$R_b = \frac{M_{LP}}{M_{CR}} = .203, \quad R_s = \frac{V_T}{V_{CR}} = .766$$

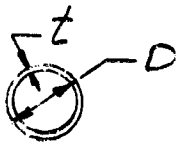
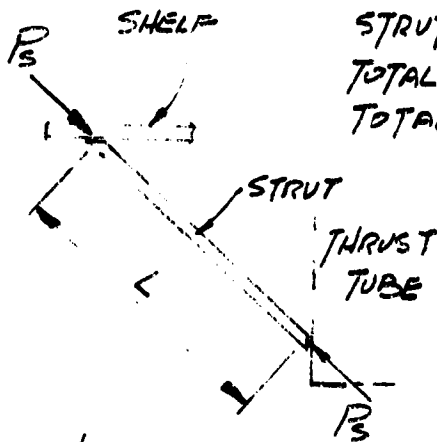
$$MS = .150$$

## SHELF SUPPORTS

THE SHELF SUPPORT STRUTS TRANSMIT A PORTION OF THE EQUIPMENT LOADS TO THE THRUST TUBE. THEY ALSO PROVIDE THE REQUIRED ADDITIONAL STIFFNESS TO THE EQUIPMENT SHELF IN ORDER TO SATISFY THE DYNAMIC ENVIRONMENT.

### 1- DESIGN LOAD

$$F_s = F_{ST} \left( \frac{W_P}{W_S} \right) = 6640 \text{ N (1492 LB)}$$



SECT

$$\left. \begin{aligned} L &= 38.3 \text{ IN} \\ D &= 1.313 \text{ IN} \\ t &= .025 \text{ IN} \\ A_s &= .103 \text{ IN}^2 \end{aligned} \right\} \text{ALUM.}$$

STRUT LOAD ( $F_{ST}$ ) = 4760 N (1068 LB) (REF. 1, APP. 1, FIG. 2)

TOTAL SHELF LOAD ( $W_P$ ) = 2300 N (517 LB)

TOTAL SHELF LOAD ( $W_S$ ) = 1645 N (369.7 LB) (REF. 1)

### 2- COMPRESSION IN STRUT (AL 2024-T3)

#### (a) COMPRESSIVE STRESS

$$f_c = \frac{F_s}{A_s} = 9570 \text{ N/CM}^2 \text{ (14470 LB/IN}^2\text{)}$$

#### (b) COMPRESSION YIELD STRESS

$$F_{CY} = 28900 \text{ N/CM}^2 \text{ (42000 LB/IN}^2\text{)}$$

#### (c) GENERAL INSTABILITY

USING THE EULER EQN.

$$F_{CR} = \frac{\pi^2 E_c C}{(L/\rho)^2} \quad (\text{REF. 3})$$

$C = 1.0$  (PINNED ENDS)

$E_c = 10.7 \times 10^6 \text{ LB/IN}^2$

$\rho = .452 \text{ IN.}$  (RADIUS OF GYRATION)

$$F_{CR} = 10120 \text{ N/CM}^2 \text{ (14700 LB/IN}^2\text{)}$$

#### (d) MARGIN OF SAFETY

$$MS = \frac{F_{CR}}{f_c} - 1 = \underline{\underline{.015}}$$

REPRODUCIBILITY OF THE ORIGINAL PAGE IS POOR.

## SMALL PROBE SUPPORTS

THE VERTICAL STRUTS ARE REQUIRED TO TRANSMIT THE SMALL PROBE FORCES IN THE LONGITUDINAL DIRECTION TO THE EQUIPMENT SUPPORT SHELF. THE LATERAL SUPPORT BEAM TRANSMITS THE SMALL PROBE LATERAL FORCES TO THE LARGE PROBE SUPPORT.

### 1- DESIGN LOADS

WEIGHT OF SMALL PROBE ( $W_s$ ) = 34 KG. (74.9 LB.)  
SMALL PROBE VERT. LOAD FACTOR ( $\eta_z$ ) = 23.7 (REF. 1, APP. 1, § 338)

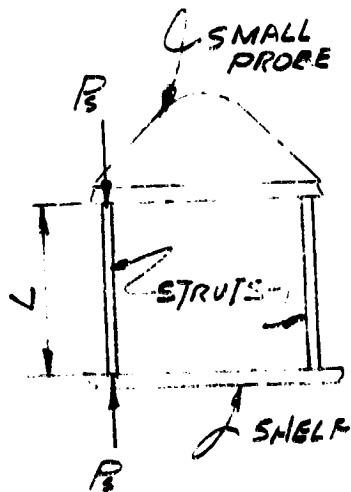
$$F_s = \left(\frac{1}{2}\right)(W_s)(\eta_z) = 3950 \text{ N (888 LB.)}$$

$$V_s = \left(\frac{1}{3}\right) V_{SP} \quad V_{SP} = 7520 \text{ N (REF. LARGE PROBE SUPPORT)}$$

$$V_s = 2507 \text{ N (563 LB.)}$$

### 2- VERTICAL STRUTS (AL 2024-73)

#### 1- COMPRESSION IN STRUT



$$L = 17.50 \text{ IN.}$$

$$D = .750 \text{ IN.}$$

$$t = .020 \text{ IN.}$$



#### (a) COMPRESSIVE STRESS

$$f_c = \frac{F_s}{A_s} \quad A_s = .0458 \text{ IN}^2$$

$$f_c = 13300 \text{ N/CM}^2 \text{ (19350 LB/IN}^2\text{)}$$

#### (b) COMPRESSION YIELD STRESS

$$F_{CY} = 28900 \text{ N/CM}^2 \text{ (42000 LB/IN}^2\text{)}$$

#### (c) GENERAL INSTABILITY

USING THE EULER CRN.

$$F_{CR} = \frac{\pi^2 E_c C}{(L/\rho)^2} \quad (\text{REF. 3})$$

$$E_c = 10.7 \times 10^6 \text{ LB/IN}^2$$

$$C = 1.0 \text{ (PINNED ENDS)}$$

$$\rho = .258 \text{ IN. (RADIUS OF GYRATION)}$$

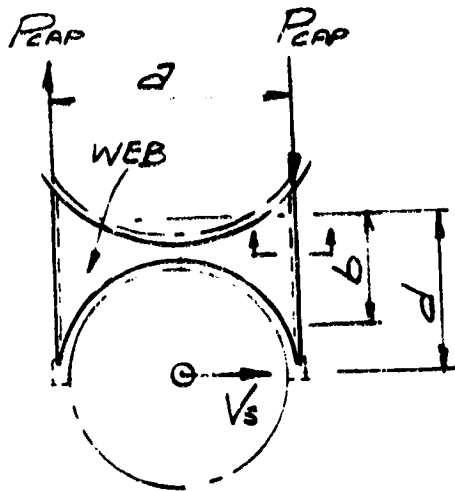
$$F_{CR} = 15750 \text{ N/CM}^2 \text{ (22900 LB/IN}^2\text{)}$$

#### (d) MARGIN OF SAFETY

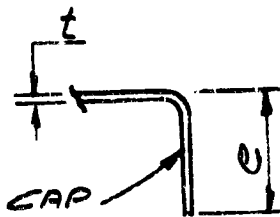
$$MS = \frac{F_{CR}}{f_c} - 1 = .185$$

SMALL PROBE SUPPORTS (CONTINUED)

3- LATERAL SUPPORT BEAM (AL 2024-T3)



$a = 24.0 \text{ IN.}$   
 $b = 12.0 \text{ IN.}$   
 $t = .039 \text{ IN.}$   
 $d = 17.0 \text{ IN.}$



SECTION

$e = .650 \text{ IN.}$   
 $K_e = .416 \text{ (ONE EDGE FREE)}$

1- SHEAR IN WEB

(a) SHEAR STRESS

$$f_s = \frac{V_s}{t a} \quad t a = .935 \text{ IN}^2$$

$$f_s = 416 \text{ N/CM}^2 \text{ (603 LB/IN}^2\text{)}$$

(b) ALLOWABLE BUCKLING STRESS

$$F_{scr} = \frac{K_e E_c}{1 - \mu^2} \left( \frac{t}{b} \right)^2 \text{ (REF 3)}$$

$$K_e = 5.43 \text{ (ALL EDGES SIMPLY SUP.)}$$

$$\mu = .33$$

$$F_{scr} = 442 \text{ N/CM}^2 \text{ (643 LB/IN}^2\text{)}$$

(c) MARGIN OF SAFETY

$$MS = \frac{F_{scr}}{f_s} - 1 = \underline{\underline{.07}}$$

2- COMPRESSION IN CAP

(a) FORCE IN CAP

$$P_{cap} = \frac{V_s (d)}{a} = 1772 \text{ N (399 LB)}$$

(b) COMPRESSIVE STRESS

$$f_c = \frac{P_{cap}}{e t} = 10820 \text{ N/CM}^2 \text{ (15710 LB/IN}^2\text{)}$$

(c) LOCAL BUCKLING ALLOWABLE

$$F_{cr} = \frac{K_e E_c}{1 - \mu^2} \left( \frac{t}{e} \right)^2 \text{ (REF 3)}$$

$$F_{cr} = 12250 \text{ N/CM}^2 \text{ (17800 LB/IN}^2\text{)}$$

(d) MARGIN OF SAFETY

$$MS = \frac{F_{cr}}{f_c} - 1 = \underline{\underline{.13}}$$

# BAPTA SUPPORT

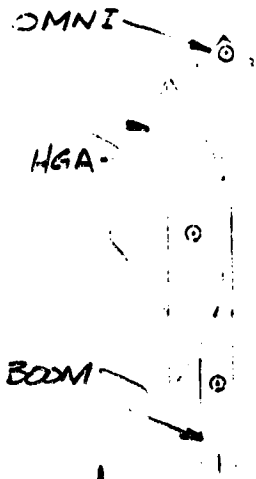
THE BAPTA SUPPORT IS REQUIRED TO TRANSMIT THE FORCES FROM THE MAIN BEARING AND POWER TRAIN ASSEMBLIES TO THE THRUST TUBE.

## 1- DESIGN LOADS

ITEM	WEIGHT (LB.)	LAT. L.F. (IN.)	V (LB)	h (IN.)	MOM. (IN. LB)
HGA	3.90	55.2	215	37.5	8080
OMNI	.50	107.6	53.8	56.5	3040
BOOM	2.15	39.5	84.7	36.5	3088
MBA	2.75	3.47	9.5	1.50	14

REF. 1  
APP 2.  
SINE VIB. Y

$$\Sigma V = 363 \text{ (LB)} \quad \Sigma M = 14222 \text{ (IN. LB)}$$



## 2- CONE INSTABILITY (AL 2024-T3)

$$t = .023 \text{ IN.}, \quad E_c = 10.7 \times 10^6 \text{ LB./IN.}^2$$

$$C_2 = .202 \quad \left. \begin{array}{l} \text{BUCKLING COEFF.} \\ \text{FROM TEST DATA} \end{array} \right\}$$

$$C_3 = 388$$

$$\mu = .33$$

### (a) ALLOWABLE BUCKLING LOADS

$$M_{CR} = C_2 E_c \pi \left(\frac{D_1}{2}\right)^2 t^2 \cos^2 \phi$$

$$M_{CR} = 192200 \text{ CM. N (16991 IN. LB)}$$

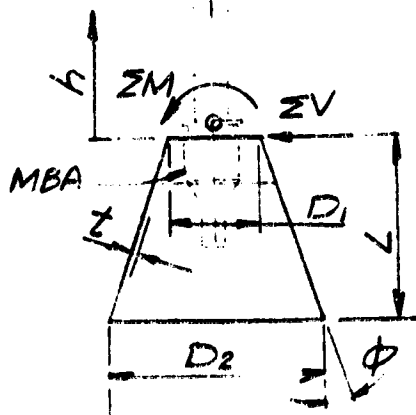
$$V_{CR} = \frac{C_3 \pi E_c \left(\frac{D}{2}\right)^2}{(12) L^2 (1 - \mu^2)} = 12680 \text{ N (2847 LB)}$$

### (b) MARGIN OF SAFETY

$$MS = \frac{2}{R_b + \left[ (R_b)^2 + 4(R_s)^2 \right]^{1/2}} - 1 \quad (\text{REF 2})$$

$$R_b = \frac{\Sigma M}{M_{CR}} = .838, \quad R_s = \frac{\Sigma V}{V_{CR}} = .127$$

$$MS = \underline{\underline{.165}}$$



$$\phi = 19.1^\circ$$

$$D_1 = 22.50 \text{ IN.}$$

$$D_2 = 9.0 \text{ IN.}$$

$$L = 19.50 \text{ IN.}$$

$$D = \frac{1}{2} (D_1 + D_2)$$

REFERENCES

- HUGHES AIRCRAFT CO., HS 507-0022-88,  
1) DYNAMIC LOADS ANALYSIS  
TASK NO. V14, 23 FEB 1973  
APPENDIX 1, 16 FEB 1973  
APPENDIX 2, 16 FEB 1973
- 2) METALLIC MATERIALS AND ELEMENTS FOR  
AEROSPACE VEHICLE STRUCTURES (MIL-HDBK-5B)  
DEPARTMENT OF DEFENSE, REVISED, 1 JULY 1972
- 3) FORMULAS FOR STRESS AND STRAIN,  
RAYMOND J. ROARK, FOURTH EDITION,  
McGraw Hill Book Co., N.Y.



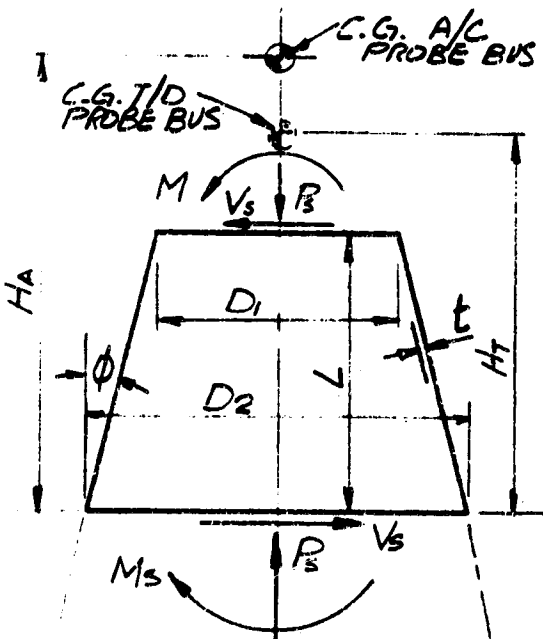
APPENDIX B  
ATLAS/CENTAUR SPACECRAFT STRESS ANALYSIS

# THRUST TUBE

THE THRUST TUBE IS REQUIRED TO TRANSMIT THE SPACECRAFT LOADS TO THE LAUNCH VEHICLE ATTACH FITTING

## 1- DESIGN LOADS & GEOMETRY

$H_A = 53.0 \text{ IN.}$        $H_T = 39.53 \text{ IN. (REF. A, FIG 12)}$   
 WEIGHT OF A/C PROBE BUS ( $W_A$ ) = 1792.6 LB  
 WEIGHT OF T/D PROBE BUS ( $W_T$ ) = 845.1 LB (REF A, FIG 12)  
 $M_{ST} = 223800 \text{ IN. LB.}$  } REF. A, APP I  
 $V_{ST} = 5012 \text{ LB.}$  } COND 3, FIG 51  
 $P_{ST} = 3786 \text{ LB.}$



$$M_s = M_{ST} \left( \frac{H_A}{H_T} \right) \left( \frac{W_A}{W_T} \right) (1.30) = 935000 \text{ CM}\cdot\text{N} \quad (825000 \text{ IN}\cdot\text{LB})$$

$$V_s = V_{ST} \left( \frac{W_A}{W_T} \right) (1.30) = 61400 \text{ N} \quad (13800 \text{ LB})$$

$$P_s = P_{ST} \left( \frac{W_A}{W_T} \right) (1.30) = 46600 \text{ N} \quad (10450 \text{ LB})$$

$$M = M_s - V_s L = 383,000 \text{ IN}\cdot\text{LB}$$

## 2- CONE INSTABILITY (AL 2024-T3)

$C_1 = .202$   
 $C_2 = .303$   
 $C_3 = 186$  } BUCKLING COEFF.  
 FROM TEST DATA

$$E_c = 10.9 \times 10^6 \text{ LB/IN}^2$$

$$t = .068 \text{ IN.}$$

$$\mu = .33 \text{ (POISSON'S RATIO)}$$

$$D_1 = 29.0 \text{ IN, } D_2 = 43.0 \text{ IN}$$

$$D = \frac{1}{2} (D_1 + D_2)$$

$$\phi = 12.3^\circ, \quad L = 32.0 \text{ IN}$$

### (a) ALLOWABLE BUCKLING LOADS

$$M_{CR} = C_2 \pi E_c \left( \frac{D_1}{2} \right) t (\cos \phi)^2 = 7,609,000 \text{ CM}\cdot\text{N} \quad (671,700 \text{ IN}\cdot\text{LB})$$

$$P_{CR} = C_1 \pi (2.0) E_c t (\cos \phi)^2 = 275,000 \text{ N} \quad (61,800 \text{ LB})$$

$$V_{CR} = \frac{C_3 \pi E_c t^3 D}{24 L^2 (1 - \mu^2)} = 121,000 \text{ N} \quad (27,200 \text{ LB})$$

### (b) MARGIN OF SAFETY

$$MS = \frac{2}{R_a + R_b + [(R_a + R_b)^2 + 4(R_s)^2]^{1/2}} - 1 \quad (\text{REF B})$$

$$R_a = \frac{P_s}{P_{CR}} = .169, \quad R_b = \frac{M}{M_{CR}} = .57, \quad R_s = \frac{V_s}{V_{CR}} = .51$$

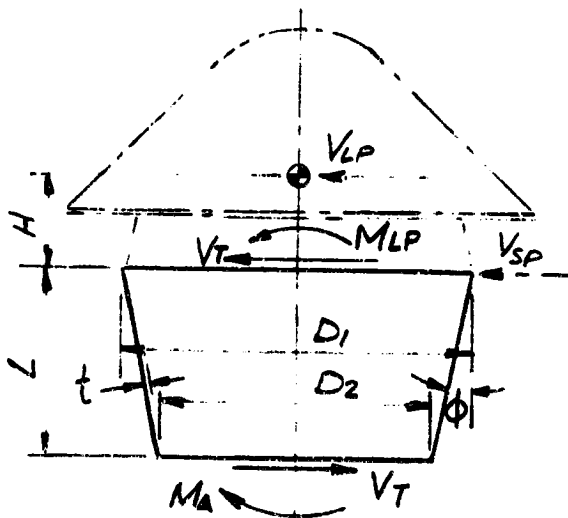
$$MS = .003$$

## LARGE PROBE ATTACH STRUCTURE

THE LARGE PROBE ATTACH STRUCTURE TRANSMITS ALL FORCES PRODUCED IN THE LARGE PROBE AND THE LATERAL FORCES PRODUCED IN THE SMALL PROBES TO THE THRUST TUBE.

### 1- DESIGN LOADS

WEIGHT OF SMALL PROBES ( $W_{SP}$ ) = (430.2 LB)  
 SMALL PROBE LAT. LOAD FACTOR ( $M_{SP}$ ) = 7.52 (REF. A, APP. 1)  
 WEIGHT OF LARGE PROBE ( $W_{LP}$ ) = (534.6 LB)  
 LARGE PROBE LAT. LOAD FACTOR ( $M_{LP}$ ) = 7.399 (REF. A, APP. 1)



$L = 22.0$  IN.  
 $H = 10.0$  IN.  
 $D_1 = 39.50$  IN.  
 $D_2 = 31.0$  IN.  
 $D = \frac{1}{2}(D_1 + D_2)$   
 $\phi = 10.93^\circ$

$V_T = V_{LP} + V_{SP}$   
 $V_{LP} = (W_{LP})(M_{LP})(1.30) = 24450$  N (5490 LB)  
 $V_{SP} = (W_{SP})(M_{SP})(1.30) = 18850$  N (4210 LB)  
 $V_T = 43300$  N (9700 LB)  
 $M_{LP} = (V_{LP})(H) = 622500$  CM·N (54900 IN·LB)

### 2- CONE INSTABILITY (AL 2024-T3)

$C_2 = .249$  } BUCKLING COEFF.  
 $C_3 = 155$  } FROM TEST DATA  
 $t = .040$  IN.       $\mu = .33$   
 $E_c = 10.7 \times 10^6$  LB/IN<sup>2</sup>

### (a) ALLOWABLE BUCKLING LOADS

$M_{CR} = C_2 \pi E_c \left(\frac{D_1}{2}\right) t^2 (\cos \phi)^2$   
 $M_{CR} = 2875000$  CM·N (254429 IN·LB)  
 $V_{CR} = \frac{C_3 \pi E_c t^3 D}{(24) L^2 (1 - \mu^2)} = 50100$  N (11249 LB)

### (b) MARGIN OF SAFETY

$MS = \frac{2}{R_b + [(R_b)^2 + (R_s)^2]^{\frac{1}{2}}} - 1$  (REF B)

$R_b = \frac{M_{LP}}{M_{CR}} = .206$        $R_s = \frac{V_T}{V_{CR}} = .862$

$MS = .023$

## SHELF SUPPORTS

THE SHELF SUPPORT STRUTS TRANSMIT A PORTION OF THE EQUIPMENT LOADS TO THE THRUST TUBE. THEY ALSO PROVIDE THE REQUIRED ADDITIONAL STIFFNESS TO THE EQUIPMENT SHELF IN ORDER TO SATISFY THE DYNAMIC ENVIRONMENT.

### 1 - DESIGN LOAD

$$P_S = P_{ST} \left( \frac{W_P}{W_S} \right) \left( \frac{N_S}{N_P} \right) (1.30)$$

$$\text{STRUT LOAD } (P_{ST}) = 4760 \text{ N } (1068 \text{ LB.}) \text{ (REF. A, APP1, P. 90)}$$

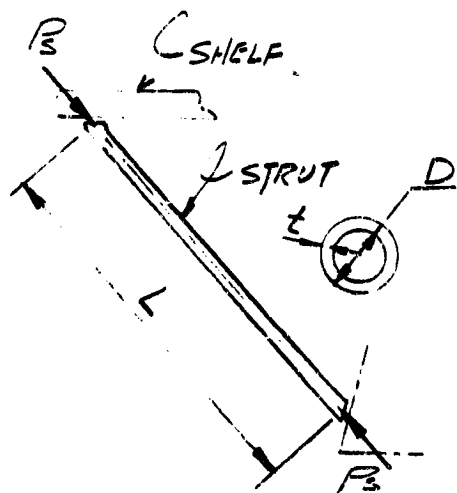
$$\text{TOTAL SHELF LOAD } (W_P) = (748.3 \text{ LB.})$$

$$\text{TOTAL SHELF LOAD } (W_S) = (369.7 \text{ LB.}) \text{ (REF. A)}$$

$$\text{NO. OF STRUTS } (N_P) = 12$$

$$\text{NO. OF STRUTS } (N_S) = 6 \text{ (REF. A)}$$

$$P_S = 6260 \text{ N } (1405 \text{ LB.})$$



$$L = 35.0 \text{ IN.}$$

$$D = 1.250 \text{ IN.}$$

$$t = .025 \text{ IN.}$$

$$A_s = .0963 \text{ IN}^2$$

ALUM.

### 2 - COMPRESSION IN STRUT (AL 2024-T3)

#### (a) COMPRESSIVE STRESS

$$f_c = \frac{P_S}{A_s} = 10500 \text{ N/CM}^2 \text{ (14600 LB/IN}^2\text{)}$$

#### (b) COMPRESSION YIELD STRESS

$$F_{CY} = 28900 \text{ N/CM}^2 \text{ (42000 LB/IN}^2\text{)}$$

#### (c) GENERAL INSTABILITY

USING THE EULER EQN.

$$F_{CR} = \frac{\pi^2 E_c C}{(L/\rho)^2} \text{ (REF. C)}$$

$$C = 1.0 \text{ (PINNED ENDS)}$$

$$E_c = 10.7 \times 10^6 \text{ LB/IN}^2$$

$$\rho = .928 \text{ IN. (RADIUS OF GYRATION)}$$

$$F_{CR} = 10850 \text{ N/CM}^2 \text{ (15750 LB/IN}^2\text{)}$$

#### (d) MARGIN OF SAFETY

$$M_F = \frac{F_{CR}}{f_c} - 1 = \underline{\underline{.080}}$$

## SMALL PROBE SUPPORTS

THE VERTICAL STRUTS ARE REQUIRED TO TRANSMIT THE SMALL PROBE FORCES IN THE LONGITUDINAL DIRECTION TO THE EQUIPMENT SUPPORT SHELF. THE LATERAL SUPPORT BEAM TRANSMITS THE SMALL PROBE LATERAL FORCES TO THE LARGE PROBE SUPPORT.

### 1- DESIGN LOADS

$$\text{WEIGHT OF SMALL PROBE } (W_s) = 65.2 \text{ KG. (143.4 LB.)}$$

$$\text{SMALL PROBE VERT. LD. FACTOR } (M_s) = 23.7 \text{ (REF. A, APP 1, P. 38)}$$

$$F_s = \left(\frac{1}{2}\right) (W_s) (M_s) (1.30) = 9860 \text{ N (2215 LB)}$$

$$V_s = \left(\frac{1}{3}\right) V_{SP} \quad V_{SP} = 18850 \text{ N (REF. LARGE PROBE SUPPORT)}$$

$$V_s = 6283 \text{ N (1403 LB.)}$$

### 2- VERTICAL STRUTS (AL 2024-T3)

#### 1- COMPRESSION IN STRUT

##### (a) COMPRESSIVE STRESS

$$f_c = \frac{F_s}{A_s} = 23200 \text{ N/cm}^2 (33800 \text{ LB/in}^2)$$

##### (b) COMPRESSION YIELD STRESS

$$F_{CY} = 28900 \text{ N/cm}^2 (42000 \text{ LB/in}^2)$$

##### (c) GENERAL INSTABILITY

USING THE EULER EQN

$$\frac{F_{CR}}{\eta} = \frac{\pi^2 E_c C}{(L/\rho)^2} \quad (\text{REF C})$$

$$E_c = 10.7 \times 10^9 \text{ LB/in}^2$$

$$C = 1.0 \text{ (FINNED ENDS)}$$

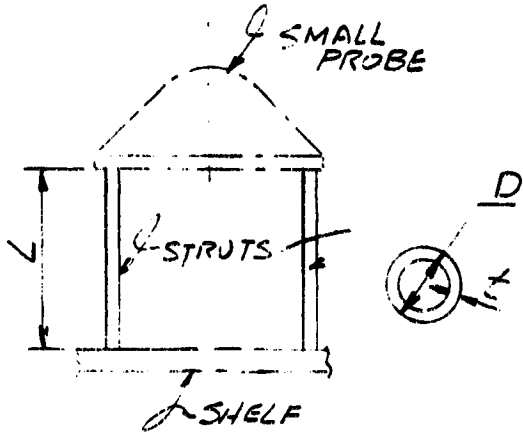
$$\rho = .369 \text{ IN}$$

$$\eta = .855 \text{ (PLASTICITY REDUCTION FACTOR)}$$

$$F_{CR} = 23350 \text{ N/cm}^2 (34000 \text{ LB/in}^2)$$

#### (d) MARGIN OF SAFETY

$$MS = \frac{F_{CR}}{f_c} - 1 = .005$$



$$L = 19.0 \text{ IN.}$$

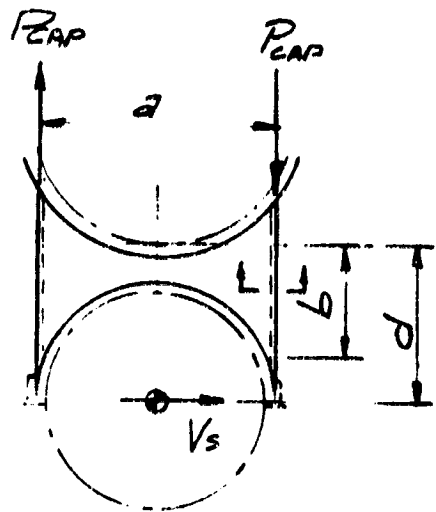
$$D = 1.063 \text{ IN}$$

$$t = .020 \text{ IN.}$$

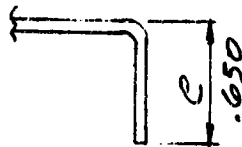
$$A_s = .0656 \text{ IN}^2$$

# SMALL PROBE SUPPORTS (CONTINUED)

## 3- LATERAL SUPPORT BEAM (AL 2024-T3)



$$\begin{aligned} a &= 24.0 \text{ IN.} \\ b &= 12.0 \text{ IN.} \\ t &= .051 \text{ IN.} \\ d &= 17.0 \text{ IN.} \end{aligned}$$



SECTION

$$K_c = .416$$

### 1- SHEAR IN WEB

#### (a) SHEAR STRESS

$$f_s = \frac{V_s}{t a} \quad t a = 1.222 \text{ IN}^2$$

$$f_s = 790 \text{ N/cm}^2 \quad (1148 \text{ LB/IN}^2)$$

#### (b) ALLOWABLE BUCKLING STRESS

$$F_{SCR} = \frac{K_s E_c}{(1-\mu^2)} \left(\frac{t}{b}\right)^2 \quad (\text{REF. C})$$

$$K_s = 5.43 \quad (\text{ALL EDGES SIMPLY SUPPORTED})$$

$$\mu = .33$$

$$F_{SCR} = 803 \text{ N/cm}^2 \quad (1168 \text{ LB/IN}^2)$$

#### (c) MARGIN OF SAFETY

$$MS = \frac{F_{SCR}}{f_s} - 1 = \underline{\underline{.015}}$$

### 2- COMPRESSION IN CAP

#### (a) FORCE IN CAP

$$P_{CAP} = V_s \left(\frac{d}{a}\right) = 4420 \text{ N} \quad (994 \text{ LB})$$

#### (b) COMPRESSIVE STRESS

$$f_c = \frac{P_{CAP}}{e t} = 20650 \text{ N/cm}^2 \quad (30000 \text{ LB/IN}^2)$$

#### (c) COMPRESSION YIELD STRESS

$$F_{CY} = 26800 \text{ N/cm}^2 \quad (39000 \text{ LB/IN}^2)$$

#### (d) LOCAL BUCKLING ALLOWABLE

$$F_{CR} = \frac{K_c E_c}{(1-\mu^2)} \left(\frac{t}{e}\right)^2 \quad (\text{REF. C})$$

$$F_{CR} = 20950 \text{ N/cm}^2 \quad (30500 \text{ LB/IN}^2)$$

#### (d) MARGIN OF SAFETY

$$MS = \frac{F_{CR}}{f_c} - 1 = \underline{\underline{.015}}$$

## REFERENCES

- A) DYNAMIC LOADS ANALYSIS, HS 507-0022-83  
TASK NO. VI 4, 23 FEB 1973  
APPENDIX I, 16 FEB 1973  
APPENDIX 2, 16 FEB 1973
- B) METALLIC MATERIALS AND ELEMENTS FOR  
AEROSPACE VEHICLE STRUCTURES (MIL-HDBK-5A)
- C) FORMULAS FOR STRESS AND STRAIN  
FOURTH EDITION, ROARK, R.J.